

# NOTE TO USERS

This reproduction is the best copy available.

**UMI**<sup>®</sup>



**University of Alberta**

**Air Flow in Sanitary Sewer Systems:  
A Physically-Based Approach**

by

**Stephen Edwini-Bonsu** ©

A thesis submitted to the Faculty of Graduate Studies and  
Research in partial fulfillment of the requirements for the  
degree of Doctor of Philosophy

in

Water Resources Engineering  
Department of Civil and Environmental Engineering  
Edmonton, Alberta  
Fall, 2004



Library and  
Archives Canada

Bibliothèque et  
Archives Canada

Published Heritage  
Branch

Direction du  
Patrimoine de l'édition

395 Wellington Street  
Ottawa ON K1A 0N4  
Canada

395, rue Wellington  
Ottawa ON K1A 0N4  
Canada

*Your file* *Votre référence*  
*ISBN: 0-612-95926-0*  
*Our file* *Notre référence*  
*ISBN: 0-612-95926-0*

The author has granted a non-exclusive license allowing the Library and Archives Canada to reproduce, loan, distribute or sell copies of this thesis in microform, paper or electronic formats.

L'auteur a accordé une licence non exclusive permettant à la Bibliothèque et Archives Canada de reproduire, prêter, distribuer ou vendre des copies de cette thèse sous la forme de microfiche/film, de reproduction sur papier ou sur format électronique.

The author retains ownership of the copyright in this thesis. Neither the thesis nor substantial extracts from it may be printed or otherwise reproduced without the author's permission.

L'auteur conserve la propriété du droit d'auteur qui protège cette thèse. Ni la thèse ni des extraits substantiels de celle-ci ne doivent être imprimés ou autrement reproduits sans son autorisation.

---

In compliance with the Canadian Privacy Act some supporting forms may have been removed from this thesis.

Conformément à la loi canadienne sur la protection de la vie privée, quelques formulaires secondaires ont été enlevés de cette thèse.

While these forms may be included in the document page count, their removal does not represent any loss of content from the thesis.

Bien que ces formulaires aient inclus dans la pagination, il n'y aura aucun contenu manquant.

# Canada



*'I do not know what I may appear to the world; but to myself I seem to have been only like a boy playing on the seashore, and diverting myself in now and then finding a smoother pebble or a prettier shell than ordinary, whilst the great ocean of truth lay all undiscovered before me'*

*Isaac Newton, (Brewster (1855), Memoirs of Newton)*

**Dedicated To**

**Veronica Yaa Serwaah (my dear mother)**

**&**

**All children who have lost a parent**

## ACKNOWLEDGEMENT

I am thankful to the Almighty God who in His mercy upholds me everyday.

I wish to express my gratitude to my supervisor, Dr. Peter Steffler, who throughout the research has been very resourceful in providing valued suggestions and initiatives. His encouragement is very much acknowledged. My thanks are also to Dr. Bryan Karney, my external examiner, and my committee members for their time in appraising the thesis and also for their valuable comments in improving this thesis. I wish also to thank Dr. M. Sterling, University of Birmingham, and Dr. W. Pescod of Motherwell Bridge, England, for providing me with their experimental data.

I gratefully acknowledge the financial support from the Natural Sciences and Engineering Research Council of Canada (NSERC) through my supervisor, and teaching assistantship and tuition scholarship from the University of Alberta. Thanks also to the staff of the Department of Civil and Environmental Engineering, especially Perry Fedun, for their technical support. I wish also to extend thanks to my colleagues at the University of Alberta, especially George Dogbe, Kwame Ofei, Emmanuel Ewusie, Aqeel Jalil and Karen Kow for their encouragement and prayers. Thanks also to the members of Victory Christian Centre, Edmonton, for their prayers and spiritual support.

I am truly grateful to my mother, Veronica, and sister, Afriyie, for their

encouragement, concern and love which are the secrets that have propelled me on all these years. A tribute to my father, Mosi, who inculcated the spirit of hard work in me right from my childhood, but sadly passed away before my 10<sup>th</sup> birthday. I am highly indebted to my wife, Aba, for her encouragement, forbearance and love. Finally, to my three great sons: Kwadwo, Kofi and Brefo, for providing joyful moments at all times.

# TABLE OF CONTENTS

<b>CHAPTER ONE</b>	1
<b>INTRODUCTION</b>	1
1.1 GENERAL	1
1.2 FACTORS AFFECTING SEWER AIR FLOW	3
1.3 RESEARCH APPROACH AND OBJECTIVES	6
1.4 THESIS ORGANIZATION	10
REFERENCES	12
<b>CHAPTER TWO</b>	15
<b>AIR FLOW IN SANITARY SEWER CONDUITS</b>	15
<b>DUE TO WASTEWATER DRAG</b>	15
2.1 INTRODUCTION	15
2.1.1 Background	15
2.1.2 Review of Existing Models and Knowledge-Base	17
2.2 MATHEMATICAL FORMULATION	26
2.2.1 Mean Flow Equations	26
2.2.2 Turbulence Closure	29
2.2.2.1 <i>Modeling the Reynolds shear stresses</i>	29
2.2.2.2 <i>Modeling the Reynolds normal stresses</i>	31
2.3 COMPUTATIONAL APPROACH	32
2.3.1 Boundary Conditions	33

2.3.2 Numerical Solution	35
2.4 VALIDATION AND SIMULATIONS	40
2.5 CONCLUSIONS	56
REFERENCES	59
<b>CHAPTER THREE</b>	<b>64</b>
<b>DYNAMICS OF AIR FLOW IN SANITARY SEWER</b>	<b>64</b>
<b>CONDUITS DUE TO DIFFERENTIAL PRESSURE</b>	<b>64</b>
3.1 INTRODUCTION	64
3.2 MODEL FORMULATION	68
3.2.1 Flow Equations	68
3.2.2 Turbulence Closure	71
3.3 SOLUTION PROCEDURE	73
3.4 VALIDATION AND PREDICTIONS	75
3.5 CONCLUSIONS	87
REFERENCES	89
<b>CHAPTER FOUR</b>	<b>92</b>
<b>COMBINED EFFECTS OF WASTEWATER DRAG AND</b>	<b>92</b>
<b>PRESSURE GRADIENT ON AIR FLOW IN SANITARY SEWER</b>	<b>92</b>
<b>CONDUITS</b>	<b>92</b>
4.1 INTRODUCTION	92
4.2 MATHEMATICAL FORMULATION	97
4.2.1 Governing Equations	97

4.2.2 Modeling the Reynolds Stress Tensor	99
4.3 SOLUTION PROCEDURE	101
4.3.1 Modeling the Ventilating Forces	101
4.3.2 Numerical Modeling	102
4.4 SIMULATIONS AND DISCUSSIONS	104
4.4.1 Velocity Field	105
4.4.2 Interfacial Coefficient of Drag	127
4.5 CONCLUSIONS	133
REFERENCES	136
<b>CHAPTER FIVE</b>	141
<b>SYSTEM THEORETIC FRAMEWORK FOR MODELING</b>	141
<b>SANITARY SEWER SYSTEM VENTILATION</b>	141
5.1 INTRODUCTION	141
5.1.1 Background	141
5.1.2 Existing Knowledge-Base	142
5.2 VENTILATION AND EMISSION RATE RELATIONSHIP	145
5.3 SYSTEM THEORY AND FORMULATION	146
5.3.1 Basic Philosophy	146
5.3.2 Continuity and Energy Formulation	147
5.3.3 Pressure Head Difference-Flow Rate Relationships	149
5.3.3.1 Sewer conduit atmosphere	149
5.3.3.2 Manhole eduction/induction	152
5.3.3.3 Dropstructure pumping effect	154

5.3.3.4 <i>Auxiliary ventilators: scrubbers and mechanical blowers</i>	155
5.4 MODEL APPLICATIONS	156
5.4.1 Case I: A Hypothetical Sewer System	156
5.4.2 Case II: The Kenilworth Sewer System	168
5.4.2.1 <i>System configuration and available data</i>	168
5.4.2.2 <i>Theoretical predictions</i>	175
5.5 DESIGN CONSIDERATIONS FOR A NEW SEWER SYSTEM	184
5.6 CONCLUSIONS	186
REFERENCES	190
<b>CHAPTER SIX</b>	194
<b>SUMMARY, CONCLUSIONS AND RECOMMENDATIONS</b>	194
6.1 SUMMARY AND CONCLUSIONS	194
6.1.1 Headspace Ventilation and Pressurization	194
6.1.2 System Modeling	198
6.2 RECOMMENDATIONS FOR FUTURE WORK	200
REFERENCE	202
<b>APPENDIX A</b>	203
<b>COMPUTATIONAL METHOD: FINITE ELEMENT METHOD</b>	203
A.1 INTRODUCTION	203
A.2 FEMLAB IMPLEMENTATION	204
A.2.1 Geometric Modeling	205
A.2.2 Generation of Unstructured Meshes	206



A.2.3 Discretization of PDEs	210
A.2.4 Solution of the Discretized Equations	217
A.3 ASSESSING THE PREDICTIVE CAPACITY	220
A.3.1 Analytical Modeling	221
A.3.2 Finite Difference Modeling	228
A.3.3 Comparisons of Developed Models	234
REFERENCES	240
<b>APPENDIX B</b>	<b>242</b>
<b>NETWORK FORMULATION AND DATA FOR THE</b>	<b>242</b>
<b>KENILWORTH SEWER SYSTEM</b>	<b>242</b>

## LIST OF TABLES

Table 2-1: Comparing existing and developed models with experiments of Pescod and Price (1978)	42
---	----

## LIST OF FIGURES

Figure 1.1: Primary driving forces affecting sewer air movement	3
Figure 2-1: Theorized streamwise velocity contour due to sewage drag (Pescod and Price 1978)	18
Figure 2-2(a & b): Empirical curves of Pescod and Price (1978): a) using unwetted perimeter, b) using hydraulic radius	20
Figure 2-3(a & b): Variability of streamwise velocity in the headspace: a) at a specific position, b) across the headspace (Pescod and Price 1978)	21
Figure 2-4: A sewer conduit model	27
Figure 2-5(a & b): Examples of finite element meshes: a) laminar, b) turbulent	39
Figure 2-6(a & b): Comparing contour plot of mean primary velocity for Test no. 7, $Re_c = 3,000$ : a) experiment, b) simulated	43
Figure 2-7(a & b): Comparing contour plot of mean primary velocity for Test no. 8, $Re_c = 7,800$ : a) experiment, b) simulated	44
Figure 2-8(a & b): Comparing contour plot of mean primary velocity for Test no. 9, $Re_c = 7,440$ : a) experiment, b) simulated	45
Figure 2-9(a, b & c): Longitudinal velocity profiles at headspace center: a) Test No. 7, b) Test No. 8, c) Test No. 9	46
Figure 2-10: Variation of simulated average mean secondary flow velocity with relative depth (b/D)	50
Figure 2-11: Typical non-dimensionalized velocity ( $U/U_w$ ) contour	

distribution for $b/D= 50 \%$ in laminar flow regime	50
Figure 2-12: Non-dimensionalized average longitudinal velocity ( $U_{av}/U_w$ ) plotted as a function of headspace perimetric shape factor; Also compared is the USEPA (1994) model	53
Figure 2-13: Non-dimensionalized average longitudinal velocity curves ( $U_{av}/U_w$ ) as a function of the relative depth ( $b/D$ ); Also compared is the USEPA (1994) model	54
Figure 2-14: Non-dimensionalized average longitudinal velocity curves ( $U_{av}/V_w$ ) as a function of the relative depth ( $b/D$ ); Also compared is the $\frac{1}{2}$ -WWV model	55
Figure 3-1: A model sewer conduit	70
Figure 3-2(a, b & c): Predicted and measured flow rate compared: a) $b/D= 27 \%$ , b) $b/D = 20 \%$ , c) $b/D= 10 \%$	76
Figure 3-3(a & b): Contour of mean primary velocity ( $U/U_{pt}$ ), $b/D= 27 \%$ , $Re_t = 22,816$ : a) experimental, b) simulated	79
Figure 3-4(a & b): Contour of mean primary velocity ( $U/U_{pt}$ ), $b/D = 20 \%$ , $Re_t = 18,634$ : a) experimental, b) simulated	80
Figure 3-5(a & b): Contour of mean primary velocity ( $U/U_{pt}$ ), $b/D = 10 \%$ , $Re_t = 8,640$ : a) experimental, b) simulated	80
Figure 3-6: Typical non-dimensionalized center velocity profiles for laminar and turbulent flows (compared are the power law and the parabolic profiles)	81

- Figure 3-7(a & b): Typical non-dimensionalized velocity contour distribution  
for  $b/D = 50\%$ : a) laminar regime, b) turbulent,  $Re_t = 30,000$  82
- Figure 3-8(a & b): Cross-sectional average velocity curves as a function of the  
relative depth  $b/D$ : a) laminar, b) turbulent 85
- Figure 3-9(a & b): Cross-sectional average velocity curves as a function of  
the perimetric shape factor: a) laminar, b) turbulent 86
- Figure 4-1: Sewer atmosphere subjected to both pressure gradient and  
wastewater drag 98
- Figure 4-2(a, b, c & d): Typical non-dimensionalized laminar velocity  
contour distributions: a) wastewater-driven only,  $\alpha = 0$ , b)  
pressure-induced only, non-dimensionalized with  $(-dP/dx)b^2/(\rho v)$ ,  
c) forward flow, cases a) & b) combined,  $\alpha = 5.35$ , d) reverse flow,  
cases a) & positive pressure gradient in b) combined,  $\alpha = -5.35$  108
- Figure 4-3(a, b, c & d): Typical turbulent velocity contour distributions:  
a) wastewater-driven only,  $\lambda = 0$ , b) pressure-induced only,  
non-dimensionalized with  $\sqrt{(-dP/dx)b}/(\rho)$ , c) forward flow,  
cases a) & b) combined,  $\lambda = 0.005$ , d) reverse flow, cases a)  
& positive pressure gradient in b) combined,  $\lambda = -0.005$ .  
Superimposed on each plot are the corresponding velocity vectors 110
- Figure 4-4(a, b, c & d): Effect of increasing negative pressure gradient  
against continuously forward moving wastewater on isovels in  
laminar flow: a)  $\alpha = 2.5$ , b)  $\alpha = 10$ , c)  $\alpha = 25$ , d)  $\alpha = 50$  112
- Figure 4-5(a, b & c): Effect of increasing negative pressure gradient

against continuously forward moving wastewater on isovels in turbulent flow: a) $\lambda = 0.01$ , b) $\lambda = 0.025$ , c) $\lambda = 0.1$	114
Figure 4-6(a, b, c & d): Effect of increasing positive pressure gradient against continuously forward moving wastewater on isovels in laminar flow: a) $\alpha = -2.5$ , b) $\alpha = -10$ , c) $\alpha = -25$ , d) $\alpha = -50$	115
Figure 4-7(a, b & c): Effect of increasing positive pressure gradient against continuously forward moving wastewater on isovels in turbulent flow: a) $\lambda = -0.01$ , b) $\lambda = -0.025$ , c) $\lambda = -0.1$	117
Figure 4-8(a, b & c): Average primary velocity curves for turbulent flow regime due to the combined forces of wastewater drag and negative pressure gradient for range of values of $U_R$ and $b/D$	121
Figure 4-9(a, b, c & d): Average primary velocity curves for turbulent flow regime due to the combined forces of wastewater drag and positive pressure gradient for range of values of $U_R$ and $b/D$	123
Figure 4-10: Zero average velocity criterion curve in laminar flow regime	126
Figure 4-11: Predicted interfacial drag coefficient (due to wastewater) compared with plane Couette flow data available in the literature	128
Figure 4-12: Comparison of calculated average wall friction coefficient and interfacial drag coefficient due to wastewater drag	129
Figure 4-13(a, b & c): Interfacial drag coefficient for some values of $\lambda$ : a) $b/D= 25\%$ , b) $b/D= 50\%$ , c) $b/D= 75\%$	130
Figure 4-14(a, b & c): Comparison of calculated average wall friction coefficient and interfacial drag coefficient-combined flow:	

a) $b/D= 25\%$ , b) $b/D= 50\%$ , c) $b/D= 75\%$	131
Figure 5-1a: Schematic of an isolated municipal sewer system	157
Figure 5-1b: Network representation of Figure 5-1a	159
Figure 5-2a: Influence of auxiliary ventilation on manhole velocity, $C_d= 0.65$ , $b/D= 50\%$ , $U_{wc}= 1\text{ m/s}$ , $P_5= 0\text{ m}$ , $k= 0$	165
Figure 5-2b: Influence of auxiliary ventilation on manhole flow rate, $C_d= 0.65$ , $b/D= 50\%$ , $U_{wc}= 1\text{ m/s}$ , $P_5= 0\text{ m}$ , $k= 0$	165
Figure 5-2c: Influence of auxiliary ventilation on headspace flow rate, $C_d= 0.65$ , $b/D= 50\%$ , $U_{wc}= 1\text{ m/s}$ , $P_5= 0\text{ m}$ , $k= 0$	166
Figure 5-3a: Effect of outfall pressure head, $P_5$ , (m) on air eduction, $C_d= 0.65$ , $Q_{AV}= 0\text{ m}^3/\text{min}$	166
Figure 5-3b: Effect of outfall pressure head, $P_5$ , (m) on headspace flow rate, $Q_{AV} = 0\text{ m}^3/\text{min}$ , $U_{wc}= 1\text{ m/s}$ , $C_d= 0.65$ , $b/D= 50\%$	167
Figure 5-4: Effect of coefficient of discharge on eduction, $Q_{AV} = 0\text{ m}^3/\text{min}$ , $P_5= 0\text{ m}$ , $b/D= 50\%$	167
Figure 5-5: The Kenilworth sewer system (Not drawn to scale)	170
Figure 5-6a: Diurnal wastewater velocity in pipe [1] (May/June2003)	171
Figure 5-6b: Diurnal wastewater flow depth in pipe [1] (May/June 2003)	171
Figure 5-7a: Diurnal wastewater velocity in pipe [33] (July/Oct 2003)	172
Figure 5-7b: Diurnal wastewater flow depth in pipe [33] (July/Oct 2003)	172
Figure 5-8a: Diurnal wastewater velocity in pipe [44] (June/July 2003)	173
Figure 5-8b: Diurnal wastewater flow depth in pipe [44] (June/July 2003)	173
Figure 5-9a: Field measurement of average educting velocity	174

Figure 5-9b: Field measurement of average educting/inducting velocity	175
Figure 5-10: Network representation of Figure 5-5	176
Figure 5-11(a & b): Influence of scrubber on eduction/induction, $C_d=0.65$	179
Figure 5-12(a, b, c & d): Influence of scrubber on headspace flow rate	180
Figure 5-13(a & b): Effect of wastewater level changes on eduction/induction, $C_d= 0.65$	183
Figure A-1(a & b): Typical unstructured mesh: a) initial finite element mesh; nodes= 173, boundary elements = 39, elements = 305, b) corresponding mesh quality histogram	207
Figure A-2(a & b): Typical unstructured mesh: a) refined finite element mesh; nodes= 650, boundary elements = 78, elements = 1220, b) corresponding mesh quality histogram	208
Figure A-3: Typical unstructured mesh using selective refinement close to the boundary regions: nodes= 5177, boundary elements = 535, elements = 9817, minimum $q= 0.78$	209
Figure A-4: Headspace in an elliptic system	222
Figure A-5: Correspondence between physical and computational domains	231
Figure A-6(a, b & c): Wastewater-induced isovels for $b/D= 10 \%$ : a) finite element, b) analytical, c) finite difference	235
Figure A-7(a, b & c): Pressure-induced isovels for $\alpha = -5$ , $b/D= 10 \%$ : a) finite element, b) analytical, c) finite difference	236
Figure A-8(a, b & c): Combined pressure and wastewater induced isovels for $\alpha = -5$ , $b/D= 10 \%$ : a) finite element, b) analytical,	



c) finite difference	237
Figure A-9: Comparative performance of the three models in computing wastewater-induced average velocity	238
Figure A-10: Comparative performance of the three models in computing pressure-induced average velocity for $(dp/dx)/(v\rho) = -100$	238
Figure A-11: Comparative performance of the three models in computing combined average velocity for $(dp/dx)/(v\rho U_w) = -100$	239
Figure B-1: Network representation of the Kenilworth sewer system	242
Figure B-2: Sewer system showing available slopes and assumed boundary pressure heads (m) (Not drawn to scale)	250

## LIST OF SYMBOLS/ABBREVIATIONS •

$A$	= Cross-sectional area [5],[A]
$A_s$	= Surface area [5]
$AT$	= Atmosphere [5],[A]
$A_{wy}, A_{vy}, A_{wn}, A_{vn}$	= Empirical constants for turbulent intensity distributions [2],[3],[4]
$b$	= Maximum headspace depth [2],[3],[4],[5],[A]
$B_{wy}, B_{vy}, B_{wn}, B_{vn}$	= Empirical constants for turbulent intensity distributions [2],[3],[4]
$C$	= Width of the air-water interface [2],[3],[4],[5],[A]; concentration [5]
$C_d$	= Coefficient of discharge [5],[A]
$CJ$	= Closed junction [5],[A]
$d$	= Diameter of orifice [5]
$D$	= Diameter of sewer pipe [2],[3],[4],[5],[A]
$dx$	= Longitudinal distance between any two openings along a sewer [3],[4]
$e$	= Eccentricity [A]
$E$	= Emission rate [5]
$f$	= Drag coefficient/friction factor [2],[4]
$F$	= Vector of equations [5],[A]

---

• The number in square brackets [ ] denotes relevant chapter number. [A] denotes Appendix

FD(M)	= Finite difference(model/method) [2],[3],[4],[A]
FE(M)	= Finite element (model/method) [2],[3],[4],[A]
$g$	= Acceleration due to gravity (= 9.81 m/s <sup>2</sup> ) [2],[5],[A]
$h$	= Channel flow depth [2],[4]
$H$	= Drop height [5]
$H_c$	= Henry's law coefficient [5]
$i$	= Elements of the incidence matrix [5]
<b>I</b>	= Incidence matrix [5]
<b>J</b>	= Jacobian matrix [5]
$k$	= Turbulent kinetic energy [2],[3]; incidence index [5]; mass transfer coefficient [5]; constant for duct in Darcy-Weisbach equation [5]
$k_s$	= Effective roughness height [2]
$k_s^+$	= Dimensionless effective roughness height  ( $k^+ = u_\tau k_s / \nu$ ) [2]
$K_L$	= Overall mass transfer coefficient [5]
$K_l$	= Loss coefficient [2]
$l$	= Length of pipe [2]
$\ell_m$	= Mixing length [2],[3],[4]
$L$	= Perimeter of the unwetted headspace [2],[3],[4],[5]
LP	= Loop [5],[A]
$\dot{m}$	= Mass flow rate [2]
MH	= Manhole [5],[A]

$n$	= Normal to or from the boundary [2],[3],[4],[A]; Manning coefficient [2]; pipe number [5]; exponent in Darcy-Weisbach equation [5]
$P$	= Mean pressure [3],[4],[5]; Pressure head [5],[A]
$Q$ or $(\mathbf{Q})$	= Flow rate or flow rate vector [3],[5],[A]
$R$	= Coefficient of determination [2],[3]
$Re$	= Reynolds number ( $Re_w = U_w b / \nu$ [2],[4], $Re_c = U_{wc} b / \nu$ [2],[4],[A], $Re_t = U_{pt} b / \nu$ [3], $Re_l = U_{pl} b / \nu$ [3], $Re = V_E d / \nu$ [5])
$R_h$	= Hydraulic radius of water section [2]
$R_{hs}$	= Hydraulic radius of the headspace [2]
SOR	= Successive over-relation [A]
$S_0$	= Channel slope [2]
$t$	= Time [2]
$u_\tau$	= Shear velocity [2],[3],[4]
$U$	= Longitudinal mean velocity [2],[3],[4],[A]
$U_{av}$	= Cross-sectional average velocity [2],[3],[4],[A]
$U_{pl}$	= Laminar velocity scale [3]
$U_{pt}$	= Turbulent velocity scale [3]
$U_R$	= $\lambda(L + C) / C$ [4],[5]
$U_w$	= Average water surface velocity [2],[4],[5],[A]

$U_{wc}$	= Water surface velocity at channel center [2],[4],[5]
$U_{ws}$	= Interfacial velocity [2],[4],[A]
$u', v', w'$	= Velocity fluctuations in x, y and z directions, respectively [2],[3],[4],[A]
$\sqrt{v'^2}, \sqrt{w'^2}$	= r.m.s. of turbulence in y and z directions, respectively [2],[3],[4],[A]
V, W	= Secondary velocities in y and z directions, respectively [2],[3],[4],[A]
$V_E$	= Average velocity via manhole [5]
$V_{net}$	= Net velocity [2]
$V_w$	= Average water velocity [2],[5]
$V_{w1}, V_{w2}$	= Wind speeds at two points along the sewer pipe [3],[4]
$VW$	= Magnitude of the secondary flow vectors (V, W) [2]
$\dot{w}$	= Rate of work [2]
W	= Flow rate due to wastewater drag [5],[A]
x	= Axial/longitudinal Cartesian co-ordinate [1],[2],[3],[4]
X	= Length of pipe [5]
$X^*$	= $x/b$ [2],[3],[4],[A]
y	= Vertical Cartesian co-ordinate [2],[3],[4]
$y^+$	= Normalized wall distance ( $y^+ = u_{\tau} n_i / \nu$ ) [2]
$Y^*$	= $y/b$ [2],[3],[4],[A]

$z$	= Transverse/lateral Cartesian co-ordinate [2],[3],[4]
$Z^*$	= $z/b$ [2],[3],[4],[A]
$\alpha$	= $(-dP/dx)b^2/(\rho\nu U_w)$ [4]; dropstructure/pump/fan characteristic function parameter [5],[A]
$\beta$	= Sewer pipe slope [2],[3],[4]; dropstructure/pump/fan characteristic function parameter [5],[A]
$\Delta$	= Change [5],[A]
$\varepsilon$	= Rate of turbulent kinetic energy dissipation [2],[3]
$\gamma$	= Dropstructure/pump/fan characteristic function parameter [5],[A]
$\eta$	= Co-ordinate related to the elliptic and generalized co- ordinate systems [A]; dimensionless parameter equal to 0.67 [2]
$\tau$	= Shear stress [2],[4]
$\Phi$	= Vector of unknowns [2],[A]
$\psi$	= Reduction factor [5]
$\kappa$	= von Karman constant (= 0.41) [2],[4]
$\lambda$	= $(-dP/dx)b/(\rho U_{wc}^2)$ [4],[5]; relaxation parameter in SOR method [A]
$\nu$	= Kinematic viscosity (= $1.5 \times 10^{-5}$ m <sup>2</sup> /s); turbulent eddy viscosity ( $\nu_t$ ) [2],[3],[4],[5],[A]
$\theta$	= Angle related to the elliptic co-ordinate system [A]

$\rho$	= Mass density of air (= 1.28 kgm <sup>-3</sup> ) [2],[3],[4],[5],[A]
$\xi$	= Co-ordinate related to the generalized system [A]

## SUBSCRIPTS

AT	= Atmospheric [5],[A]
av	= Spatial average [2],[3],[4],[A]
AV	= Auxiliary ventilator [5]
DS	= Pertaining to dropstructure [5],[A]
E	= Pertaining to eduction/induction [5],[A]
g	= Gas [5]
h	= Pertaining to dropstructure [5]
i	= Pertaining to interface [2],[4]
id	= Ideal [2]
i, j	= Co-ordinates directions; tensor indices [2],[3],[4]
j	= Pertaining to manhole [5]
l	= Laminar [3]; liquid [5]
n	= Pipe number [5]
0	= Pertaining to orifice [5],[A]
s	= Pertaining to water surface [3]; pertaining to scrubber [A]
sec	= Pertaining to secondary flow [2]
t	= Turbulent [3]
w	= Pertaining to wall; pertaining to water [2],[3],[4]
*	= Dimensionless [2],[3],[4],[A]

---

# CHAPTER ONE

## INTRODUCTION

---

### 1.1 GENERAL

Municipal wastewater collection systems, due to the nature of their functions, carry varying concentrations of hydrogen sulphide gas and other lethal gaseous compounds such as ammonia, carbon monoxide, methane, to mention just a few. The effects of emission of these gaseous products are various and include toxicity, odour nuisance, explosion hazards, and acid attack of the sewer fabric and appurtenances (ASCE 1989; Davidson et al. 2004; Haecker et al. 2004; Thistlethwayte 1972; Zytner et al. 1997). In some developed countries (e.g. United States) odour nuisance can be a source of litigation for sewerage and municipal authorities with concomitant financial liability in some cases (Apgar et al. 2004; ASCE 1989).

The production and emission rate of the sewer gases as well as their transport within and out of sewer systems strongly depend on air flow dynamics in the system piping (Davidson et al. 2004; Haecker et al. 2004; Odor and Corrosion Technology Consultants 1999b; Olson 1996; Olson et al. 1997; Pescod and Price



1978; Thistlethwayte 1972). If the air stays within the sewer atmosphere there will be no release of odorous or hazardous pollutants into ambient localities and therefore no complaints, although corrosion from hydrogen sulphide gas and threats to the safety of maintenance workers (owing to oxygen deficiency and poisoning) will undoubtedly persist. To effectively understand the production, emission and transport mechanisms of these gaseous products, to provide a quantitative basis for deciding on the form and frequency of engineering interventions necessary to induce adequate ventilation or control odour in sanitary sewer systems, and to reliably model corrosion phenomenon, the air flow dynamics must be quantitatively predicted.

There have been limited scientific studies on air flow in municipal wastewater collection systems. Sewer systems are designed to transport only sewage flow without giving consideration to the air flow field. As a consequence, the movement of air into, along and out of wastewater collection systems is for the most part uncontrolled. The few air flow models currently in use are generally noted to overestimate the air flow rate due to incorrect representation of the motive forces and inappropriate formulation of the physics of the flow phenomena (Davidson et al. 2004; Odor and Corrosion Technology Consultants 1999b; Olson 1996; Olson et al. 1997; Pescod and Price 1978, 1982; USEPA 1994). The main purpose of this research project therefore is to improve and build on the existing knowledge-base related to the dynamics of air flow in sewer systems with a view to providing a design protocol for engineers and environmentalists. The research

study considers air flow in sewer conduit headspaces in addition to air exchanges via manhole openings.

## 1.2 FACTORS AFFECTING SEWER AIR FLOW

The driving forces responsible for air movement in sanitary sewer systems are well-documented (Corsi et al. 1989; Odor and Corrosion Technology Consultants 1999b; Olson 1996; Olson et al. 1997; Pescod and Price 1978, 1981, 1982; Pomeroy 1945; Quigley and Corsi 1995; USEPA 1994; Thistlethwayte 1972). Broadly, ventilation of sewers can be classified as natural (environmental) or artificial (structural) as depicted in Figure 1.1. Natural ventilation is that where movement of air occurs as a consequence of natural barometric, wind or drag exerted by the flow of the sewage. Artificial ventilation is that where air moves by the application of mechanically power-driven equipment or by dropstructure pressurization.

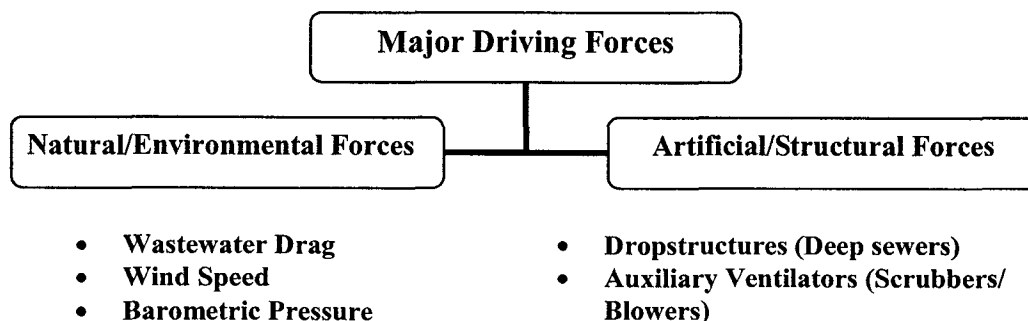


**Figure 1.1: Primary driving forces affecting sewer air movement**

The effects of these driving forces can be summarized as follows:

- Wastewater/sewage drag: momentum is transferred from wastewater to air due to shear forces at the air-water interface which translates into an induced flow of air. Changes in wastewater velocity, most often the result of changing slopes in the sewer, have perhaps the greatest effects on the air pressure in a sewer. Increasing velocities pull harder on the air through friction, while decreasing velocities act to slow the air down. This pushing and pulling of air through the sewer establishes positive and negative pressure zones which can cause movement of air into and out of the sewer.
- Wind speed: wind speeds across sewer openings such as manholes can cause dynamic pressure differences between the sewer pipe headspaces and the atmospheres above the openings. These pressure differences can lead to air flow circuits between the sewer and ambient atmospheres.
- Barometric pressure: variations in barometric pressure within a locality can cause air flow into, along and out of sewers depending upon the relative pressures inside and outside the sewers.
- Dropstructures: in some cases, dropstructures are the single greatest contributors to ventilation and odour releases from deep tunnel sewers. The function of dropstructures is simple: contain wastewater as it falls under the effect of gravity until it enters a lower pipe. As in sewer conduit headspace, drag is also the primary air movement mechanism except that the drag is further enhanced due to increased surface contact area and dispersion of wastewater.

- Auxiliary ventilators (also known as forced draft): scrubbers and blowers fall into this category. These auxiliary ventilators are usually used to combat corrosive, odorous and other hazardous gases. These mechanical ventilators act to induce air flow in sewer headspaces and openings such as manhole covers.

Aside from the above major motive forces, other factors that can add to or detract from the ventilation rate and magnitude of odour emission of sewer systems are:

- A decrease in pipe diameter in the downstream direction (which should not happen in any well-designed sewer system) limiting the air carrying capacity and causing a localized pressure zone with a possibility of venting.
- Opposing or perpendicular flows entering a junction sewer structure causing a temporary back up of air resulting in locally increased air pressure and leading to the expulsion of air via available outlets.
- A gravity sewer entering an inverted siphon or a pump station wet well causing all of the air being carried in the sewer to be immediately ejected to the atmosphere or forced back upstream to the nearest point of release.
- Sudden rising wastewater levels forcing air out of an unsealed sewer opening. Conversely, sudden declining water levels can draw air into sewers.
- Hydraulic jump (mostly formed due to supercritical to subcritical flow conditions at exits of dropstructures) can generate huge amount of air

which could potentially be carried into the receiving sewer or be trapped at the bottom of the dropstructure where it could pressurize.

- Air temperature differential between the sewer air and the ambient air (for example, in winter the sewer air is likely to be warmer) can result in a density difference producing a net air movement.

### **1.3 RESEARCH APPROACH AND OBJECTIVES**

Air movement in sanitary sewer systems is one of the complex hydraulic flow phenomena. There are a large number of variables involved and the relationships between them are too complex to assemble readily any sort of reliable mathematical relationships. The effects and relationships between variables are affected by distance, hydraulic flow variations, interfacial waves, pipe constrictions, pipe roughness, ambient environmental conditions and many other variations. A physical or generalized theoretical model that would accurately consider all the factors together is not currently feasible. The appropriate step, in the author's view, toward understanding the air flow dynamics in sewer systems is to isolate and model flows in the various major units (manhole, sewer conduit headspace, dropstructure, etc.,) that make up the collection system. In this direction, the entity of sewer system air pressurization and ventilation can be assumed to be an independent system, in the sense that it can be divided into interconnected components each of which can be modelled mathematically. This approach serves as the keystone for this research.

This study is limited to ventilation and pressurization in sewer headspace and eduction via manholes due to the driving forces of wastewater drag phenomenon and pressure. The pressure may result from wind speed, barometric pumping, pressurization from dropstructures, scrubbers/blowers, and other pressure causing conditions. The separate effects of wastewater drag, pressure as well as the combined effect of wastewater drag and pressure on sewer headspace ventilation and pressurization are thoroughly investigated using techniques of computational fluid dynamics (CFD). The effect of sudden rise and fall of wastewater level on ventilation in sewers has been discussed qualitatively by several authors (e.g. Pescod and Price 1978, 1981, 1982; Pomeroy 1945; Thistlethwayte 1972). Thistlethwayte (1972) noted that the overall change in air headspace volume due to sudden rise and fall may be temporal and as such is not discussed further in this research. In sanitary sewers unlike industrial sewers, the effect of temperature gradient may be minimal in comparison to other driving forces. To this end, temperature effect is also not modelled in this study. The dynamics of air entrainment and eduction in dropstructures and hydraulic jumps is also not considered in this study.

The current models used in practice provide only the spatial averaged value of the longitudinal headspace air velocity and also fail to account for the physics behind the flow field (Davidson et al. 2004; Odor and Corrosion Technology Consultants 1999b; Olson 1996; Olson et al. 1997; Pescod and Price 1978, 1981; USEPA 1994). Any improvement should not only be limited to the average streamwise

velocity computations, but also offer a framework upon which the flow patterns in the sewer headspace could be properly elucidated. The improvements in the flow modeling should also include more physics, and correct representation of the airspace cross-section and the driving forces.

Specific research objectives include:

- Development of an improved understanding of the separate effects of wastewater drag and pressure gradient on sewer headspace air dynamics.
- Assessment of the effects of combined mechanism of wastewater drag and pressure gradient on sewer headspace ventilation and pressurization.
- Investigation of the effects of turbulence-driven secondary motions on the longitudinal (mean) turbulent headspace velocity field.
- Development of a generalized system model for eduction/induction computations.

In modeling the air flow field in the sewer conduit atmosphere, the Navier-Stokes equations (Reynolds-averaged-Navier-Stokes equations, in the case of turbulent flow) have been adopted and place the flow field in a 2-D framework. The modeling approach considers an isolated section of wastewater collection system without intersecting sewer lines, changes in channel slope, or changes in pipe diameter thus making the assumption of fully-developed flow ( i.e.  $\partial(\cdot)/\partial x = 0$ , except the longitudinal pressure gradient) strictly valid. Both turbulent and laminar flow regimes are considered. A generalized eddy viscosity-mixing length

model is selected for closing the averaged Navier-Stokes equations governing the flow field in the turbulent flow regime. In this study, the effect of wastewater drag is formulated as a boundary condition at the air-wastewater interface whilst conduit pressurization effects are represented as longitudinal pressure gradients in the streamwise momentum equation. A Galerkin finite element method is developed to approximate the resulting formulations.

Owing to the limited experimental data against which the computational results may be compared, alternative means of assessing the predictive capacity of the numerical tool are implemented. In this case the finite element method is tested against approximate analytical and finite difference models developed for the laminar flow regime. The computed turbulent flow characteristics are restricted to (i) the longitudinal mean velocity; (ii) the secondary mean flow pattern in the plane of the cross-section due to turbulence anisotropy and (iii) the interfacial drag coefficient. Accurate predictions of these constitute the accurate prediction of the air flow field in the sewer conduit headspace. Laminar flow modeling in the conduit is limited to only the longitudinal velocity.

The study further adopts system theory to formulate a generalized framework for analysing ventilation and pressurization in sewer systems. In this framework, eduction/induction via manholes and dropstructure pressurization phenomena are conceptually formulated by invoking an orifice model and a quadratic characteristics pump model, respectively. Auxiliary ventilators such as scrubbers



and blowers are treated as fans and pumps of known performance characteristic curves.

## **1.4 THESIS ORGANIZATION**

This thesis is written in accordance with the University of Alberta paper-based format where each chapter is made independent as possible. This chapter (Chapter 1) provides a brief review regarding sanitary sewer ventilation factors and also points out the scope of the present study as well as the main flow features of interest to be studied in the subsequent chapters.

The papers in Chapters 2-5 present the main research contributions. Chapters 2 and 3 are respectively devoted to studying the effects of wastewater drag and pressure gradient on air flow field in an isolated section of partially-full, straight gravity-flow circular sewer conduit without intersecting sewer lines, changes in channel slope, or changes in pipe diameter. Chapter 4 examines the combined effects of wastewater drag and pressure gradient on air flow field in an isolated sewer conduit. Each of these chapters employs the Navier-Stokes equations (Reynolds-averaged-Navier-Stokes equations in the case of turbulent flows) to describe the air flow field. In the turbulent flow the unknown Reynolds stresses in the Reynolds-averaged-Navier-Stokes equations are resolved via a Boussinesq's eddy viscosity hypothesis in combination with semi-empirical models. The effects of secondary flow on the streamwise mean velocity field are examined in

Chapters 2-4. The model computations are validated with experimental data (available in the literature) in Chapters 2 and 3 and subsequently used to develop generalized curves and formulae for practical use.

Chapter 5 is devoted to modeling air flow in sewer systems using system theory and the formulae developed in the preceding chapters. The main driving forces involved in causing air eduction/induction via manholes are discussed. The approach adopted applies both continuity and work-energy principles and models eduction/induction using the standard orifice equation. A quadratic characteristic pump model, whose parameters have to be calibrated for a given system, is proposed to describe the pumping effects of dropstructures in deep sewer systems. The main conclusions of the study and recommendations for future work are presented in Chapter 6. The finite element method which is the main numerical tool in Chapters 2-4 is described in Appendix A. Also presented in Appendix A are the analytical and finite difference laminar models developed to assess the predictive capacity of the finite element method used in Chapters 2-4. Appendix B gives the system formulation and data assumed in Chapter 5 for theoretically deducing air flows in the Kenilworth sewer system in the City of Edmonton.

## REFERENCES

- Apgar, D., Witherspoon, J., Finger, D. 2004. Odor complaint investigation and response. WEF/A & WMA Odors and Air Emission Conference, Bellevue, Seattle.
- ASCE. 1989. Sulphide in wastewater collection and treatment systems. ASCE Manuals and Reports on Engineering Practice, No. 69.
- Bowker, R. P. G., Smith, J. M., Webster, N. A. 1989. Odor and corrosion control in sanitary sewerage systems and treatment plants. Hemisphere Publishing Corporation, N. Y.
- Corsi, R. L., Chang, P. Y., Schroeder, E. D. 1989. Assessment of the effect of ventilation rates on VOC emission from sewers. Air & Water Management Ass. 82nd Annual Meeting & Exhibition. Anaheim, California.
- Corsi, R. L., Chang, P. Y., Schroeder, E. D. 1992. A modeling approach for VOC emissions from sewers, Water Env. Research. **64** (5), 734-741.
- Davidson, S., Green, J., Mann, J., Lamb, E. 2004. Design challenges in sewer foul air extraction and treatment. WEF/A & WMA Odors and Air Emission Conference, Bellevue, Seattle.
- Haecker, S., Cheatham, J. B, Gaudes, R. J. 2004. Biological treatment of collection system odors is the most cost effective solution. WEF/A & WMA Odors and Air Emission Conference, Bellevue, Seattle.
- Matos, J. S., de Sousa, E. R. 1992. The forecasting of hydrogen sulphide gas build-up in sewerage collection systems. Wat. Sci. Tech. **26** (3-4): 915-922.

- Odor and Corrosion Technology Consultants, Inc. 1999a. The dropstructures ventilation phenomena. TM No.2, City of Edmonton Odour Control Project, Alberta.
- Odor and Corrosion Technology Consultants, Inc. 1999b. The use of modeling techniques to evaluate and correct odour releases from trunk sewers. TM No.4, City of Edmonton, Odour Control Project, Alberta.
- Odor and Corrosion Technology Consultants, Inc. 1999c. Trunk sewer odour monitoring program. TM No.1, City of Edmonton, Odour Control Project, Alberta.
- Olson, D. 1996. Gas exchange rates between industrial process drains and the ambient atmosphere. MSc. Thesis, University of Texas.
- Olson, D., Rajagopalan, S., Corsi, R. L. 1997. Ventilation of industrial process drains: mechanisms and effects on VOC emissions, *Jr. Env. Eng.* **123** (9), 939-947.
- Pescod, M. B., Price, A. C. 1978. A study of sewer ventilation for the Tyneside sewerage scheme. Final Research Report, Department of Civil Engineering, University of Newcastle Upon Tyne, U. K.
- Pescod, M. B., Price, A. C. 1981. Fundamentals of sewer ventilation as applied to the Tyneside sewerage scheme. *Water Pollution Control*: **90** (1), 17-33.
- Pescod, M. B., Price, A. C. 1982. Major factors in sewer ventilation. *J. Water Pollution Control Fed.*, **54** (4), 385-397.
- Pomeroy, R. 1945. Pros and cons of sewer ventilation. *Sewage Works Journal*, **17** (2), 203-208.

Quigley, C. J., Corsi, R. L. 1995. Emission of VOCs from a municipal sewer.

J. Air and Waste Mgmt. Assn., **45** (5), 395-403.

Thistlethwayte, D. K. B. (Ed.). 1972. The control of sulphides in sewerage systems. Butterworths, Sydney.

U. S. Environmental Protection Agency (EPA). 1994. Air emission models for waste and wastewater. EPA-453/R-94-080A-Part 1.

Zytner, R. G., Madani-Isfahani, M., Corsi, R. L. 1997. Oxygen uptake and VOC emissions at enclosed sewer dropstructures, Water Env. Research. **69** (3), 286-294.

---

# CHAPTER TWO<sup>1</sup>

## AIR FLOW IN SANITARY SEWER CONDUITS

### DUE TO WASTEWATER DRAG

---

## 2.1 INTRODUCTION

### 2.1.1 Background

Air flow modeling in sanitary sewer conduits is a key input for efficient design of ventilation systems, and improved understanding of emission of volatile organic compounds (VOCs) from and occurrence of corrosion in sewer piping systems (ASCE 1989; Bowker et al. 1989; Matos and de Sousa 1992; Pescod and Price 1978; Odor and Corrosion Technology Consultants 1999b; Olson et al. 1997; Quigley and Corsi 1995; Thistlethwayte 1972). Unfortunately, collection systems are designed to carry only liquid flow without regard to what happens to the airspace. Therefore the effects of friction drag, acceleration and deceleration of wastewater, and headspace pressurization are largely misunderstood and ignored.

---

<sup>1</sup> The main content of this chapter is accepted for publication in the *J. Environ. Eng. Sci.*; Some model results are also presented at WEF/A & WMA Odors & Air Emission Conference, Bellevue, Seattle, 2004.

As a consequence, the movement of air into, along and out of wastewater collection systems is for the most part uncontrolled. This causes odour complaints and points of aggressive corrosion that may be totally unexpected and are identified only after system startup.

Field and laboratory studies indicate that wastewater drag and other factors such as wind speed, barometric pressure, dropstructures and scrubber/blower are the major forces responsible for air flow in sanitary sewer channels (Odor and Corrosion Technology Consultants 1999b; Olson 1996; Olson et al. 1997; Pescod and Price 1978, 1981, 1982; Pomeroy 1945; Quigley and Corsi 1995; Thistlethwayte 1972; USEPA 1994). The effects of these driving forces do not only accelerate the sewer air along the sewer pipe, but also cause air ejection and hence odour releases via available openings. Air movement in sanitary sewer conduits resulting from pressure gradient has been studied using computational fluid dynamics (CFD) techniques by Edwini-Bonsu and Steffler (2004b) (also Chapter 3 of this thesis) and also studied somewhat quantitatively or qualitatively in the literature (Olson 1996; Olson et al. 1997; Pescod and Price 1978, 1981, 1982; Thistlethwayte 1972; USEPA 1994).

In this paper only the driving force of wastewater drag is considered. Wastewater flowing down the sewer results in friction at the air-water interface and this translates into an induced flow of air. Of all the factors that affect the movement of sewer gases, the wastewater drag is the one that acts continuously. With no

other ventilation mechanism present, air and wastewater flow should be co-current. However, re-circulation flow patterns may exist when openings between sewer and ambient atmospheres are restricted (Olson 1996). Quigley and Corsi (1995) measured air exchange rates using both anemometric methods and sulphur hexafluoride injections within a municipal sewer interceptor. The system conveyed wastewater containing significant industrial discharges and was characterized by numerous openings for air exchange. Air exhaust rates from a single manhole cover containing 66 1-inch diameter pickholes ranged from a low of 140 m<sup>3</sup>/h at 6 a.m. to a high of 590 m<sup>3</sup>/h at 12 p.m. The profile of air exchange rates was consistent with wastewater flow rates, suggesting that ventilation was driven by liquid drag. Pescod and Price (1978) also referenced field studies in Tyneside sewerage scheme in England. The sewer section studied had an internal diameter of 1650 mm and slope of 1/202. During the time of the tests, sewage was flowing at a depth of 150-200 mm and a surface velocity of about 1 m/s. The measured air flow rates within the sewer ranged from 105 to 315 m<sup>3</sup>/h. The above field examples demonstrate the capacity of wastewater drag phenomenon to transport air in sewer systems.

### **2.1.2 Review of Existing Models and Knowledge-Base**

A literature review of current models and their limitations is given below.

**Pescod and Price (1978) empirical curves:** Pescod and Price (1978) were perhaps the first to present a scientific experimental study (described briefly in



Section 2.4) on wastewater-driven air movement in sewer conduit atmosphere. Based on their study, they theorized that the streamwise air flow pattern in the sewer headspace due to wastewater drag is as shown in Figure 2-1 and that the velocity profile decreases exponentially from the interface with increasing vertical distance (from the water surface) except near the pipe wall.

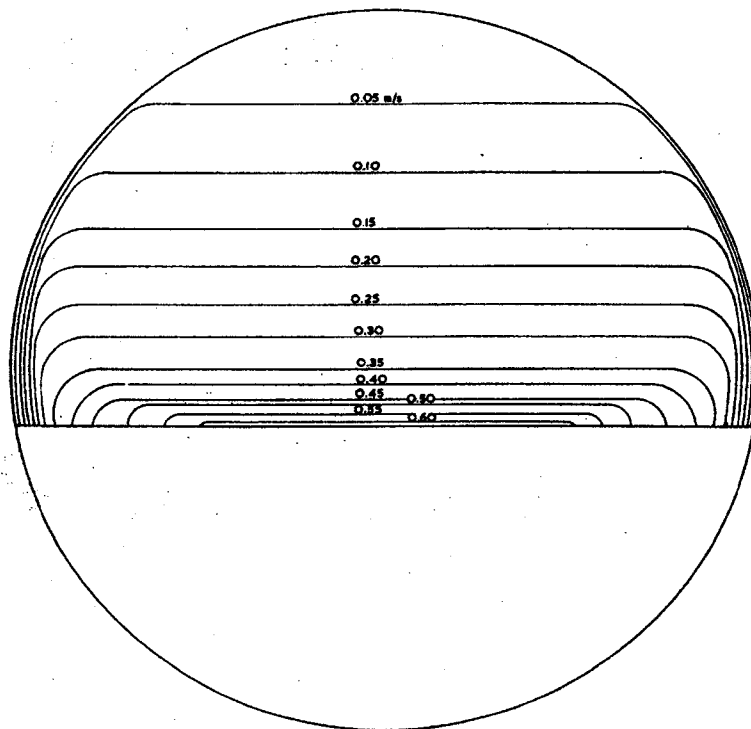


**Figure 2-1: Theorized streamwise velocity contour due to sewage drag  
(Pescod and Price 1978)**

Figure 2-1 is possibly the only known scientific deduction insofar as headspace air velocity distribution is concerned. Although this flow pattern is an ideal one, it has had some useful impact in the sewer corrosion modeling industry. Pescod and Price (1978) further developed empirical curves for the estimation of the average

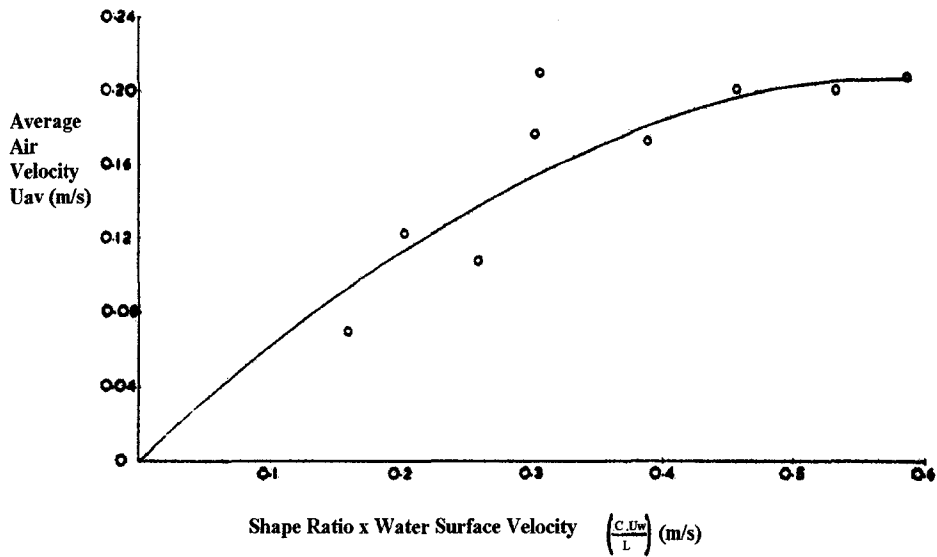
air velocity. They showed that the measured average air velocity correlated with the product of water surface velocity and a shape ratio. They defined the shape ratio as either the width of the air-water interface ( $C$ ) divided by the unwetted perimeter of the headspace ( $L$ ) or the width of the air-water interface divided by the hydraulic radius of the headspace ( $R_{hs}$ ). The two definitions are given as:

$$\text{Shape ratio} = \frac{C}{L} \text{ or } \frac{C}{R_{hs}} \quad [2.1]$$

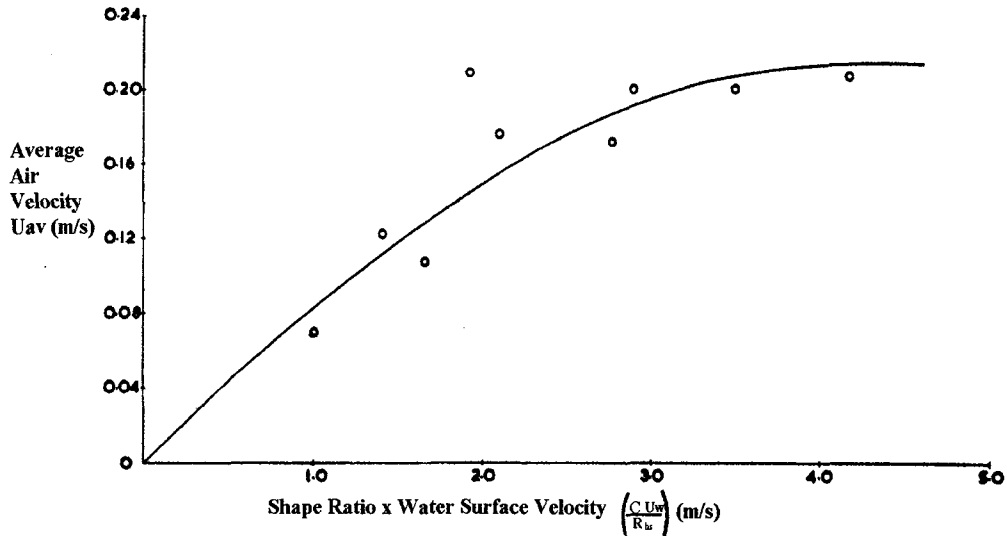
The shape ratios were chosen with the belief that both energy transfer to the headspace and frictional resistance of the pipe wall were important quantities. These two parameters were represented by the air-water interfacial width ( $C$ ) and the unwetted perimeter ( $L$ ), respectively. The mean air velocity was plotted as a function of the product of the water surface velocity and the shape ratio as shown in Figure 2-2. In the figure  $U_{av}$  is the average air velocity and  $U_w$  is the average water surface velocity.

As can be seen from the plots, the average air velocity increases with increasing shape ratio and approaches a limiting value of approximately 0.2 m/s. Clearly the curves are not capable of predicting velocities more than this value and hence can not adequately characterize all possible range of hydraulic flow conditions expected in an in-service sewer. The data collected were too limited to attempt any empirical modeling. Again the curves are difficult to apply in practice. In a related field study Pescod and Price (1978) indicated that their empirical models were not directly applicable to sewer diameters larger than the one used in their

laboratory studies and that predictions could be higher.

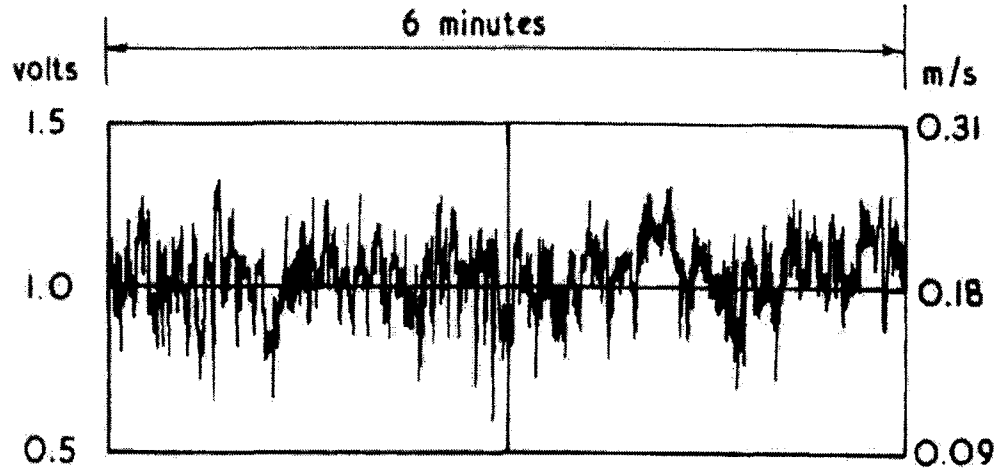


a)

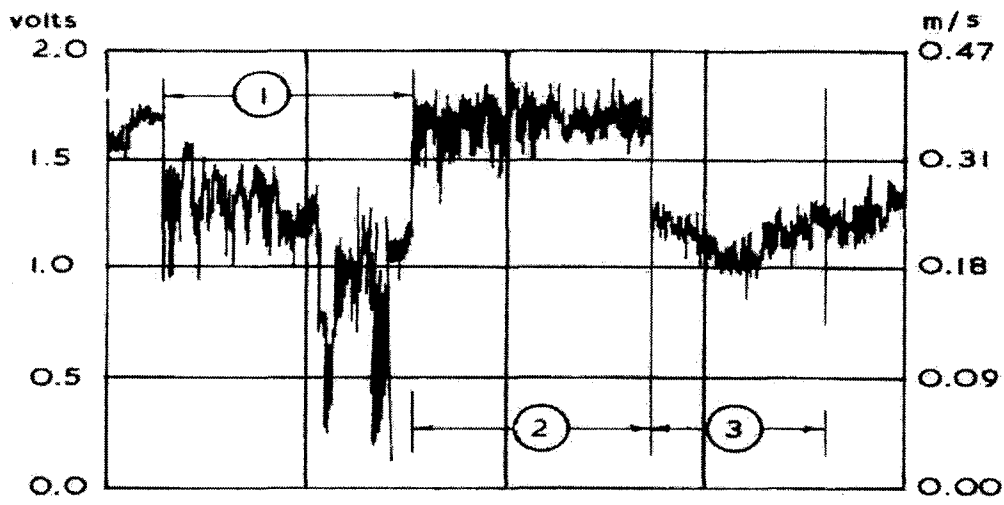


b)

Figure 2-2 (a & b): Empirical curves of Pescod and Price (1978): a) using unwetted perimeter, b) using hydraulic radius



a)



b)

**Figure 2-3 (a & b): Variability of streamwise velocity in the headspace: a) at a specific position, b) across the headspace (Pescod and Price 1978)**

Pescod and Price (1978) further elucidated the variability of the longitudinal air velocity in the sewer headspace as illustrated in Figure 2-3 which clearly indicates some degree of turbulence in the headspace even at the low Reynolds numbers

studied. The upper trace of the figure shows a 6-minute chart record for a specific location and in the lower trace, the variability across the headspace. These figures convey a strong impression that the airspace turbulence is composed of a wide range of scales (whether interpreted in terms of time or distance).

**United States EPA (1994) model:** In response to the limited knowledge-base associated with hazardous air pollutant (HAP) emissions from industrial sewers, the United States Environmental Protection Agency (USEPA 1994) commissioned the development of a model known as COLLECT which estimates emissions from sewer channels. This model is also detailed by Olson (1996). The COLLECT model computes the average air velocity due to wastewater drag using:

$$U_{av} = U_w \frac{C}{L + C} \quad [2.2]$$

This relation is expected to predict higher velocities since no consideration is given to the possibility of interfacial waves and upshots of secondary motions associated with the shape of the headspace. Interestingly this model is the only one currently available for estimating ventilation rates from sewers regardless of whether the flow regime is turbulent or laminar.

**Olson (1996) and Olson et al. (1997) model:** Olson (1996) and Olson et al. (1997) developed a theoretical model using energy concepts to estimate the effect of liquid drag on sewer ventilation as an improvement over the USEPA (1994) model. They identified the two forces acting on the air as the liquid drag (at the

air-water interface) and the shear stress at the pipe wall. These two forces were then quantified using empirical modeling and boundary layer theory. The shear stress from the liquid drag at the air-water interface was quantified as:

$$\tau_i = \frac{1}{2} \rho f_i V_{net}^2 \quad [2.3]$$

where  $\tau_i$  is the interfacial shear stress,  $f_i$  is the interfacial drag coefficient,  $\rho$  is density of air and  $V_{net}$  is the net velocity. The interfacial drag coefficient was derived from the simultaneous solution of Equation [2.4] and an oceanic-resistance model (a modified Charnock-Sinai based model (Sinai 1983) which is based on wind-ocean resistance formulation) given by Equation [2.5]:

$$f_i = 2 \left( \frac{u_a}{U_w} \right)^2 \quad [2.4]$$

$$\frac{U_w}{u_a} = 5.75 \log_{10} \left( \frac{20.1 g R_h L_w}{\eta C u_a^2} \right) \quad [2.5]$$

where  $u_a$  is the interfacial friction velocity,  $g$  is the acceleration due to gravity,  $L_w$  is the water perimeter,  $\eta$  is a dimensionless parameter equal to 0.67 for an air-water system and  $R_h$  is the hydraulic radius of the water section. They used the concept that work is the product of force and velocity, and that force is the product of shear stress and surface area, and arrived that the rate of work at the interface can be written as:

$$\dot{w}_i = \frac{1}{2} \rho f_i (U_w - U_{id})^2 C I U_{id} \quad [2.6]$$

where  $\dot{w}_i$  is the rate of work along the interface and  $U_{id}$  ('ideal' air velocity) is

defined as the average air velocity for a system with zero head loss. They went further to use the concept of turbulent boundary layer to evaluate the wall shear stress as:

$$\tau_w = u_{tw}^2 \rho \quad [2.7a]$$

where  $u_{tw}$  is the wall shear velocity obtained from the full pipe flow as:

$$\frac{u_{tw}}{U_{av}} = \sqrt{\frac{f_w}{8}} \quad [2.7b]$$

where  $f_w$  is the wall friction factor taken as 0.006. In a manner similar to the development of Equation [2.6], the rate of work at the wall was derived from Equation [2.7] as:

$$\dot{w}_w = \rho \frac{f_w}{8} U_{av}^3 L l \quad [2.8]$$

where  $\dot{w}_w$  is the rate of work along the pipe wall and  $l$  is the length of the pipe.

Including the head loss in the system, energy balance was written as:

$$-\frac{1}{2} \rho f_i (U_w - U_{id})^2 C I U_{id} + \rho \frac{f_w}{8} U_{av}^3 L l + \dot{m} g K_l \frac{U_{av}^2}{2g} = 0 \quad [2.9]$$

where  $\dot{m}$  is the mass flow rate and  $K_l$  is a head loss coefficient. The drawback of this approach is that the headspace has to be converted into an equivalent circular pipe and total head loss in the system calculated using full pipe flow coefficient. Again the use of wind-ocean resistance model which is different in character from air-water interface in internal gravity flow may be inappropriate. The relative error of this model is reported to be about 20 % (Olson 1996).

**One-half average wastewater model (½-WWV model):** A very crude approach, presumably based on the premise of a 1-D flow field and linear velocity profile, is also in use (Odor and Corrosion Technology Consultants 1999a). This method simply assumes that the average air velocity is one-half the average wastewater velocity irrespective of the sewer hydraulics. Thus,

$$U_{av} = 0.5V_w \quad [2.10]$$

where  $V_w$  is the average wastewater velocity. Some researchers have introduced safety factors (e.g. Davidson et al. 2004 used a safety factor of 15 %) to this model without any scientific basis. Equation [2.10] does not take into consideration the prevailing flow regime (turbulent or laminar), the water-air surface conditions or the headspace geometry effects.

Clearly, there are inadequacies in the existing models. Any improvement in the flow modeling, therefore, should include more physics, and correct representation of the airspace cross-section and the driving force. Furthermore, the improvement should not be limited to the average streamwise velocity computations, but also offer a thorough understanding of the flow patterns in the sewer headspace. This is especially relevant in corrosion modeling. The present paper therefore introduces CFD models for predicting the air flow field in which the Reynolds-averaged-Navier-Stokes (RANS) equations with incompressible, fully-developed and steady-state assumptions govern the flow field. The Reynolds stresses in the governing equations are computed using an anisotropic turbulence model which takes into account the effect of the sewer headspace geometry to generate



turbulence-driven secondary flows. This consists of two sub-models: a generalized eddy viscosity-mixing length model for the shear stresses and a semi-empirical model for the normal stresses. A finite element solution of the resulting set of parabolic equations is implemented. The effect of wastewater drag is formulated at the air-wastewater interface as in separated flows. To cover all possible flow scenarios, a laminar model is also developed. Calculations from these models are compared with experimental data of Pescod and Price (1978) and the above-mentioned models. Generalized curves and formulae for the average velocities have been developed to be used in practice since it would be too difficult to use the full CFD models.

## **2.2 MATHEMATICAL FORMULATION**

### **2.2.1 Mean Flow Equations**

Figure 2-4 shows a schematic representation of a partially-full, gravity-flow circular sewer conduit, including the co-ordinate system and nomenclature. Here an isolated section of the wastewater collection system without intersecting sewer lines, changes in channel slope, or changes in pipe diameter is assumed thus making the assumption of fully-developed flow ( $\partial(\cdot)/\partial x = 0$ ) strictly valid. A steady state condition (time-invariant,  $\partial(\cdot)/\partial t = 0$ ) is further assumed.

Under the aforementioned assumptions, the Reynolds-averaged-Navier-Stokes equations together with the continuity equation of turbulent incompressible flow

lead to:

$$V \frac{\partial U}{\partial y} + W \frac{\partial U}{\partial z} = g \sin \beta + \nu \left( \frac{\partial^2 U}{\partial y^2} + \frac{\partial^2 U}{\partial z^2} \right) - \left( \frac{\partial \overline{u'v'}}{\partial y} + \frac{\partial \overline{u'w'}}{\partial z} \right) \quad [2.11a]$$

$$V \frac{\partial V}{\partial y} + W \frac{\partial V}{\partial z} = -\frac{1}{\rho} \frac{\partial P}{\partial y} + g \cos \beta + \nu \left( \frac{\partial^2 V}{\partial y^2} + \frac{\partial^2 V}{\partial z^2} \right) - \left( \frac{\partial \overline{v'^2}}{\partial y} + \frac{\partial \overline{w'v'}}{\partial z} \right) \quad [2.11b]$$

$$V \frac{\partial W}{\partial y} + W \frac{\partial W}{\partial z} = -\frac{1}{\rho} \frac{\partial P}{\partial z} + \nu \left( \frac{\partial^2 W}{\partial y^2} + \frac{\partial^2 W}{\partial z^2} \right) - \left( \frac{\partial \overline{v'w'}}{\partial y} + \frac{\partial \overline{w'^2}}{\partial z} \right) \quad [2.11c]$$

$$\frac{\partial V}{\partial y} + \frac{\partial W}{\partial z} = 0 \quad [2.11d]$$

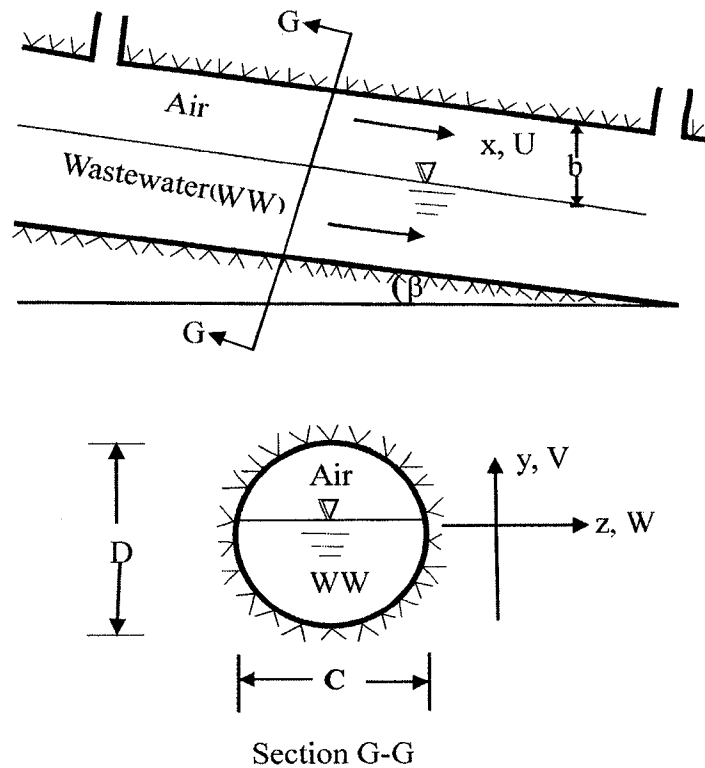


Figure 2-4: A sewer conduit model

where  $P$  is the total pressure, i.e., the sum of pressure resulting from the normal components of the molecular forces and the pressure arising from anisotropy of turbulence,  $\nu$  is the kinematic viscosity of air,  $U$  is the streamwise mean velocity in the  $x$  direction and  $\beta$  is the slope of the sewer pipe.  $u'$ ,  $v'$  and  $w'$  are components of the turbulent velocities in  $x$ ,  $y$  and  $z$  directions, respectively. The velocities  $V$  and  $W$  are secondary mean flow in the plane perpendicular to the primary longitudinal ( $x$ ) direction. These secondary velocities are caused by the anisotropy of the normal Reynolds stress terms  $\overline{v'^2}$  and  $\overline{w'^2}$  (Demuren and Rodi 1984; Gerard 1978; Rodi 1984).

The Reynolds stresses in the mean flow equations have to be modelled. The simplest turbulence models employ the Boussinesq eddy viscosity approximation to compute the Reynolds stresses. For computational simplicity, the eddy viscosity is, in turn, often computed in terms of the mixing length that is analogous to the mean free path of molecules in the kinetic theory of gases. Prandtl's mixing length hypothesis (MLH) is among the simplest turbulence models for modeling the turbulent shear stresses. Unfortunately, Prandtl's MLH does not include any information on the normal stresses. For homogenous turbulence, the normal stresses are usually included in the pressure and they do not have to be calculated. This is not the case here, because the flow in the headspace is not homogeneous. Thus, in addition to specifying the shear stresses, modeling of the turbulent normal stresses is needed. This problem is discussed below.

## 2.2.2 Turbulence Closure

The Reynolds stresses appearing in Equation [2.11(a-c)] are modelled using an anisotropic turbulence closure model which comprises the use of an eddy viscosity concept for the shear stresses and a semi-empirical model for the normal stresses. This approach allows us to compute the turbulence-driven secondary motions owing to the differences in the normal stresses ( $\overline{v^2} - \overline{w^2}$ ).

### 2.2.2.1 Modeling the Reynolds shear stresses

The eddy viscosity concept which is based on the assumption that the Reynolds stresses are a local property of the mean flow and are related to the mean flow gradients via a turbulent viscosity is used. For the flow under consideration this concept may be expressed as:

$$-\overline{u'v'} = \nu_t \frac{\partial U}{\partial y} \quad [2.12a]$$

$$-\overline{u'w'} = \nu_t \frac{\partial U}{\partial z} \quad [2.12b]$$

$$-\overline{v'w'} = \nu_t \left( \frac{\partial W}{\partial y} + \frac{\partial V}{\partial z} \right) \quad [2.12c]$$

where  $\nu_t$  is the eddy viscosity. The introduction of Equation [2.12] alone does not constitute a turbulent model for the shear stresses, but only offers the framework for constructing such a model; the main problem is now shifted to determining the distribution of  $\nu_t$ . There are several ways of determining this distribution (Rodi 1984). In a preliminary study two closure models have been investigated. These are the low Reynolds number  $k - \varepsilon$  model of Lam and Bremhorst (1981), and a

generalized bi-harmonic mixing length model of Robert et al. (1998). Although these models give comparable average longitudinal mean velocities, the mixing length model provides better air velocity patterns in the headspace (in comparison with experimental data of Pescod and Price (1978)). In view of this, the mixing length model has been chosen for this study.

Hence the eddy viscosity is obtained from a generalized mixing length formulation given as (Rodi 1984):

$$v_t = \ell_m^2 \left[ \left( \frac{\partial U_i}{\partial X_j} + \frac{\partial U_j}{\partial X_i} \right) \frac{\partial U_i}{\partial X_j} \right]^{\frac{1}{2}} \quad [2.13]$$

wherein the Einstein summation is used.  $\ell_m$  is the mixing length. Equation [2.13] in a fully-developed 3-D flow is expanded as:

$$v_t = \ell_m^2 \left[ \left( \frac{\partial U}{\partial y} \right)^2 + \left( \frac{\partial U}{\partial z} \right)^2 + 2 \left( \frac{\partial V}{\partial y} \right)^2 + 2 \left( \frac{\partial W}{\partial z} \right)^2 + \left( \frac{\partial V}{\partial z} + \frac{\partial W}{\partial y} \right)^2 \right]^{\frac{1}{2}} \quad [2.14]$$

The mixing length is prescribed using Robert et al. (1998)'s bi-harmonic model given as:

$$\frac{\partial^4 \ell_m}{\partial z^4} + 2 \frac{\partial^4 \ell_m}{\partial z^2 \partial y^2} + \frac{\partial^4 \ell_m}{\partial y^4} = 0 \quad [2.15]$$

with the rigid boundary conditions:

$$\ell_m = 0 \quad [2.16a]$$

$$\frac{\partial \ell_m}{\partial n} = -\kappa \quad [2.16b]$$

where  $n$  is the normal outside the domain on the boundaries and  $\kappa$  is von

Karman's constant. These formulations make the mixing length concept applicable to complex geometries thus removing the bottlenecks associated with Prandtl's original mixing length hypothesis.

### 2.2.2.2 Modeling the Reynolds normal stresses

To calculate the secondary velocities, the distribution of the main driving forces (Reynolds normal stresses) needs to be determined. In order to obtain a visual impression of the circulation due to secondary flows, Gerard (1978) pioneered a semi-empirical approach which enabled the prediction of the secondary flow streamlines. Tominaga et al. (1989) have successfully modified Gerard's approach and verified it experimentally. Tominaga et al. derived a semi-empirical relation for the distribution of  $\sqrt{v'^2}$  and  $\sqrt{w'^2}$  for a two-dimensional closed-channel as:

$$\sqrt{v'^2}(y) = u_\tau \left( A_{vy} e^{-B_{vy} \frac{y}{h}} \right), \quad \sqrt{w'^2}(y) = u_\tau \left( A_{wy} e^{-B_{wy} \frac{y}{h}} \right) \quad [2.17]$$

where  $A_{vy} = 1.45$ ,  $A_{wy} = 1.15$ ,  $B_{wy} = 0.92$ ,  $B_{vy} = 0.69$ ,  $h$  is the depth of the channel and  $u_\tau$  is the boundary shear velocity.

Using a weighted average method, Tominaga et al. extended these semi-empirical formulations to three-dimensions. Czernuszenko and Rylov (2002) have successfully employed a version of Tominaga et al.'s relations for open-channels in modeling a three-dimensional velocity field in open-channel flows. The pattern of secondary flow was accurately simulated. Here the semi-empirical relations of

Tominaga et al. (1989) are adopted for the normal stresses given in this case as:

$$\sqrt{v'^2}(n_i) = u_a (A_{vi} e^{-B_{vi} n_i}), \sqrt{v'^2}(n_w) = u_{tw} (A_{wi} e^{-B_{wi} n_w}) \quad [2.18a]$$

$$\sqrt{w'^2}(n_i) = u_a (A_{wi} e^{-B_{wi} n_i}), \sqrt{w'^2}(n_w) = u_{tw} (A_{wi} e^{-B_{wi} n_w}) \quad [2.18b]$$

where  $A_{wi} = 1.45$ ,  $A_{vi} = 1.15$ ,  $B_{wi} = 0.92$  and  $B_{vi} = 0.69$

The weighted average contribution from the wall and the interface can be expressed as:

$$\sqrt{w'^2} = \left( \sqrt{w'^2}(n_i) \right)^{\Gamma_{n_i}} \left( \sqrt{w'^2}(n_w) \right)^{\Gamma_{n_w}}, \sqrt{v'^2} = \left( \sqrt{v'^2}(n_i) \right)^{\Gamma_{n_i}} \left( \sqrt{v'^2}(n_w) \right)^{\Gamma_{n_w}} \quad [2.19]$$

where  $\Gamma_{n_i} = \frac{n_w}{n_w + n_i}$ ,  $\Gamma_{n_w} = \frac{n_i}{n_w + n_i}$ ,  $n_i$  and  $n_w$  are dimensionless normal distances from the interface and the wall, respectively.

## 2.3 COMPUTATIONAL APPROACH

The air flow in the sewer atmosphere could be laminar or turbulent contingent upon the magnitude of the driving force. Pescod and Price (1978), and Olson (1996) reported low Reynolds number flow regimes in their studies. It has been reported that the friction between the wastewater and air can be increased through steep slopes or wastewater velocities in excess of 1.5 m/s (Odor and Corrosion Technology Consultants 1999b). Given this added impact of increased friction the volume of moving air can be quite large and turbulent. Consequently any modeling technique should take these regimes into consideration. Discussed below are the boundary conditions and the numerical solution methods for the two

regimes of interest.

### 2.3.1 Boundary Conditions

Boundary conditions are required at both the stationary wall and the interface. The only resistance to the air movement in the sewer pipe is friction between the air and the stationary wall of the sewer. Given this set of simple boundary conditions, it is possible to generate the air flow field for the air movement in the sewer airspace. In the present study the integration of the flow equations is carried out to the wall which makes the no-slip condition applicable. This means that the velocities tangential and normal to the stationary wall are zero. The use of the no-slip condition calls for a modification of the mixing length boundary condition (Equation [2.16b]). This is realized by applying the Van Driest damping function (Wilcox 2000) to bridge the fully turbulent zones away from the wall and the near-wall regions where viscosity effects are substantial such that:

$$\frac{\partial \ell_m}{\partial n} = -\kappa [1 - (1 + S(n)) \text{Exp}(S(n))] \quad [2.20]$$

where  $S(n) = -nu_\tau / vA$  and  $A = \text{empirical constant} = 26$ .

Throughout this paper, it is assumed that there is negligible momentum transfer from the air to the underlying wastewater. This assumption is adequate since the air motion is caused by the air being dragged along by the wastewater (i.e. without the wastewater there is no air flow). The air-water interface is hence modelled as a rigid-moving lid as in Couette-flows. Practically, the interface may



not be sharp and could contain a mixture of air and water with concomitant generation of waves and ‘whitecaps’. Consequently the interface should be treated with caution if detailed features are required. Four possible cases for prescribing the interfacial boundary for the longitudinal mean velocity are proposed as follows:

$$U = U_w : \text{Smooth interface} \quad [2.21]$$

$$U = U_{ws} : \text{Rippled interface (small amplitude and well-organized waves)} \quad [2.22]$$

$$\frac{U - U_{ws}}{u_a} = -\frac{1}{\kappa} \ln(9y^+) : \text{Rippled interface (large amplitude and well-organized waves)} \quad [2.23]$$

$$\frac{U - U_{ws}}{u_a} = -\frac{1}{\kappa} \ln\left(\frac{9y^+}{(1 + 0.3k_s^+)}\right) : \text{Fully rough interface (a precursor to a transition to slug flow)} \quad [2.24]$$

where  $U_{wc}$  is the water surface velocity at center of pipe,  $U_{ws}$  is the surface velocity distribution (Equation [2.25]),  $k^+ = u_a k_s / \nu$ ,  $y^+ = u_a n_i / \nu$ , and  $k_s$  is the effective interfacial boundary roughness height. The application of the fully rough interface regime requires knowledge of the interfacial boundary roughness parameter,  $k_s$ . This regime is likely to occur in very steep slopes and is therefore not considered further. Following Nordsveen and Bertelsen (1996), a relation between the water surface velocity at channel center  $U_{wc}$  and velocity distribution at the interface  $U_{ws}$  is obtained as:

$$U_{ws}(z) = U_{wc} \left( \frac{C - 2|z|}{C} \right)^{1/4} \quad [2.25]$$

where  $C$  is the width of the interface. In modeling the laminar flow, it is assumed that the air-water interface is devoid of interfacial waves and therefore the assumptions of smooth interfacial boundary and constant interfacial drag are satisfactory. In this paper Equation [2.22] together with Equation [2.25] is used as a boundary condition for all simulated turbulent flows. This boundary condition is justified since we are dealing with large diameter pipes (Vlachos et al. 1999). Secondary velocities are assigned zero at the interface.

### 2.3.2 Numerical Solution

For computational reasons, all variables are non-dimensionalized as:

$$X_* = x/b, Y_* = y/b, Z_* = z/b, U_* = U/U_{wc}, V_* = V/U_{wc}, W_* = W/U_{wc},$$

$$\overline{v_*'^2} = \overline{v'^2}/U_{wc}^2, \overline{w_*'^2} = \overline{w'^2}/U_{wc}^2, \text{ and } g_* = gb/U_{wc}^2, \text{ where the length scale } b$$

is the maximum headspace depth and  $U_{wc}$  is the velocity scaling parameter in turbulent flow case. The Reynolds number then becomes  $Re_c = U_{wc}b/\nu$  in the turbulent flow case. Using the turbulent closure models introduced above, the system of equations to solve, in dimensionless forms, becomes:

$$V_* \frac{\partial U_*}{\partial Y_*} + W_* \frac{\partial U_*}{\partial Z_*} - \frac{\partial}{\partial Y_*} \left[ (1/Re_c + \nu_{t*}) \frac{\partial U_*}{\partial Y_*} \right] - \frac{\partial}{\partial Z_*} \left[ (1/Re_c + \nu_{t*}) \frac{\partial U_*}{\partial Z_*} \right] = g_* \sin \beta \quad [2.26a]$$

$$V_* \frac{\partial V_*}{\partial Y_*} + W_* \frac{\partial V_*}{\partial Z_*} - \frac{1}{Re_c} \left[ \frac{\partial^2 V_*}{\partial Y_*^2} + \frac{\partial^2 V_*}{\partial Z_*^2} \right] = g_* \cos \beta - \frac{\partial P_*}{\partial Y_*} - \frac{\partial \overline{v_*'^2}}{\partial Y_*} + \frac{\partial}{\partial Z_*} \left[ \nu_{t*} \left( \frac{\partial V_*}{\partial Z_*} + \frac{\partial W_*}{\partial Y_*} \right) \right] \quad [2.26b]$$

$$V_* \frac{\partial W_*}{\partial Y_*} + W_* \frac{\partial W_*}{\partial Z_*} - \frac{1}{Re_c} \left[ \frac{\partial^2 W_*}{\partial Y_*^2} + \frac{\partial^2 W_*}{\partial Z_*^2} \right] = -\frac{\partial P_*}{\partial Z_*} - \frac{\partial \overline{w_*'^2}}{\partial Z_*} + \frac{\partial}{\partial Y_*} \left[ \nu_{t*} \left( \frac{\partial V_*}{\partial Z_*} + \frac{\partial W_*}{\partial Y_*} \right) \right] \quad [2.26c]$$

$$\frac{\partial V_*}{\partial Y_*} + \frac{\partial W_*}{\partial Z_*} = 0 \quad [2.26d]$$

$$v_{i*} = \ell_m^2 \left[ \left( \frac{\partial U_*}{\partial Y_*} \right)^2 + \left( \frac{\partial U_*}{\partial Z_*} \right)^2 + 2 \left( \frac{\partial V_*}{\partial Y_*} \right)^2 + 2 \left( \frac{\partial W_*}{\partial Z_*} \right)^2 + \left( \frac{\partial V_*}{\partial Z_*} + \frac{\partial W_*}{\partial Y_*} \right)^2 \right]^{\frac{1}{2}} \quad [2.27]$$

In laminar flow, the flow field has only one component velocity  $U_*(Y_*, Z_*)$  and the remaining governing equation simply reduces to:

$$-\frac{\partial}{\partial Y_*} \left[ (1/\text{Re}_w) \frac{\partial U_*}{\partial Y_*} \right] - \frac{\partial}{\partial Z_*} \left[ (1/\text{Re}_w) \frac{\partial U_*}{\partial Z_*} \right] = g_* \sin \beta \quad [2.28]$$

Here,  $U_w$  is used as the velocity scaling parameter and the Reynolds number of the flow becomes  $\text{Re}_w = U_w b / \nu$ . The upper limit of the laminar flow regime is set at a Reynolds number of 1,500 based on a plane Couette-flow of moving wall velocity  $U_w$  and depth of flow  $b$  (Wilcox 2000).

A finite element method (FEM) based on FEMLAB programming language which stores data structures in MATLAB (FEMLAB 2002) has been implemented to solve the above equations (See Appendix A for the description of the FEM). The method involves geometric modeling (using rational Bezier patches and curves), generation of unstructured meshes using an automatic mesh generator (created using Delaunay triangulation algorithm in MATLAB), numerical integration of the equations and boundary conditions in Galerkin framework, and post processing using MATLAB commands. All variables are discretized with quadratic Lagrange elements.

In the laminar flow modeling, the linearized matrix resulting from the spatial discretization is solved using the Gaussian elimination method. We have a system of coupled parabolic equations in  $U_*$ ,  $V_*$ ,  $W_*$  and  $P_*$  in the turbulent flow case. Due to the non-linear nature of these equations the solution is achieved via a combination of a parametric sweeping algorithm (with the Reynolds number,  $Re_c$ , as a sweeping parameter) and a Good Broyden iterative (GBIT) procedure with an exact (analytical) evaluation of the Jacobian derivatives. In this way the solution of a low Reynolds number flow is subsequently used as an initial guess for the next iteration step. This method leads to a fast and efficient convergence. To improve the efficiency of the iterative solver in relation to coping with any bad condition number, an Incomplete LU factorization preconditioner is used. The convergence of the solution to the next iterative step within a given parametric sweep is assessed using the solution error criterion formulation of Deuffhand et al. (1990) given as:

$$\frac{\sqrt{\sigma_{k+1}}}{\|\Phi_{k+1}\|} \leq \text{'tolerance'} \quad [2.29]$$

where  $\|\Phi_{k+1}\|$  is the norm of vector of unknowns at  $k+1$  iterative step and the numerator is simply the norm of the preconditioned residual of the iterate  $\Phi_{k+1}$ .

A tolerance of  $10^{-6}$  has been used in this convergence criterion. The equation for mixing length is first decomposed into Laplace and Poisson PDEs and combined with the momentum and continuity equations using a multiphysics method in FEMLAB.

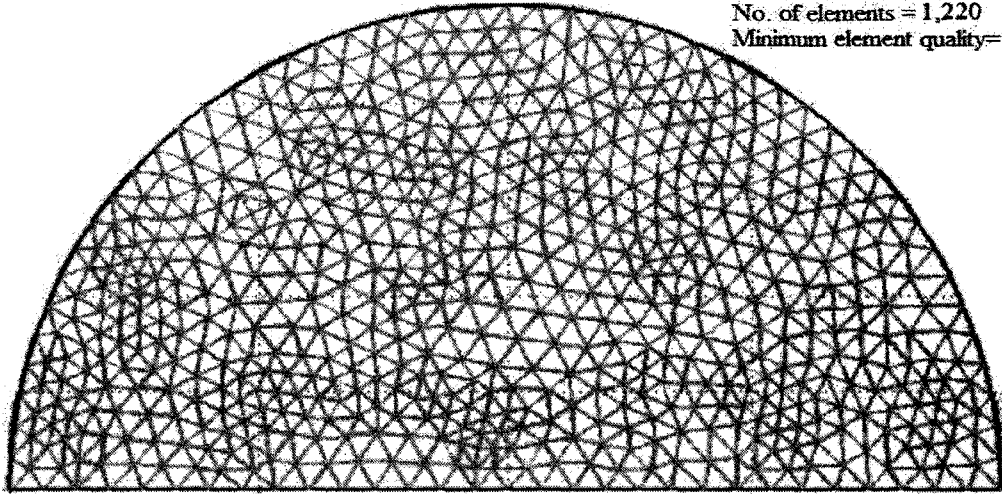
Examples of grids used in both laminar and turbulent simulations are illustrated in Figure 2-5 in which mesh statistics are also indicated. Due to the sharp velocity gradient expected in the viscous sublayer, more nodes are placed close to the boundaries for the turbulent case (Figure 2-5(b)). This is done using selective refinement, where the triangles near the boundaries are further divided into four triangles of the same shape, but ensuring that the triangle quality (Equation [2.30]) is at least 0.7 for all triangles in order to decrease the number of iterations. The triangular quality has been assessed using the formula (FEMLAB 2002):

$$q = \frac{4\sqrt{3}a}{h_1^2 + h_2^2 + h_3^2} \quad [2.30]$$

where  $a$  is the area and  $h_1$ ,  $h_2$ , and  $h_3$  the side length of the triangle.  $q$  is a number between 0 and 1. If  $q > 0.6$  the triangle is of acceptable quality. To ensure that the solution outputs are mesh-independent, the differences in the cross-sectional average velocity in a sequence of successively refined meshes are compared with a preset tolerance. A tolerance of  $10^{-6}$  has been used here.

**Mesh Statistics**

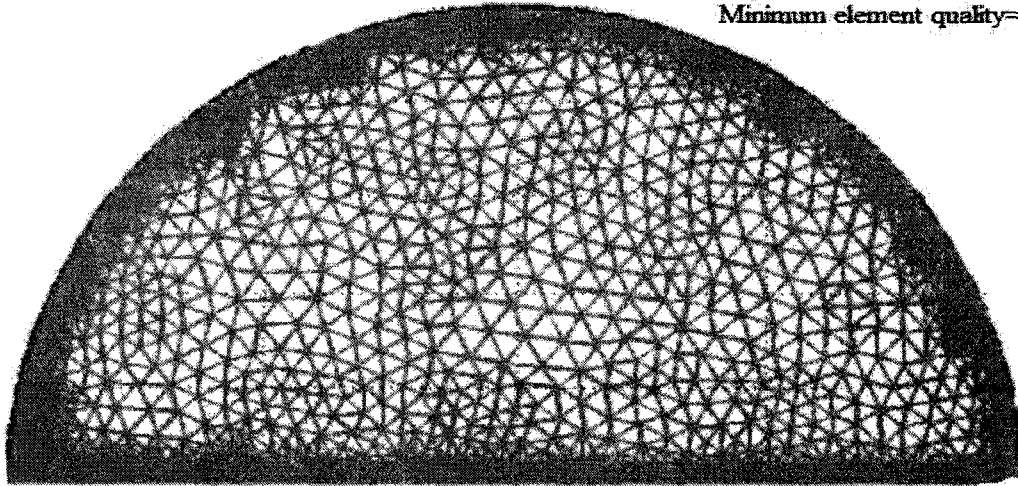
No. of nodes= 650  
No. of boundary elements=78  
No. of elements = 1,220  
Minimum element quality= 0.78



a)

**Mesh Statistics**

No. of nodes= 5,177  
No. of boundary elements= 535  
No. of elements = 9,817  
Minimum element quality= 0.78



b)

**Figure 2-5(a & b): Examples of finite element meshes: a) laminar,  
b) turbulent**

## 2.4 VALIDATION AND SIMULATIONS

Validation of the finite element model is implemented by comparing modeling results with other solution techniques and experimental data reported in the literature. Comparisons with the existing sewer ventilation models are also made.

In preliminary test computations, the laminar formulation (Equation [2.28]) has been solved using analytical, finite difference and finite element methods. The first two methods have been used with the primary aim of checking the predictive capability of the finite element discretization scheme, which is the core numerical tool in this paper. In the analytical method, the airspace cross-section is approximately transformed into half-elliptic shape facilitating the use of elliptic orthogonal and conformal curvilinear co-ordinates. The resulting equation is subsequently solved using the method of eigenfunction expansion. The finite difference approach uses the generalized co-ordinate system and employs the transfinite algebraic grid generation technique to transform the governing equation and the flow geometry into a body-fitted unit-square co-ordinate system that allows co-incidence of all boundary lines with a co-ordinate line. The discretization is then evaluated using central difference formulae. Satisfactory agreements have been obtained between the finite element scheme and the other two methods (shown in Appendix A). Both the analytical and finite difference methods are detailed in Appendix A. The preference of the finite element method to the other computational techniques stems from its capability to handle complex flow geometries, consistency and generality.

Experimental data for validation are scanty in this research area. Arguably the only detailed data available as of now in the literature are those of Pescod and Price (1978). These experiments were conducted in a 15 m long 300 mm diameter UPVC open-ended laboratory sewer pipe. Velocity measurements using a portable anemometer consisting of a thermister sensing device (air velocity meter, AVM) were taken at several locations over the headspace cross-section in order to develop isovels for each experiment. It is unclear at what channel slopes these measurements were taken. However, based on uniform flow conditions, the channel slope can be computed using the Manning's formula  $S_0 = \left( V_w n / R_h^{2/3} \right)^2$ , where  $S_0 \approx \sin \beta$ . Here  $n$  is the Manning coefficient taken as 0.009 for smooth UPVC pipe. Hydraulic parameters of the selected experiments are shown in Table 2-1 below.

The proposed models are validated by simulating three selected experimental data (Test 7, Test 8 and Test 9) of Pescod and Price (1978) which seemingly exhibit fully-developed flow characteristics and are less influenced by environmental factors in the laboratory during the time of the experiment (as pointed out in the original reference).

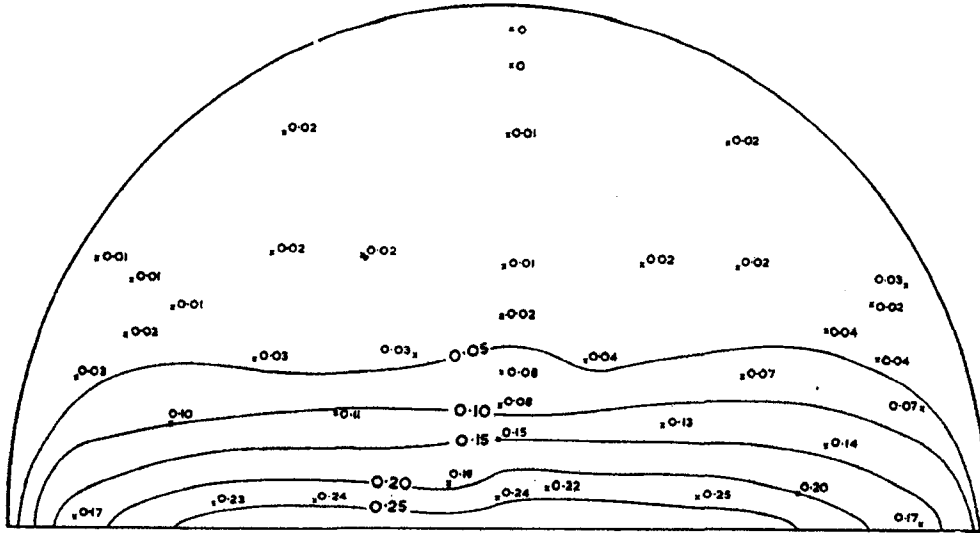


**Table 2-1: Comparing existing and developed models with experiments of Pescod and Price (1978)**

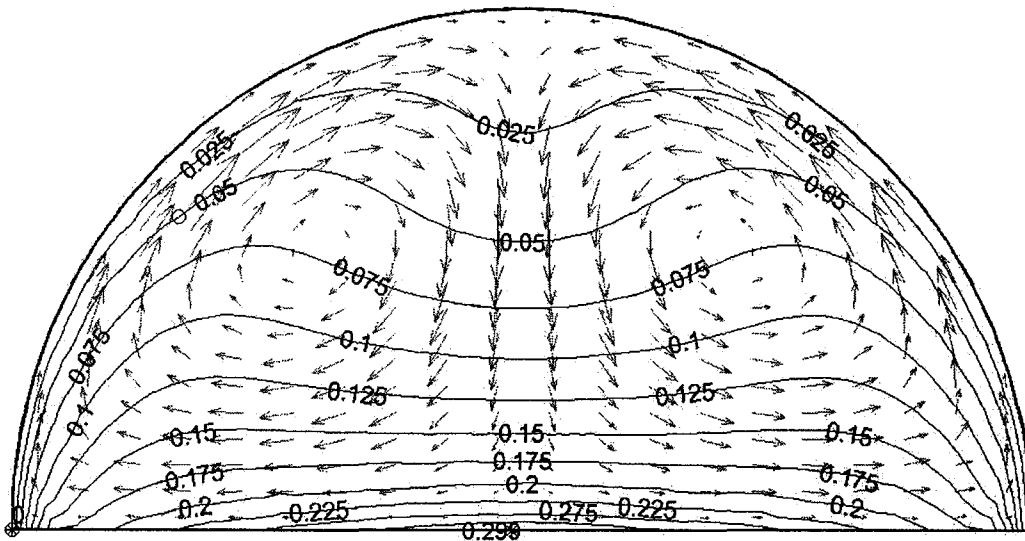
<b>Hydraulic parameters</b>					<b>Cross-sectional average velocity, <math>U_{av}</math>, (m/s)</b>					
Test No.	b/D	$V_w$ (m/s)	$U_w$ (m/s)	$U_{wc}$ (m/s)	Expe- riment	USEPA model	$\frac{1}{2}$ - WWV model	Olson & Olson et al.*	Present models <sup>+</sup>	
									Turbu- lent	Lam- inar
7	0.500	0.200	0.250	0.300	0.070	0.097	0.100	0.135	0.081	0.101
8	0.600	0.800	0.960	0.650	0.200	0.342	0.400	0.356	0.272	0.360
9	0.620	0.400	0.490	0.600	0.110	0.171	0.200	0.173	0.149	0.181

\*open-ended and smooth pipe assumption. + gravity term included.

Figures 2-6 to 2-8 compare simulated axial velocity contours with the selected experiments, where the isovel lines are in m/s. Also displayed on the simulated velocity contours are the corresponding computed secondary flow vectors. Figure 2-9 also shows the comparison between experimental and computed velocity profiles for the same experiments. Data in Figure 2-9 refers to the middle of the channel cross-section.



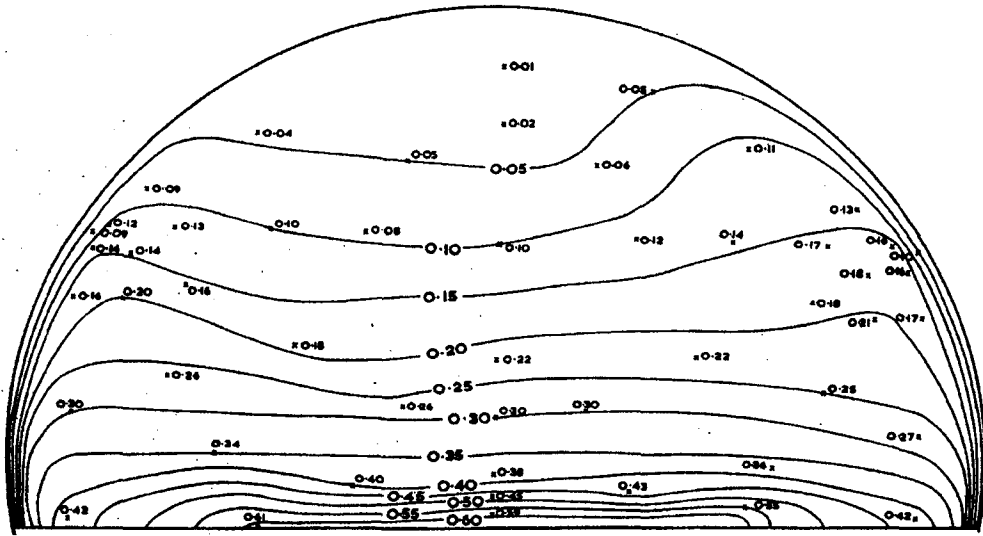
a)



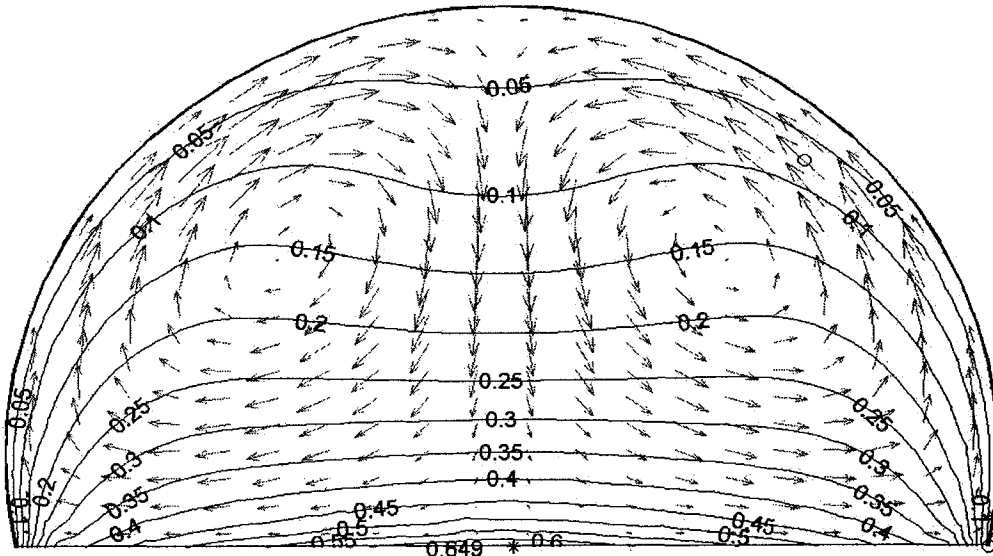
b)

**Figure 2-6(a & b): Comparing contour plot of mean primary velocity for**

**Test no. 7,  $Re_c = 3,000$  : a) experiment, b) simulated**

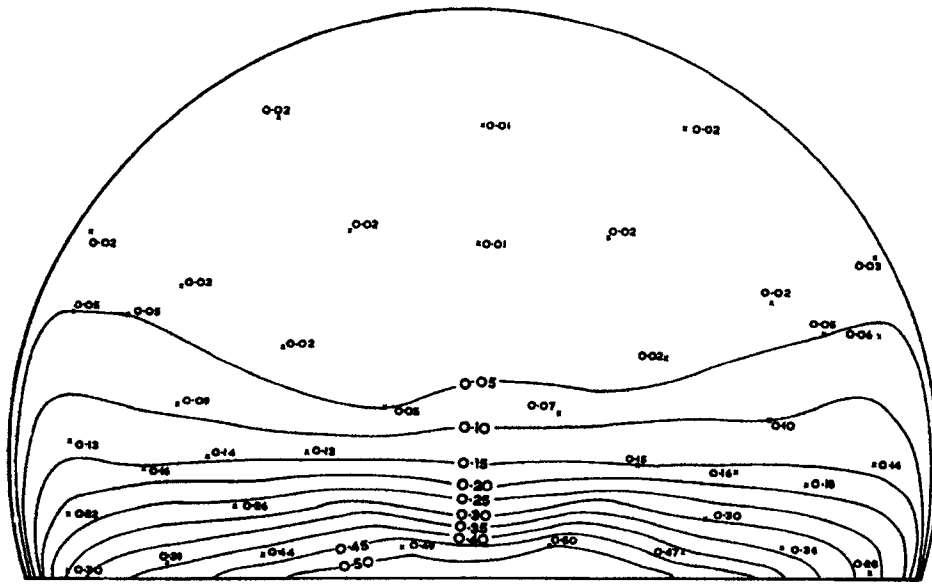


a)

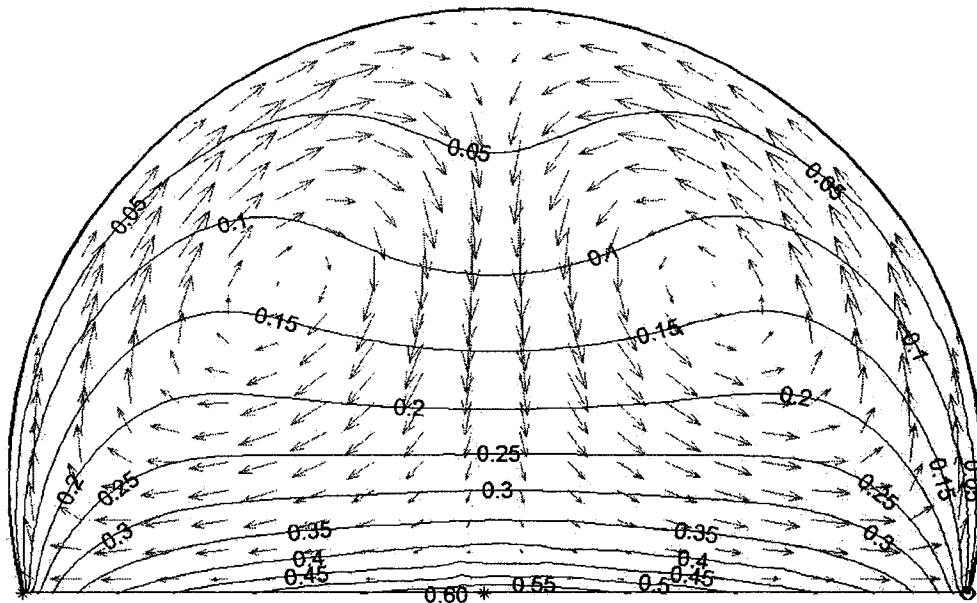


b)

**Figure 2-7(a & b): Comparing contour plot of mean primary velocity for  
Test no. 8,  $Re_c = 7,800$  : a) experiment, b) simulated**

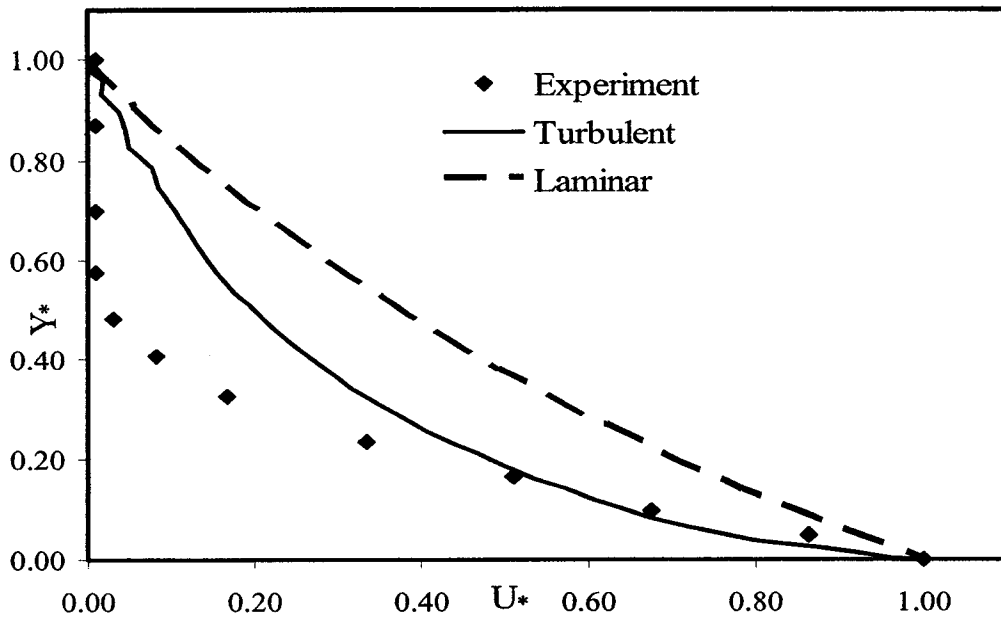


a)

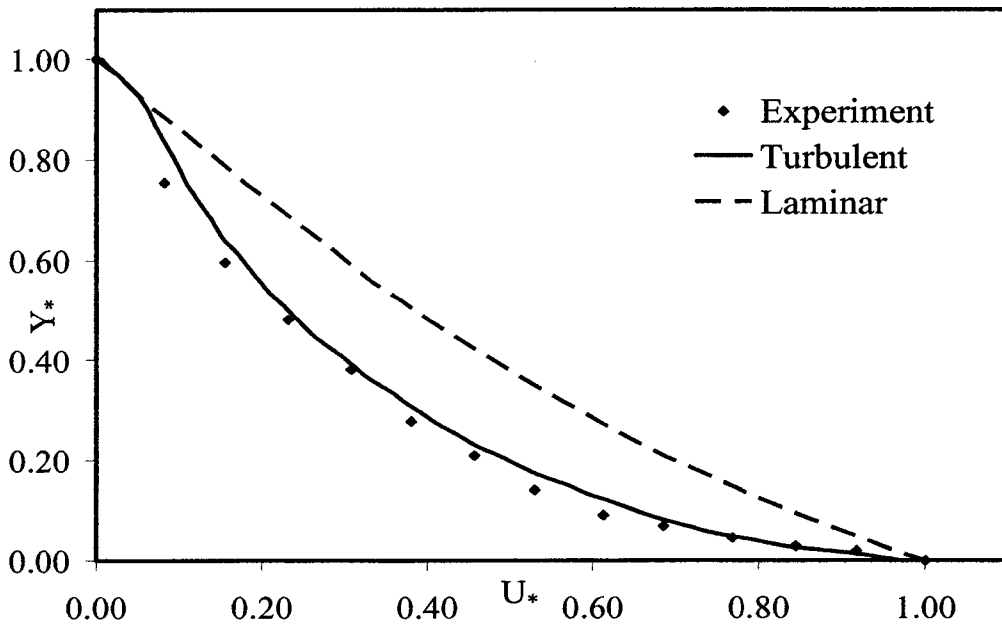


b)

**Figure 2-8(a & b): Comparing contour plot of mean primary velocity for Test no. 9,  $Re_c = 7,440$  : a) experiment, b) simulated**



a)



b)

Figure 2-9(a, b & c): Longitudinal velocity profiles at headspace center: a)

Test No. 7, b) Test No. 8, c) Test No. 9

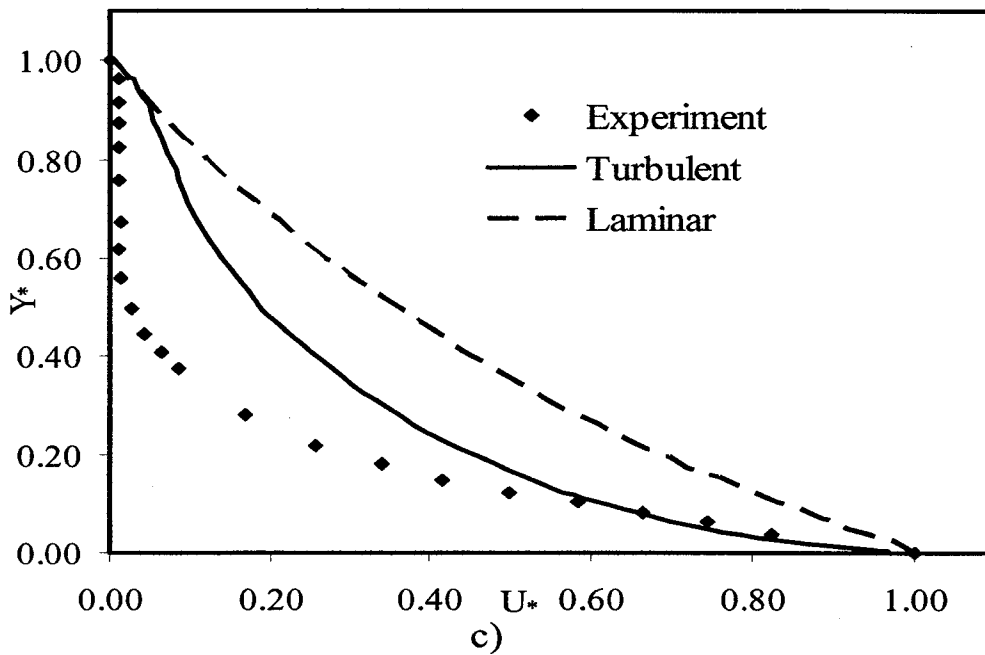


**Figure 2-9(Continued): Longitudinal velocity profiles at headspace center: a) Test No. 7, b) Test No. 8, c) Test No. 9**

The analysis of the velocity profiles and isovels shows overall good accordance between the turbulent model and experimental data. The flow pattern is well predicted. Over prediction of the mean velocity profile in the top-half of the headspace for Test 9 and Test 7 is however acknowledged. Experimental data in Test 9 and Test 7 suggest almost zero velocity profiles for  $y/b (Y^*) > 0.55$  which is not simulated by the numerical model. The apparent discrepancies might be due to a number of factors. Three reasons are advanced here.

- The first reason could be that either the numerical model underpredicts the secondary flows or there is an additional secondary flow in the data other than that due to turbulence anisotropy.

- A second reason could be that there was an adverse pressure gradient counteracting the forward moving wastewater-induced flow during the time of the experiments (See Chapter 4). Under such circumstance the top part of the headspace is likely to have negative velocities that the measuring device ignored and registered as zero.
- A question also arises as to whether fully-developed flow conditions were attained during these experiments. For fully-developed flow to occur in non-circular ducts, the measurement section (entrance length) should be 50 times the headspace depth or longer because the secondary motion may take longer to reach a developed state (Demuren and Rodi 1984). Pescod and Price (1978) only indicated that measurements were taken slightly downstream of the centre of the length which is about 7.5 m from the inlet. This does not satisfy the entrance length requirement for full flow development to occur.

Also superimposed on Figure 2-9 is the laminar model simulation. It is observed that even at the channel center the laminar velocity profile is not linear and that the lateral boundary to some extent influences the flow field. It is evident in the velocity contours (Figures 2-6 to 2-8) that the primary mean velocity near the central region of the channel is advected towards the interface and the wall by the secondary currents. The pattern of air isovels, as evident in the plots, underscores the importance of the inclusion of the secondary velocities in the turbulent flow calculations. This is particularly relevant in sewer corrosion studies and emission

modeling (using mass transfer techniques) where not only the mean bulk velocity is needed, but also the air flow patterns. The transfer of heat to the sewer wall and the spreading of VOCs/odour within the sewer headspace are expected to be influenced significantly by the secondary motions. In the plots (Figures 2-6b to 2-8b) a single secondary flow cell on either side of the channel quadrant is observed. The secondary flow pattern calculated here is in good agreement with that of Hoohlo (1994) who numerically simulated secondary currents in water pipe flowing partly full using an anisotropic non-linear  $k-\varepsilon$  model for the turbulent Reynolds stresses. The pattern of the secondary flow simulated is found to be independent of Reynolds number as evident in Figures 2-6b to 2-8b. The cross-sectional average secondary velocity on the other hand is noted to depend on the relative depth  $b/D$ . This latter observation is depicted in Figure 2-10 in which the cross-sectional average secondary velocity is non-dimensionalized with the water surface velocity. In the figure, the secondary velocity,  $VW_{sec}$  is obtained from its two components  $V$ ,  $W$  .i.e.  $VW_{sec} = \sqrt{V^2 + W^2}$ . The computed average mean secondary velocity is within 1-3 % of the water surface velocity. The plot observed here shows that the strength of the average secondary velocity (non-dimensionalized with the water surface velocity) generally stays somewhat constant in the range  $0.30 \leq b/D \leq 0.65$ . On one hand, the variation of the average secondary velocity non-dimensionalized with the average streamwise velocity ( $VW_{sec(av)}/U_{av}$ ) with relative depth ( $b/D$ ) is found not to follow any definite pattern. The relationship is found to be spurious (not shown here), but the average secondary velocities are within 5-8 % of the average streamwise velocity.



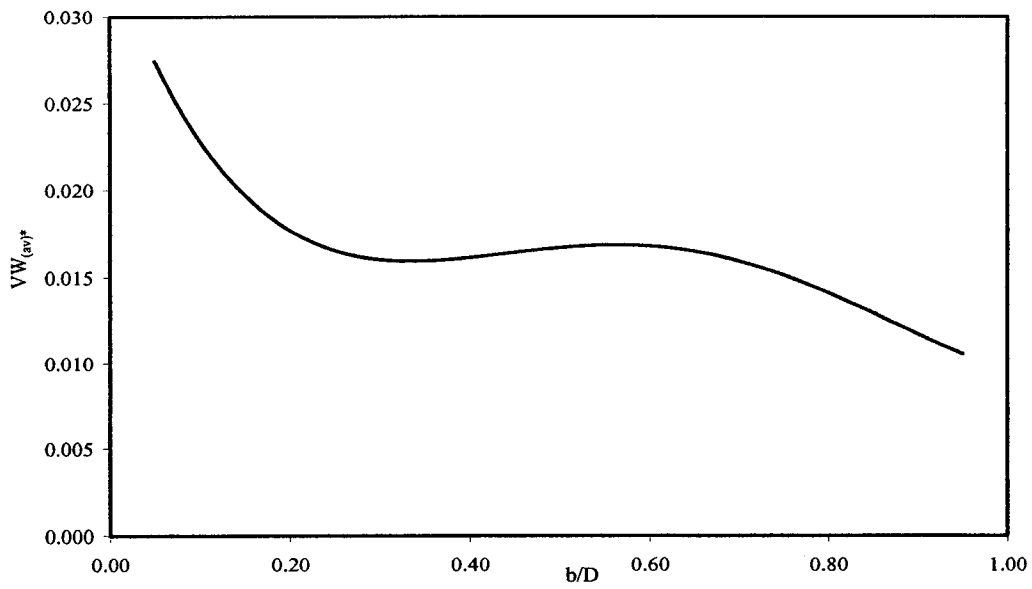


**Figure 2-10: Variation of simulated average mean secondary flow velocity with relative depth (b/D)**

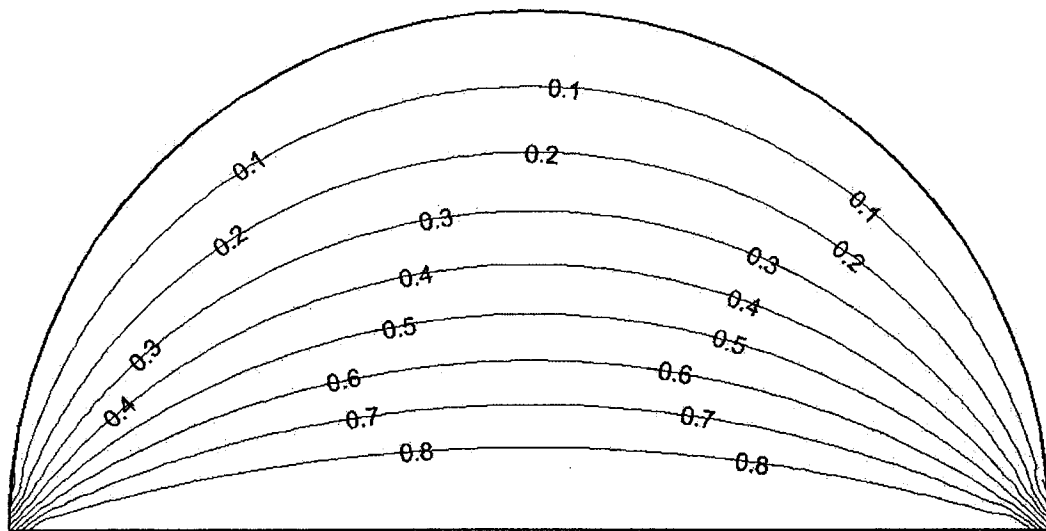


**Figure 2-11: Typical non-dimensionalized velocity ( $U/U_w$ ) contour distribution for  $b/D= 50\%$  in laminar flow regime**

A typical computed non-dimensionalized velocity contour in the laminar regime is shown in Figure 2-11 for  $b/D = 50\%$ . Unlike turbulent flow, the laminar isovels approximately follow the shape of the sewer wall further away from the interface.

Comparisons of cross-sectional average velocity computed from the present models, the one-half wastewater velocity model ( $1/2$ -WWV model), Olson and Olson et al.'s model, and the USEPA model are made with the experiments of Pescod and Price as shown in Table 2-1. As can be seen from the Table, all the models over predict the measured average air velocity. High predictions from Olson and Olson et al.'s model are possibly due to the interfacial drag coefficient expression used in their model. It must be mentioned here that the physical processes at the interface of a horizontal stratified air-water flow (where each fluid flows under its own driving force in addition to the interfacial shear) are quite different from those in air-wastewater flow in sewers where the only force driving the air in this case is that of the wastewater drag. Their model which is in a form of a non-linear algebraic expression (combination of Equations [2.4],[2.5], [2.9]) has been solved using a non-linear solver in MATLAB.

Given the importance of the USEPA model in the current practice of estimating ventilation rates, the simulated data obtained from the proposed models are expressed in the same form of this model given by Equations [2.31] and [2.32]:

$$U_{av}/U_w = 1.028 \frac{C}{(L+C)}, R^2 = 0.993 \quad (\text{Simulated laminar}) \quad [2.31]$$

$$U_{av}/U_{wc} = 0.856 \frac{C}{(L+C)}, R^2 = 0.994 \quad (\text{Simulated turbulent}) \quad [2.32]$$

where  $R$  is the coefficient of determination. Thirty simulated points have been used in fitting these relations.

The turbulent relation (Equation [2.32]) requires the center water surface velocity,  $U_{wc}$ , as an input. To make any meaningful comparisons, it would be therefore appropriate to find a relationship between  $U_{wc}$  and  $U_w$ . This of course would require experimental data. For example using experimental data of Pescod and Price (1978) a relation between these velocities has been established as  $U_{wc} = 1.033U_w$ . Additionally, using Replogle and Chow (1966)'s Pitot tube water velocity data in circular channels, we also establish that  $U_{wc} = 1.072U_w$ . Clearly, the two relations do not differ appreciably. These relations are only provided as a guide and should not be accepted as a general norm. Such relationship should be established for a given sewer system where appropriate. Equation [2.32] is therefore modified using above substitutions to:

$$U_{av}/U_w = 0.885 \frac{C}{(L+C)} \quad (\text{Using Pescod and Price (1978)'s data}) \quad [2.33]$$

$$U_{av}/U_w = 0.918 \frac{C}{(L+C)} \quad (\text{Using Replogle and Chow (1966)'s data}) \quad [2.34]$$

These equations are plotted together with the simulated data in Figure 2-12. Also shown in the same figure is the USEPA model.

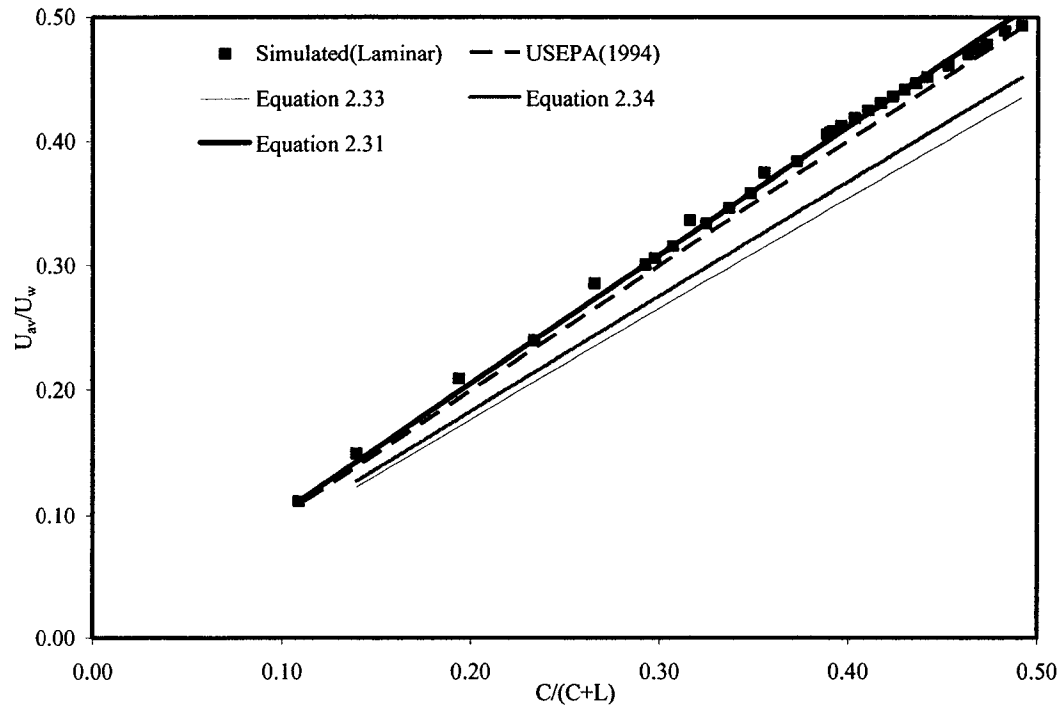


**Figure 2-12: Non-dimensionalized average longitudinal velocity ( $U_{av}/U_w$ ) plotted as a function of headspace perimetric shape factor; Also compared is the USEPA (1994) model**

In Figure 2-13, average velocity curves for different wastewater levels (in terms of relative depth) for laminar, and Equations [2.33] and [2.34] for the turbulent regimes are presented. The figure clearly shows that the average streamwise velocity is less than half the water surface velocity irrespective of the wastewater level or the flow regime. The simulations from the present models suggest that the USEPA model is more accurate for laminar than turbulent. The difference in estimated average velocity between the USEPA model and the proposed laminar model is about 5 %. It however overestimates the average streamwise turbulent velocity computed from the modified turbulent models. At this juncture, the exact

accuracy of the USEPA model with respect to the turbulent models can only be assessed only if the exact relationship between  $U_{wc}$  and  $U_w$  is fittingly established.

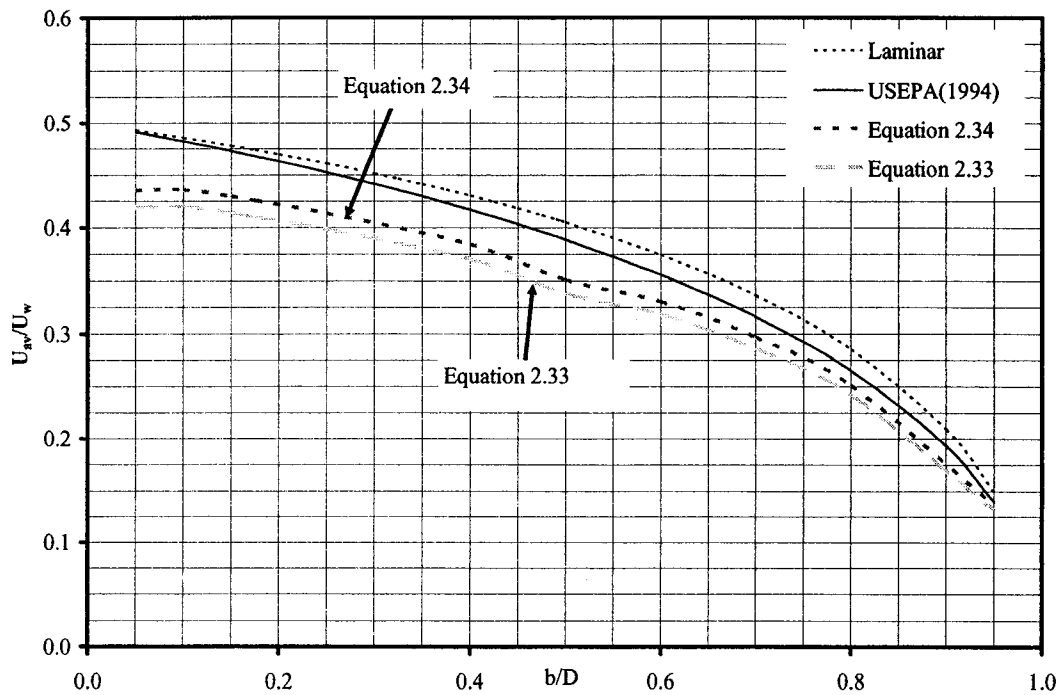


**Figure 2-13: Non-dimensionalized average longitudinal velocity curves ( $U_{av}/U_w$ ) as a function of the relative depth ( $b/D$ ); Also compared is the USEPA (1994) model**

To further make comparison of the present models to that of the  $\frac{1}{2}$ -WWV model, we again use the Replogle and Chow (1966)'s water velocity data to establish a relation between  $U_w$  and  $V_w$ . Based on their data, we find that  $U_w = 1.12V_w$ .

Figure 2-14 compares these models based on this relation. In general, the  $\frac{1}{2}$ -

WWV model over predicts the mean velocity in turbulent flow regime at all relative depths.

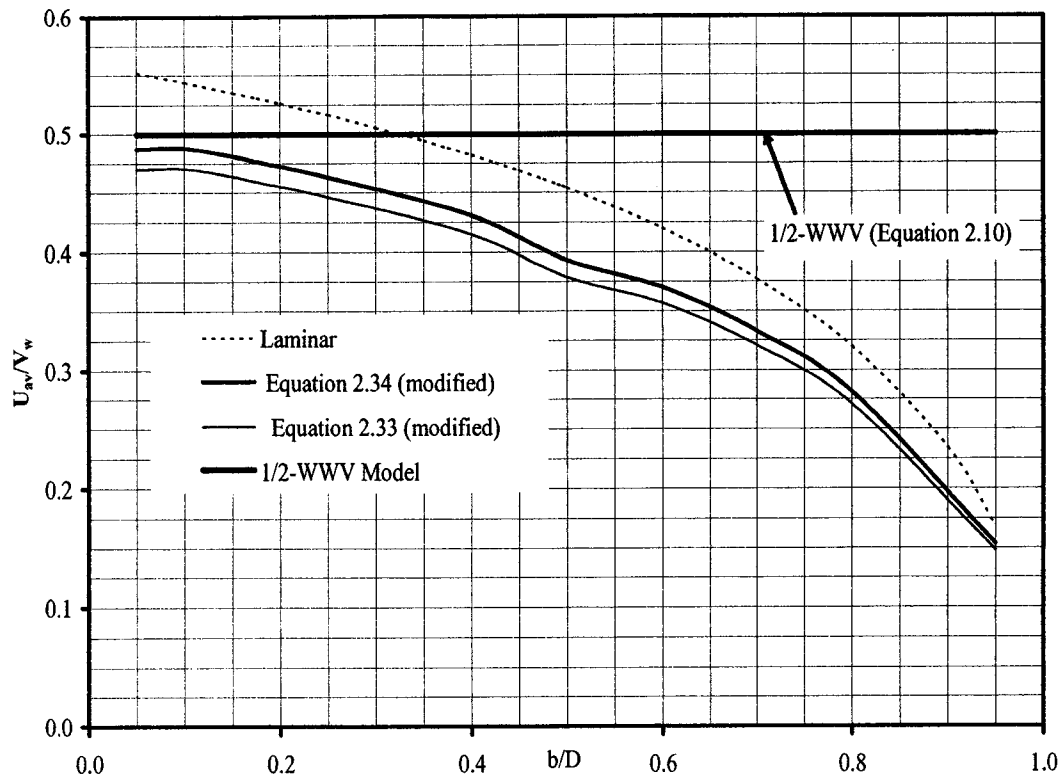


**Figure 2-14: Non-dimensionalized average longitudinal velocity curves ( $U_{av}/V_w$ ) as a function of the relative depth ( $b/D$ ); Also compared is the  $\frac{1}{2}$ -WWV model**

Overall, it is demonstrated that the present models are quite useful in obtaining detailed flow field information. In particular, it is valuable in understanding the flow feature changes due to changes in wastewater level and velocity.

## 2.5 CONCLUSIONS

Models that can be used to assess the magnitude and nature of sewage drag effect in transporting air along sewers have been presented. The effect of the interfacial drag due to the wastewater is conceptually viewed as a Couette-flow. The outputs from these models are essential for the implementation of any efficient odour and corrosion control technology in both turbulent and laminar flow regimes. In the turbulent modeling, the Reynolds equations are closed with a relatively simple turbulence model which consists of an eddy viscosity hypothesis for the shear stresses and a semi-empirical model for the normal stresses. Finite element solution of the parabolic approximation of the model equations gives good secondary flow patterns as well as longitudinal velocity distribution in the headspace cross-section. The models have been validated with experimental data of Pescod and Price (1978). Overall, it is found that the models are capable of reproducing observed flow characteristics, and agreement with experimental data is also favorable. Using the models, average velocity curves and formulae that can be used for calculating the average longitudinal velocity relative to the wastewater have been developed. These curves and formulae suggest that the amount of ventilation induced by wastewater drag is dependent upon the unwetted wall perimeter, interfacial surface width and the headspace depth in addition to the wastewater surface velocity.

Specifically, the following conclusions can be drawn:

- The previously available ventilating models used for emission estimates and in corrosion modeling are incapable of detailing the air flow structure and generally over predict the mean velocity, especially in turbulent flow.
- In order to understand the flow structure in the headspace under different flow conditions, it is necessary to elucidate the secondary current structures in turbulent flow regimes. Although these secondary velocities are within 5-8 % of the average streamwise mean velocity, these currents may have important consequences on the air flow field.
- An interesting relationship is found to exist between the cross-sectional average secondary velocity (non-dimensionalized with the water surface velocity) and the relative depth ( $b/D$ ). The relationship indicates that although the strength of the cross-sectional average secondary velocity depends on the relative depth, it remains almost constant for headspace proportional depth range of about 30-65 %. The average secondary velocity is calculated to be within 1-3 % of the water surface velocity.
- The isovels in the laminar flow regime decrease from the air-water interface with increasing vertical distance from the water surface and follow approximately the wall boundary.
- The computed average streamwise velocity is consistently less than half the water surface velocity. This is found to be independent of the wastewater level or the flow regimes studied.

In spite of the progress and the optimistic results reported herein, there are still



significant areas where modeling refinements are needed. For instance the effects of fully rough interfacial waves and roughness of the collection conduit wall, subjects not addressed in this paper, still remain major challenges.

## REFERENCES

- ASCE. 1989. Sulphide in wastewater collection and treatment systems. ASCE Manuals and Reports on Engineering Practice, No. 69.
- Bowker, R. P. G., Smith, J. M., Webster, N. A. 1989. Odor and corrosion control in sanitary sewerage systems and treatment plants. Hemisphere Publishing Corporation, N. Y.
- Corsi, R. L., Chang, P. Y., Schroeder, E. D. 1992. A modeling approach for VOC emissions from sewers. *Water Env. Research.* **64** (5): 734-741.
- Czernuszenko, W., Rylov, A. A. 2002. Modeling of three-dimensional velocity field in open channel flows. *Journal of Hydraulic Research*, **40** (2): 135-143.
- Davidson, S., Green, J., Mann, J., Lamb, E. 2004. Design challenges in sewer foul air extraction and treatment. WEF/A & WMA Odors and Air Emission Conference, Bellevue, Seattle.
- Demuren, A. O., Rodi, W. 1984. Calculation of turbulence-driven secondary motions in non-circular ducts. *Journal of Fluid Mechanics.* **140**: 189-222.
- Deuflhard, P., Freund, R., Walter, A. 1990. Fast secant methods for the iterative solution of large non-symmetric linear systems. *IMPACT Comp. Sci. Eng.* **2**: 244-276.
- Edwini-Bonsu, S., Steffler, P. M. 2004a. A physically-based model for computing natural ventilation rate in sanitary sewer atmosphere. WEF/A & WMA Odors and Air Emission Conference, Bellevue, Seattle.
- Edwini-Bonsu, S., Steffler, P. M. 2004b. Dynamics of air flow in sanitary sewer

- conduits due to differential pressure. J. of Envir. Engrg. ASCE. Submitted.
- FEMLAB. 2002. Version 2.3a. Comsol Inc.
- Fletcher, C. A. J. 1988. Computational techniques for fluid dynamics 2. Springer-Verlag, N. Y.
- Gerard, R. 1978. Secondary flow in non-circular conduits. Journal of the Hydraulic Division, ASCE. **104** (HY5): 603-616.
- Gessner, F. B., Jones, J. B. 1965. On some aspects of fully-developed turbulent flow in rectangular channels. Journal of Fluid Mechanics, **23** (part 4), 689-713.
- Hager, H. W. 1999. Wastewater hydraulics-Theory and practice. Springer-Verlag, Berlin.
- Hinze, J. O. 1975. Turbulence. MacGraw-Hill, London.
- Hooхло, C. A. 1994. A numerical and experimental study of open channel flow in a pipe of circular cross-section with a flat bed. PhD. Thesis, University of Newcastle.
- Lam, C. K. G., Bremhorst, K. 1981. A modified form of the  $k - \varepsilon$  model for predicting wall turbulence. ASME Journal of Fluids Engineering. **103**, 456-460.
- Leutheusser, H. J., Chu, V. H. 1971. Experiments on plane Couette flow. Proc. ASCE., J. Hyd. Div. **97**, 1269-1284.
- Matos, J. S., de Sousa, E. R. 1992. The forecasting of hydrogen sulphide gas build-up in sewerage collection systems. Wat. Sci. Tech. **26** (3-4): 915-922.
- Moon, P., Spencer, D. E. 1961. Field theory handbook. Springer-Verlag, Berlin.
- Nezu, I., Nakagawa, H. 1993. Turbulence in open-channel flows. A. A. Belkema, Rotterdam.

- Nordsveen, M., Bertelsen, F. A. 1996. Waves and secondary flows in stratified gas/liquid duct flow: Waves and Non-linear Processes in Hydrodynamics (Ed. Grue et al.), Kluwer Academic Publishers, Netherlands, 279-290.
- Odor and Corrosion Technology Consultants, Inc. 1999a. The use of modeling techniques to evaluate and correct odour releases from trunk sewers. TM No.4, City of Edmonton Odour Control Project, Alberta.
- Odor and Corrosion Technology Consultants, Inc. 1999b. Trunk sewer odour monitoring program. TM No.1, City of Edmonton Odour Control Project, Alberta.
- Olson, D. 1996. Gas exchange rates between industrial process drains and the ambient atmosphere. MSc. Thesis, University of Texas.
- Olson, D., Rajagopalan, S., Corsi, R. L. 1997. Ventilation of industrial process drains: mechanisms and effects on VOC emissions, Jr. *Env. Eng.* **123** (9): 939-947.
- Perkins, H. J. 1970. The formation of streamwise vorticity in turbulent flow. *Journal of Fluid Mechanics.* **44** (4), 721-740.
- Pescod, M. B., Price, A. C. 1978. A study of sewer ventilation for the Tyneside sewerage scheme. Final research report, Department of Civil Engineering, University of Newcastle upon Tyne, U. K.
- Pescod, M. B., Price, A. C. 1981. Fundamentals of sewer ventilation as applied to the Tyneside sewerage scheme. *Water Pollution Control:* **90** (1): 17-33.
- Pescod, M. B., Price, A. C. 1982. Major factors in sewer ventilation. *J. Water Pollution Control Fed.* **54** (4): 385-397.

- Pomeroy, R. 1945. Pros and cons of sewer ventilation. *Sewage Works Journal*, **17** (2): 203-208.
- Quigley, C. J., Corsi, R. L. 1995. Emission of VOCs from a municipal sewer. *J. Air and Waste Mgmt. Assn.* **45** (5): 395-403.
- Reichardt, H. 1959. *Gesetzmässigkeiten der geradlinigen turbulenten Couettestromung*. Mitt. Max-Planck-Inst. Fur Stromungsforschung, no. 22, Gottingen.
- Replogle, J. A., Chow, V. T. 1966. Tractive force distribution in open channels. *J. Hyd. Div. ASCE.*, **92**(2), 169-191.
- Robert, J-L., Khelifi, M., Ghanmi, A. 1998. Use of the mixing length concept to correctly reproduce velocity profiles of turbulent flows. *Can. J. Civ. Eng.* **25**: 232-240.
- Robertson, J. M. (1959). On turbulent plane Couette flow. Proc. 6<sup>th</sup> Midwestern Conf. on Fluid Mech. University of Texas, Austin. 169-182.
- Robertson, J. M., Johnson, H. F. (1970). Turbulence structure in plane Couette flow. Proc. ASCE., J. Eng. Mech. Div. **96**, 1171-1182.
- Rodi, W. 1984. Turbulence models and their application in hydraulics. A state of the art review. International Association for Hydraulic Research, Delft, the Netherlands.
- Schlichting, H. 1969. *Boundary layer theory*. McGraw Hill, N.Y.
- Sinai, Y. L. 1983. A Charnock-based estimate of interfacial resistance and roughness for internal, fully-developed, stratified, two-phase horizontal flow. *Int. J. Multiphase Flow.* **9** (1), 13-19.
- Speziale, C. G. 1982. On turbulent secondary flows in pipes of non-circular cross-

- section. *International Journal of Engineering Science*. **20** (7), 863-872.
- Thistlethwayte, D. K. B. (Ed.). 1972. *The control of sulphides in sewerage systems*. Butterworths, Sydney. .
- Tominaga, A., Nezu, I., Ezaki, K., Nakagawa, H. 1989. Three-dimensional turbulent structures in straight open channel flows. *Journal of Hydraulic Research*. **27** (1): 149-173.
- U. S. Environmental Protection Agency (EPA). 1994. *Air emission models for waste and wastewater*. EPA-453/R-94-080A-Part 1.
- Vlachos, N. A., Paras, S. V., Karabelas, A. J. 1999. Prediction of holdup, axial pressure gradient and wall shear stress in wavy stratified and stratified/atomization gas/liquid flow. *Int. J. of Multiphase Flow*. **25**, 365-376.
- Wilcox, D. C. 2000. *Turbulence modeling for CFD*. 2<sup>nd</sup> ed. DCW Industries, Inc., California, U. S.

---

## CHAPTER THREE<sup>2</sup>

### DYNAMICS OF AIR FLOW IN SANITARY SEWER CONDUITS DUE TO DIFFERENTIAL PRESSURE

---

#### 3.1 INTRODUCTION

Ventilation and pressurization in sanitary sewer conduits are primarily caused by differences in environmental conditions along the collection system as well as the two-phase fluid mechanic phenomenon within. Three such driving conditions, namely; barometric pressure, wind speed, and wastewater flowing down the sewer, have been identified as the main natural factors influencing the flow of air in sewer piping systems (Pescod and Price 1978, 1981, 1982; Pomeroy 1945; Odor and Corrosion Technology Consultants 1999b; Olson et al. 1997; Quigley and Corsi 1995; USEPA 1994). Physical structures such as dropstructures associated with deep trunk and interceptor sewer systems can also cause significant pressurization to headspaces of downstream sewer conduits and cause air to move. Furthermore, sewer conduit headspace can be pressurized with mechanical scrubbers/blowers which are usually used to combat corrosive,

---

<sup>2</sup> The main content of this chapter is submitted for publication in the J. of Envir. Engrg. ASCE; Some model results are also presented at WEF/A & WMA Odors & Air Emission Conference, Bellevue, Seattle, 2004.

odorous and other hazardous gases. Computational fluid dynamics modeling of the effect of wastewater drag has been presented by Edwini-Bonsu and Steffler (2003), and also in Chapter 2 of this thesis and therefore not considered in this paper. The present study is only concerned with sewer headspace pressurization.

Calculations of the air flow field are key inputs for the design of ventilation systems, and modeling of odorous-compound emissions from and occurrence of corrosion in sewer conduit systems (Bowker et al. 1989; Matos and de Sousa 1992; Pescod and Price 1978; Odor and Corrosion Technology Consultants 1999b; Olson et al. 1997; Quigley and Corsi 1995). The study undertaken here typifies a situation where wastewater flow is stagnant or too low to transfer any appreciable momentum into the sewer atmosphere. An example of this situation can be found in bypasses where wastewater flow is sluggish. Under this circumstance pressure gradients may be the primary ventilating force.

Differential wind speed may occur when one opening along the sewer is shielded from the wind and another opening is exposed to it or may be due to climatic differences between any two locations along the sewer reach. This differential wind speed can set up a dynamic pressure difference and cause air to flow. Another scenario under which pressure can result is where alternating high and low vents are used in the design of wastewater collection systems to enhance ventilation by maximizing the effect of wind eduction, a technique which has been used successfully in controlling corrosion in municipal sewers



(Thistlethwayte 1972).

Pescod and Price (1978), and Olson (1996) developed a theoretical model to assess the effect of wind speed on air eduction in sewer channels with openings along the reach. Their model, which is not different from that of the United States Environmental Protection Agency (USEPA 1994)'s for estimating air emissions from wastewater collection systems, is based on the energy concept and the approximation of the headspace to an equivalent circular pipe. This approximation is a serious handicap for accurate predictions of the air flow rate. Ignoring the 'horizontal' portion formed by the air-water interface in any theoretical modeling completely alters the cross-sectional shape and ultimately gives different flow phenomenon in the sewer headspace. A complicated situation exists when the depth of water is greater than half the diameter of the conduit, since the top width of the channel decreases and the boundary curves inwards.

There has been no attempt to either theoretically or experimentally quantify the effect of barometric pressure on sewer air flow. All facts to date are based on qualitative descriptions (Pescod and Price 1978, 1981, 1982; Olson 1996). Differences in barometric pressure along various parts of the sewer system are noted to produce gradients which sustain air flow. It has been reported that a barometric pressure gradient of one millibar per kilometre (mb/km) can lead to ventilation rates that rival those caused by other ventilation factors (Quigley and Corsi 1995; Olson 1996). Thistlethwayte (1972) noted that a change of one

millibar of pressure for a typical sewer corresponds to an air velocity of approximately 1.5 m/s. These examples illustrate that the pressure gradient does not necessarily have to be substantial in order to cause air (odour) transport in sewer systems. Since a high barometric pressure gradient usually occurs with unstable atmospheric conditions and therefore at a time of significant wind velocity, the resultant effect on sewer ventilation will depend on the magnitude and direction of the two air flows. If both act in the same direction, an air flow rate of greatest magnitude can be expected. However if the barometric pressure difference acts in the opposite direction to wind, a reduced rate of ventilating air flow is probable. Headspace pressurizations resulting from dropstructures or scrubbers/blowers have also not been modelled.

In this paper, mathematical models that not only represent these driving forces correctly, but also account for the possibility of the sewer headspace to generate secondary currents in a turbulent flow regime are proposed. The governing equations are those of the Reynolds averaged momentum and continuity equations with fully-developed and steady state assumptions. The Reynolds shear stresses in the turbulent governing equations are computed using an eddy viscosity-mixing length model in conjunction with universal semi-empirical relations for the turbulent normal intensities thus making it possible to account for turbulence anisotropy. The headspace pressurization is conceptually analyzed as a 2-D Poiseuille-flow. A finite element solution of the model formulation is first validated with air velocity and flow rate measurements in lenticular channels

subjected to pressure gradients and then used to develop generalized curves and formulae for the bulk streamwise mean velocity. To ensure that most flow situations in in-service sewers are covered, laminar flow regime is also considered.

## 3.2 MODEL FORMULATION

### 3.2.1 Flow Equations

The governing equations for turbulent fluid flows are those of the Reynolds-averaged-Navier-Stokes (RANS) equations. With the assumptions of incompressible and fully-developed flows, and steady-state conditions, these equations are written together with the continuity as:

Streamwise averaged momentum equation:

$$x - \quad V \frac{\partial U}{\partial y} + W \frac{\partial U}{\partial z} = -\frac{1}{\rho} \frac{dP}{dx} + \nu \left( \frac{\partial^2 U}{\partial y^2} + \frac{\partial^2 U}{\partial z^2} \right) - \left( \frac{\overline{\partial u' v'}}{\partial y} + \frac{\overline{\partial u' w'}}{\partial z} \right) \quad [3.1]$$

Secondary averaged momentum equations:

$$y - \quad V \frac{\partial V}{\partial y} + W \frac{\partial V}{\partial z} = -\frac{1}{\rho} \frac{\partial P}{\partial y} + \nu \left( \frac{\partial^2 V}{\partial y^2} + \frac{\partial^2 V}{\partial z^2} \right) - \left( \frac{\overline{\partial v'^2}}{\partial y} + \frac{\overline{\partial v' w'}}{\partial z} \right) \quad [3.2]$$

$$z - \quad V \frac{\partial W}{\partial y} + W \frac{\partial W}{\partial z} = -\frac{1}{\rho} \frac{\partial P}{\partial z} + \nu \left( \frac{\partial^2 W}{\partial y^2} + \frac{\partial^2 W}{\partial z^2} \right) - \left( \frac{\overline{\partial v' w'}}{\partial y} + \frac{\overline{\partial w'^2}}{\partial z} \right) \quad [3.3]$$

Continuity:

$$\frac{\partial V}{\partial y} + \frac{\partial W}{\partial z} = 0 \quad [3.4]$$

where  $\rho$  and  $\nu$  are respectively the density and kinematic viscosity of air,  $U$  is the streamwise mean velocity in the  $x$  direction, and  $u'$ ,  $v'$  and  $w'$  are components of the turbulent velocities in  $x$ ,  $y$  and  $z$  directions, respectively.  $V$  and  $W$  are secondary mean flow velocities in the  $y$  and  $z$  directions. These velocities are produced due to anisotropy of turbulence. The assumption of fully-developed flow in the above formulation requires that the section under consideration be well removed from exit and entrance of junctions, and the diameter of the sewer pipe remain constant along the reach as depicted in Figure 3-1. The figure shows a partially-full, gravity-flow circular sewer conduit, including the co-ordinate system and nomenclature. The longitudinal pressure gradient term ( $dP/dx$ ) in Equation [3.1] is the average piezometric pressure gradient (i.e. with gravitational force per unit mass included) which may be due to differential wind speed, barometric pressure differential, upstream dropstructure pressurization or application of a scrubber/blower.  $P$  in Equations [3.2] and [3.3] arises mainly from anisotropy of turbulence. In Figure 3-1 the wind speeds at the two openings are denoted by  $V_{w1}$  and  $V_{w2}$ , and the pressures at the ends of the pipe resulting from any of the above motive forces are denoted by  $P_1$  and  $P_2$ .

The turbulent stresses in the mean flow equations have to be computed. Many turbulence models, from simple to very complicated ones, are available at present (Rodi 1984; Wilcox 2000). The simplest turbulence closure models usually employ the Boussinesq eddy viscosity approximation to model these apparent stresses. For computational simplicity, the turbulent eddy viscosity is, in turn,

often calculated using the Prandtl's mixing length hypothesis (MLH). Unfortunately, Prandtl's MLH does not offer any means of determining the normal stresses. For homogenous turbulence, the normal stresses are usually included in the pressure term and they do not have to be calculated. This is not the case here, because the flow in the headspace is nonhomogeneous. Thus, in addition to specifying the shear stresses, the turbulent normal stresses need to be modelled. A relatively simple way of achieving this is discussed below.

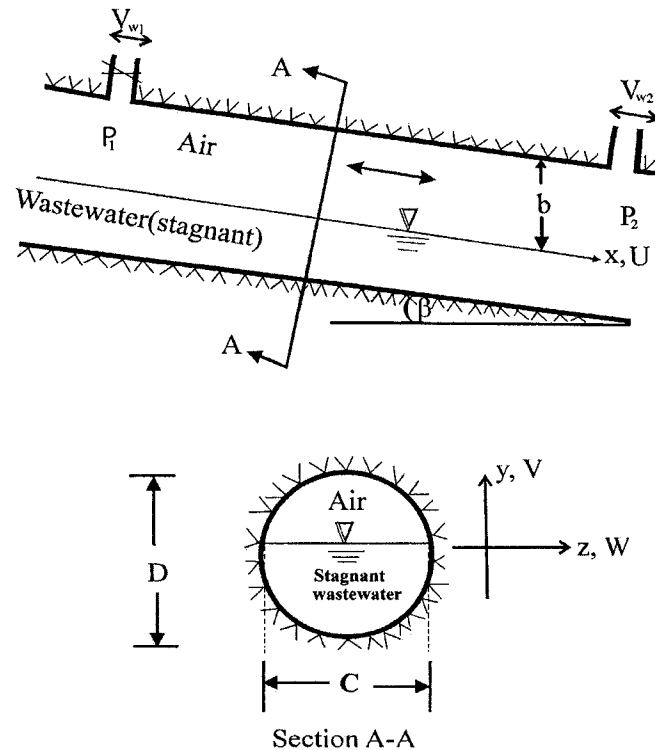


**Figure 3-1: A model sewer conduit**

### 3.2.2 Turbulence Closure

Turbulence closure of the momentum equations is achieved with the use of semi-empirical relations for the Reynolds normal stress terms and an eddy viscosity modeling concept for the Reynolds shear stress terms (Chapter 2). This approach offers a means of assessing the turbulence-driven secondary effects on the mean flow. Turbulence-driven secondary motion associated with fully-developed flows in non-circular conduits such as the one under study is caused mainly by the differences between the normal stress terms,  $\overline{v'^2}$  and  $\overline{w'^2}$  (Naot and Rodi 1982; Demuren and Rodi 1984; Gerard 1978; Tominaga et al. 1989). As a consequence, the two terms must be modelled in a mathematical simulation in order to describe realistically the secondary flow phenomenon.

From Chapter 2, the distributions of the turbulent intensities  $\sqrt{\overline{v'^2}}$  and  $\sqrt{\overline{w'^2}}$  are obtained as:

$$\sqrt{\overline{v'^2}} = \left( \sqrt{\overline{v'^2}}(n_s) \right)^{\Phi_{n_s}} \left( \sqrt{\overline{v'^2}}(n_w) \right)^{\Phi_{n_w}} \quad [3.5]$$

$$\sqrt{\overline{w'^2}} = \left( \sqrt{\overline{w'^2}}(n_s) \right)^{\Phi_{n_s}} \left( \sqrt{\overline{w'^2}}(n_w) \right)^{\Phi_{n_w}} \quad [3.6]$$

where

$$\sqrt{\overline{v'^2}}(n_s) = u_{zs} \left( A_{vn} e^{-B_{vn} n_s} \right), \sqrt{\overline{v'^2}}(n_w) = u_{zw} \left( A_{vn} e^{-B_{vn} n_w} \right), \sqrt{\overline{w'^2}}(n_s) = u_s \left( A_{wn} e^{-B_{wn} n_s} \right)$$

$$, \sqrt{\overline{w'^2}}(n_w) = u_{zw} \left( A_{wn} e^{-B_{wn} n_w} \right), \Phi_{n_s} = n_w / (n_w + n_s), \Phi_{n_w} = n_s / (n_w + n_s),$$

$$A_{wn} = 1.45, \quad A_{vn} = 1.15, \quad B_{wn} = 0.92, \quad B_{vn} = 0.69, \quad n_s \text{ and } n_w \text{ are dimensionless}$$

normal distances from the water surface and the curved wall, respectively.  $u_{\tau}$  and  $u_{\tau w}$  are shear velocities respectively for water surface and curved wall.

In a preliminary study, three closure models have been used to calculate the Reynolds shear stresses  $\overline{u'v'}$ ,  $\overline{u'w'}$ ,  $\overline{v'w'}$  appearing in Equations [3.1]-[3.3]. These are the low Reynolds number  $k-\varepsilon$  model of Lam and Bremhorst (1981) with non-slip boundary conditions and damping functions, the standard  $k-\varepsilon$  model with wall function approach and a generalized bi-harmonic mixing length model of Robert et al. (1998) (also discussed in Chapter 2). Although these models give comparable bulk longitudinal mean velocities, the mixing length approach provides best air velocity patterns in the headspace (in comparison with experimental data). In this direction, the mixing length model has been chosen for this study.

Thus the eddy viscosity is computed from the mixing length model as (Chapter 2):

$$\nu_t = \ell_m^2 \left[ \left( \frac{\partial U_i}{\partial X_j} + \frac{\partial U_j}{\partial X_i} \right) \frac{\partial U_i}{\partial X_j} \right]^{\frac{1}{2}} \quad [3.7]$$

where  $\ell_m$  is the mixing length described in Chapter 2. In a fully-developed 3-D flow, Equation [3.7] can be written as:

$$\nu_t = \ell_m^2 \left[ \left( \frac{\partial U}{\partial y} \right)^2 + \left( \frac{\partial U}{\partial z} \right)^2 + 2 \left( \frac{\partial V}{\partial y} \right)^2 + 2 \left( \frac{\partial W}{\partial z} \right)^2 + \left( \frac{\partial V}{\partial z} + \frac{\partial W}{\partial y} \right)^2 \right]^{\frac{1}{2}} \quad [3.8]$$

### 3.3 SOLUTION PROCEDURE

The RANS equations are now closed and amenable to solution. In this paper, the pressure effects are modelled with the supposition that the wastewater flow is stagnant and also that the water surface is rigid. This means that there is no momentum transfer from the wastewater to the headspace and vice versa. The resistance to the air movement is the friction between the air and the boundaries (both 'flat' portion and curved sewer wall). Given this set of simple boundary conditions, it is possible to generate the air flow field for the air movement in the sewer airspace. In the present study the integration of the flow equations is carried out to the boundaries. This means that the velocities tangential and normal to the boundaries are set to zero.

To present generalized solutions, the Reynolds similarity criterion is employed. The length scale is chosen to be  $b$ , where  $b$  is the maximum headspace depth of the sewer pipe. Two velocity scales, one for the turbulent case and another for the laminar regime, are introduced. The velocity scale for the turbulent flow case is defined as:  $U_{pt} = \sqrt{(|-dP/dx|)b/\rho}$ . These scales lead to the following non-

dimensional quantities:  $X_* = x/b$ ;  $Y_* = y/b$ ;  $Z_* = z/b$ ;  $U_* = U/U_{pt}$ ;

$P_* = P/(\rho U_{pt}^2)$ ;  $V_* = V/U_{pt}$ ;  $W_* = W/U_{pt}$ ;  $\overline{v_*'^2} = \overline{v'^2}/U_{pt}^2$  and

$\overline{w_*'^2} = \overline{w'^2}/U_{pt}^2$ . The corresponding 'turbulent Reynolds number' then becomes



$Re_t = U_{pl}b/\nu$ . The governing equations yield a set of non-dimensionalized parabolic equations as:

Streamwise averaged momentum equation:

$$X_* - V_* \frac{\partial U_*}{\partial Y_*} + W_* \frac{\partial U_*}{\partial Z_*} - \frac{\partial}{\partial Y_*} \left[ (1/Re_t + \nu_{t*}) \frac{\partial U_*}{\partial Y_*} \right] - \frac{\partial}{\partial Z_*} \left[ (1/Re_t + \nu_{t*}) \frac{\partial U_*}{\partial Z_*} \right] = 1 \quad [3.9]$$

Secondary averaged momentum equations:

$$Y_* - V_* \frac{\partial V_*}{\partial Y_*} + W_* \frac{\partial V_*}{\partial Z_*} - \frac{1}{Re_t} \left[ \frac{\partial^2 V_*}{\partial Y_*^2} + \frac{\partial^2 V_*}{\partial Z_*^2} \right] = -\frac{\partial P_*}{\partial Y_*} - \frac{\overline{\partial \nu_*^2}}{\partial Y_*} + \frac{\partial}{\partial Z_*} \left[ \nu_{t*} \left( \frac{\partial V_*}{\partial Z_*} + \frac{\partial W_*}{\partial Y_*} \right) \right] \quad [3.10]$$

$$Z_* - V_* \frac{\partial W_*}{\partial Y_*} + W_* \frac{\partial W_*}{\partial Z_*} - \frac{1}{Re_t} \left[ \frac{\partial^2 W_*}{\partial Y_*^2} + \frac{\partial^2 W_*}{\partial Z_*^2} \right] = -\frac{\partial P_*}{\partial Z_*} - \frac{\overline{\partial \nu_*^2}}{\partial Z_*} + \frac{\partial}{\partial Y_*} \left[ \nu_{t*} \left( \frac{\partial V_*}{\partial Z_*} + \frac{\partial W_*}{\partial Y_*} \right) \right] \quad [3.11]$$

Continuity:

$$\frac{\partial V_*}{\partial Y_*} + \frac{\partial W_*}{\partial Z_*} = 0 \quad [3.12]$$

Eddy viscosity:

$$\nu_{t*} = \ell_{m*}^2 \left[ \left( \frac{\partial U_*}{\partial Y_*} \right)^2 + \left( \frac{\partial U_*}{\partial Z_*} \right)^2 + 2 \left( \frac{\partial V_*}{\partial Y_*} \right)^2 + 2 \left( \frac{\partial W_*}{\partial Z_*} \right)^2 + \left( \frac{\partial V_*}{\partial Z_*} + \frac{\partial W_*}{\partial Y_*} \right)^2 \right]^{\frac{1}{2}} \quad [3.13]$$

Under laminar flow conditions, the equation of continuity is satisfied identically and the momentum equations in the directions of  $y$  and  $z$  reduce to a statement that pressure is a constant. If a velocity scale is introduced for the laminar case such that  $U_{pl} = (-dP/dx)b^2/(\nu\rho)$ , then the streamwise momentum equation simplifies to a Poisson-type equation with a unit driving force:

$$X_* - \left( \frac{\partial^2 U_*}{\partial Y_*^2} + \frac{\partial^2 U_*}{\partial Z_*^2} \right) = 1 \quad [3.14]$$

The velocity scale used here renders the non-dimensionalized laminar velocity distribution independent of the flow Reynolds number. Using pressure flow in pipes as a basis, it is assumed that laminar flow is assured up to a Reynolds number of 8000 (Wilcox 2000). This Reynolds number is based on the laminar velocity scale (i.e.  $Re_l = U_{pl}b/\nu$ ).

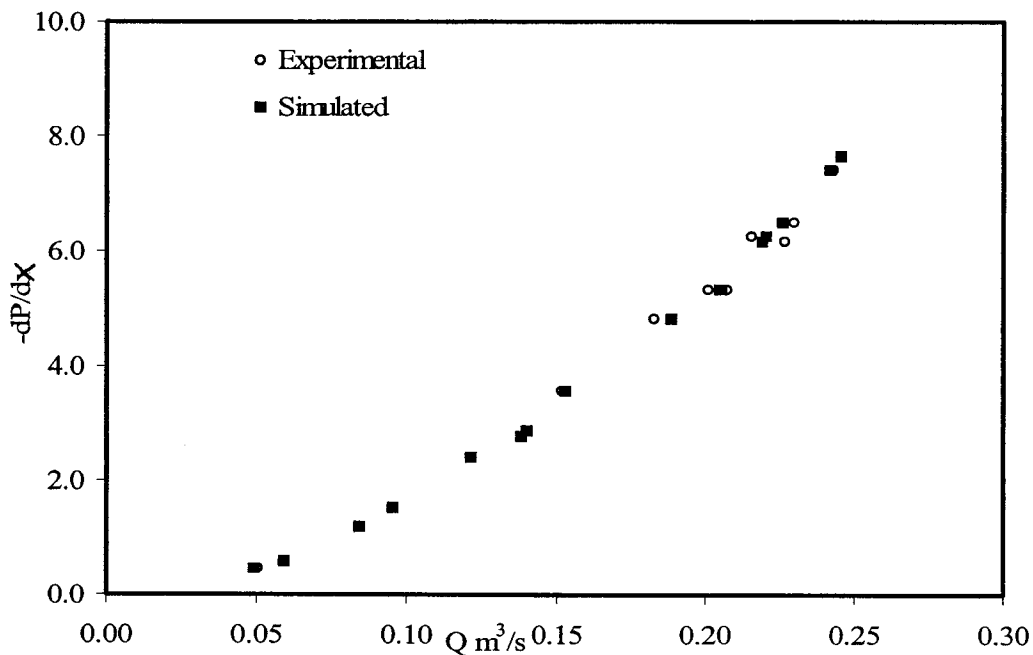
A finite element method (FEM) based on the FEMLAB programming language is implemented to solve the above non-dimensionalized equations as discussed in Chapter 2 and Appendix A.

### 3.4 VALIDATION AND PREDICTIONS

The finite element models are validated by comparing results with other solution techniques as well as experimental data in the literature. The laminar flow regime (governed by Equation [3.14]) has been modelled using analytical, finite difference (FD) and finite element (FE) techniques in preliminary test calculations. The first two methods have been used with the objective of assessing the predictive performance of the FE discretization scheme, which is the core numerical tool in this paper. Satisfactory agreements have been obtained between the finite element scheme and the other two methods. Details of the analytical and

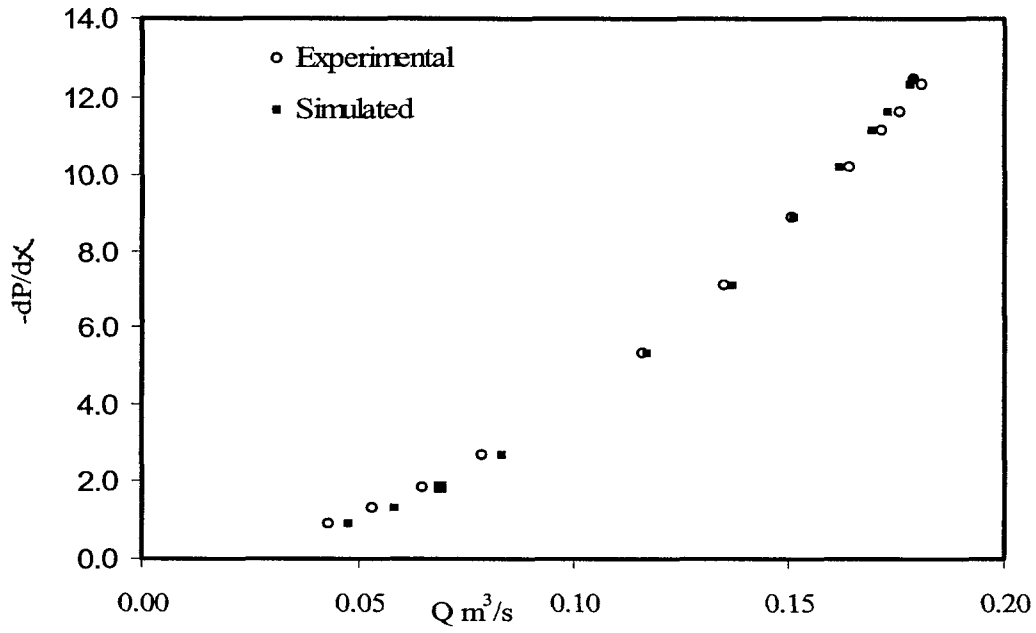
the finite difference methods as well as their comparisons are given in Appendix A.

Sterling (1998)'s air velocity distribution and flow rate data in lenticular channels subjected to pressure gradients are used to evaluate the performance of the proposed turbulent model. The measurements were conducted in a 9.2 m lenticular section cut from a 389 mm diameter circular PVC pipe. The air velocity was measured at a distance of about 8.9 m from the channel entrance using a Pitot tube. Three sets of experiments were conducted for cross-sections of relative depths  $b/D= 27, 20$  and  $10 \%$ . Details of the experimental set-up can be found in the above reference.

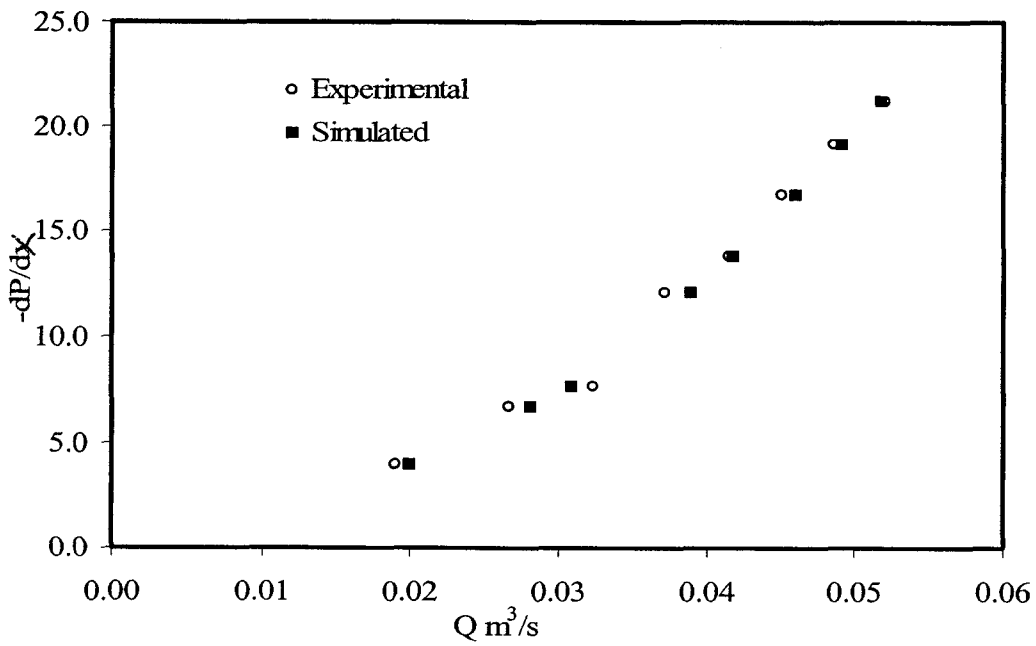


a)

**Figure 3-2(a, b & c): Predicted and measured flow rate compared: a)  $b/D= 27 \%$ , b)  $b/D= 20 \%$ , c)  $b/D= 10 \%$**



b)



c)

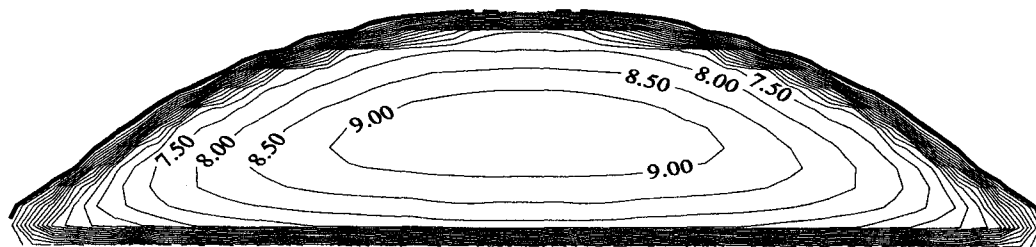
**Figure 3-2(Continued): Predicted and measured flow rate compared: a)  $b/D=$   
27 %, b)  $b/D=$  20 %, c)  $b/D=$  10 %**

Figure 3-2 shows the comparative performance of the turbulent model in predicting measured flow rate for the three cross-sections under varying pressure gradients (in  $\text{N/m}^{-3}$ ). The model is seen to accurately simulate the experimental values reasonably well with complete overlap at some points.

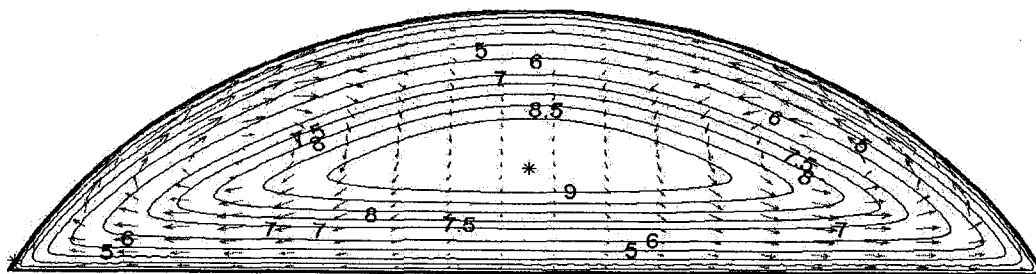
Figures 3-3 to 3-5 compare the simulated isovel plots for the three cross-sections with those of experimental measurements. Superimposed on the simulated isovel diagrams are the corresponding secondary velocity vectors. The isovel plots are non-dimensionalized with  $U_{pt}$ . Overall, it is seen from these diagrams that there are no remarkable differences between the numerical results and the measured isovels. It should however be acknowledged here that the model fails to predict the measured velocity isovels near the boundary especially in Figure 3-3. It is important to mention here that different plotting packages are used for the calculated and experimental isovels. Surfer is used in plotting the experimental data whereas the numerical simulations are post-processed using MATLAB commands.

Figure 3-6 compares center velocity profiles for the two regimes with the parabolic and  $1/7^{\text{th}}$  power-law profiles. These profiles are non-dimensionalized with the corresponding maximum center velocity. The first obvious realization is that the simulated headspace laminar profile approximately exhibits parabolic shape characteristics. All the profiles, with the exception of the simulated turbulent profile, are symmetric with the turning points occurring at the channel

center. As illustrated in the figure, the turbulent headspace velocity profile follows neither the parabolic nor the power law profiles. The relaxed and almost uniform velocity profile exhibited by the power law is not evident in the simulated turbulent profile which only undergoes uniform rapid decline near the wall. The differences may be attributed to the effects of the lateral boundary and the secondary flows. The simulated turbulent profile further indicates that the point of zero lateral apparent shear stress ( $\overline{u'v'} = 0$ ) or turning point is closer to the 'flat' portion than the curved wall boundary.



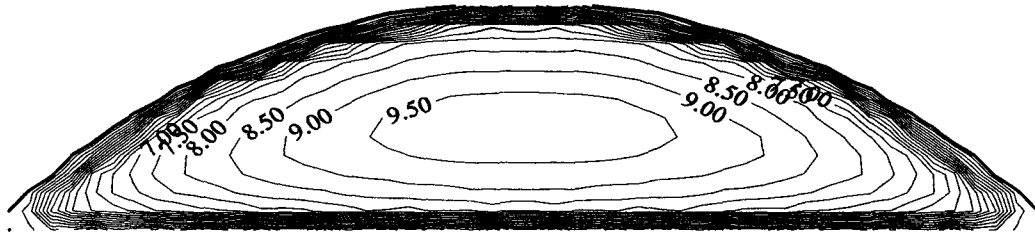
a)



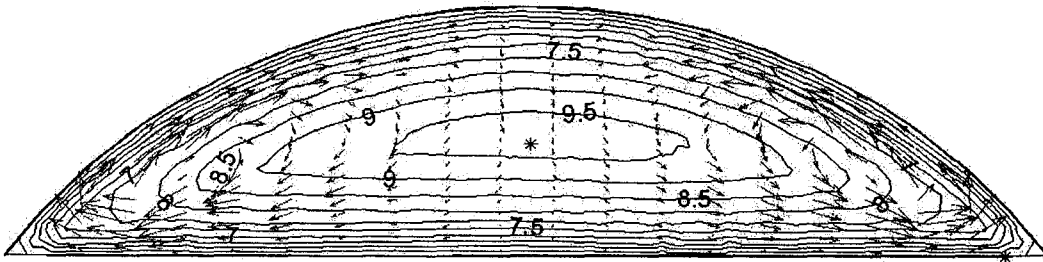
b)

**Figure 3-3(a& b): Contour of mean primary velocity ( $U/U_{pt}$ ),  $b/D= 27\%$ ,**

**$Re_t = 22,816$ : a) experimental, b) simulated**



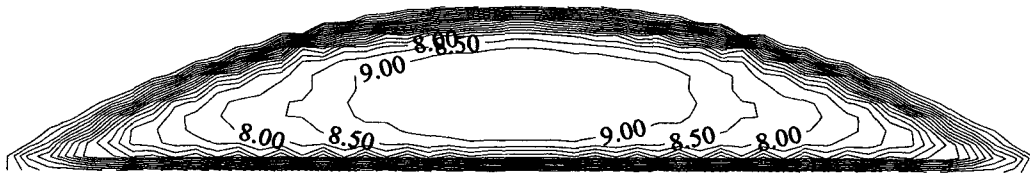
a)



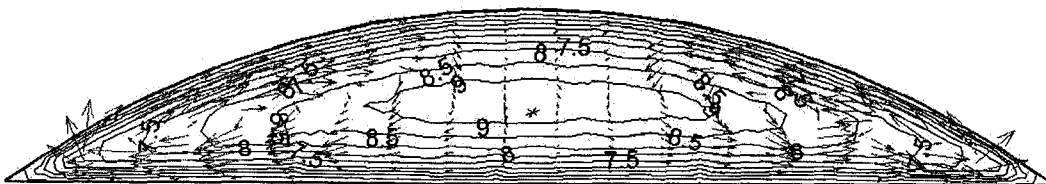
b)

Figure 3-4(a & b): Contour of mean primary velocity ( $U/U_{pt}$ ),  $b/D = 20\%$ ,

$Re_t = 18,634$  : a) experimental, b) simulated



a)



b)

Figure 3-5(a & b): Contour of mean primary velocity ( $U/U_{pt}$ ),  $b/D = 10\%$ ,

$Re_t = 8,640$  : a) experimental, b) simulated

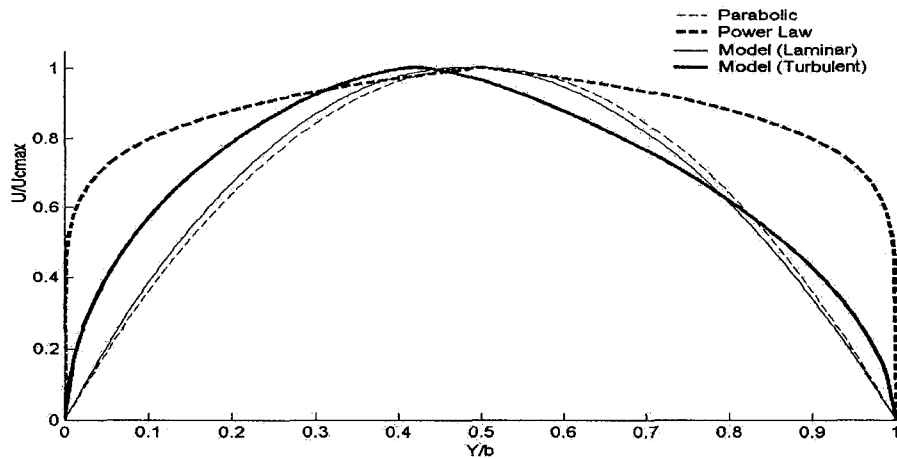


**Figure 3-6: Typical non-dimensionalized center velocity profiles for laminar and turbulent flows (compared are the power law and the parabolic profiles)**

In Figure 3-7 typical non-dimensionalized isovels in laminar and turbulent flow regimes are also compared. Again it is seen that in laminar flows the maximum local streamwise velocity occurs mid way between the curved and ‘flat’ surface unlike the turbulent flow case. Superimposed on the turbulent isovels are the secondary flow vectors. In Figure 3-7b (also in Figures 3-3b, 3-4b and 3-5b) a single secondary flow cell on either side of the channel quadrant is observed. It is also observed that the centers of the cells are closer to the wall boundary than the ‘flat’ boundary. In both laminar and turbulent cases, the maximum velocity occurs on the centre-line of the duct, but tends to be located closer to the interface than the curved boundary in turbulent flow case. This shift in the maximum velocity is due to the effect of the secondary flow which also displaces the velocity contours from the wall toward the ‘flat’ portion of the headspace. The secondary flow



pattern calculated here is in agreement with that of Hoohlo (1994), Edwini-Bonsu and Steffler (2003), and also Chapter 2 of this thesis. The pattern is also found to be independent of the flow Reynolds number as evident in Figures 3-3b, 3-4b, 3-5b and 3-7b. The calculated secondary current is generally within 6-10 % of the bulk streamwise velocity. The numerical simulation further shows that the strength of the secondary flow increases with decreasing headspace depth ( $b/D$ ). This feature is also in agreement with previous findings (Edwini-Bonsu and Steffler 2003; Chapter 2 of this thesis).

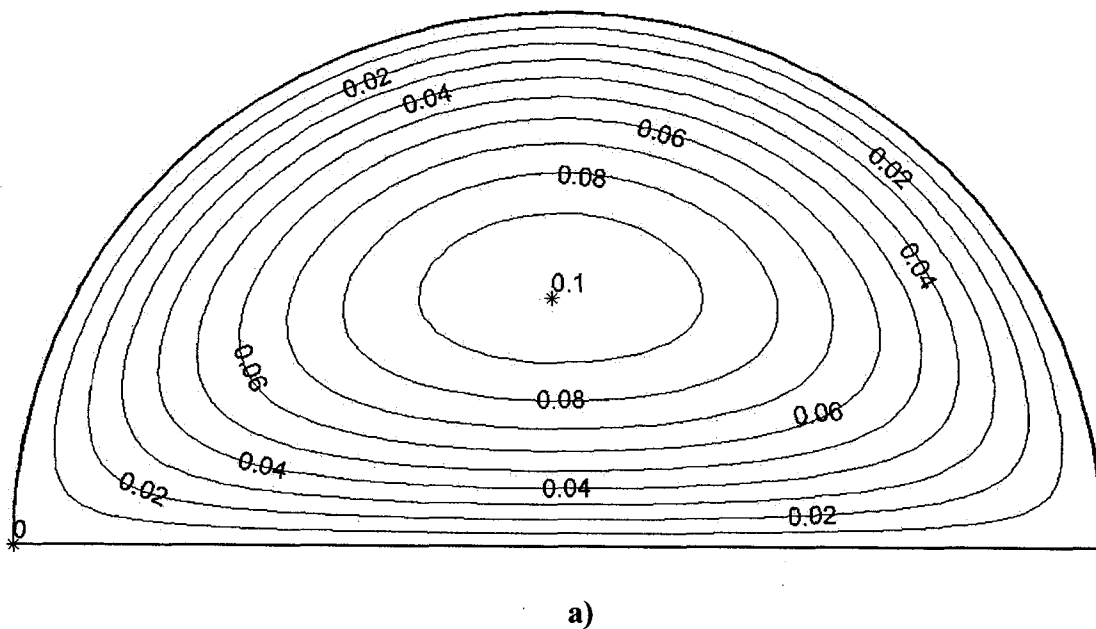
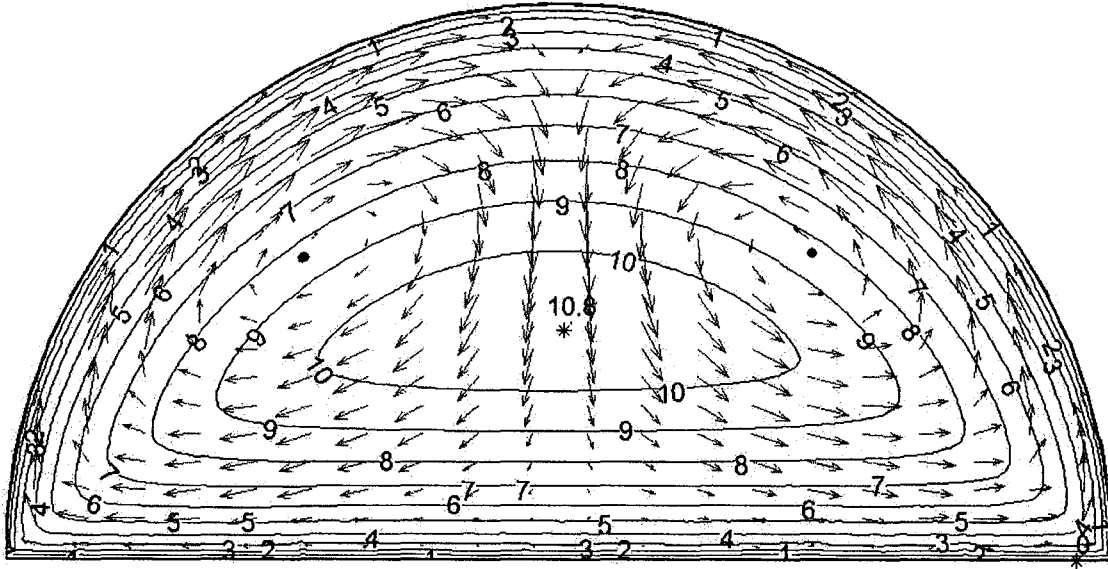


**Figure 3-7(a & b): Typical non-dimensionalized velocity contour distribution for  $b/D= 50\%$ : a) laminar regime, b) turbulent,  $Re_t= 30,000$**



b)

**Figure 3-7 (Continued): Typical non-dimensionalized velocity contour distribution for  $b/D= 50 \%$ : a) laminar regime, b) turbulent,  $Re_t= 30, 000$**

One main variable of interest to practicing engineers is the cross-sectional average longitudinal velocity. Here this variable is presented graphically and also expressed in convenient mathematical formats. Figure 3-8 shows the bulk velocity curves for laminar and turbulent flows as a function of the relative depth  $b/D$ .

These curves are best fitted to give:

$$\frac{U_{av}}{U_{pl}} = 0.0561 - 0.0142 \left[ \frac{b}{D} \right]^2 - 0.0101 \left[ \frac{b}{D} \right], R^2 = 0.99 \text{ (Laminar flow)} \quad [3.15]$$

$$\frac{U_{av}}{U_{bt}} = 1.2477 - 4.5107 \left[ \frac{b}{D} \right]^2 + 9.7641 \left[ \frac{b}{D} \right], R^2 = 0.99 \text{ (Turbulent flow)} \quad [3.16]$$

where  $R$  is the coefficient of determination and  $U_{bt}$  is the ratio of turbulent velocity scale ( $U_{pl}$ ) to the square root of the relative depth ( $b/D$ ). Using the same

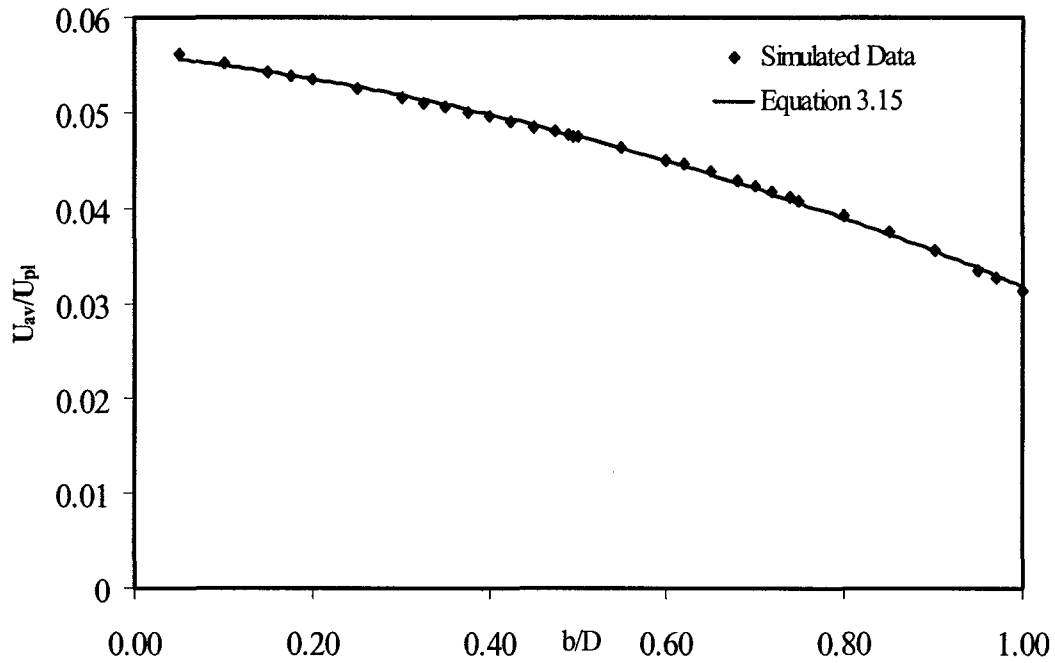
simulated data and expressing the results in terms of the perimetric shape factor, the following relations are also obtained:

$$\frac{U_{av}}{U_{pt}} = 0.088 \left[ \frac{C}{(C+L)} \right]^2 + 0.0079 \left[ \frac{C}{(C+L)} \right] + 0.0313, R^2 = 0.99 (\text{Laminar}) \quad [3.17]$$

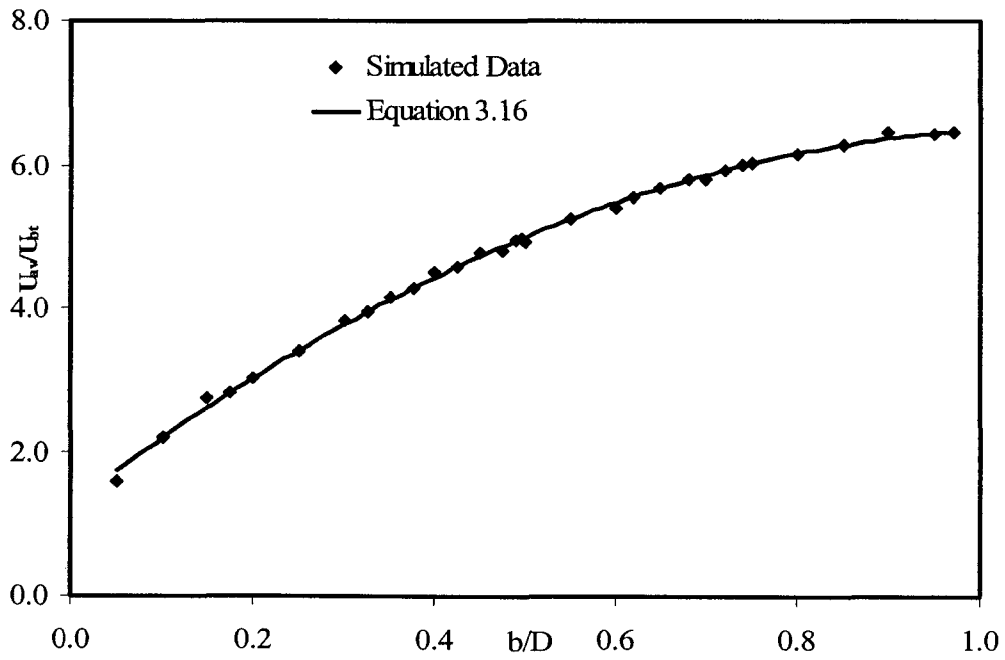
$$\frac{U_{av}}{U_{ct}} = 6.3985 \left[ \frac{C}{(C+L)} \right] + 1.8443, R^2 = 0.99 (\text{Turbulent}) \quad [3.18]$$

where  $C$  is the total width of the water surface,  $L$  is the perimeter of the unwetted headspace and  $U_{ct}$  is the ratio of turbulent velocity scale ( $U_{pt}$ ) to the square root of the perimetric shape factor ( $C/(C+L)$ ). Equations [3.17] and [3.18] are plotted together with the simulated data in Figure 3-9.

These curves and formulae can be used to estimate the cross-sectional average air velocity at different water levels when the pressure gradient, which is expressed in the velocity scales, is known. This basic calculation would allow the determination of the volume of air capable of being forced out via available opening. In general, the proposed 2-D models are found useful for providing quantitative evaluation of the headspace ventilation in addition to elucidating the patterns of the air flow field in the sewer atmosphere which are particularly relevant in corrosion modeling studies.



a)



b)

**Figure 3-8(a & b): Cross-sectional average velocity curves as a function of relative depth  $b/D$ : a) laminar, b) turbulent**

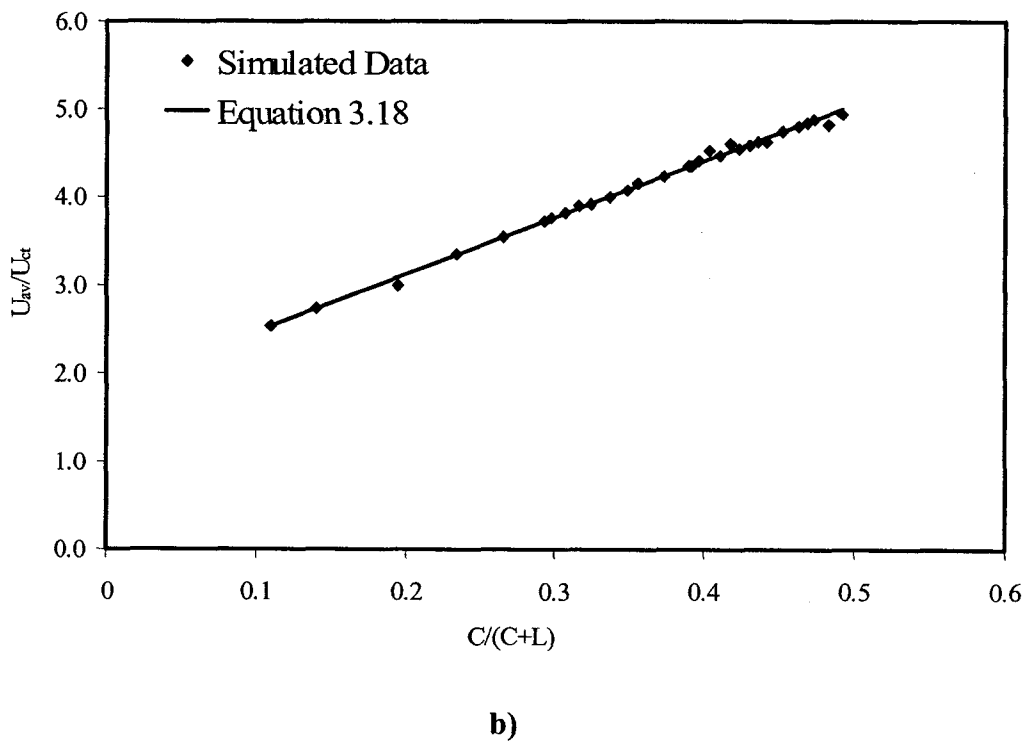
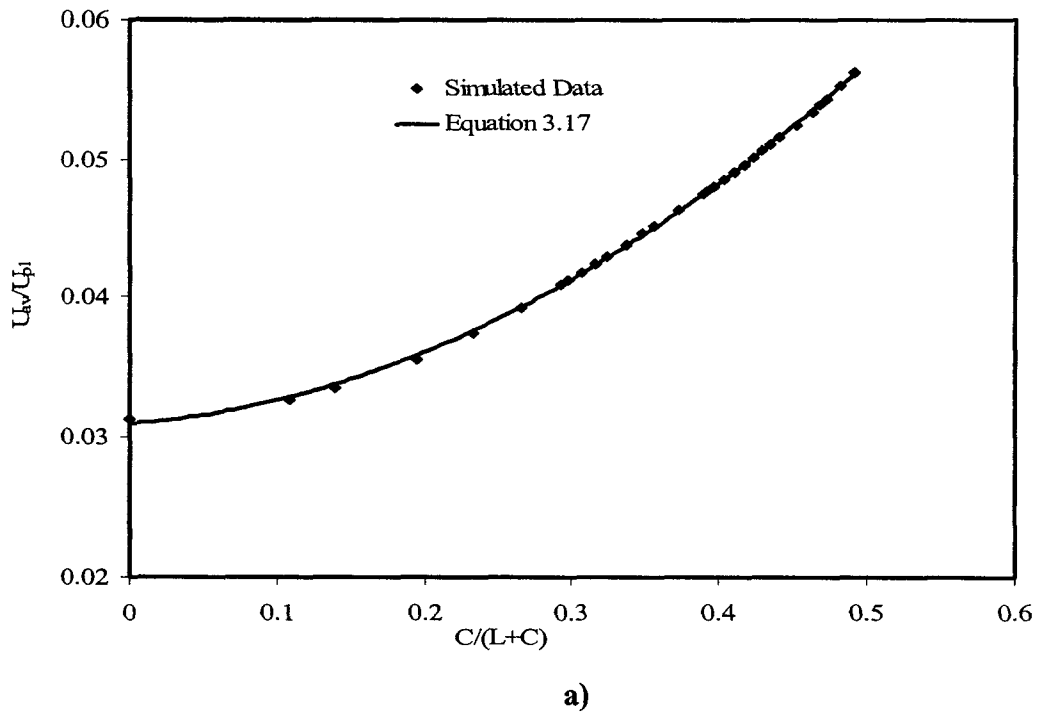


**Figure 3-9(a & b): Cross-sectional average velocity curves as a function of perimetric shape factor: a) laminar, b) turbulent**

### 3.5 CONCLUSIONS

New models for calculating laminar and turbulent air flow field due to the events of pressure gradient along circular sanitary sewers have been presented. The turbulent modeling approach takes into consideration the turbulence-driven secondary currents associated with the sewer headspace cross-section. Therefore the Reynolds equations governing the air flow field are closed with an anisotropic closure model which comprises the use of the eddy viscosity concept for turbulent shear stresses and semi-empirical relations for the turbulent normal stresses. The resulting formulations are numerically integrated using a Galerkin finite element method. The turbulent model is first validated with experimental data reported in the literature and then used to develop cross-sectional average longitudinal velocity curves and formulae that can be used for calculating either air flow rate or velocity along a given sewer reach. The model gives good secondary flow patterns as well as longitudinal velocity distribution in the sewer atmosphere. Similar curves and formulae are also developed for calculating the cross-sectional average velocity in laminar flow regime.

The following conclusions are particularly drawn from the simulations:

- The maximum local streamwise velocity occurs mid way between the curved and water surface in laminar flow. However, in turbulent flow regime the maximum value shifts closer to the water surface than the

curved wall. The maximum global longitudinal velocity however occurs at the centre-line of the headspace in both regimes.

- The transverse laminar velocity distribution across the duct follows a parabolic trend. The turbulent velocity profiles follow neither the parabolic nor the power law profiles.
- The secondary velocities computed are generally within 6-10 % of the bulk streamwise velocity and only causes minimal displacements of the headspace isovels. The strength of the secondary velocities is found to increase with decreasing headspace depth.
- The variation of the longitudinal bulk velocity with perimetric shape factor is found to be explicitly quadratic in laminar flow regime and non-linear in turbulent flow case.

The work presented in this paper is only valid for cases where the sewer pipe walls are smooth and also where the section under study is far removed from junctions where the fully-developed flow assumption breaks down. In some operating sewer conduit systems, wastewater drag and pressure forces might act altogether to sustain air movement. Under such circumstance the combined mechanisms of the two forces have to be modelled. This is the objective of the paper presented in Chapter 4 of this thesis.

## REFERENCES

- ASCE. 1989. Sulphide in wastewater collection and treatment systems. ASCE Manuals and Reports on Engineering Practice, No. 69.
- Bowker, R. P. G., Smith, J. M., Webster, N. A. 1989. Odor and corrosion control in sanitary sewerage systems and treatment plants. Hemisphere Publishing Corporation, N. Y.
- Czernuszenko, W., Rylov, A. A. 2002. Modeling of three-dimensional velocity field in open channel flows. *Journal of Hydraulic Research*, **40** (2): 135-143.
- Demuren, A. O., Rodi, W. 1984. Calculation of turbulence-driven secondary motions in non-circular ducts. *Journal of Fluid Mechanics*. **140**: 189-222.
- Deuffhard, P., Freund, R., Walter, A. 1990. Fast secant methods for the iterative solution of large non-symmetric linear systems. *IMPACT Comp. Sci. Eng.* **2**: 244-276.
- Edwini-Bonsu, S., Steffler, P. M. 2004. A physically-based model for computing natural ventilation rate in sanitary sewer atmosphere. WEF/A & WMA Odors and Air Emission Conference, Bellevue, Seattle.
- Edwini-Bonsu, S., Steffler, P. M. 2003. Air flow in sanitary sewer conduits due to wastewater drag: A CFD approach. *J. Environ. Eng. Sci.* Accepted.
- FEMLAB. 2002. Version 2.3a. Comsol Inc.
- Gerard, R. 1978. Secondary flow in non-circular conduits. *Journal of the Hydraulic Division, ASCE*. **104** (HY5): 603-616.
- Hoohlo, C. A. 1994. A numerical and experimental study of open channel flow in



- a pipe of circular cross-section with a flat bed. PhD. Thesis, University of Newcastle.
- Naot, D., Rodi, W. 1982. Calculation of secondary currents in channel flow. *Journal of Hydraulic Engineering, ASCE*. **108**: 948-968.
- Nezu, I., Nakagawa, H. 1993. *Turbulence in open-channel flows*. A. A. Belkema, Rotterdam.
- Odor and Corrosion Technology Consultants, Inc. 1999a. The use of modeling techniques to evaluate and correct odour releases from trunk sewers. TM No.4, City of Edmonton Odour Control Project, Alberta.
- Odor and Corrosion Technology Consultants, Inc. 1999b. Trunk sewer odour monitoring program. TM No.1, City of Edmonton Odour Control Project, Alberta.
- Olson, D. 1996. Gas exchange rates between industrial process drains and the ambient atmosphere. MSc. Thesis, University of Texas.
- Olson, D., Rajagopalan, S., Corsi, R. L. 1997. Ventilation of industrial process drains: mechanisms and effects on VOC emissions, *Jr. Env. Eng.* **123** (9): 939-947.
- Pescod, M. B., Price, A. C. 1978. A study of sewer ventilation for the Tyneside sewerage scheme. Final research report, Department of Civil Engineering, University of Newcastle upon Tyne, U. K.
- Pescod, M. B., Price, A. C. 1981. Fundamentals of sewer ventilation as applied to the Tyneside sewerage scheme. *Water Pollution Control*: **90** (1): 17-33.
- Pescod, M. B., Price, A. C. 1982. Major factors in sewer ventilation. *J. Water*

- Pollution Control Fed. **54** (4): 385-397.
- Pomeroy, R. 1945. Pros and cons of sewer ventilation. Sewage Works Journal, **17**(2): 203-208.
- Quigley, C. J., Corsi, R. L. 1995. Emission of VOCs from a municipal sewer. J. Air and Waste Mgmt. Assn. **45** (5): 395-403.
- Robert, J-L, Khelifi, M., Ghanmi, A. 1998. Use of the mixing length concept to correctly reproduce velocity profiles of turbulent flows. Can. J. Civ. Eng. **25**: 232-240.
- Rodi, W. 1984. Turbulence models and their application in hydraulics. A state of the art review. International Association for Hydraulic Research, Delft, the Netherlands.
- Sterling, M. 1998. A study of boundary shear stress, flow resistance and the free overfall in open channels with a circular cross section. PhD. Thesis, University of Birmingham.
- Thistlethwayte, D. K. B. (Ed.). 1972. The control of sulphides in sewerage systems. Butterworths, Sydney.
- Tominaga, A., Nezu, I., Ezaki, K., Nakagawa, H. 1989. Three-dimensional turbulent structures in straight open channel flows. Journal of Hydraulic Research. **27** (1): 149-173.
- U. S. Environmental Protection Agency (EPA). 1994. Air emission models for waste and wastewater. EPA-453/R-94-080A-Part 1.
- Wilcox, D. C. 2000. Turbulence modeling for CFD. 2<sup>nd</sup> ed. DCW Industries, Inc., California, U. S.

---

**CHAPTER FOUR<sup>3</sup>**

**COMBINED EFFECTS OF WASTEWATER**

**DRAG AND PRESSURE GRADIENT ON AIR FLOW**

**IN SANITARY SEWER CONDUITS**

---

#### **4.1 INTRODUCTION**

The airspace above flowing wastewater in municipal wastewater collection conduits contains varying concentrations of hydrogen sulphide and volatile organic compounds (VOCs). Effects of these gaseous products are various and include toxicity, odour nuisance, explosion hazards and acid attack of the sewer fabric and appurtenances (Zytner et al. 1997). Municipal engineers often fail to understand the relatively complex relationships between wastewater characteristics, sulphide production biology and chemistry, corrosion biology and ventilation dynamics. This paper is concerned with the headspace ventilation phenomenon. There are several published accounts of the effects of sewer headspace air dynamics on these hazardous- and odorous-compounds. Quigley and Corsi (1995) completed pilot studies to determine stripping efficiencies for a

---

<sup>3</sup> **The main content of this chapter is submitted for publication in the J. of Envir. Engrg. ASCE; Some model results are also presented at WEF/A & WMA Odors & Air Emission Conference, Bellevue, Seattle, 2004.**

wide range of volatile tracers. Their study indicated that headspace ventilation has a significant impact on VOC stripping, particularly for lower volatility chemicals. Whitmore and Corsi (1994) also undertook tracer experiments in an in-service municipal sewer to back-calculate mass transfer coefficients. Results were used to determine half-lengths, i.e., lengths of sewer reach necessary to strip 50 % of 1,1,1-trichloroethene. Calculated half-lengths were determined to be extremely sensitive to the headspace ventilation rate, particularly for poorly ventilated sewers. Olson et al. (1997) reported that the air exchange rate between sewer and ambient atmospheres is a prime parameter in the estimation of VOC emissions when coupled with the knowledge of air-water mass transfer or the assumption of equilibrium. It has been reported also that hydrogen sulphide build-up in sewer air does not only relate to the sulphide concentrations in the flowing sewage, but more importantly with other factors, such as turbulence, aerodynamic conditions of the ventilating air flow and roughness of the unsubmerged surfaces (Matos and de Sousa 1992).

Previous researchers have identified wastewater drag, differential wind speed and barometric pressure gradient as the primary factors responsible for natural ventilation and pressurization in sanitary sewer conduits (Corsi et al. 1989; Odor and Corrosion Technology Consultants 1999b; Olson 1996; Olson et al. 1997; Pescod and Price 1978, 1981, 1982; Pomeroy 1945; Thistlethwayte 1972; USEPA 1994). Wastewater flowing down sewer transfers momentum to the airspace due to the interfacial shear force and causes air to flow. Differential wind speed and

barometric pressure can also set up dynamic pressure gradients and cause air to move. These driving forces do not only accelerate the sewer air along the pipe, but also cause air ejection and hence odour release via available opening. Thistlethwayte (1972) referenced a set of observations made in 1933 in London from a two-mile length sewer reach with a diameter from 2 to 9 feet. No barometric measurements were reported, but it was observed that average air velocities exiting the sewer at road level were consistently between 1.0-2.0 m/s. Thistlethwayte (1972) also referenced an Austrian study which included observations of natural ventilation from sewers over a period of several years. Average air velocities ranged from as low as 0.2 m/s to as high as 4.3 m/s. In addition to the natural forces, some sewer systems such as deep trunk and interceptor sewers where dropstructures are an integral part of the physical system structures, significant pressurization of the downstream sewer conduits can result (Odor and Corrosion Technology Consultants 1999b). Sewer conduit headspace can also be pressurized by scrubbers/blowers which are usually used to combat corrosive, odorous and other hazardous gases.

Pescod and Price (1978) performed experimental studies on a sewer model reach to study the combined effects of wind speed and wastewater drag, but no mathematical model was developed. The Water Environment Research Foundation in 1998 undertook a laboratory investigation and field demonstration of the various ventilation dynamics using tracer gas techniques (Odor and Corrosion Technology Consultants 1999a). The study quantified and ranked the

relative importance of water flow rate (water velocity and volume) and wind eduction over sewer shaft on sewer ventilation rates. It was concluded that wind eduction over open sewer shaft was the primary driving force for sewer ventilation and that wastewater friction drag was a secondary motive force. However, no mathematical models were developed to describe the movement of air into, out of, or along the sewer. Also in use is a commercial air-transport computer model (KYGas) which helps identify the dynamics of air movement through sewers (Odor and Corrosion Technology Consultants 1999a). This model assumes that there is no wastewater in the sewer pipe which is a serious handicap for the accurate prediction of sewer ventilation dynamics. Some empirical and mathematical models are also available for computing wastewater-driven average velocity (e.g. Pescod and Price 1978; USEPA 1994; Olson 1996; Olson et al. 1997). These models are based on 1-D formulations and do not represent the headspace cross-section and driving forces appropriately. Edwini-Bonsu and Steffler (2003, 2004b) (also Chapters 2 and 3 of this thesis) have successfully developed models based on the results of computational fluid dynamics (CFD) for studying the individual effects of wastewater drag and differential pressure on air movements in sewer conduits, but not the combined effects. Their models have been validated with encouraging results and can be used to provide quantitative accounts of ventilation and pressurization in sewer atmosphere under the individual motive forces. Olson (1996) also proposed a method for calculating the cross-sectional average air velocity due to the simultaneous ventilating mechanisms of liquid drag and wind speed based on a simple algebraic

superposition of the individual effects. It must however be stressed here that the simple addition of individual effects may not be generally valid particularly in a turbulent flow regime where the degree and scales of turbulence may depend upon the driving mechanisms.

The main purpose of this paper is to provide municipal engineers and experts with a tool for the prediction of the air flow field in sewer conduits due to the simultaneous effects of wastewater drag and differential pressure. The models developed here are based on the Reynolds-averaged transport equations (with incompressible, fully-developed and steady-state assumptions) and a turbulence closure model. In fact, there are two models for the turbulent stresses: The first model stems from a 2-D eddy viscosity-mixing length formulation for the turbulent shear stresses and the second one which deals with the turbulent normal stresses incorporates empirical formulae based on precise measurements of turbulent quantities. Solution of the resulting set of equations is implemented in a finite element framework. The analysis of the flow field is conceptually viewed as a 2-D Poiseuille-Couette flow where the effect of wastewater is formulated as a boundary condition at the air-wastewater interface and that of pressure motive forces is represented as a pressure gradient in the longitudinal momentum equation. To ensure that most flow situations are covered, laminar flow regime is also considered. The models are used to develop generalized bulk velocity curves (in the case of a turbulent flow regime) and formula (in the case of a laminar flow regime) for use in practice. Interfacial drag coefficients are also predicted.

## 4.2 MATHEMATICAL FORMULATION

### 4.2.1 Governing Equations

Three-dimensional, steady, incompressible, turbulent flow in channels can be described by the Reynolds-averaged-Navier-Stokes equations. Mean continuity and momentum equations, written in Cartesian tensor notation, take the following form:

-Continuity equation

$$\frac{\partial U_i}{\partial x_i} = 0 \quad [4.1]$$

- Momentum equation in the  $i$ -direction

$$U_j \frac{\partial U_i}{\partial x_j} = -\frac{1}{\rho} \frac{\partial P}{\partial x_i} + \nu \frac{\partial^2 U_i}{\partial x_j \partial x_j} - \frac{\partial \overline{u'_i u'_j}}{\partial x_j} \quad [4.2]$$

Here,  $U_i$  ( $i = 1, 2, 3$ ) = ( $U, V, W$ ) and  $u'_i$  are the mean and fluctuating velocities in the  $x_i$  direction, respectively,  $\overline{u'_i u'_j}$  is the Reynolds stress tensor,  $P$  is the piezometric pressure,  $\nu$  and  $\rho$  are respectively the kinematic viscosity and density of air. A notation of  $x$  for the horizontal (longitudinal),  $y$  for the vertical and  $z$  for the lateral co-ordinates as well as  $U$ ,  $V$ ,  $W$  for corresponding velocity components will be used further in the paper. Note that  $V$  and  $W$  are the secondary velocities due to the anisotropy of turbulence. Figure 4-1 shows a theoretical model of a partially-full, gravity-flow circular sewer conduit, including the co-ordinate system and nomenclature. In the figure the wind speeds at the two



openings are denoted by  $V_{w1}$  and  $V_{w2}$ , and the pressures at the ends of the sewer pipe resulting from any of the motive forces (other than wastewater drag) are denoted by  $P_1$  and  $P_2$ . It should be noted that the air flow direction can be in any direction as shown in the figure.

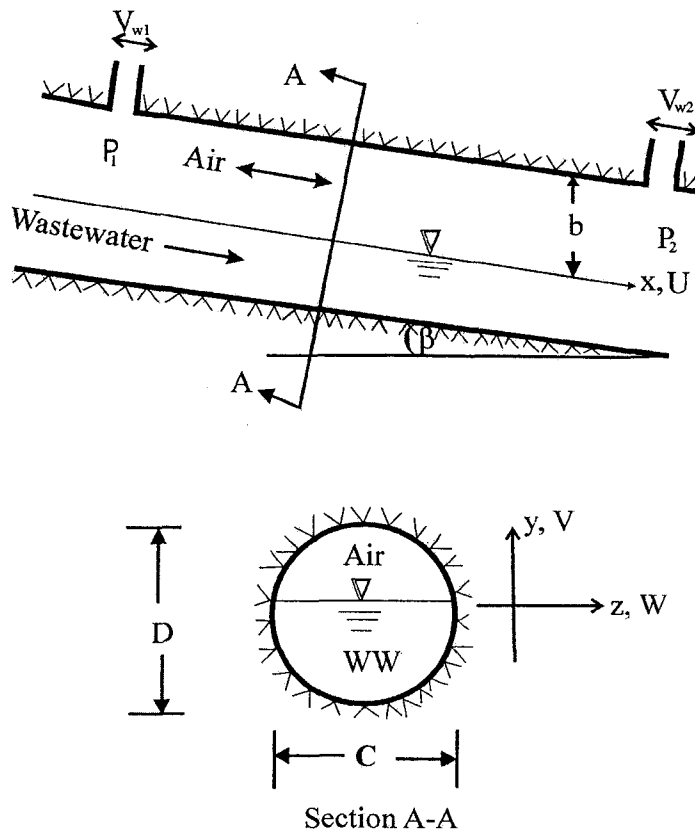


**Figure 4-1: Sewer atmosphere subjected to both pressure gradient and wastewater drag**

The Reynolds stresses  $\overline{u'_i u'_j}$  in the mean flow equations have to be modelled. Due to the anisotropy of turbulence associated with the flow in the sewer atmosphere, both shear and normal stresses have to be calculated. Rodi (1984)

and Wilcox (2000) give authoritative reviews of turbulence modeling based on Reynolds-averaging. Most popular turbulence closure models are based on the Boussinesq's eddy viscosity concept. However, the eddy viscosity concept is limited by its inability to predict the anisotropy of turbulence. This drawback can be accounted for by the use of universal semi-empirical models (Gerard 1978; Tominaga et al. 1989; Czernuszenko and Rylov 2002) in conjunction with the eddy viscosity closure. This composite version is used in this paper as discussed below.

#### 4.2.2 Modeling the Reynolds Stress Tensor

The Reynolds shear stresses are calculated using eddy viscosity-mixing length hypothesis whilst the turbulent normal stresses are modelled using semi-empirical relations. The eddy viscosity concept for the shear stresses can be expressed as:

$$-\overline{u_i u_j} = \nu_t \left( \frac{\partial U_i}{\partial x_j} + \frac{\partial U_j}{\partial x_i} \right), \quad i \neq j \quad [4.3]$$

where the turbulent viscosity,  $\nu_t$ , is in turn modelled using the mixing length model (Rodi 1984, Chapter 2):

$$\nu_t = \ell_m^2 \left[ \left( \frac{\partial U_i}{\partial x_j} + \frac{\partial U_j}{\partial x_i} \right) \frac{\partial U_i}{\partial x_j} \right]^{\frac{1}{2}} \quad [4.4]$$

where  $\ell_m$  is the mixing length. The mixing length  $\ell_m$  is evaluated using the Robert et al. (1998)'s bi-harmonic model given as:

$$\nabla^2 (\nabla^2 \ell_m) = 0 \quad [4.5]$$

with the modified boundary conditions given as (Chapter 2):

$$\bar{n}(\Delta \ell_m) = -\kappa [1 - (1 + S(n)) \text{Exp}(S(n))] \text{ and } \ell_m = 0 \quad [4.6]$$

where  $S(n) = -nu_\tau / \nu A$ ,  $A = \text{empirical constant} = 26$ ,  $\kappa$  is von Karman constant and  $\bar{n}$  is a unit normal vector outside the domain of the boundary.

Several authors (e.g. Tominaga et al. 1989; Nezu and Nakagawa 1993) have published semi-empirical relations for the turbulence intensities (r.m.s of turbulent velocities) in two-dimensional, fully-developed closed-channel and open-channel flows. These relations are usually in the form of an exponential law as:

$$\frac{u_i'}{u_\tau} = A_i \exp(-B_{i\xi} \xi), \quad i = j \quad [4.7]$$

in which  $A_i (i=1,2,3)$  and  $B_{i\xi}$  are empirical constants,  $\xi$  is a dimensionless coordinate measured from the boundary,  $u_\tau$  is the boundary shear velocity,  $u_i' (i=1,2,3)$  are intensities of turbulence in longitudinal, vertical and lateral direction, respectively. Tominaga et al. (1989) evaluated the empirical constants for the vertical and lateral intensities for a closed-channel and obtained:

$$\sqrt{v'^2}(y) = u_\tau \left( A_{vy} e^{-B_{vy} \frac{y}{h}} \right) \quad [4.8]$$

$$\sqrt{w'^2}(y) = u_\tau \left( A_{wy} e^{-B_{wy} \frac{y}{h}} \right) \quad [4.9]$$

where  $h$  is the depth of the channel. The constants were calibrated as  $A_{wy} = 1.45$ ,  $A_{vy} = 1.15$ ,  $B_{vy} = 0.92$  and  $B_{wy} = 0.69$ . These values are proved to be

independent of the flow Reynolds number. Again, following Tominaga et al. (1989) or as explained in Chapter 2, these normal stresses are extended using a weighted average method to the present cross-section as:

$$\sqrt{v'^2} = \left( \sqrt{v'^2}(n_i) \right)^{\Gamma_{n_i}} \left( \sqrt{v'^2}(n_w) \right)^{\Gamma_{n_w}} \quad [4.10]$$

$$\sqrt{w'^2} = \left( \sqrt{w'^2}(n_i) \right)^{\Gamma_{n_i}} \left( \sqrt{w'^2}(n_w) \right)^{\Gamma_{n_w}} \quad [4.11]$$

wherein the contribution from each boundary is expressed as:

$$\sqrt{v'^2}(n_i) = u_{ai} \left( A_{vn} e^{-B_{vn} n_i} \right), \quad \sqrt{v'^2}(n_w) = u_{aw} \left( A_{vn} e^{-B_{vn} n_w} \right) \quad [4.12]$$

$$\sqrt{w'^2}(n_i) = u_{ai} \left( A_{wn} e^{-B_{wn} n_i} \right), \quad \sqrt{w'^2}(n_w) = u_{aw} \left( A_{wn} e^{-B_{wn} n_w} \right) \quad [4.13]$$

where

$\Gamma_{n_i} = n_w / (n_w + n_i)$ ,  $\Gamma_{n_w} = n_i / (n_w + n_i)$ ,  $A_{wn} = 1.45$ ,  $A_{vn} = 1.15$ ,  $B_{wn} = 0.92$  and  $B_{vn} = 0.69$ .  $n_i$  and  $n_w$  are dimensionless normal distances from the interface and the wall, respectively.

## 4.3 SOLUTION PROCEDURE

### 4.3.1 Modeling the Ventilating Forces

In this paper the sewer headspace flow field is analysed as 2-D Poiseuille-Couette flow. The wastewater drag is prescribed as a Dirichlet boundary condition and consequently the momentum transfer from the air to the underlying water is neglected. Following Edwini-Bonsu and Steffler (2003) (also Chapter 2 of this

thesis), the interfacial boundary conditions for the mean longitudinal velocity in laminar and turbulent flow regimes are respectively given as:

$$U = U_w \quad [4.14]$$

$$U = U_{wc} \left( \frac{C - 2|z|}{C} \right)^{1/4} \quad [4.15]$$

where  $U_w$  is the average velocity at the interface,  $U_{wc}$  is the water surface velocity at channel center and  $C$  is the interfacial width. In modeling the laminar flow, it is assumed that the air-water interface is devoid of interfacial waves and therefore the assumptions of smooth interfacial boundary and constant interfacial drag are satisfactory. In the turbulent case, it is assumed that the interfacial waves are well-organized and of small amplitudes (Chapter 2).

Differential wind speed and barometric pressure, and pressurization due to dropstructures and scrubber/blower are represented as pressure gradient ( $dP/dx$ ) in the longitudinal mean momentum equation as in Edwini-Bonsu and Steffler (2004b) (Chapter 3 of this thesis). We should note that the pressure forces determine the overall air flow direction since in an operating sewer system the pressure gradient could belong to adverse, favorable or zero regime.

### 4.3.2 Numerical Modeling

Equations [4.1]-[4.6], and [4.10]-[4.13] constitute a closed system. In order to present generalized solutions, the governing equations are appropriately non-dimensionalized. If a dimensionless parameter  $\lambda = (-dP/dx)b/(\rho U_{wc}^2)$  and a

length scale equal to the maximum headspace depth  $b$  are defined, then equations for the turbulent flow yield a set of non-dimensionalized equations in fully-developed flow regime as:

Momentum:

$$X_*: V_* \frac{\partial U_*}{\partial Y_*} + W_* \frac{\partial U_*}{\partial Z_*} - \frac{\partial}{\partial Y_*} \left[ (1/\text{Re} + v_{t*}) \frac{\partial U_*}{\partial Y_*} \right] - \frac{\partial}{\partial Z_*} \left[ (1/\text{Re} + v_{t*}) \frac{\partial U_*}{\partial Z_*} \right] = \lambda \quad [4.16]$$

$$Y_*: V_* \frac{\partial V_*}{\partial Y_*} + W_* \frac{\partial V_*}{\partial Z_*} - \frac{1}{\text{Re}} \left[ \frac{\partial^2 V_*}{\partial Y_*^2} + \frac{\partial^2 V_*}{\partial Z_*^2} \right] = -\frac{\partial P_*}{\partial Y_*} - \frac{\overline{v_*'^2}}{\partial Y_*} + \frac{\partial}{\partial Z_*} \left[ v_{t*} \left( \frac{\partial V_*}{\partial Z_*} + \frac{\partial W_*}{\partial Y_*} \right) \right] \quad [4.17]$$

$$Z_*: V_* \frac{\partial W_*}{\partial Y_*} + W_* \frac{\partial W_*}{\partial Z_*} - \frac{1}{\text{Re}} \left[ \frac{\partial^2 W_*}{\partial Y_*^2} + \frac{\partial^2 W_*}{\partial Z_*^2} \right] = -\frac{\partial P_*}{\partial Z_*} - \frac{\overline{w_*'^2}}{\partial Z_*} + \frac{\partial}{\partial Y_*} \left[ v_{t*} \left( \frac{\partial V_*}{\partial Z_*} + \frac{\partial W_*}{\partial Y_*} \right) \right] \quad [4.18]$$

Continuity:

$$\frac{\partial V_*}{\partial Y_*} + \frac{\partial W_*}{\partial Z_*} = 0 \quad [4.19]$$

where

$$v_{t*} = \ell_{m*}^2 \left[ \left( \frac{\partial U_*}{\partial Y_*} \right)^2 + \left( \frac{\partial U_*}{\partial Z_*} \right)^2 + 2 \left( \frac{\partial V_*}{\partial Y_*} \right)^2 + 2 \left( \frac{\partial W_*}{\partial Z_*} \right)^2 + \left( \frac{\partial V_*}{\partial Z_*} + \frac{\partial W_*}{\partial Y_*} \right)^2 \right]^{\frac{1}{2}} \quad [4.20]$$

and the dimensionless quantities are given as:

$$X_* = x/b, Y_* = y/b, Z_* = z/b, \ell_{m*} = \ell_m/b, U_* = U/U_{wc}, V_* = V/U_{wc},$$

$$W_* = W/U_{wc}, \overline{v_*'^2} = \overline{v'^2}/U_{wc}^2, \overline{w_*'^2} = \overline{w'^2}/U_{wc}^2, R_e = U_{wc}b/\nu. \text{ If } \lambda = 0, \text{ the air is}$$

wastewater-driven.  $\lambda$  could be negative or positive contingent upon the direction of the pressure forces. For negative values of  $\lambda$ , the velocity field can be in the reverse direction in certain portions of the sewer atmosphere.

A system of coupled parabolic equations in  $U_*$ ,  $V_*$ ,  $W_*$  and  $P_*$  results in the turbulent flow case. Due to the non-linear nature of these equations, the solution is implemented using a parametric sweeping algorithm (with the Reynolds number,  $Re$ , as a sweeping parameter) together with a Good Broyden iterative (GBIT) procedure with an exact (analytical) evaluation of the Jacobian derivatives as discussed in Appendix A.

In a fully-developed laminar flow regime, the equation of continuity is satisfied identically and the momentum equations in the directions of  $y$  and  $z$  reduce to a statement that pressure is a constant. The streamwise momentum equation in non-dimensionalized form simplifies to a Poisson-type equation:

$$X_* : -\left(\frac{\partial^2 U_*}{\partial Y_*^2} + \frac{\partial^2 U_*}{\partial Z_*^2}\right) = \alpha \quad [4.21]$$

where  $\alpha = (-dP/dx)b^2/(\rho\nu U_w)$  and  $U_* = U/U_w$ . This equation is discretized subject to the boundary conditions described above. The matrix resulting from the spatial discretization is solved using the Gaussian elimination method.

#### 4.4 SIMULATIONS AND DISCUSSIONS

Currently there is no headspace velocity data for validating the case where wastewater and pressure gradient act altogether. Since the same models have been validated with experimental data under the individual effects in Chapters 2 and 3, it is assumed here that the models would also perform under the simultaneous

effects of the two forces. Two investigations are undertaken here: velocity field modeling and interfacial drag coefficient predictions.

#### **4.4.1 Velocity Field**

In attempting to validate the finite element models, the laminar flow regime (governed by Equation [4.21]) has been modelled using analytical, finite difference method (FDM) and finite element techniques in preliminary test calculations. The first two methods have been used with the objective of assessing the predictive performance of the FEM discretization scheme, which is the core numerical tool in this paper. In the analytical solution technique, the headspace cross-section and Equation [4.21] are approximately transformed into elliptic orthogonal and conformal curvilinear co-ordinate systems. The resulting equation is subsequently solved using the method of eigenfunction expansion. The FDM approach on the other hand uses the generalized co-ordinate system and further employs the transfinite algebraic grid generation technique to transform the governing equation and the flow geometry into a body-fitted unit-square co-ordinates system that allows co-incidence of all boundary lines with a co-ordinate line. The discretization of the transformed equation is evaluated using central difference formulae. Satisfactory agreements have been obtained between the finite element scheme and the other two methods. Details of the analytical and the finite difference methods as well as their comparisons are given in Appendix A.

Having validated the finite element models this way, we are in a position to use

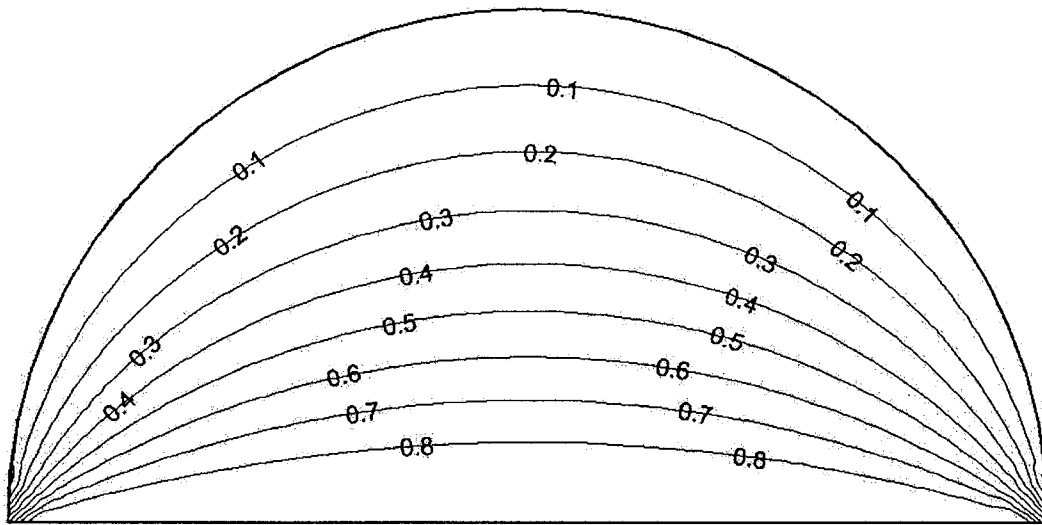


them to perform detailed flow investigations. Both forward and reverse flows are investigated here. Figures 4-2 and 4-3 show simulated non-dimensionalized streamwise isovels in laminar and turbulent flow regimes, respectively for  $b/D=50\%$ . Diagrams in each figure show isovels of separate effects of wastewater drag phenomenon and pressure gradient as well as the combined effect of wastewater drag and pressure gradient. The isovels in Figures 4-2c, 4-2d, 4-3c and 4-3d are due to the simultaneous effects of wastewater drag and pressure gradient. In Figures 4-2d and 4-3d, the effect of positive pressure gradients on the velocity distribution is clearly observed. With application of a positive pressure gradient, the airspace flow field exhibits distinct zones of positive and negative velocity fields. It can be seen that apart from the non-slip conditions on the wall, there are also spots where the streamwise velocity is zero. As might be anticipated, for wastewater-only-driven flows (as shown in Figures 4-2a and 4-3a) the velocity of air is maximum at the surface of the water and decreases with increasing distance from the interface. There is no stagnant air zone and every region is moving in this case.

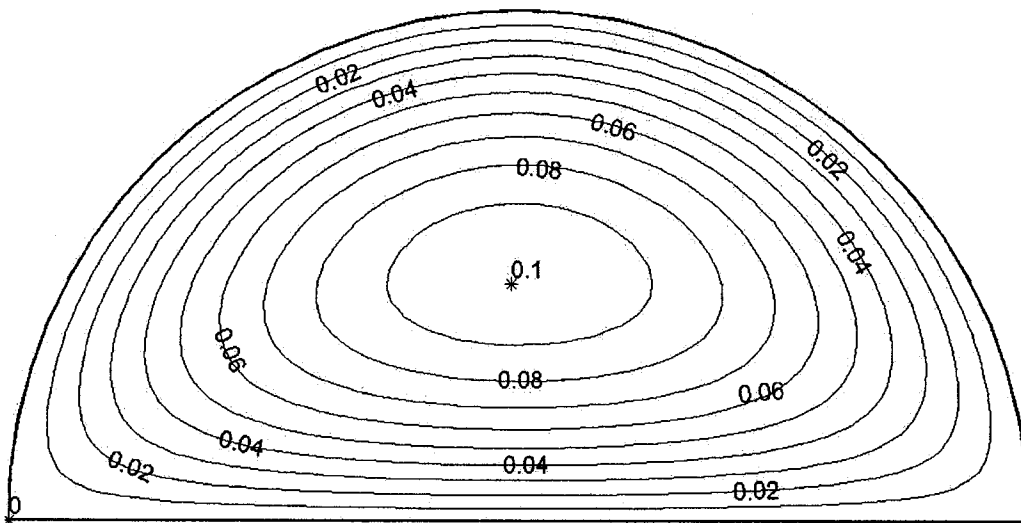
In Figure 4-3, the corresponding secondary velocity vectors are superimposed on the isovels to elucidate the pattern and effects of the secondary currents under individual mechanisms as well as when they are combined. It is evident that the pattern of the secondary flow is independent of the air driving force. There is a single identical secondary flow cell on either side of the vertical plane dividing the headspace into symmetric quadrants. The only apparent observed difference of

the secondary flow lies in the location of the center of the secondary flow cell. It is observed that the centers of the secondary cells shown in these diagrams, to some extent, are located nearer the curved wall than the interface in the presence of a pressure force. The secondary motion is also noted to depress the location of the maximum velocity towards the interface in pressure-driven flows as well as in the combined case. The distortion of the isovels by the secondary current is observed to be strongest in wastewater-driven flows than either pressure-induced or when the two forces act altogether.

In Figures 4-4 to 4-7 the effect of increasing pressure gradient (negative or positive) against a continuously forward moving wastewater drag on air velocity contour distribution is further examined. The isovels in these figures demonstrate that the wastewater drag effect seems subservient to pressure gradient with increasing  $\alpha$  (in laminar regime) or  $\lambda$  (in turbulent regime). This feature is particularly pronounced where there is a large space above low-velocity fluid flow (not shown here).

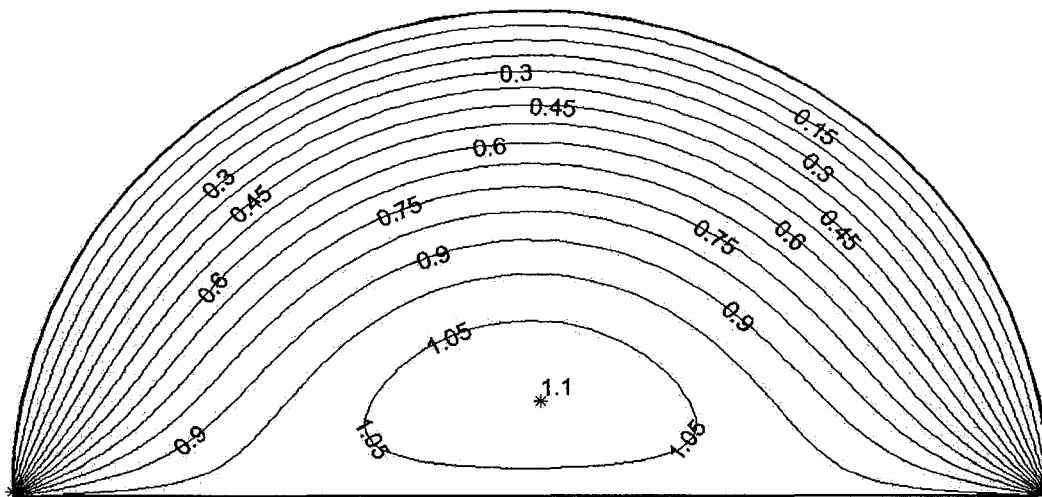


a)

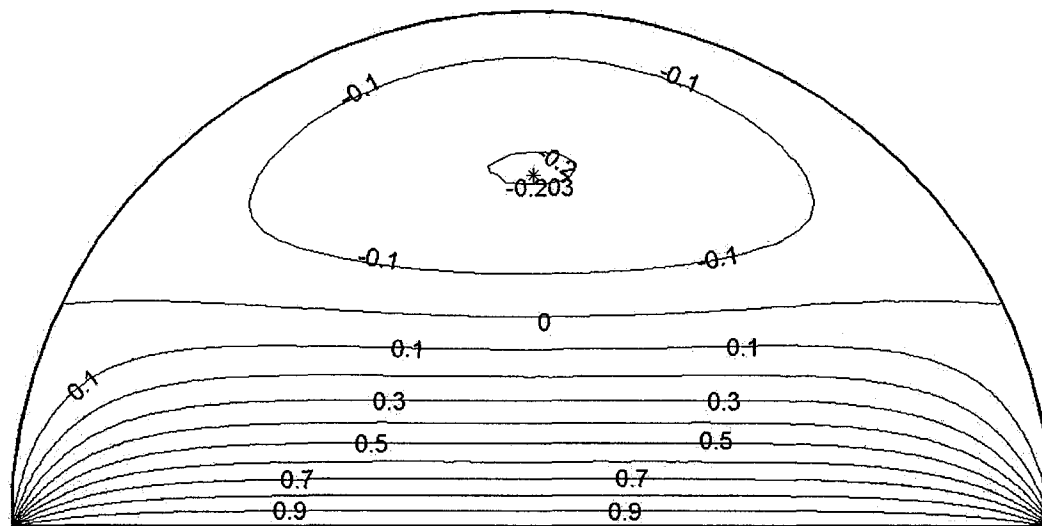


b)

**Figure 4-2(a, b, c & d): Typical non-dimensionalized laminar velocity contour distributions: a) wastewater-driven only,  $\alpha = 0$ , b) pressure-induced only, non-dimensionalized with  $(-dP/dx)b^2/(\rho\nu)$ , c) forward flow, cases a) & b) combined,  $\alpha = 5.35$ , d) reverse flow, cases a) & positive pressure gradient in b) combined,  $\alpha = -5.35$**

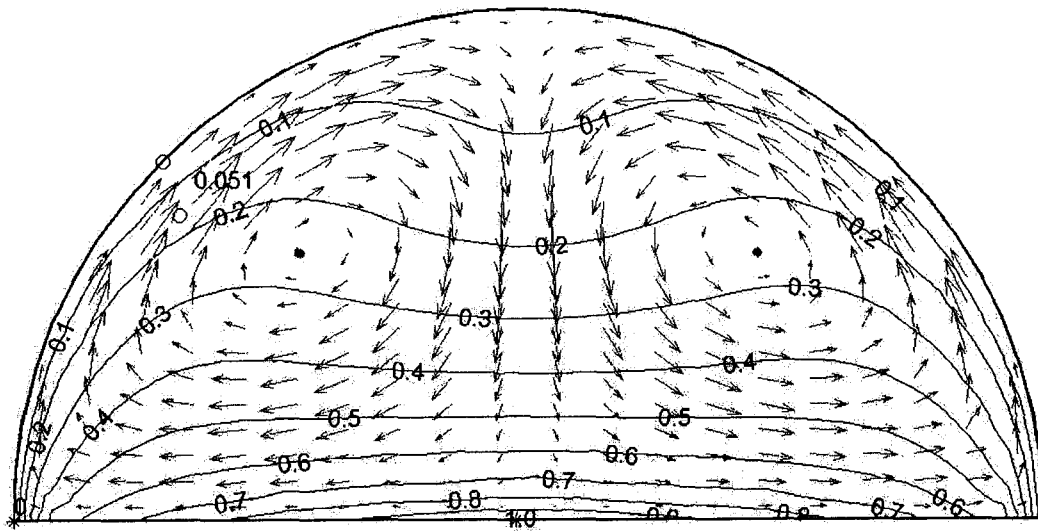


c)

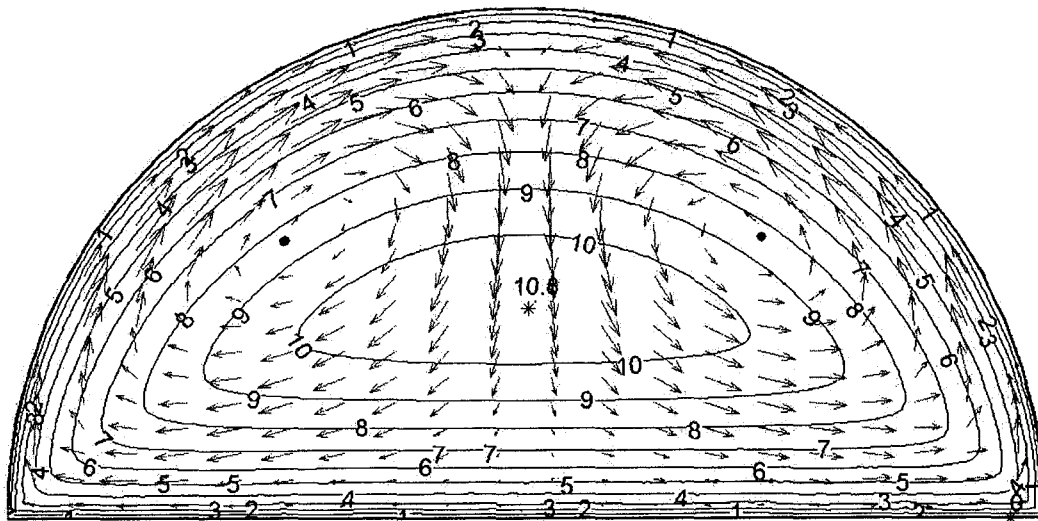


d)

**Figure 4-2(Continued): Typical non-dimensionalized laminar velocity contour distributions: a) wastewater-driven only,  $\alpha = 0$ , b) pressure-induced only, non-dimensionalized with  $(-dP/dx)b^2/(\rho\nu)$ , c) forward flow, a )& b) combined,  $\alpha = 5.35$ , d) reverse flow, a) & positive pressure gradient in b) combined,  $\alpha = -5.35$**



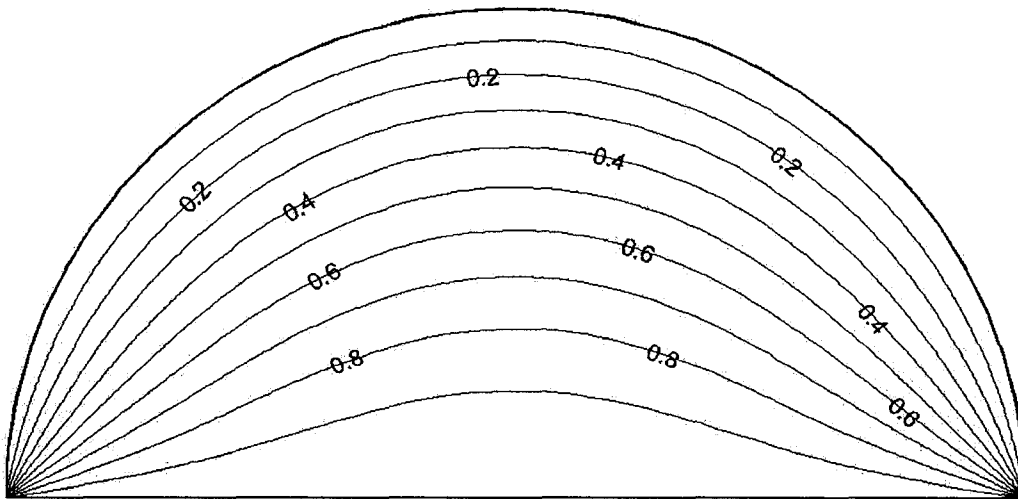
a)



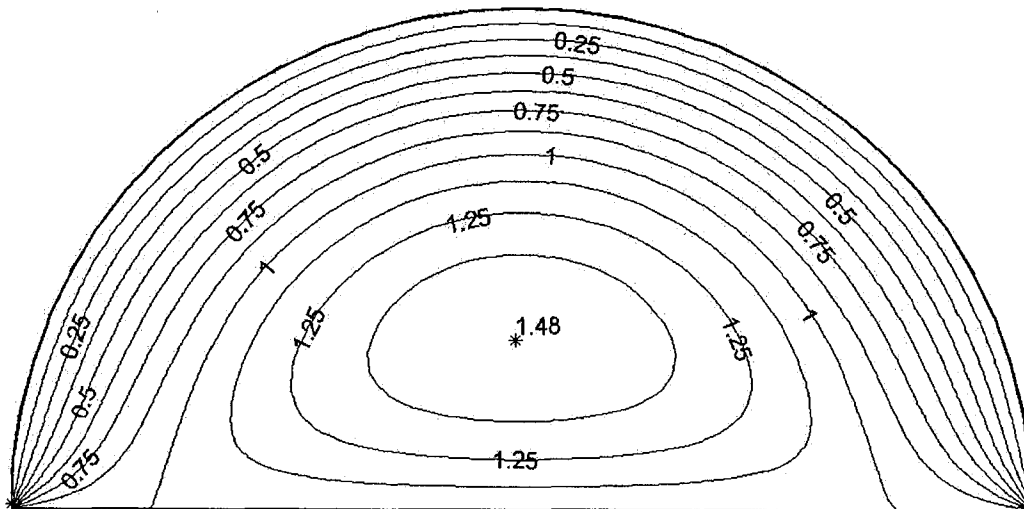
b)

Figure 4-3(a, b, c & d): Typical turbulent velocity contour distributions: a) wastewater-driven only,  $\lambda=0$ , b) pressure-induced only, non-dimensionalized with  $\sqrt{(-dP/dx)b/(\rho)}$ , c) forward flow, cases a) & b) combined,  $\lambda=0.005$ , d) reverse flow, cases a) & positive pressure gradient in b) combined,  $\lambda=-0.005$ . Superimposed on each plot are the corresponding velocity vectors





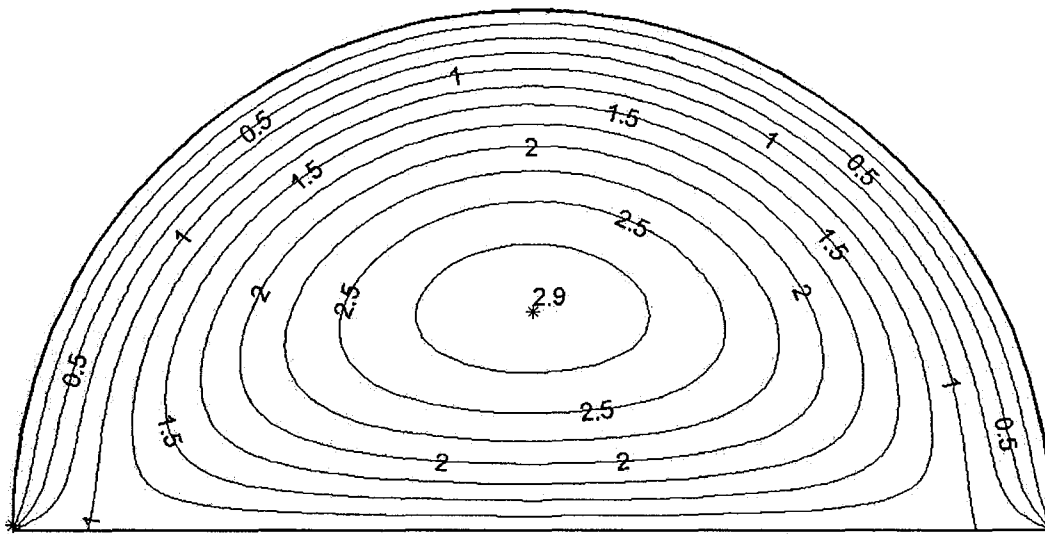
a)



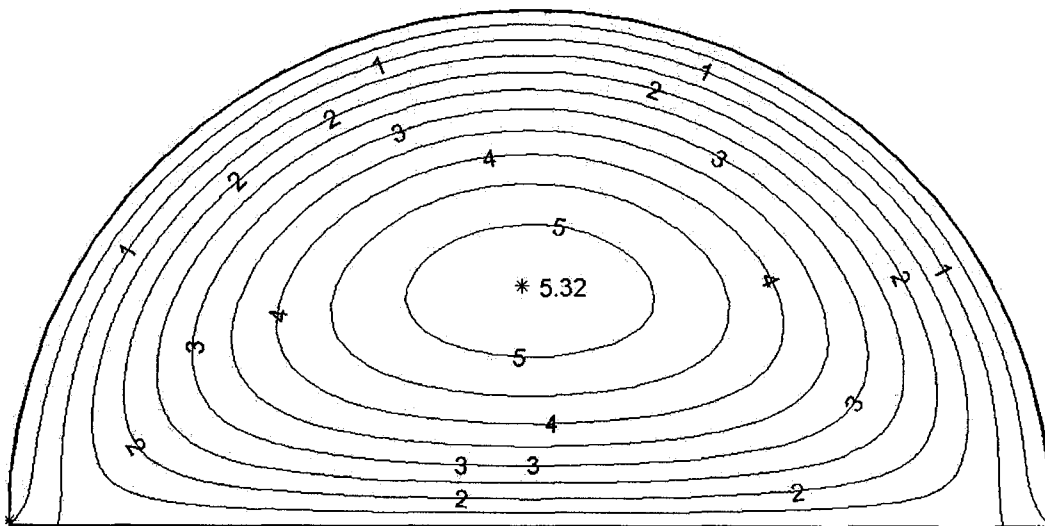
b)

**Figure 4-4(a, b, c & d): Effect of increasing negative pressure gradient against continuously forward moving wastewater on isovels in laminar flow:**

a)  $\alpha = 2.5$ , b)  $\alpha = 10$ , c)  $\alpha = 25$ , d)  $\alpha = 50$



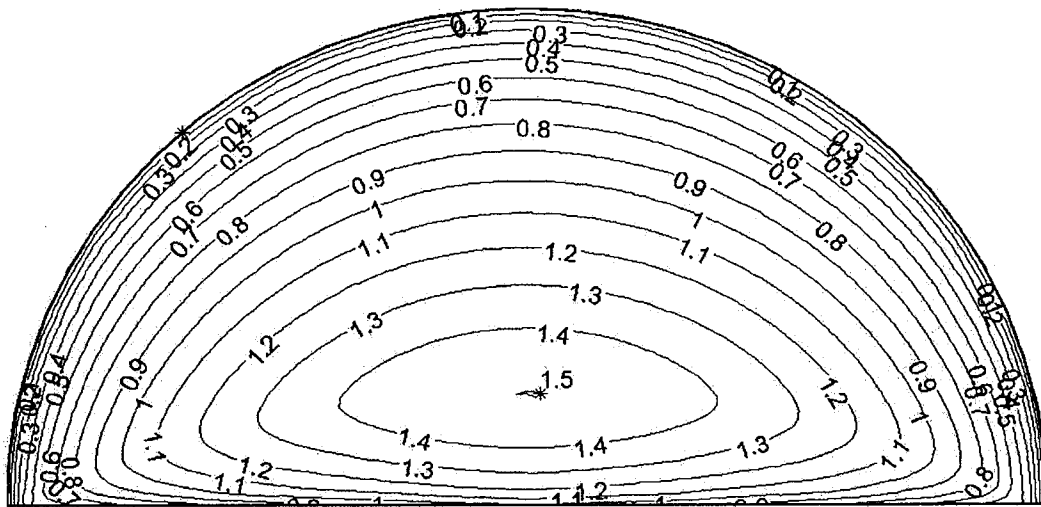
c)



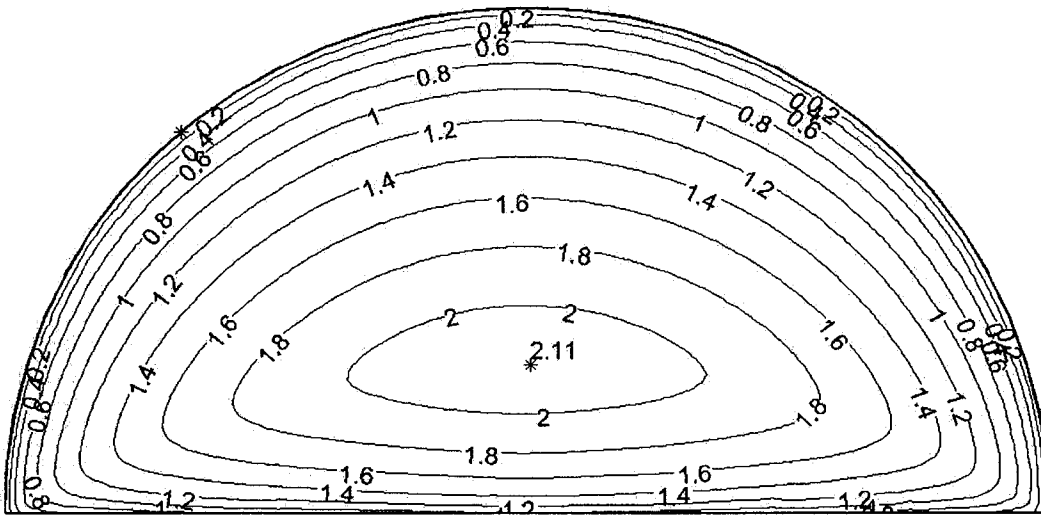
d)

**Figure 4-4(Continued): Effect of increasing negative pressure gradient against continuously forward moving wastewater on isovels in laminar flow:**  
**a)  $\alpha = 2.5$ , b)  $\alpha = 10$ , c)  $\alpha = 25$ , d)  $\alpha = 50$**





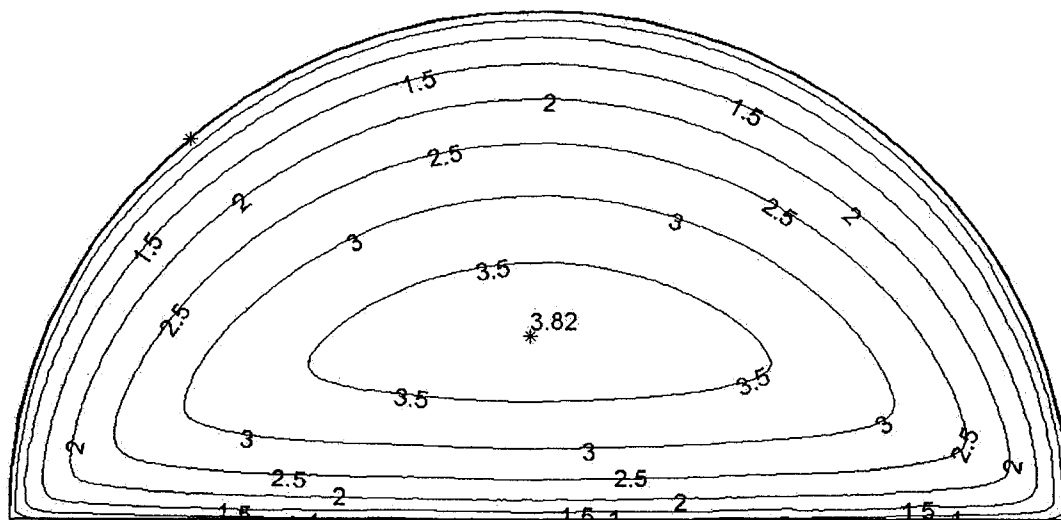
a)



b)

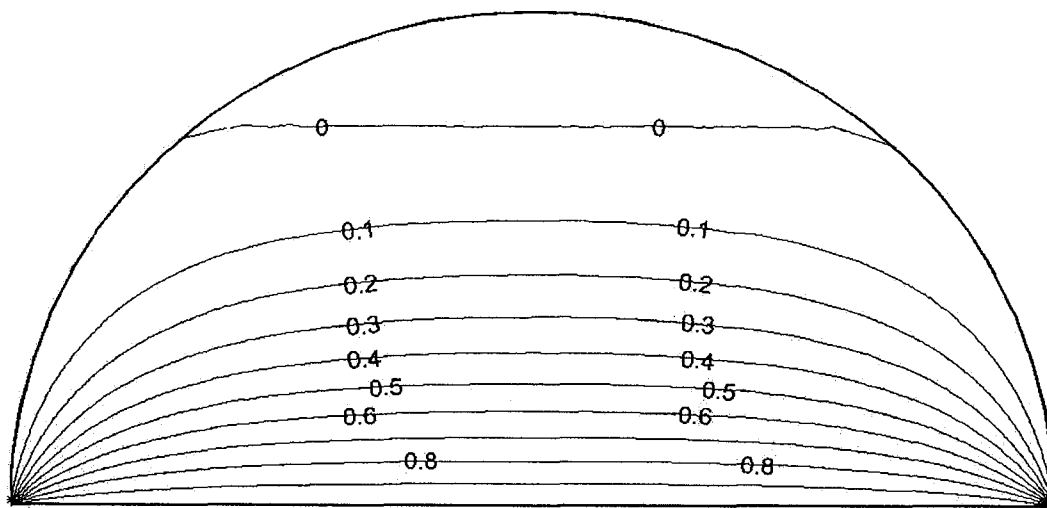
**Figure 4-5(a, b & c): Effect of increasing negative pressure gradient against continuously forward moving wastewater on isovels in turbulent flow:**

a)  $\lambda = 0.01$ , b)  $\lambda = 0.025$ , c)  $\lambda = 0.1$



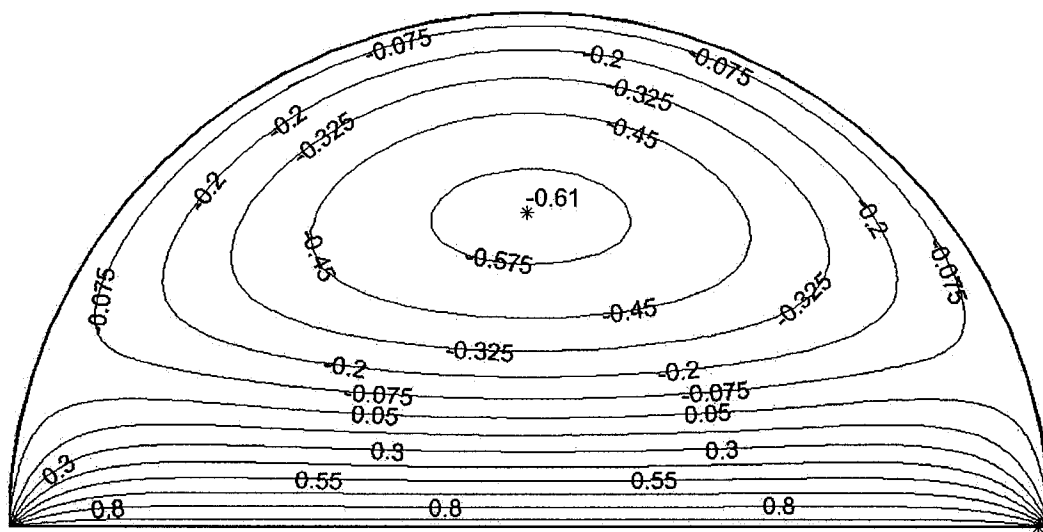
c)

Figure 4-5(Continued): Effect of increasing negative pressure gradient against continuously forward moving wastewater on isovels in turbulent flow: a)  $\lambda = 0.01$ , b)  $\lambda = 0.025$ , c)  $\lambda = 0.1$

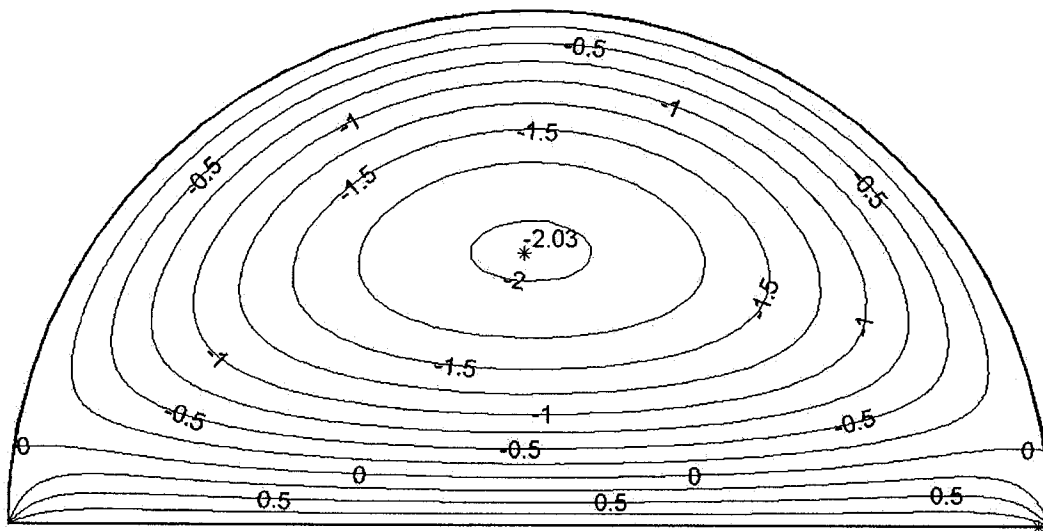


a)

Figure 4-6(a, b, c & d): Effect of increasing positive pressure gradient against continuously forward moving wastewater on isovels in laminar flow: a)  $\alpha = -2.5$ , b)  $\alpha = -10$ , c)  $\alpha = -25$ , d)  $\alpha = -50$



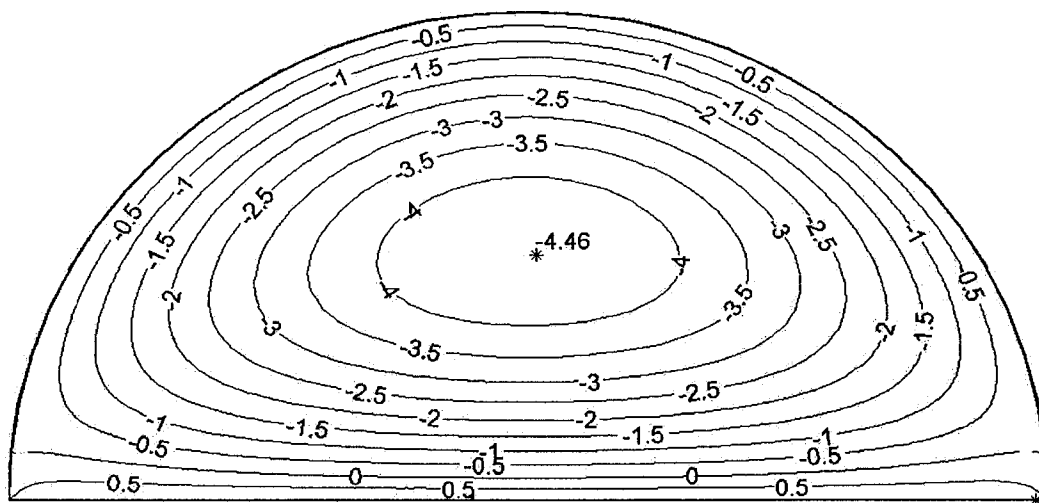
b)



c)

**Figure 4-6(Continued): Effect of increasing positive pressure gradient against continuously forward moving wastewater on isovels in laminar flow:**

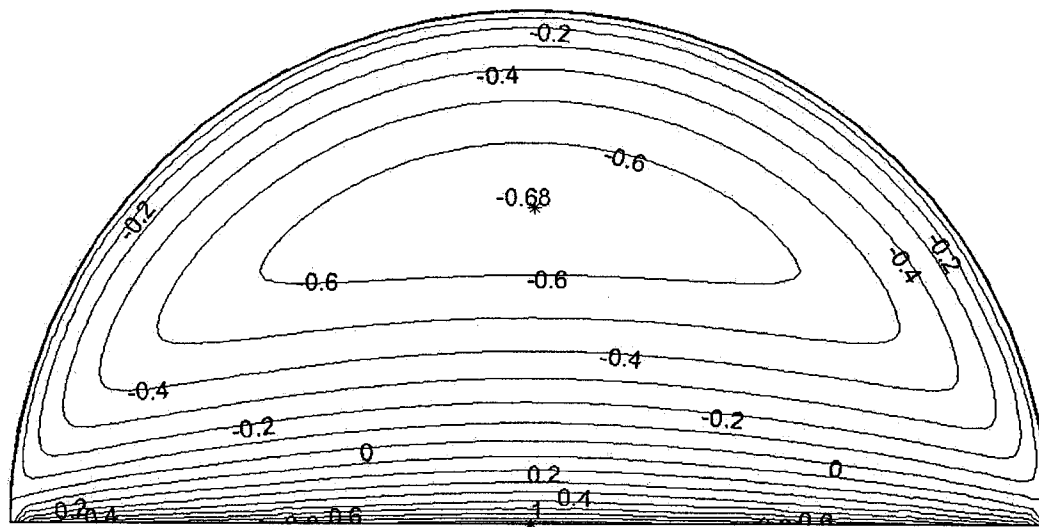
a)  $\alpha = -2.5$ , b)  $\alpha = -10$ , c)  $\alpha = -25$ , d)  $\alpha = -50$



d)

**Figure 4-6(Continued): Effect of increasing positive pressure gradient against continuously forward moving wastewater on isovels in laminar flow:**

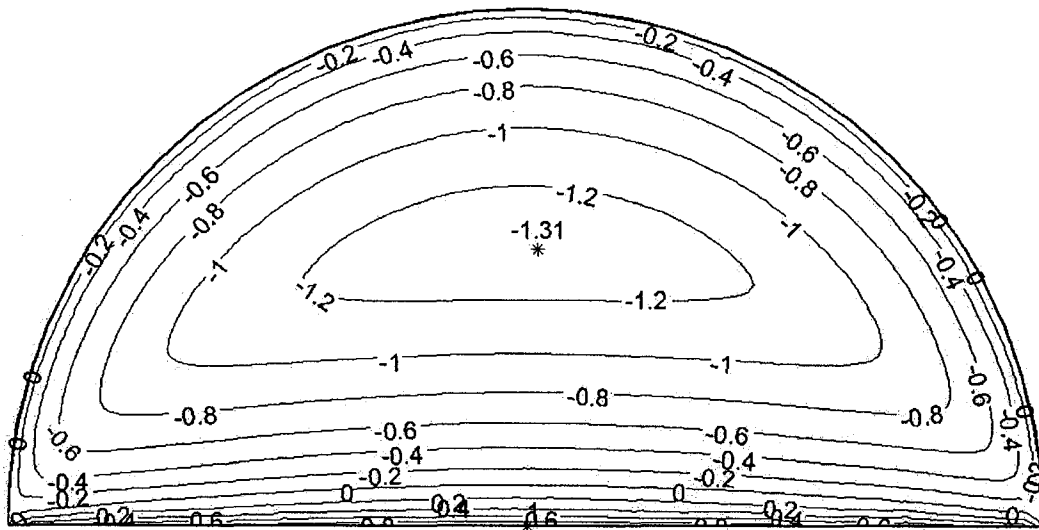
a)  $\alpha = -2.5$ , b)  $\alpha = -10$ , c)  $\alpha = -25$ , d)  $\alpha = -50$



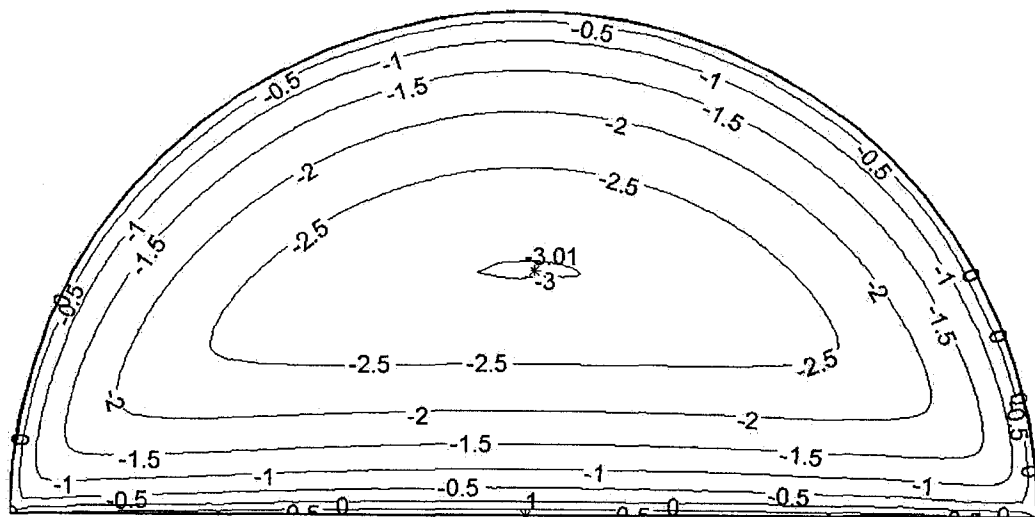
a)

**Figure 4-7(a, b & c): Effect of increasing positive pressure gradient against continuously forward moving wastewater on isovels in turbulent flow:**

a)  $\lambda = -0.01$ , b)  $\lambda = -0.025$ , c)  $\lambda = -0.1$



b)



c)

**Figure 4-7(Continued): Effect of increasing positive pressure gradient against continuously forward moving wastewater on isovels in turbulent case: a)  $\lambda = -0.01$ , b)  $\lambda = -0.025$ , c)  $\lambda = -0.1$**

One key objective of this paper is to develop relations or curves for the prediction of the average streamwise velocity to be used directly in engineering analysis or design. Both graphical and mathematical formats are provided. Figures 4-8 and 4-9 show curves of cross-sectional average air velocity ( $U_{av}$ ) relative to the wastewater surface velocity in turbulent flow regime. The curves in Figure 4-8 are due to the simultaneous effect of wastewater drag and negative pressure gradient whereas those in Figure 4-9 are due to wastewater drag and positive pressure gradient. In the plots, the horizontal scale  $U_R$  is given by the dimensionless quantity  $U_R = \lambda(L+C)/C$ , where  $\lambda = (-dP/dx)b/(\rho U_{wc}^2)$  and  $L$  is the perimeter of the unwetted headspace. These curves are simulated for the relative depth of range of  $0.05 \leq b/D \leq 0.95$  at intervals of  $b/D = 0.05$ . The numerical computations indicate that for low values of  $U_R$ , the cross-sectional average velocity in a turbulent regime for the combined case, unlike the laminar flow regime, is always less than the simple algebraic addition of the contributions from the individual mechanisms and that ventilation rates can be overestimated by employing the simple superposition of the individual models developed previously by Edwini-Bonsu and Steffler (2003, 2004b), (also in Chapters 2 and 3 of this thesis). This observation may theoretically be explained in a number of ways. Three reasons are given here:

- First, there is a possibility of an increased resistance in the turbulent flow regime when wastewater and pressure gradient together drive the sewer air and hence a reduction in the longitudinal mean velocity may be expected.

- A second reason could be attributed to the differences in magnitude of the secondary flow currents in the individual effects and the combined case. The secondary velocity computed is generally within 5-8 %, 6-10 % and 6-12 % of the cross-sectional average longitudinal mean velocity for wastewater-driven, pressure-induced and combined case, respectively. Although these values are small in comparison with the streamwise bulk velocity, they have the tendency to modify the isovels and hence the overall mean flow quantities.
- A third reason might be due to the differences in the distribution of turbulence quantities such as the eddy viscosity or the mean strain rate under the individual and combined ventilating forces which may in turn affect the bulk mean velocity.

For high values of  $U_R$  ( $U_R \geq 5.0$ ) the contribution of the wastewater drag to the bulk mean velocity is found to be insignificant and can be ignored. This finding reinforces the point that, in an operating sewer system, pressure gradient (due to forces such as wind speed, barometric pressure or dropstructure pressurization) may be a primary motive force and wastewater drag a secondary force. Under this circumstance, it is adequate to use the pressure gradient-only developed equations of Edwini-Bonsu and Steffler (2004b) or in Chapter 3 of this thesis.

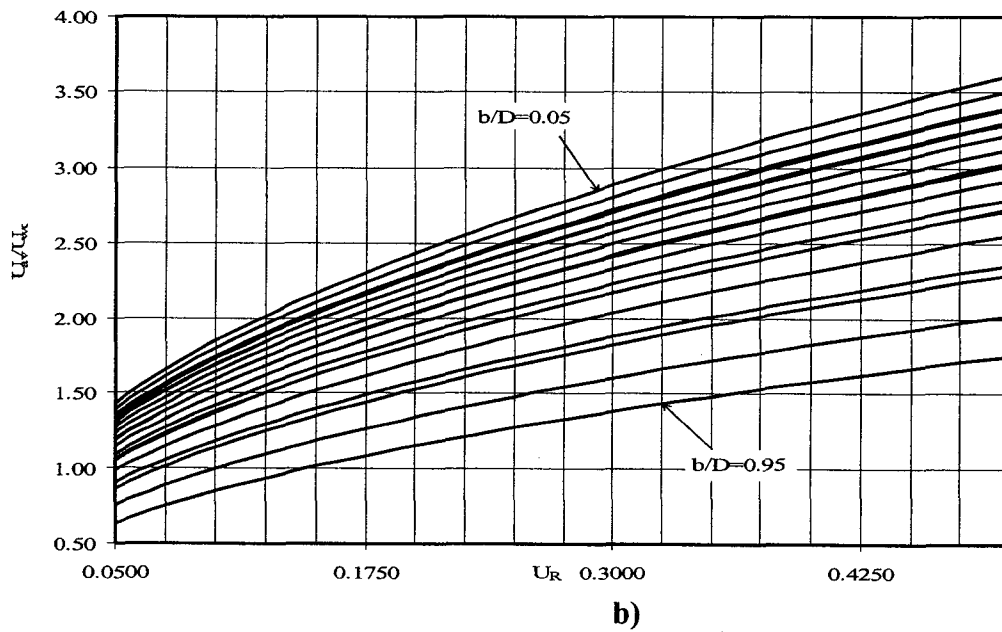
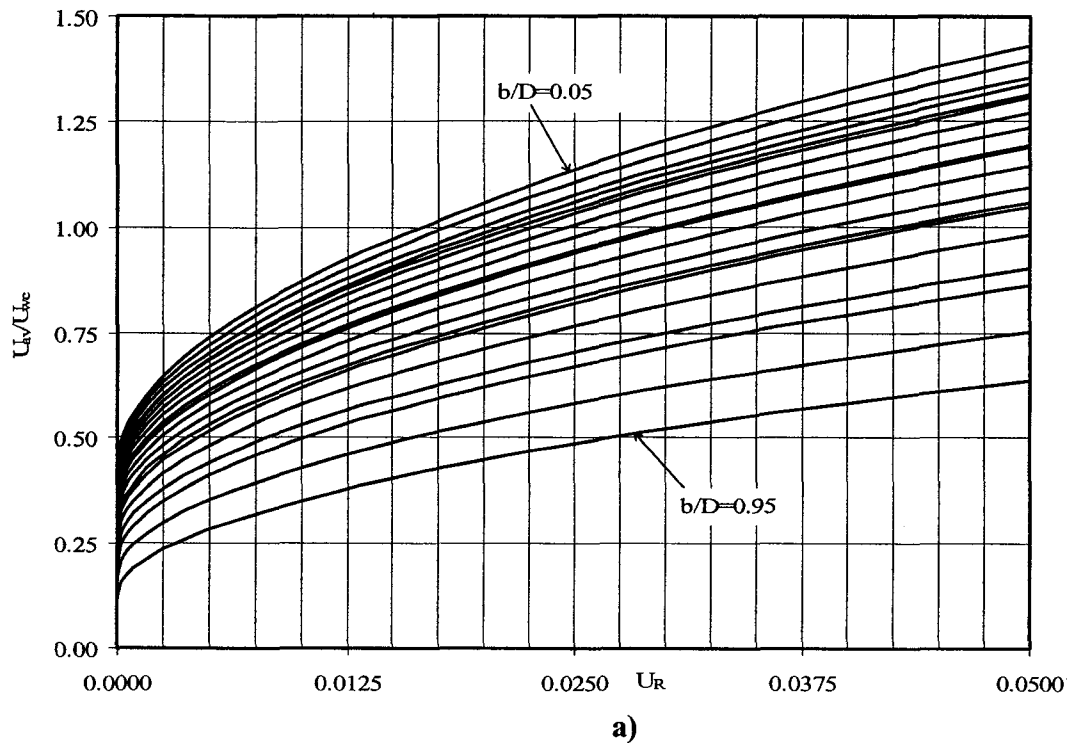
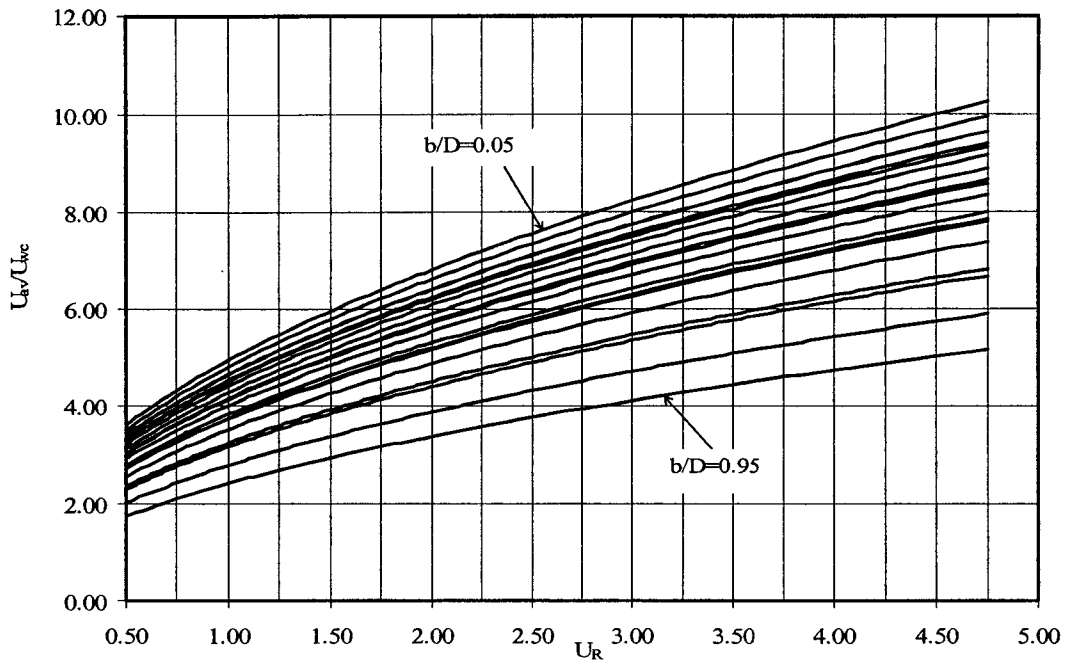


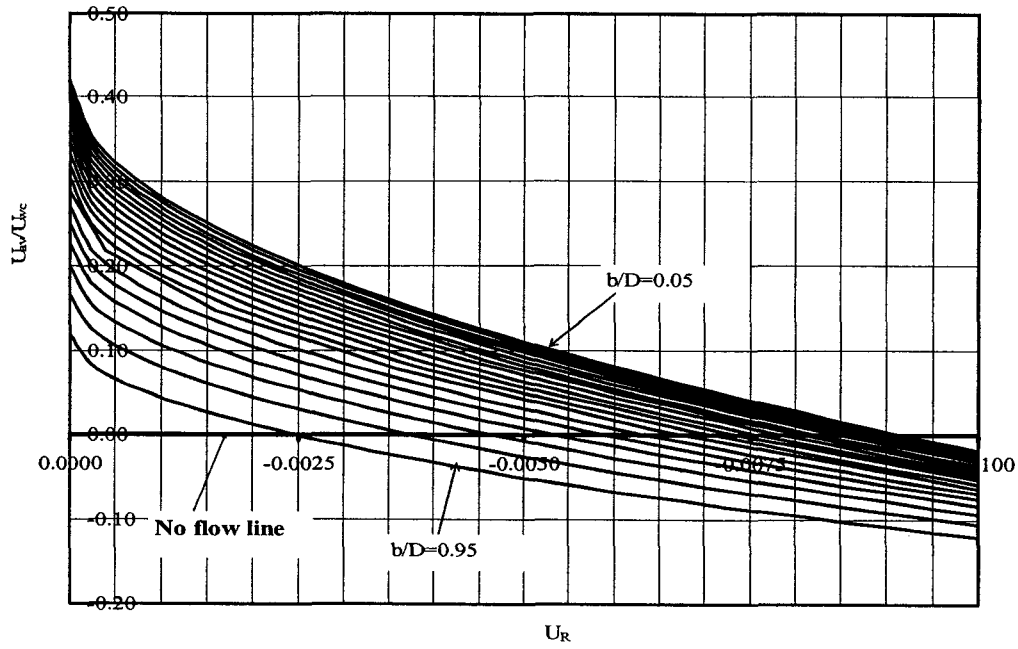
**Figure 4-8(a, b & c): Average primary velocity curves for turbulent flow regime due to the combined forces of wastewater drag and negative pressure gradient for range of values of  $U_R$  and  $b/D$**



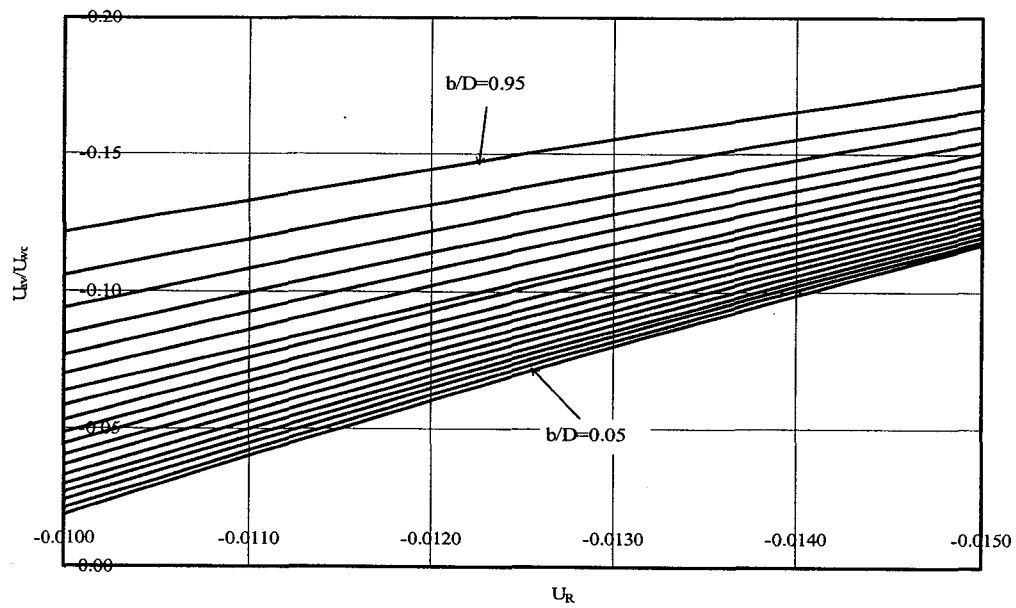


c)

**Figure 4-8(Continued): Average primary velocity curves for turbulent flow regime due to the combined forces of wastewater drag and negative pressure gradient for range of values of  $U_R$  and  $b/D$**

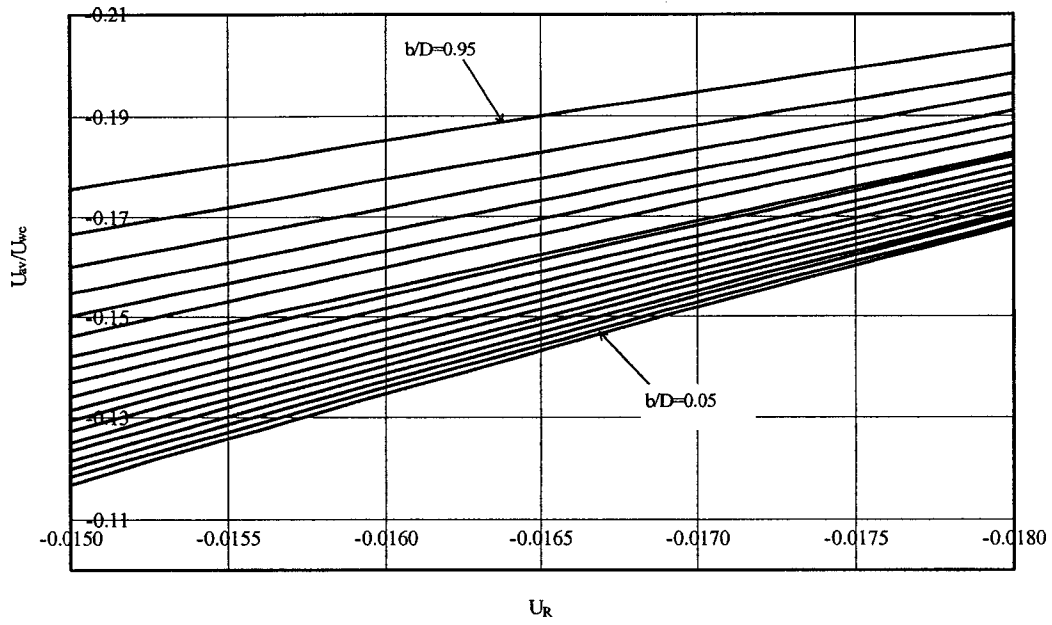


a)

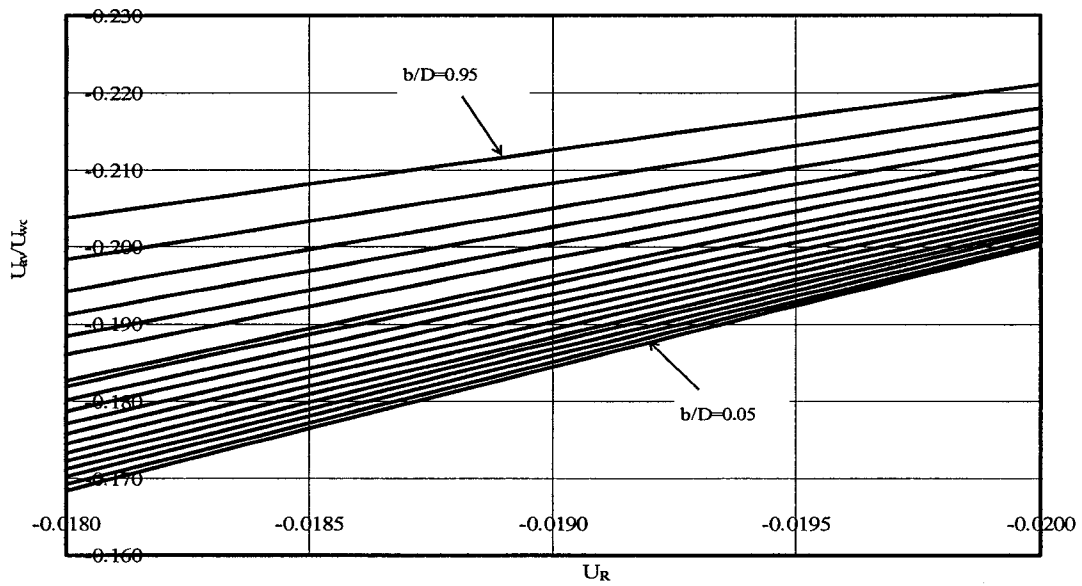


b)

**Figure 4-9(a, b, c & d): Average primary velocity curves for turbulent flow regime due to the combined forces of wastewater drag and positive pressure gradient for range of values of  $U_R$  and  $b/D$**



c)



d)

**Figure 4-9(Continued): Average primary velocity curves for turbulent flow regime due to the combined forces of wastewater drag and positive pressure gradient for range of values of  $U_R$  and  $b/D$**

As already stated, a simple additive rule is found to hold for the calculated laminar average velocity. This is true for both forward and reverse flows. This deduction allows us to decidedly write an expression for the cross-sectional average velocity due to the combined forces of wastewater drag and pressure gradient following Edwini-Bonsu and Steffler (2003, 2004b) or Chapters 2 and 3 of this thesis as:

$$\frac{U_{av}}{U_w} = 1.028 \left[ \frac{C}{(L+C)} \right] + \alpha \left( 0.088 \left[ \frac{C}{(L+C)} \right]^2 + 0.0079 \left[ \frac{C}{(L+C)} \right] + 0.0313 \right) \quad [4.22]$$

The first term in Equation [4.22] is due to wastewater drag whilst the second term is the contribution from pressure gradient. The direction of the resultant average velocity depends on the sign and magnitude of  $\alpha$ . For  $\alpha = 0$ , the air is wastewater-driven. If  $\alpha < 0$ , then the average velocity may be negative depending on the strength of the wastewater term. Obviously for  $\alpha > 0$  both air and wastewater flow in the same direction.

It must be noted here that, there is a possibility of zero cross-sectional average velocity even when both pressure and wastewater act simultaneously. Of course this will only occur when the pressure gradient is positive. Figure 4-10 offers the criterion for this scenario to occur in laminar flow regime. This figure provides a value of  $\alpha$  for a given level of the headspace for which a zero average velocity can occur. The corresponding value of  $U_R$  for zero average velocity scenario to occur in turbulent flow regime can be adduced from Figure 4-9a. Knowledge of

zero average velocity would be useful in ensuring the safety of maintenance workers working downstream of sewer reaches.

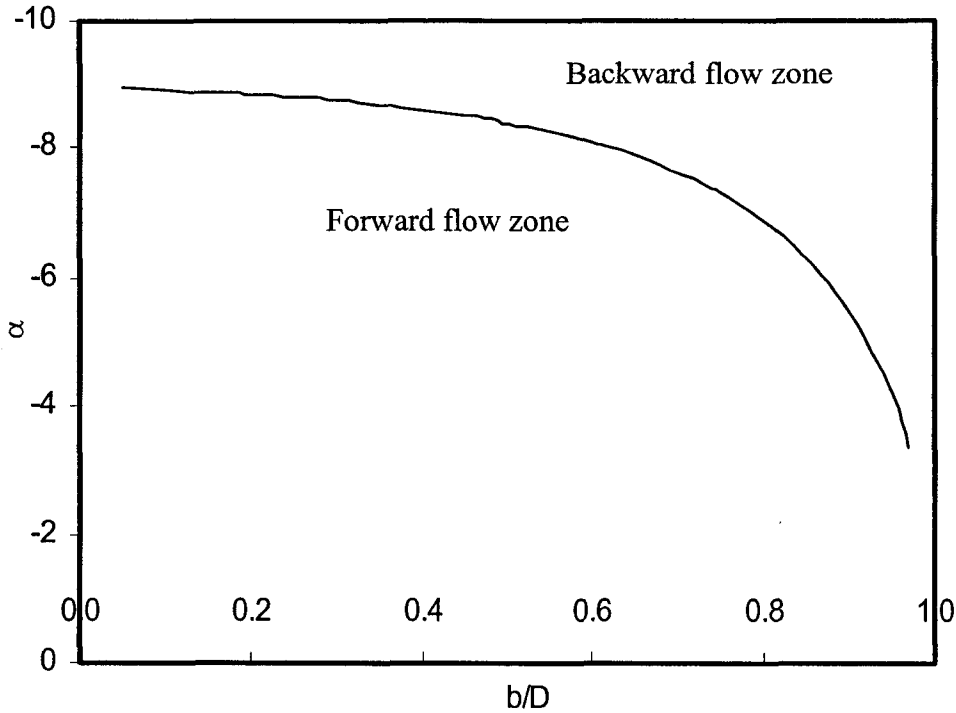


**Figure 4-10: Zero average velocity criterion curve in laminar flow regime**

The curves and formula presented herein can be used to estimate the cross-sectional average streamwise velocity including the direction of the mean air current when the water level, pressure gradient (which is expressed in the dimensionless parameters  $\alpha$  and  $\lambda$ ) and the water surface velocity are known. Aside from the average velocity provided by the models, the proposed models also offer the framework upon which a detailed air flow pattern in the sewer atmosphere, which is particularly relevant in corrosion modeling studies, could be ascertained.

#### 4.4.2 Interfacial Coefficient of Drag

The interfacial drag coefficient is calculated using the velocity field. The interfacial shear stress relates the derivative of the velocity  $U$  in the direction perpendicular to the interface as:

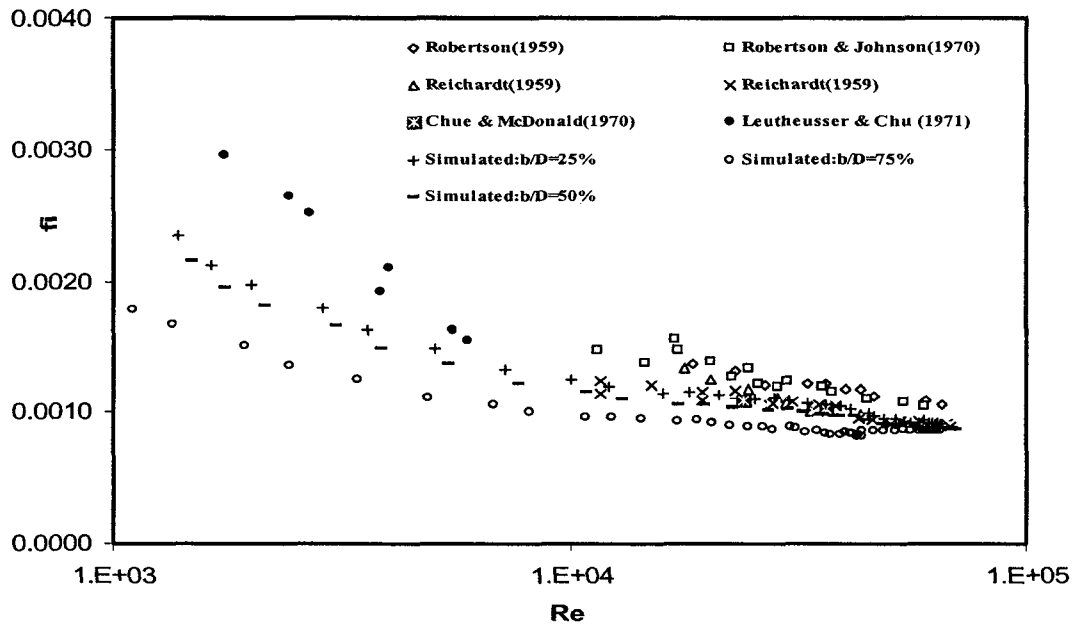
$$\tau_i = \rho(v + v_i) \frac{\partial U}{\partial n} \quad [4.23]$$

where  $\tau_i$  is the interfacial shear stress distribution. The average drag coefficient also relates the shear stress in a number of definitions. In this paper we define the average interfacial drag coefficient as:

$$f_i = \frac{\tau_{iav}}{1/2 \rho U_{av}^2} \quad [4.24]$$

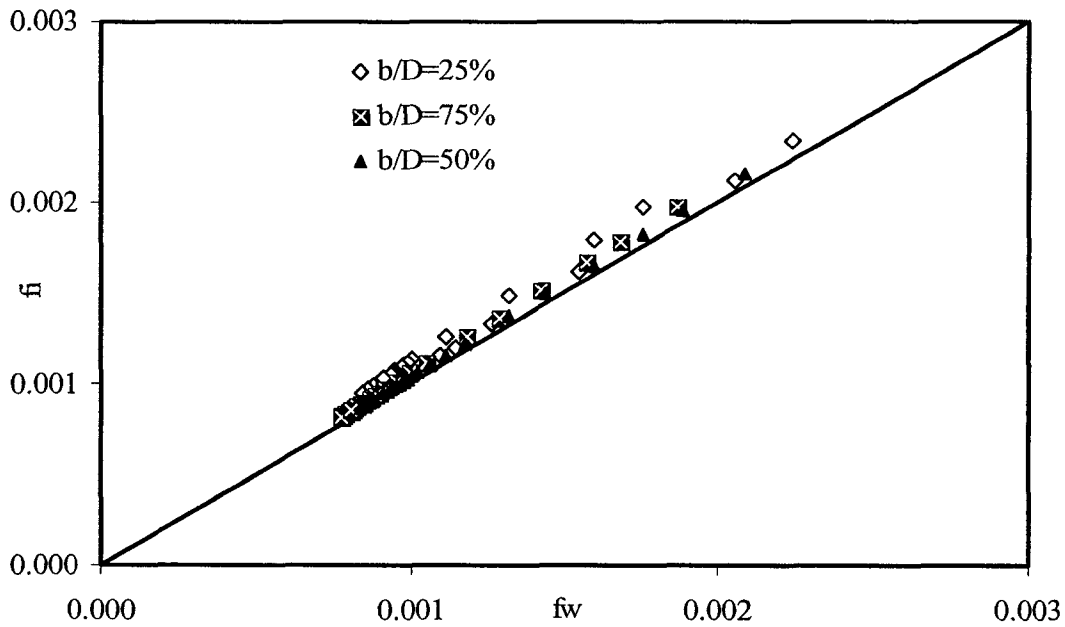
where  $\tau_{iav}$  is the average interfacial shear stress and  $f_i$  is the average interfacial drag coefficient.

Equation [4.24] is evaluated for three relative depths  $b/D= 25\%$ ,  $b/D= 50\%$  and  $b/D= 75\%$  for two cases of wastewater drag and combined flows. Currently air-water flow data in sewer conduits to validate the numerical simulations are not available hence comparison of simulated coefficient due to wastewater drag is achieved using plane Couette flow data. Drag coefficient of plane Couette flow has been studied by several investigators including Chue and McDonald (1970), Leutheusser and Chu (1971), Reichardt (1959), Robertson (1959), and Robertson and Johnson (1970). Figure 4-11 compares the simulated coefficient values with data reported by these investigators.



**Figure 4-11: Predicted interfacial drag coefficient (due to wastewater) compared with plane Couette flow data available in the literature**

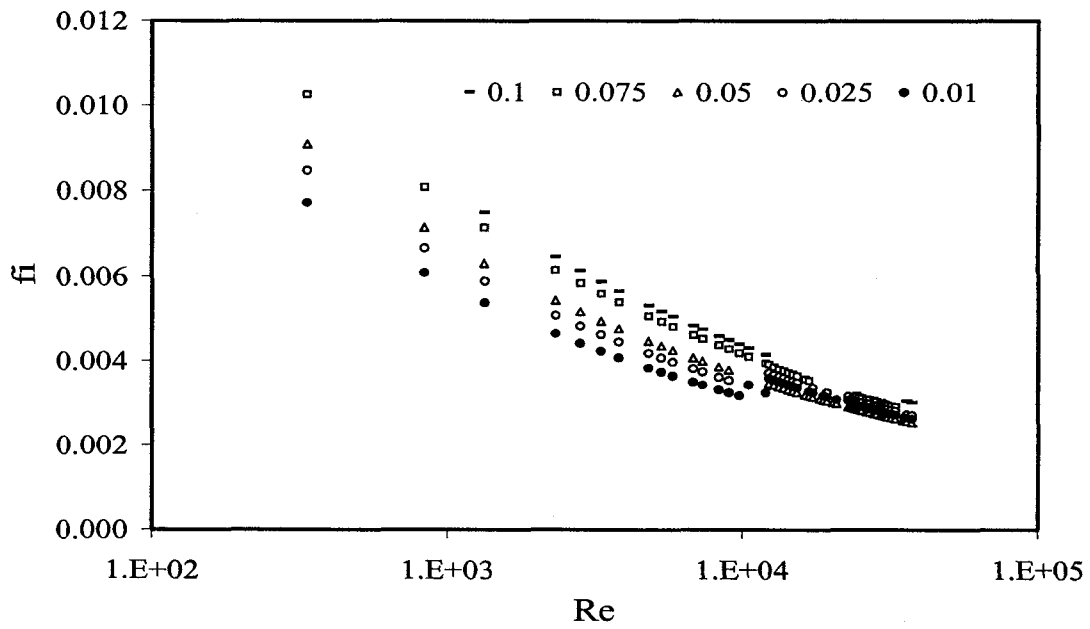
The simulated coefficients are generally found to be less than those of plane Couette flow possibly due to the effect of the flow boundary. As noted, the coefficient of drag follows a Reynolds number-relative depth dependent relationship as in the well-known Moody diagram. The coefficient is observed to increase with decreasing relative depth ( $b/D$ ) for the three relative depths studied. Also shown in Figure 4-12 is the comparison between simulated average friction coefficient of the sewer wall and that at the interface for the three relative depths. The wall friction coefficient has been computed by employing the same definition as in Equations [4-23] and [4-24], but with sewer wall inputs. From the plot, it is interesting to see that the ratio of the average interfacial coefficient to the corresponding average wall coefficient is approximately unity.



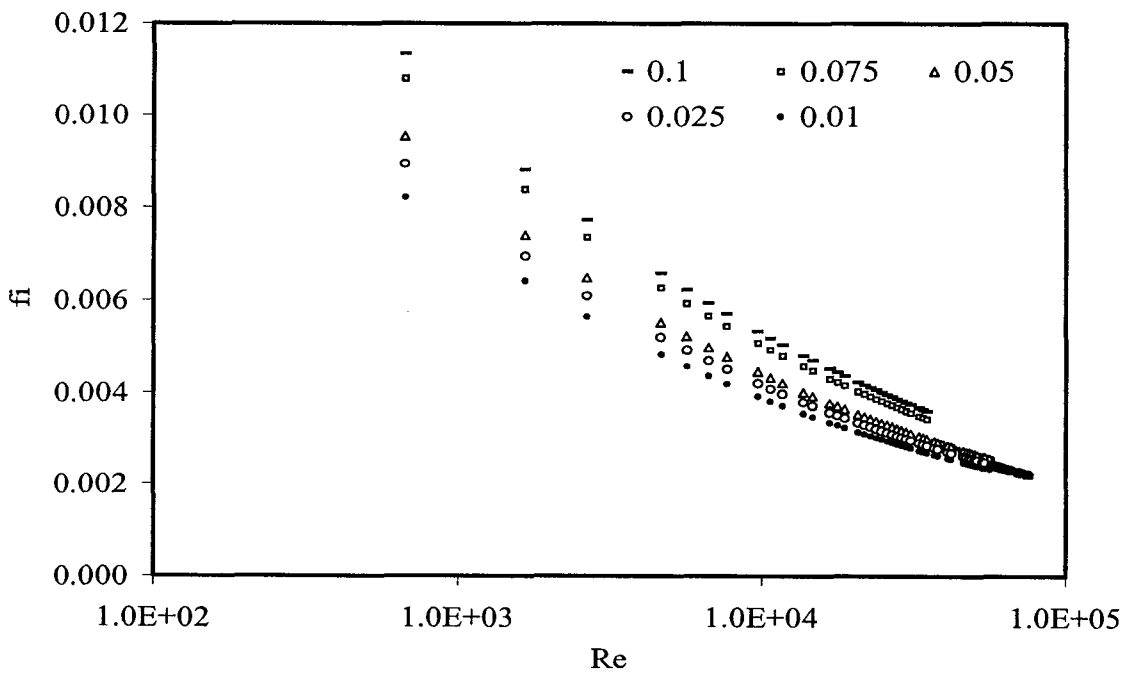
**Figure 4-12: Comparison of calculated average wall friction coefficient and interfacial drag coefficient due to wastewater drag**

Figure 4-13 shows the simulated drag coefficients when wastewater and pressure drive the flow altogether. The effect of some selected positive  $\lambda$  values on the coefficient is examined for the same three relative depths. The coefficient is observed to decrease with decreasing values of  $\lambda$ . Just as in the wastewater drag case, the coefficient is found to increase with decreasing relative depth ( $b/D$ ) for the cases investigated. On the contrary, the average interfacial coefficient is found to be less than the corresponding wall coefficient in the combined case as depicted in Figure 4-14.



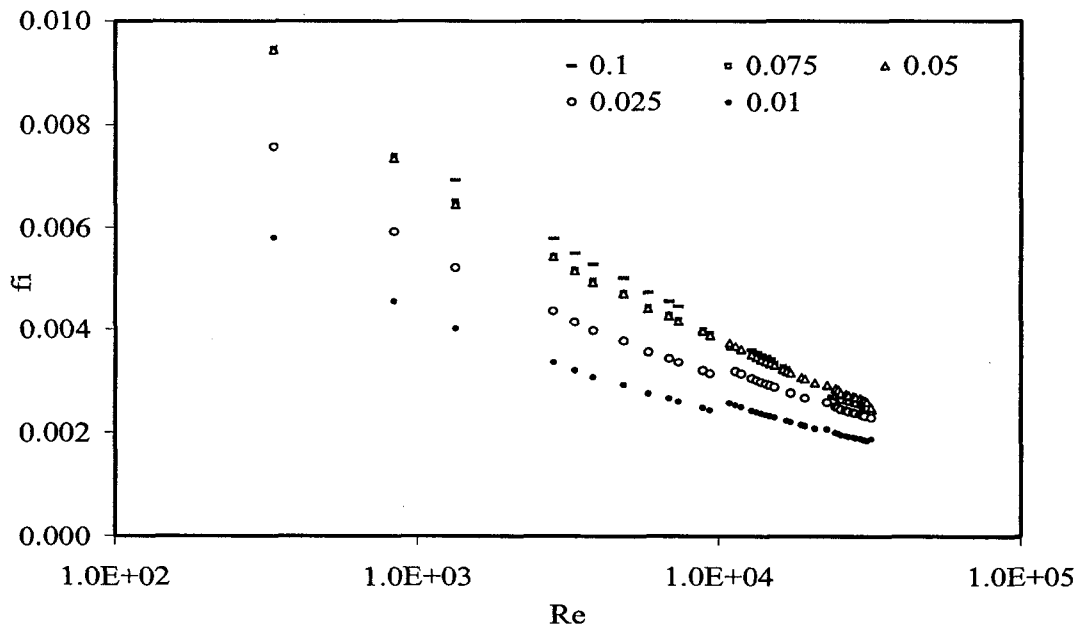


a)



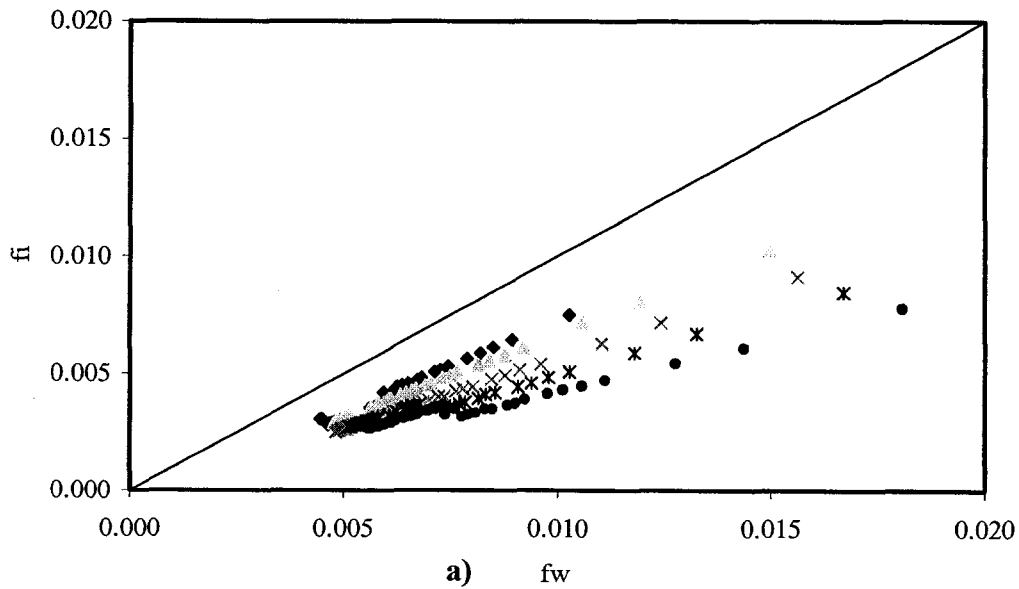
b)

**Figure 4-13(a, b & c): Interfacial drag coefficient for some values of  $\lambda$  : a)  $b/D= 25\%$ , b)  $b/D= 50\%$ , c)  $b/D= 75\%$**



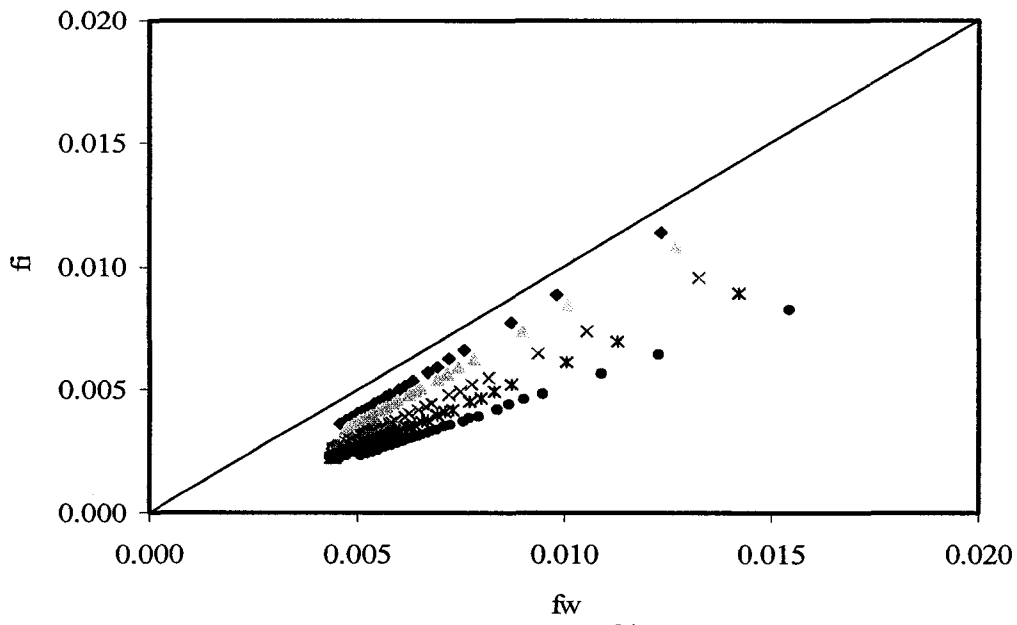
c)

**Figure 4-13(Continued): Interfacial drag coefficient for some values of  $\lambda$  : a)  $b/D= 25 \%$ , b)  $b/D= 50 \%$ , c)  $b/D= 75 \%$**

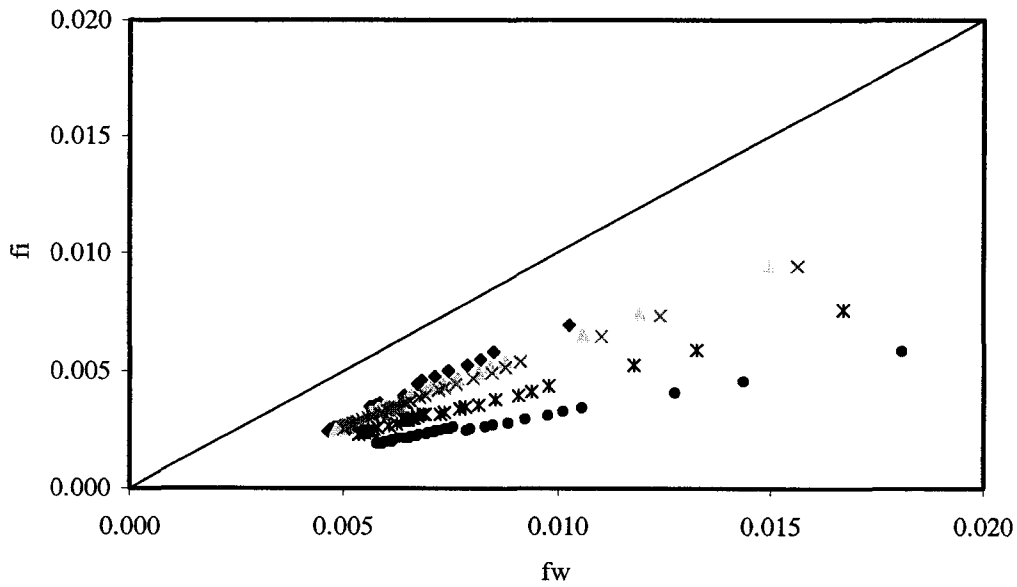


a)

**Figure 4-14(a, b & c): Comparison of calculated average wall friction coefficient and interfacial drag coefficient-combined flow: a)  $b/D= 25 \%$ , b)  $b/D= 50 \%$ , c)  $b/D = 75 \%$**



b)



c)

**Figure 4-14(Continued): Comparison of calculated average wall friction coefficient and interfacial drag coefficient-  
combined flow: a)  $b/D= 25 \%$ , b)  $b/D= 50 \%$ , c)  $b/D= 75 \%$**

## 4.5 CONCLUSIONS

Physically-based models for assessing the combined effects of sewage drag and pressure gradient on air transport in sanitary sewer conduits have been developed and presented. The models can be used for the prediction of the amount and direction of the transporting air currents.

The computational approach is conceptually viewed as a 2-D Poiseuille-Couette flow with the wastewater effect formulated as a moving boundary condition, and the effect of pressure modelled as a longitudinal pressure gradient in the momentum equation. In the turbulent flow modeling, the Reynolds transport equations are closed with a simple turbulence closure model which consists of an eddy viscosity- mixing length model for the Reynolds shear stresses and a semi-empirical model for the turbulent normal stresses. A Galerkin finite element solution of the equations provides good secondary flow patterns as well as longitudinal velocity distribution in the sewer atmosphere. The models provide novel insights about the complex nature of the air flow field at a level of detail that is not easily attainable by laboratory or field studies. Curves and formula that can be used for calculating the cross-sectional average longitudinal velocity in both turbulent and laminar flow regimes are developed. These curves and formula suggest that the amount and characteristics of ventilation induced by wastewater drag and pressure gradient depend upon the available headspace geometry as well as the magnitude of the driving forces.

Major findings stemming from this paper are as follows:

- The secondary velocities computed are within 5-12 % of the bulk streamwise mean velocity. The effect of the secondary current in distorting the streamwise velocity distribution is strongest in wastewater-driven flows.
- With application of a positive pressure gradient, the air movement could be in any direction depending on the strength of the forward moving wastewater drag. In this case apart from the sewer walls, there are also spots where the longitudinal air velocity is zero. As might be expected in wastewater-only-driven flows, all air in the headspace moves downstream due to the drag of the flowing wastewater and there is no zero velocity in the headspace. The model simulations also suggest that there is a possibility of zero average velocity even when both positive pressure gradient and wastewater act simultaneously.
- Ventilation rates caused by pressure forces are likely to be higher than those caused by wastewater drag for a given in-service trunk sewer and environmental condition. The wastewater drag effect appears subservient to pressure, particularly where there is a large space above low-velocity fluid flow. When high pressure forces act in the same direction as liquid drag, the resulting average velocity is almost the same as that with no liquid drag present.
- In turbulent flow regime, when both wastewater drag and pressure forces simultaneously act either in the same direction or in the opposite direction,

the cross-sectional average velocity due to the individual effects is not linearly additive. On the other hand, individual effects are strictly additive in the case of laminar flow.

- The variation of interfacial drag coefficient with Reynolds number follows a Moody-like diagram and decreases with increasing relative depth. Coefficient due to wastewater drag is generally less than plane Couette flow data and is found to be approximately equal to the corresponding predicted average wall friction coefficient. On the other hand the interfacial drag coefficient in the combined case is found to be consistently less than the corresponding wall friction coefficient.

The models presented in this paper are valid for cases where the sewer pipe walls are smooth and also where the section under consideration is about 50 times the depth of the headspace or longer from the entrance or exit of a junction to satisfy the requirement for full flow development. This paper and the preceding ones have focused on conditions of air flow in pipes flowing partially-full with no eduction via manholes. The models in these chapters can only provide the basic calculations that would allow the determination of the volume of air in the sewer atmosphere that is capable of being forced out. An important question that arises is how the amount educting an opening such as manhole pickhole can be quantified. This question is given consideration in the paper presented in the next chapter.

## REFERENCES

- ASCE. 1989. Sulphide in wastewater collection and treatment systems. ASCE Manuals and Reports on Engineering Practice, No. 69.
- Bowker, R. P. G., Smith, J. M., Webster, N. A. 1989. Odor and corrosion control in sanitary sewerage systems and treatment plants. Hemisphere Publishing Corporation, N. Y.
- Chue, S. H., McDonald, A. T. 1970. Application of a new effective viscosity model to turbulent plane Couette flow. *A. I. A. A. J.* **8**, 2076-2078.
- Corsi, R. L., Chang, P. Y., Schroeder, E. D. 1992. A modeling approach for VOC emissions from sewers. *Water Env. Research.* **64** (5): 734-741.
- Corsi, R. L., Chang, P. Y., Schroeder, E. D. 1989. Assessment of the effect of ventilation rates on VOC emission from sewers. *Air & Water Management Ass.* 82nd Annual Meeting & Exhibition. Anaheim, California.
- Corsi, R. L., Quigley, C. J. 1996. VOC emissions from sewer junction boxes and dropstructures: estimation methods and experimental results. *J. Air and Waste Mgmt. Assn.* **46** (3): 224-233.
- Czernuszenko, W., Rylov, A. A. 2002. Modeling of three-dimensional velocity field in open channel flows. *Journal of Hydraulic Research*, **40** (2): 135-143.
- Daly, B. J, Harlow, F. H. 1970. Transport equations in turbulence. *The Physics of Fluids*, **13** (11), 2634-2649.
- Demuren, A. O., Rodi, W. 1984. Calculation of turbulence-driven secondary motions in non-circular ducts. *Journal of Fluid Mechanics.* **140**: 189-222.

- Deuflhard, P., Freund, R., Walter, A. 1990. Fast secant methods for the iterative solution of large non-symmetric linear systems. *IMPACT Comp. Sci. Eng.* **2**: 244-276.
- Edwini-Bonsu, S., Steffler, P. M. 2004a. A physically-based model for computing natural ventilation rate in sanitary sewer atmosphere. WEF/A & WMA Odors and Air Emission Conference, Bellevue, Seattle.
- Edwini-Bonsu, S., Steffler, P. M. 2003. Air flow in sanitary sewer conduits due to wastewater drag: A CFD approach. *J. Environ. Eng. Sci.* Accepted.
- Edwini-Bonsu, S., Steffler, P. M. 2004b. Dynamics of air flow in sanitary sewer conduits due to differential pressure. *J. of Envir. Engrg. ASCE.* Submitted.
- FEMLAB. 2002. Version 2.3a. Comsol Inc.
- Fletcher, C. A. J. 1988. Computational techniques for fluid dynamics 2. Springer-Verlag, N. Y.
- Gerard, R. 1978. Secondary flow in non-circular conduits. *Journal of the Hydraulic Division, ASCE.* **104** (HY5): 603-616.
- Leutheusser, H. J., Chu, V. H. 1971. Experiments on plane Couette flow. *Proc. ASCE., J. Hyd. Div.* **97**, 1269-1284.
- Matos, J. S., de Sousa, E. R. 1992. The forecasting of hydrogen sulphide gas build-up in sewerage collection systems. *Wat. Sci. Tech.* **26** (3-4): 915-922.
- Nezu, I., Nakagawa, H. 1993. Turbulence in open-channel flows. A. A. Belkema, Rotterdam.
- Odor and Corrosion Technology Consultants Inc. 1999a. The use of modeling techniques to evaluate and correct odour releases from trunk sewers. TM No.4,



- City of Edmonton Odour Control Project, Alberta.
- Odor and Corrosion Technology Consultants Inc. 1999b. Trunk sewer odour monitoring program. TM No.1, City of Edmonton Odour Control Project, Alberta.
- Olson, D. 1996. Gas exchange rates between industrial process drains and the ambient atmosphere. MSc. Thesis, University of Texas.
- Olson, D., Rajagopalan, S., Corsi, R. L. 1997. Ventilation of industrial process drains: mechanisms and effects on VOC emissions, Jr. *Env. Eng.* **123** (9): 939-947.
- Pescod, M. B., Price, A. C. 1978. A study of sewer ventilation for the Tyneside sewerage scheme. Final research report, Department of Civil Engineering, University of Newcastle upon Tyne, U. K.
- Pescod, M. B., Price, A. C. 1981. Fundamentals of sewer ventilation as applied to the Tyneside sewerage scheme. *Water Pollution Control*: **90** (1): 17-33.
- Pescod, M. B., Price, A. C. 1982. Major factors in sewer ventilation. *J. Water Pollution Control Fed.* **54** (4): 385-397.
- Pomeroy, R. 1945. Pros and cons of sewer ventilation. *Sewage Works Journal*, **17** (2): 203-208.
- Quigley, C. J., Corsi, R. L. 1995. Emission of VOCs from a municipal sewer. *J. Air and Waste Mgmt. Assn.* **45** (5): 395-403.
- Reichardt, H. 1959. *Gesetzmässigkeiten der geradlinigen turbulenten Couettestromung*. Mitt. Max-Planck-Inst. Fur Stromungsforschung, no. 22, Gottingen.
- Robert, J-L., Khelifi, M., Ghanmi, A. 1998. Use of the mixing length concept to

- correctly reproduce velocity profiles of turbulent flows. *Can. J. Civ. Eng.* **25**: 232-240.
- Robertson, J. M. 1959. On turbulent plane Couette flow. *Proc. 6<sup>th</sup> Midwestern Conf. on Fluid Mech.* University of Texas, Austin. 169-182.
- Robertson, J. M., Johnson, H. F. 1970. Turbulence structure in plane Couette flow. *Proc. ASCE., J. Eng. Mech. Div.* **96**, 1171-1182.
- Rodi, W. 1984. Turbulence models and their application in hydraulics. A state of the art review. International Association for Hydraulic Research, Delft, the Netherlands.
- Strand, Ø. 1993. An experimental investigation of stratified two-phase flow in horizontal pipes. PhD. Thesis, University of Oslo.
- Thistlethwayte, D. K. B. (Ed.). 1972. The control of sulphides in sewerage systems. Butterworths, Sydney.
- Tominaga, A., Nezu, I., Ezaki, K., Nakagawa, H. 1989. Three-dimensional turbulent structures in straight open channel flows. *Journal of Hydraulic Research.* **27** (1): 149-173.
- Whitmore, A., Corsi, R. L. 1994. Measurement of gas-liquid mass transfer coefficients for volatile organic compounds in sewers. *Envir. Progress*, **13** (2), 114-123.
- Wilcox, D. C. 2000. Turbulence modeling for CFD. 2<sup>nd</sup> ed. DCW Industries, Inc. California, U. S.
- Zytner, R. G., Madani-Isfahani, M., Corsi, R. L. 1997. Oxygen uptake and VOC emissions at enclosed sewer dropstructures, *Water Env. Research.* **69** (3), 286-

294.

---

# CHAPTER FIVE<sup>4</sup>

## SYSTEM THEORETIC FRAMEWORK FOR MODELING SANITARY SEWER SYSTEM VENTILATION

---

### 5.1 INTRODUCTION

#### 5.1.1 Background

In municipal collection systems of today, large volumes of wastewater are transported long distances, odorous compounds abound, and pressurization and ventilation of sewer airspaces prevails. The pressurization and ventilation phenomenon in most cases leads to odour releases via manhole pickholes into ambient neighborhoods. Before odour problems in such neighborhoods can adequately be addressed, the cause and severity of the odour emission episodes must first be established so that appropriate technologies can be applied. Sometimes the appropriate technology can be as simple as modification of the system hydraulics to reduce pressurization of the sewer conduits and hence reduce air eduction or as complicated as air withdrawal and treatment at a remote

---

<sup>4</sup> Some content of this chapter is presented at WEF/A & WMA Odors & Air Emission Conference, Bellevue, Seattle, 2004.

location (Davidson et al. 2004; Haecker et al. 2004; Odor and Corrosion Technology Consultants 1999a, b; Pomeroy 1945; Thistlethwayte 1972). In any of these technologies the basic control parameters must be determined. The basic control parameters are the amount of air being released and hydrogen sulphide or other offending odour compound concentration. This paper is concerned with the first parameter given that the driving forces responsible for the air movement can be appropriately identified. The combination of the primary odour compound gas concentration and the volume of air being forced out can yield total mass flux of the gas, which can yield treatment cost data for various treatment alternatives, if treatment is the odour control prescription. Again a complete understanding of the response of the air dynamics to sewer system variables and ambient environmental conditions would also help identify odour 'hot spot' areas within a given sewer system for the necessary corrective or design interventions to be implemented.

### **5.1.2 Existing Knowledge-Base**

The modeling approaches presented in the preceding chapters and also in Edwini-Bonsu and Steffler (2003, 2004a) focused on air flow dynamics in an isolated single sewer pipe headspace with no additional inlet or outlet for either water or air. Even in this situation, it is easy to see how wastewater velocity and pressure gradient can enhance or retard air flow through the conduit. Add to this the increased complexity of other tributary gravity collection sewer conduits, with each tributary pipe adding both water and air to the downstream receiving sewer

and the ventilation phenomenon becomes complicated. If the cumulative volumes and flow rates of water and air in the sewer conduits are added as you move through the system, it becomes a physical impossibility to convey 100 percent of both the water and air to the treatment plant. Given the relative density and specific gravity of air and water it is equally easy to envisage which fluid wins the competition for space in the downstream sewer and which is forced out into the ambient atmosphere via interconnected manhole pickholes. In addition to this increased complexity, many factors such as barometric pressure variations, wind speed differentials, a decrease in downstream sewer pipe diameter (which should not occur in any well-designed sewer system), junction turbulence (which may cause some circulation), hydraulic jumps and dropstructures can contribute to the odour ventilation problems from sewers (Edwini-Bonsu and Steffler 2003, 2004a; Odor and Corrosion Technology Consultants 1999a, b; Olson 1996; Olson et al. 1997; Pescod and Price 1978, 1981, 1982; USEPA 1994).

The Water Environment Research Foundation in 1998 undertook a laboratory investigation and field demonstration of ventilation dynamics using tracer gas techniques (Odor and Corrosion Technology Consultants 1999a). The study quantified and ranked the relative importance of water flow rate and wind eduction over sewer shafts on ventilation rates. It was concluded that wind eduction was the primary motive force for ventilation and that wastewater drag phenomenon was secondary force. However, no mathematical models were developed to describe the movement of air into, out of, or along the sewer. Also in

use is a commercial air-transport computer model (KYGas) which helps identify the dynamics of air movement through sewers (Odor and Corrosion Technology Consultants 1999a). This model assumes that there is no wastewater in the sewer conduits which is a serious handicap for the accurate prediction of sewer system ventilation dynamics.

In this paper a system formulation incorporating system variables and major energy inputs (driving forces) is presented for analyzing air movement in sanitary sewer systems. The formulation accounts for combined wastewater drag and pressure air flows, and manhole pressurization. Derivation of relationships between system variables and energy inputs is based on the principles of nodal mass continuity and work-energy, and on the validity of system theory. The formulation makes use of the developed mathematical formulae in the preceding chapters (also in Edwini-Bonsu and Steffler 2003, 2004a). The modeling approach conceptually considers air eduction (or induction) via manholes as an orifice and system pressurization effect from dropstructures as a pump unit. Auxiliary ventilators such as scrubbers/blowers are treated as fans/pumps of known performance characteristic curves. Input data for system simulations are: meteorological data (wind and barometric pressures), system configuration and dimension, anticipated or known wastewater flow data, and other ~~known~~ driving forces. Outputs from the simulations are air flow rates throughout the system airspaces. Analyses of air flow dynamics in both hypothetical and real sewer systems are presented to show procedural calculations and to demonstrate the

applicability of the modeling formulation. The Kenilworth sewer system in the City of Edmonton is modelled in the latter case. This isolated sewer system consists of nine (9) dropstructures whose pumping characteristic functions are unknown at this stage and have to be assumed. The analysis presented for this case study therefore can only serve as groundwork for future design of corrective ventilation measures to control odour emission from this system.

## 5.2 VENTILATION AND EMISSION RATE RELATIONSHIP

Emissions in sewer systems can be estimated using an equilibrium-based or a kinetic-based approach. Regardless of the approach employed, the ventilation rate must be accurately quantified. In the equilibrium-based approach, chemical equilibrium is assumed between wastewater and adjacent air and the rate of mass transfer of a contaminant is expressed as (Olson 1996; Olson et al. 1997):

$$E = QC_l H_c \quad [5.1]$$

where  $E$  is the emission rate,  $Q$  is the air flow rate,  $H_c$  is the Henry's law coefficient for the chemical and  $C_l$  is the concentration of the chemical in the underlying wastewater. It can be adduced from Equation [5.1] that emission estimates, using the equilibrium assumption, is directly proportional to the ventilation rate.

A more rigorous approach for estimating emissions incorporates mass transfer kinetics. In this approach, the rate of mass transfer of a chemical can be written as



follows (Olson 1996; Olson et al. 1997):

$$E = K_L A_s \left( C_l - \frac{C_g}{H_c} \right), \quad \frac{1}{K_L} = \frac{1}{k_l} + \frac{1}{k_g H_c} \quad [5.2]$$

where  $K_L$  is the overall mass transfer coefficient,  $k_l$  and  $k_g$  are the mass transfer coefficients for liquid- and gas-phase, respectively,  $A_s$  is the surface area (between the liquid and adjacent gas) and  $C_g$  is the concentration of the chemical in the gas-phase. There are two possible ways in which the ventilation rate can influence the rate of mass transfer. First, the ventilation rate affects the gas accumulation term, i.e., the quantity  $C_g / H_c$ . For example, a system approaching infinite ventilation would have negligible compound accumulation in the gas phase, thereby creating the largest possible driving force for mass transfer to the sewer atmosphere (Olson et al. 1997). On the other hand, a system with restricted ventilation would have a higher gas-phase concentration and hence a lower driving force for mass transfer. Second, ventilation can affect the overall mass transfer coefficient ( $K_L$ ), particularly in cases where gas-phase resistance to mass transfer ( $1/(k_g H_c)$ ) is significant.

## 5.3 SYSTEM THEORY AND FORMULATION

### 5.3.1 Basic Philosophy

There are a large number of variables involved in the prediction of air movement in sewer systems. The relationships between variables are too complex to

assemble readily any sort of reliable mathematical relationships. The effects and relationships between variables are affected by distance, hydraulic flow variations, interfacial waves, pipe constrictions, environmental conditions, and many other variations.

Notwithstanding these complexities, the air flow dynamics in sewer systems, like any other system, can be modelled mathematically with an application of system theoretic techniques and invoking of realistic simplifications. In this direction, the entity of air pressurization and ventilation of a sewer system is assumed to be an independent system, in the sense that it can be divided into interconnected elements and the air flow paths in these elements can be independently and uniquely described by mathematical relations. In a typical municipal wastewater collection system, connecting sewer conduits, manholes, and in some cases dropstructures and auxiliary ventilators (forced draft) such as scrubbers and blowers are the basic physical elements and these elements are linked, among them, by nodes (e.g. manhole junctions). Furthermore, the air pressurization and ventilation system is considered to be time-invariant.

### **5.3.2 Continuity and Energy Formulation**

In a complex sewerage collection system made up of a number of nodes (air inflow and outflow points) and elements, a set of independent governing equations can be derived using the basic principles of air mass continuity and work-energy. At a given node, assuming constant air density, the equation of

continuity can be expressed as:

$$\sum kQ = 0 \quad [5.3a]$$

where the summation includes all elements connected to the node and  $k$  is known as the incidence index defined as follows:

$$k = \begin{cases} 1 & \text{if element is connected to node and flow is oriented towards it} \\ -1 & \text{if element is connected to node and flow is oriented away from it} \\ 0 & \text{otherwise} \end{cases} \quad [5.3b]$$

Equation [5.3] is the key mathematical model for a single node which can easily be extended to a network of  $j$ -nodes. This leads to a set of linear nodal  $Q$ -equations in matrix form:

$$\mathbf{I}\mathbf{Q} = \mathbf{0} \quad [5.4a]$$

where  $\mathbf{Q}$  is the air flow rate vector and  $\mathbf{I}$  is known as the incidence matrix, the structure of which is dependent on the given sewer system structure. The elements of the incidence matrix are defined as follows:

$$i = \begin{cases} 1 & \text{if element is connected to node and flow is oriented towards it} \\ -1 & \text{if element is connected to node and flow is oriented away from it} \\ 0 & \text{otherwise} \end{cases} \quad [5.4b]$$

An example matrix is illustrated by Equation [5.10b] for a hypothetical system.

The energy principle can provide additional equations which must be satisfied. These equations are obtained by using work-energy along loops to produce independent equations. Such equations usually have the form:

$$\sum \Delta P = 0 \quad [5.4c]$$

in which the summation includes the elements that form the loop and  $\Delta P$  is the

pressure head loss or developed in an element. The pressure head difference is usually expressed in terms of the flow rates as discussed in Section 5.3.3. Combination of Equations [5.4a] and [5.4c] provides a system of independent equations which offers the capacity to link system elements and non-elements as well as the driving forces that sustain sewer air flow.

### 5.3.3 Pressure Head Difference-Flow Rate Relationships

This section proposes algebraic expressions for relating pressure head drop or pressure head developed across major system elements with air flow rate.

#### 5.3.3.1 Sewer conduit atmosphere

Analogous to the Darcy-Weisbach or Hazen-Williams equations for pressurized pipe flows, we can similarly define a relation between the pressure head loss in sewer headspace and the air flow rate. The air flow rate in the connecting sewer conduit headspace depends on the wastewater surface velocity, pressure head between the ends of the sewer pipe, pipe length and the available headspace geometry which can be written mathematically as (Chapters 2, 3 and 4; Edwini-Bonsu and Steffler 2003, 2004a, b, c):

$$Q_n = f(\Delta P_n, X_n, U_{wn}, G_n) \quad [5.5]$$

where the subscript "n" denotes the connecting pipe number,  $\Delta P_n$  is the pressure head loss between the ends of the pipe,  $U_{wn}$  is the wastewater surface velocity in the connecting sewer pipe,  $G_n$  is a quantity representing available headspace

geometry and  $X_n$  is the length of the sewer reach. In order to handle Equation [5.5] in mathematical sense, it must be an algebraic expression. The air flow rate in laminar flow regime under the combined forces of wastewater drag and pressure gradient from Chapter 4 (also in Edwini-Bonsu and Steffler 2004a, b) can be obtained as:

$$Q_n = A_{hn} U_{wn} (1.028 R_n + \alpha_n S_n) \quad [5.6a]$$

where  $A_{hn}$  is the headspace cross-sectional area,  $S_n = 0.088 R_n^2 + 0.0079 R_n + 0.0313$ ,  $R_n = C_n / (L_n + C_n)$ ,  $L_n$  is the perimeter of the unwetted headspace,  $C_n$  is the interfacial width,  $\alpha_n = ((\Delta P_n) / X_n) g b_n^2 / (\nu U_{wn})$ ,  $g$  is the acceleration due to gravity and  $\nu$  is the kinematic viscosity of air (assumed constant throughout the system). The first term on the right hand side of Equation [5.6a] is due to wastewater drag whilst the second term is the contribution from the pressure head differential. From Equation [5.6a], the pressure head loss can be deduced as:

$$\Delta P_n = \frac{\nu (Q_n - W_n)}{b_n g T_n} \quad [5.6b]$$

where  $T_n = A_{hn} b_n S_n / X_n$  and  $W_n = 1.028 A_{hn} U_{wn} R_n$ .

In turbulent flow regime, the use of the charts presented in Chapter 4 (also in Edwini-Bonsu and Steffler 2004a, b) would present mathematical difficulties and would not be appropriate here. In view of this we would assume that the effects of wastewater drag and pressure are additive (contrary to our findings in Chapter 4).

This supposition would allow us to write a generalized algebraic flow rate expression in the headspace as:

$$Q_n = 0.8560R_n A_{hn} U_{wcn} + m_n \sqrt{\frac{g(\Delta P_n) b_n}{X_n R_n}} \quad [5.7a]$$

where  $m_n = A_{hn}(6.3985R_n + 1.8443)$ . The first term of Equation [5.7a] is due to wastewater drag whilst the second term is the contribution from pressure differential. It should be acknowledged here that the use of Equation [5.7a] instead of the chart would over predict the air flow rate in the connecting pipes especially in high wastewater flow and low pressure gradient induced flow regimes (Chapter 4). In this case, a reduction factor is proposed to account for the overestimation resulting from the superposition of the individual effects such that  $Q_n^* = (1-\psi)Q_n$ , where  $Q_n^*$  is the corrected flow rate and  $\psi$  is the reduction factor. This factor should vary with the relative strength of the two driving forces. It is found to be near zero for  $U_{Rn} = \lambda_n / R_n \geq 5.0$ , where  $\lambda_n = (|\Delta P| b_n g) / (X_n U_{wcn}^2)$ . In most cases, the factor is found to range between  $0.082 \leq \psi \leq 0.145$  for  $U_{Rn} < 5.0$ .

In the present case, since we are dealing with high pressure flows (resulting from auxiliary ventilator (scrubber/blower), dropstructure, wind and barometric pumping) the use of Equation [5.7a] is adequate. The corresponding pressure head loss in the sewer headspace can therefore be given as:

$$\Delta P_n = \frac{|(Q_n - W_n)|(Q_n - W_n)}{gT_n^2} \quad [5.7b]$$

here  $T_n = m_n \sqrt{b_n / (X_n R_n)}$  and  $W_n = 0.8560 A h_n U_{wcn} R_n$ .

### 5.3.3.2 Manhole eduction/induction

The air flow rate educted or inducted via manholes is a function of the pressure head in the manhole with respect to the local atmospheric pressure head. If we conceptually consider eduction (or induction) as an orifice flow, then the flow rate through the manhole opening, for an incompressible air, can be modelled using the standard orifice equation as:

$$Q_{Ej} = C d_j A_{0j} \sqrt{2g(P_{Ej} - P_{ATj})} \quad [5.8a]$$

from which the pressure head loss in the manhole element is obtained as:

$$P_{Ej} - P_{ATj} = \Delta P_j = \frac{|Q_{Ej}| Q_{Ej}}{2g(A_{0j} C d_j)^2} \quad [5.8b]$$

where the subscript "j" denotes manhole number,  $C d_j$  and  $A_{0j}$  are respectively the discharge coefficient and the cross-sectional area of the orifice (manhole pickhole),  $P_{ATj}$  is the ambient atmospheric pressure head above the j-th manhole location (which should be corrected for ambient wind effect),  $P_{Ej}$  is the pressure head in the manhole, and  $Q_{Ej}$  is the educted (or inducted) air flow rate.

It should be noted from Equation [5.8b] that when the ambient atmospheric pressure  $P_{ATj}$  is greater than the manhole pressure there will be suction of fresh air from the ambient environment into the sewer system and vice versa.

Obviously when  $P_{ATj} = P_{Ej}$  there will be no flow of air via the manhole. The occurrence of this phenomenon does not mean that there is no air flow in the adjoining sewer pipes. It simply indicates that there is not enough pressure head to drive the air out. The following assumptions and approximations are further made in the development of the theoretical formulation at the manhole structure: (1) the air is incompressible since we are dealing with low pressures. (2) the adjoining sewer conduits and manhole node are not surcharged with wastewater. (3) the cross-sectional area of and velocity distribution across a manhole element are uniform.

The only coefficient needed in Equation [5.8b] is the coefficient of discharge. Strictly speaking, this coefficient is affected by many factors, including the manhole opening size and shape, the inlet and exiting conditions, the flow rate, the specific weight of air, the viscosity of air, the specific heat of the air, and differential pressure. Other factors that may affect the coefficient include the surface roughness and dents in the edge of the manhole (Zhou 2000). Accurate estimation of this coefficient constitutes an accurate prediction of the air flow rate. The discharge coefficient is usually determined experimentally or from experience. For example the value for a sharp-edged orifice ranges from 0.59 to 0.68 (Arora 1993). In some cases, the coefficient of discharge is given as a function of the Reynolds number in the relation:

$$Cd_j = 0.592 + \frac{4.50}{\sqrt{Re}} \quad [5.8c]$$



where  $Re = V_{Ej}d_j/\nu$ ,  $d_j$  is the diameter of the orifice and  $V_{Ej}$  is the velocity through the orifice.

### **5.3.3.3 Dropstructure pumping effect**

Aside from the basic sewer ventilation dynamics caused by wastewater drag and other natural driving forces, there are other physical structures and functions of a deep tunnel sewer that can add to or detract from the general ventilation rate and odour magnitude of a given sewer system. In many cases, dropstructures are the single greatest contributors to ventilation and hence odour releases from deep trunk sewers. Dropstructure usually drops wastewater from a higher elevation smaller diameter sewer pipe into a lower elevation larger diameter sewer pipe. The fall of wastewater through a height could cause severe turbulence and air entrainment. Several complex inter-relationships between hydraulics and pneumatics come into play. Like in sewer atmospheres, drag is also the main driving force except that the drag is further enhanced due to increased surface contact area and dispersion of the wastewater.

The emphasis here is not to model the dynamics of air flow in a dropstructure per se, but of particular interest is to have a means of assessing its pressurization or pumping effect on the overall system air flow dynamics. In this paper, the effect of dropstructure, where it exists, is conceptually modelled as a pump unit whose characteristic curve has to be prescribed. With this supposition, the net pressure head developed across the dropstructure can be expressed as a function of the

outlet flow rate in a form of a polynomial. The simplest approach that is reasonably general would be to invoke a second-order pumping characteristic function of the form:

$$\Delta P_{DS} = f(Q) = \gamma Q^2 + \alpha Q + \beta \quad [5.9]$$

in which  $Q$  is the dropstructure outlet or pumping flow rate,  $\Delta P_{DS}$  is the head increase across the dropstructure, and  $\gamma$ ,  $\alpha$  and  $\beta$  are constants. We should note that if this function is to be concave down and always sloping downwards for increasing  $Q$  (which should presumably be the general trend), then  $\gamma < 0$ ,  $\alpha < 0$ , and  $\beta > 0$ . These constants would depend on a number of variables including the quantity of wastewater being dropped, and size, height and shape of the dropstructure. It is recommended that future research effort be devoted to establishing the exact nature of these constants or even the form of the equation.

#### **5.3.3.4 Auxiliary ventilators: scrubbers and mechanical blowers**

Some municipal sewer system reaches are sometimes mechanically ventilated using auxiliary ventilators (forced draft) such as blowers and scrubbers to combat corrosive, odorous and other hazardous gases. These ventilators act to induce sewer air flow at openings such as perforated manhole covers. In this paper, the effects of scrubbers and blowers are represented (in a network) as fans and pumps, respectively. Scrubber/blower performance curve (pressure head as a function of air quantity flowing through the ventilator) characteristically depends on a number of factors including speed, motor horsepower and efficiency. The exact relationship (in most cases a polynomial) can be obtained from the technical

manual that comes with the equipment.

## **5.4 MODEL APPLICATIONS**

An effective determination of ventilation and pressurization dynamics of any sewer system airspaces would require the use of both theoretical analysis and a limited field data gathering efforts. These two requirements are strongly stressed in the two model applications discussed in this section. Modeling of air flow dynamics in both hypothetical and real sewer systems is presented to illustrate the applicability of the modeling formulation. The Kenilworth sewer system in the City of Edmonton is used for the latter case. This sewer system consists of nine (9) dropstructures whose pumping characteristic curves are not yet established.

### **5.4.1. Case I: A Hypothetical Sewer System**

In this section a procedural computation is illustrated to show the applicability of the theoretical formulation outlined above to a hypothetical, yet a typical section of a modern municipal trunk sewer entity as shown in Figure 5-1a. The terms needed for the analysis are shown in the figure. The system consists of three junction manholes (1, 2 and 3) with pickholes which serve as potential sources of malodourous sanitary air releases into the ambient atmosphere or fresh air into the system, an auxiliary ventilator (both scrubber and blower are considered) of known performance curve installed between manhole 1 and manhole 2, and a dropstructure at the upstream of the system. The dropstructure depicted here drops

wastewater from sewer pipe [0] into sewer pipe [1] through elevation difference  $H$ . The combination of the effects of the dropstructure, scrubber/blower, wastewater flow in the sewer conduits and environmental driving forces such as wind speed and barometric pressure variations within the locality would act to sustain air movement in the entire system.

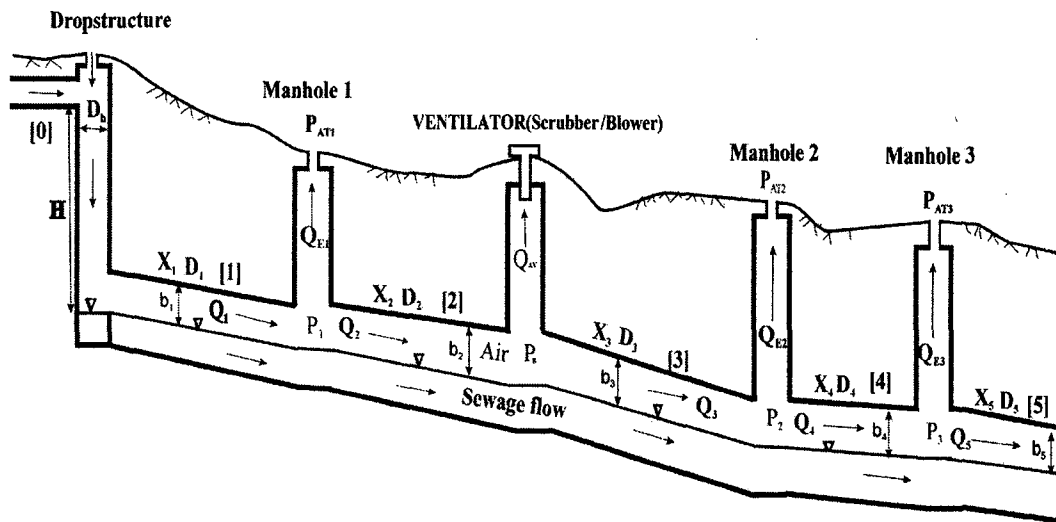


**Figure 5-1a: Schematic of an isolated municipal sewer system**

To apply the system theory to this example, the sewer system is first represented as a closed network with the atmosphere as a reference line as shown in Figure 5-1b. In this network there are four (4) junction nodes and five (5) loops. It is also assumed that pipe [5] ends at an outfall of known pressure head  $P_5$ . It should be noted here that the directions of the air flow rates are arbitrarily assumed. The actual directions would depend upon the magnitude and nature of the driving forces as well as upon the system variables.

Applying Equation [5.3] to the junction manholes (MH1, MH2 and MH3) and the ventilator location, we have the following system of equations:

$$\text{MH1: } F_1 = Q_1 - Q_2 - Q_{E1} = 0$$

$$\text{CJ1: } F_2 = Q_2 - Q_{AV} - Q_3 = 0 \text{ (location of the auxiliary ventilator)}$$

$$\text{MH2: } F_3 = Q_3 - Q_4 - Q_{E2} = 0 \quad [5.10a]$$

$$\text{MH3: } F_4 = Q_4 - Q_{E3} - Q_5 = 0$$

where  $Q_1, \dots, Q_5$  are the unknown air flow rates in the sewer pipes,  $Q_{E1}$ ,  $Q_{E2}$  and  $Q_{E3}$  are the unknown air flow rates via manholes MH1, MH2 and MH3, respectively, and  $Q_{AV}$  is the air flow rate through the auxiliary ventilator (scrubber or blower). The matrix form of these set of nodal equations can be written as:

$$\begin{bmatrix} 1 & -1 & -1 & 0 & 0 & 0 & 0 & 0 & 0 \\ 0 & 1 & 0 & -1 & -1 & 0 & 0 & 0 & 0 \\ 0 & 0 & 0 & 0 & 1 & -1 & -1 & 0 & 0 \\ 0 & 0 & 0 & 0 & 0 & 1 & 0 & -1 & -1 \end{bmatrix} \begin{bmatrix} Q_1 \\ Q_2 \\ Q_{E1} \\ Q_{AV} \\ Q_3 \\ Q_4 \\ Q_{E2} \\ Q_{E3} \\ Q_5 \end{bmatrix} = \begin{bmatrix} 0 \\ 0 \\ 0 \\ 0 \\ 0 \\ 0 \\ 0 \\ 0 \\ 0 \end{bmatrix} \quad [5.10b]$$

from which the incidence matrix **I** and its elements can easily be recognized. In Equation [5.10a]  $F_i$  for any number  $i$  is any equation which has been arranged into the form  $F_i = 0$ ; this format is useful for identification purposes and also for

subsequent mathematical and numerical developments.

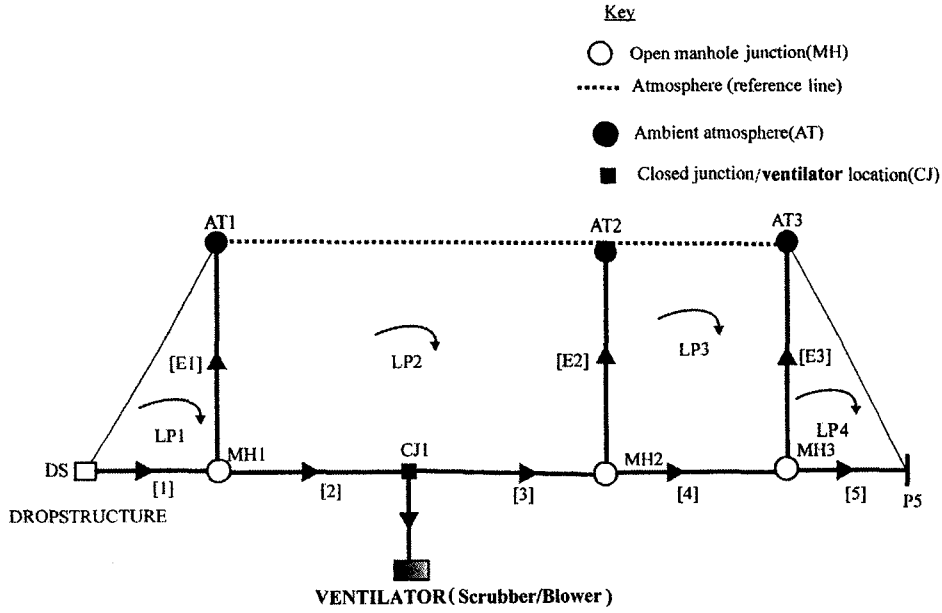


**Figure 5-1b: Network representation of Figure 5-1a**

If we further assume that both wastewater and pressure are responsible for the air flow dynamics and that flow is turbulent, then the work-energy equation (Equation [5.4c]) around the four (4) main loops may be expressed as:

$$\begin{aligned}
 \text{LP1: } F_5 &= \Delta P_{DS}(Q_1) - \frac{|Q_{E1}|Q_{E1}}{2g(A_{01}C_{d1})^2} - \frac{|(Q_1 - W_1)|(Q_1 - W_1)}{gT_1^2} - P_{AT1} = 0 \\
 \text{LP2: } F_6 &= \frac{|Q_{E1}|Q_{E1}}{2g(A_{01}C_{d1})^2} + P_{AT1} - P_{AT2} - \frac{|Q_{E2}|Q_{E2}}{2g(A_{02}C_{d2})^2} - \\
 &\quad \frac{|(Q_3 - W_3)|(Q_3 - W_3)}{gT_3^2} - \frac{|(Q_2 - W_2)|(Q_2 - W_2)}{gT_2^2} = 0 \\
 \text{LP3: } F_7 &= \frac{|Q_{E2}|Q_{E2}}{2g(A_{02}C_{d2})^2} + P_{AT2} - P_{AT3} - \frac{|Q_{E3}|Q_{E3}}{2g(A_{03}C_{d3})^2} - \\
 &\quad \frac{|(Q_4 - W_4)|(Q_4 - W_4)}{gT_4^2} = 0
 \end{aligned} \tag{5.11a}$$

$$\text{LP4: } F_8 = \frac{|Q_{E3}|Q_{E3}}{2g(A_{03}C_{d3})^2} - \frac{|(Q_5 - W_5)|(Q_5 - W_5)}{gT_5^2} + P_{AT3} - P_5 = 0$$

These work-energy equations (Equation [5.11a]) are obtained by starting at MH1, MH2 and MH3, and traversing the loops in the clockwise direction. If the assumed direction of flow opposes this traverse, a minus sign precedes the head loss term for that element. An additional equation can be obtained from the loop formed from the ventilator location to the atmosphere as:

$$F_9 = \Delta P_{AV}(Q_{AV}) + kQ^n - \frac{|Q_{E1}|Q_{E1}}{2g(A_{01}C_{d1})^2} + \frac{|(Q_2 - W_2)|(Q_2 - W_2)}{gT_2^2} - P_{AT1} = 0 \quad [5.11b]$$

where  $\Delta P_{AV}(Q_{AV})$  is the pressure head generated by the ventilator, the term  $kQ^n$  is the head loss in the ventilator ducting using Darcy-Weisbach equation,  $k$  is a constant for the duct and  $n=2$ . In Equation [5.11],  $P_{AT}$ 's are the local atmospheric pressure heads at the manhole locations. These heads may be due to barometric pressure or wind speed or a combination of the two. Since a high barometric pressure gradient usually occurs with unstable atmospheric conditions and therefore at a time of significant wind velocity, the resultant effect on sewer ventilation will depend on the magnitude and direction of the two forces. If both act in the same direction, an air flow rate of greatest magnitude can be expected. However, if the barometric pressure difference acts in the opposite direction to wind, a reduced rate of ventilating air flow is probable.

We now choose a way to represent the dropstructure pumping head  $\Delta P_{DS}(Q_1)$ . In this illustration we assume a characteristic function of Equation [5.9] such that:

$$\Delta P_{DS}(Q_1) = \gamma Q_1^2 + \alpha Q_1 + \beta \quad [5.12]$$

in which  $Q_1$  is the flow rate in pipe [1] which is responsible for downstream system pressurization. We choose the characteristic curve constants as  $\gamma = -0.25$ ,  $\alpha = -0.55$  and  $\beta = 9.55$  which in effect gives a quadratic relationship between the head and the output flow rate.

Substituting Equation [5.12] into Equation [5.11], leads to a system of nine (9) equations and nine (9) unknowns. The resulting set of equations, as would always be the case, is a mix of non-linear and linear algebraic system of Q-equations and has to be solved simultaneously. The most popular solution method is the Newton's iterative algorithm.

If we write the system of equations (Equations [5.10] and [5.11]) in a general form:

$$\mathbf{F}(\mathbf{Q}) = \mathbf{0} \quad [5.13a]$$

then the Newton's iterative formula for solving such equations can be written as:

$$\mathbf{Q}^{k+1} = \mathbf{Q}^k - \mathbf{J}^{-1} \mathbf{F}^k \quad [5.13b]$$

here  $\mathbf{Q}$  is an entire column vector of unknown flow rates,  $\mathbf{F}$  is an entire column vector of equations, and  $\mathbf{J}^{-1}$  is the inverse of a matrix  $\mathbf{J}$  which is the Jacobian. The elements of the Jacobian are:



$$\mathbf{J} = \begin{bmatrix} \frac{\partial F_1}{\partial Q_1} & \frac{\partial F_1}{\partial Q_2} & \cdots & \frac{\partial F_1}{\partial Q_n} \\ \frac{\partial F_2}{\partial Q_1} & \frac{\partial F_2}{\partial Q_2} & \cdots & \frac{\partial F_2}{\partial Q_n} \\ \vdots & \vdots & \ddots & \vdots \\ \frac{\partial F_n}{\partial Q_1} & \frac{\partial F_n}{\partial Q_2} & \cdots & \frac{\partial F_n}{\partial Q_n} \end{bmatrix} \quad [5.13c]$$

Likewise  $\mathbf{Q}$  and  $\mathbf{F}$  are actually

$$\mathbf{Q} = \begin{bmatrix} Q_1 \\ Q_2 \\ \vdots \\ Q_n \end{bmatrix}, \quad \mathbf{F} = \begin{bmatrix} F_1 \\ F_2 \\ \vdots \\ F_n \end{bmatrix} \quad [5.13d]$$

Basically, this iterative method calculates new values of the unknowns at each iteration step by linearization of the equations and by solving for the resultant set of system of linear equations. This algorithm has been coded in a MATLAB computer program for solving any system of equations. Outputs from the program are the air flow rates throughout the system. The solution algorithm terminates when a prescribed error tolerance on the norm of the residual  $\|\mathbf{F}(\mathbf{Q})\|$  has been achieved. Thus

$$\|\mathbf{F}(\mathbf{Q})\| \leq \text{'error tolerance'} \quad [5.14]$$

A tolerance of  $10^{-6}$  is used in this convergence criterion.

It is of interest to examine the influences of the scrubber/blower, the downstream pressure  $P_5$  and the coefficient of discharge on air movement for this hypothetical system. Figure 5-2 shows the effects of the auxiliary ventilator on the air flows via the three manholes (both velocity and flow rate) and in the atmospheres of the sewer pipes. The effects of the ventilator on the overall air dynamics are assessed for the three conditions of 'shut-down', 'blowing' (blower) and 'sucking' (scrubber). A second order polynomial performance curve given by Equation [5.15] is assumed for both blower (pump) and scrubber (fan):

$$\Delta P_{AV}(Q_{AV}) = \gamma Q_{AV}^2 + \alpha Q_{AV} + \beta \quad [5.15]$$

where the parameters  $\gamma = -0.095$ ,  $\alpha = -2.165$  and  $\beta = 15.5$  are assumed. Other assumed system variables and flow data are indicated on the figure. Evidently when the ventilator is in the 'shut-down' mode, air and wastewater flow in the same direction, with air being released from the sewer (Figures 5-2a and 5-2b). As expected when the blower injects air into the system, eduction rate is further increased and the air flow rates in the downstream sewer pipes [3], [4] and [5] as shown in Figure 5-2c are accelerated appreciably. On the contrary, air movement in the upstream pipes [1] and [2] is retarded. When the scrubber is in operation ('sucking' mode), fresh air from the ambient environment enters the system via all the three manholes and with the exception of pipes [1] and [2] which have increased flows, there is complete reversal of flows in all the downstream sewer pipes (i.e. in opposite direction to the wastewater flow). In this case, the ventilator is found to have the capacity to avert eduction (avert odour into the ambient environment) via all the three manholes.

The effects of some selected outfall pressure heads  $P_5$  (with the ventilator in 'shut down' mode) are shown in Figure 5-3. With a negative pressure head of -2 m, eduction is reduced in manholes 1 and 2 while induction occurs at manhole 3. However with a positive pressure head of 2 m, it is noticed that eduction is increased in all the three manholes. As observed in Figure 5-3b, the pressure heads investigated also have significant effects on the sewer headspace flow rates. Headspace flow rates are observed to increase with decreasing outfall pressure head and vice versa. In all the above computations, it is taken that there is no variation in wind speed or barometric pressure within the neighborhood (i.e. atmospheric pressure is assumed constant in the locality) and hence  $P_{AT1} = P_{AT2} = P_{AT3} = 0$ . Again all manholes are assumed to have the same orifice diameter of 25 mm, coefficient of discharge value of 0.65, and four (4) pickholes per manhole cover. Sewer pipes of equal diameter of 2250 mm and equal reach of 350 m are further assumed.

The effect of the coefficient of discharge on eduction is also investigated when the ventilator is in 'shut-down' mode as shown in Figure 5-4. As can be seen in the figure, the eduction velocity is found to be sensitive to the discharge coefficient. This reinforces the need for an accurate determination of the coefficient in any practical computations. As expected, eduction increases with decreasing exiting friction.

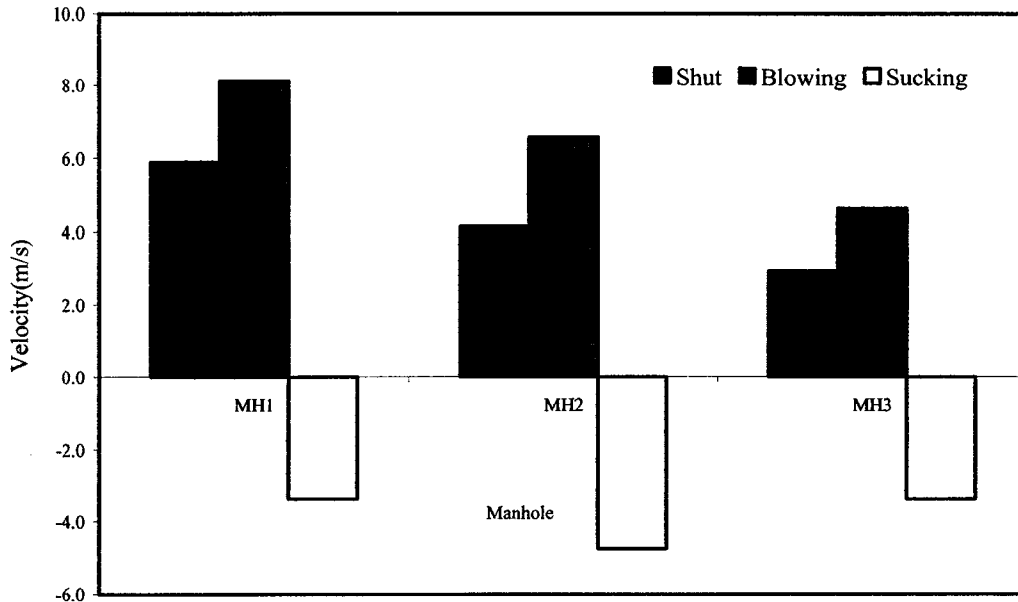


**Figure 5-2a: Influence of auxiliary ventilation on manhole velocity,  $C_d=0.65$ ,  $b/D=50\%$ ,  $U_{wc}=1\text{ m/s}$ ,  $P_5=0\text{ m}$ ,  $k=0$**

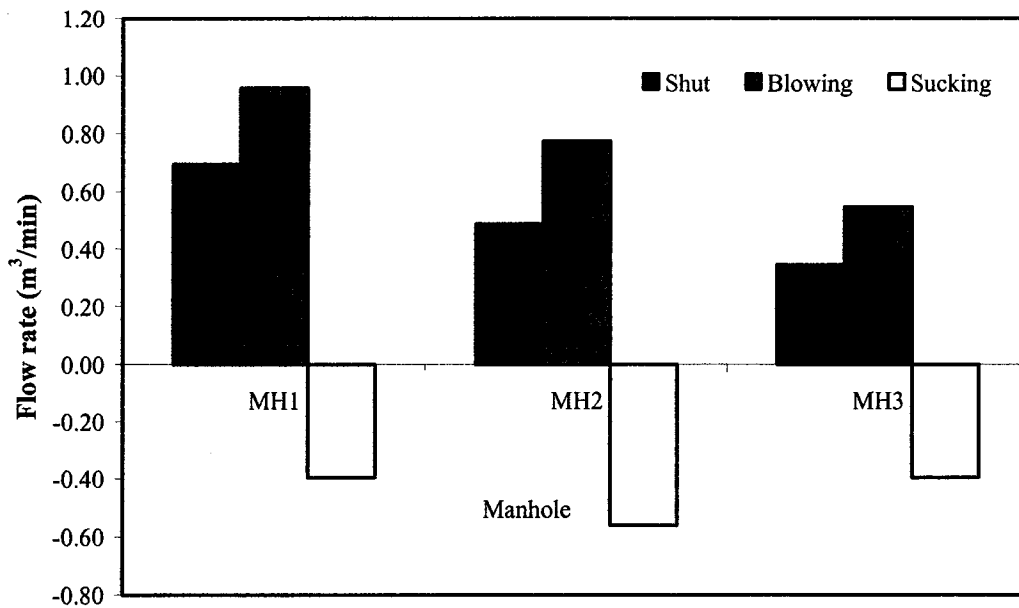


**Figure 5-2b: Influence of auxiliary ventilation on manhole flow rate,  $C_d=0.65$ ,  $b/D=50\%$ ,  $U_{wc}=1\text{ m/s}$ ,  $P_5=0\text{ m}$ ,  $k=0$**

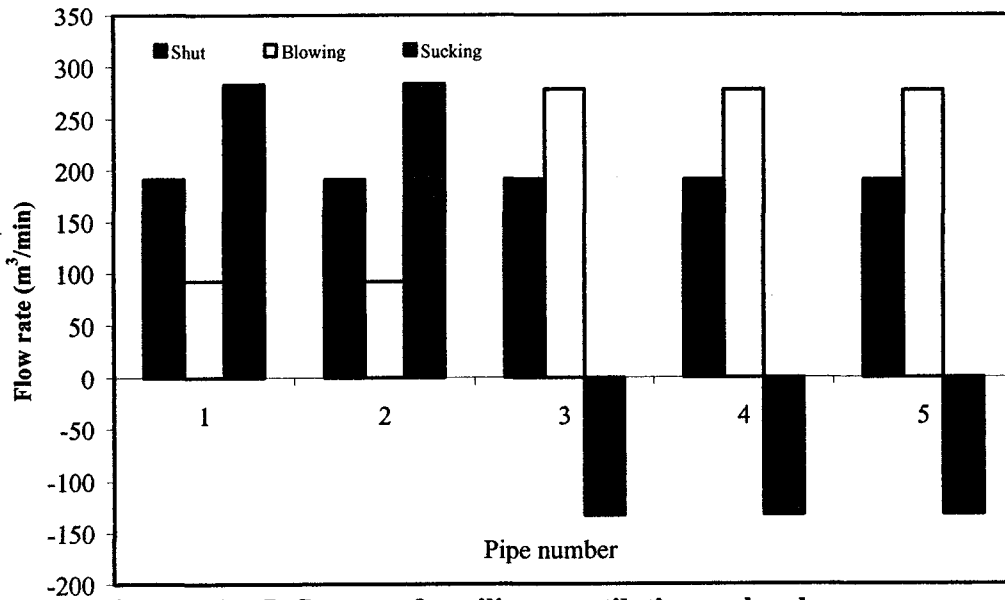


Figure 5-2c: Influence of auxiliary ventilation on headspace flow rate,  $C_d = 0.65$ ,  $b/D = 50\%$ ,  $U_{wc} = 1$  m/s,  $P_5 = 0$  m,  $k = 0$

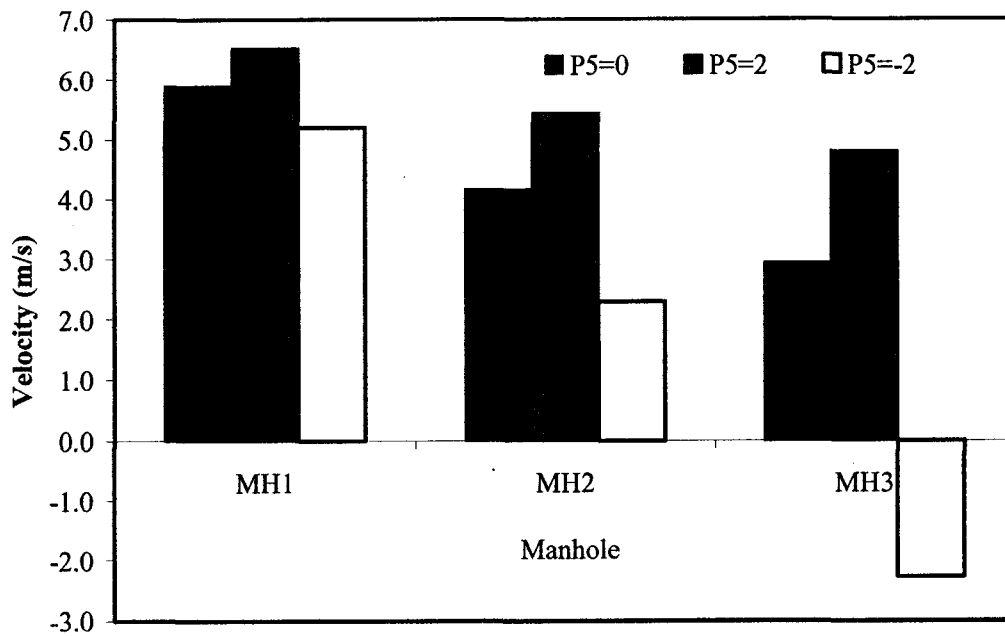
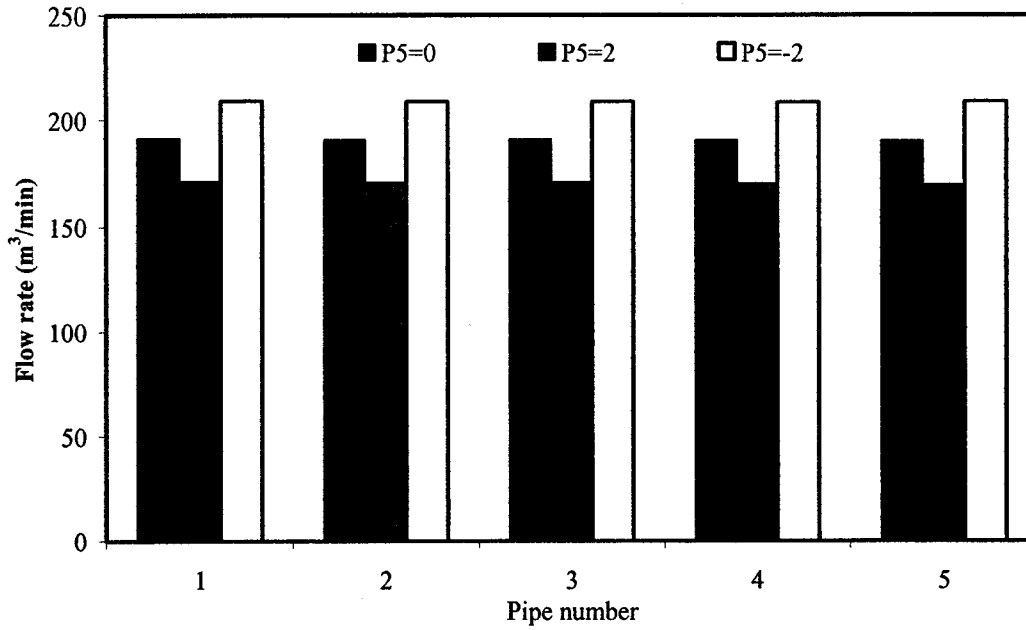
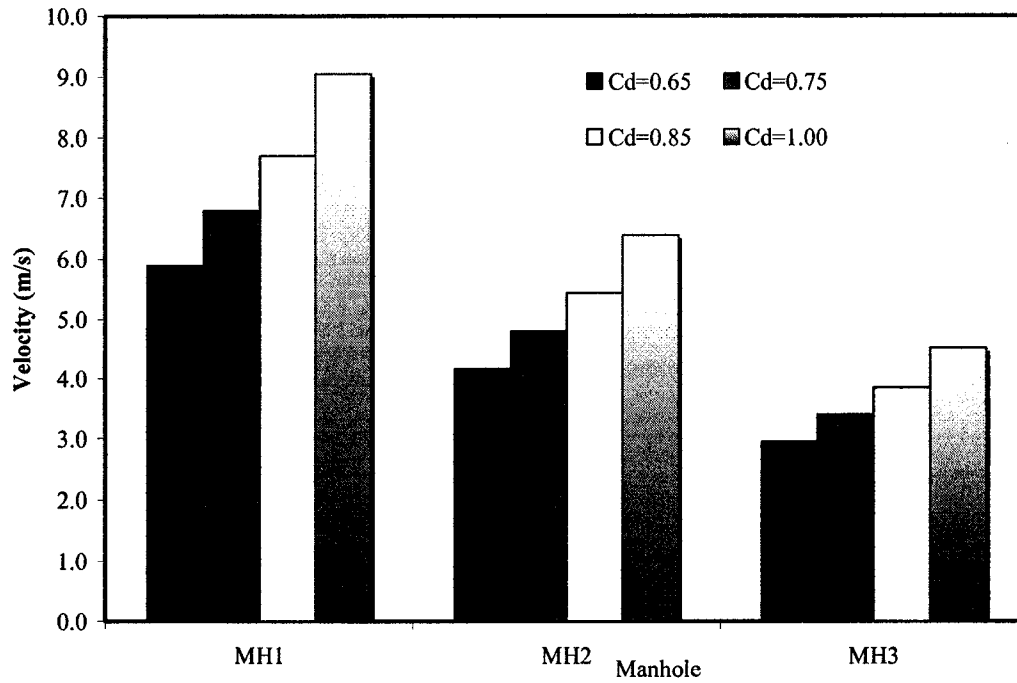


Figure 5-3a: Effect of outfall pressure head,  $P_5$ , (m) on air eduction,  $C_d = 0.65$ ,  $Q_{AV} = 0$  m³/min



**Figure 5-3b: Effect of outfall pressure head,  $P_5$ , (m) on headspace flow rate,  $Q_{AV} = 0 \text{ m}^3/\text{min}$ ,  $U_{wc} = 1 \text{ m/s}$ ,  $C_d = 0.65$ ,  $b/D = 50\%$**



**Figure 5-4: Effect of coefficient of discharge on eduction,  $Q_{AV} = 0 \text{ m}^3/\text{min}$ ,  $P_5 = 0 \text{ m}$ ,  $b/D = 50\%$**

Overall, the simulations demonstrate that the model can provide novel insights about the complex nature of the air flow dynamics at a level of detail that would not easily be attainable by field measurements. The system model can predict the causes of sewer air flow as well as the amounts and directions of the transporting air. It can also be used to assess the capacity of a ventilator to control education (odour releases). It must be said that the sewer system illustrated here is a hypothetical and over-simplified one. However in a real sewer system, wind data and barometric pumping will have to be included and again many nodal manholes and dropstructures might be involved and the system of equations could subsequently be large as we will see in the next application example.

#### **5.4.2 Case II: The Kenilworth Sewer System**

The purpose of this section is to apply the system formulation to lay down groundwork for subsequent modeling of air movement within the Kenilworth sewer system in the City of Edmonton as it relates to odour release and complaint. Based on the sewer plans and data supplied by the Drainage Services of the City of Edmonton, the system air motive forces are identified as well as the pressure causing conditions which eject odour into the locality.

##### **5.4.2.1 System configuration and available data**

The Kenilworth sewer system is made up of two main interceptor sewer tunnels located along the 71<sup>st</sup> Street and the 88<sup>nd</sup> Avenue. The two interceptors converge on the 91<sup>st</sup> Avenue into a larger pipe of diameter 2550 mm. Figure 5-5 shows a

sketch of the system based on the plans and documents supplied by the Drainage Services of the City of Edmonton. Diameters and lengths of all tributary sewer pipes and interceptors are indicated, as well as where manholes, dropstructures and scrubber are located. A diagram showing available sewer pipe slopes is provided in Figure B-2 in Appendix B. The maximum output of the scrubber is reported to be 15000 CFM ( $\sim 424.75 \text{ m}^3/\text{min}$ ) and is located about 125 m north of manhole MH5 (71<sup>st</sup> Street & N 87 Ave). The system spans about 2.11 by 3.31  $\text{km}^2$  and consists of nine (9) dropstructures. For convenience all manholes and dropstructures on the system are renumbered as shown in the figure. All junction manholes (with pickholes) and dropstructures are labeled as MH and DS, respectively. There are fifteen (15) junction manholes, each having four (4) pickholes of 25 mm diameter.

Data on natural ventilation forces within the system are not well-documented. No barometric pressure and wind speed data are available. Again, wastewater flow data in almost all the contributory pipes and laterals on the system are not available at this time. Only pipes [1], [33] and [44] have some measured wastewater flow data which are not useful because they were not measured on the same dates. The diurnal wastewater data available at the inlets of pipes [1] and [44] are displayed in Figures 5-6 and 5-8, respectively. Figure 5-7 shows wastewater data for the outlet of pipe [33]. Based on these data, the average wastewater velocity in pipes [1], [33] and [44] are respectively computed as 0.0825 m/s, 0.7405 m/s and 0.9984 m/s. The average wastewater flow depths for



the corresponding pipes in the same order are also computed as 0.2276 m, 0.9488 m and 0.5517 m. Aside from the fact that the data were measured on separate dates, they are not adequate to describe the air flow dynamics due to wastewater drag phenomenon in the entire system. It must be stressed here again that an effective determination of the air movement in the whole system would require wastewater flow data inputs for at least the main contributory pipes.

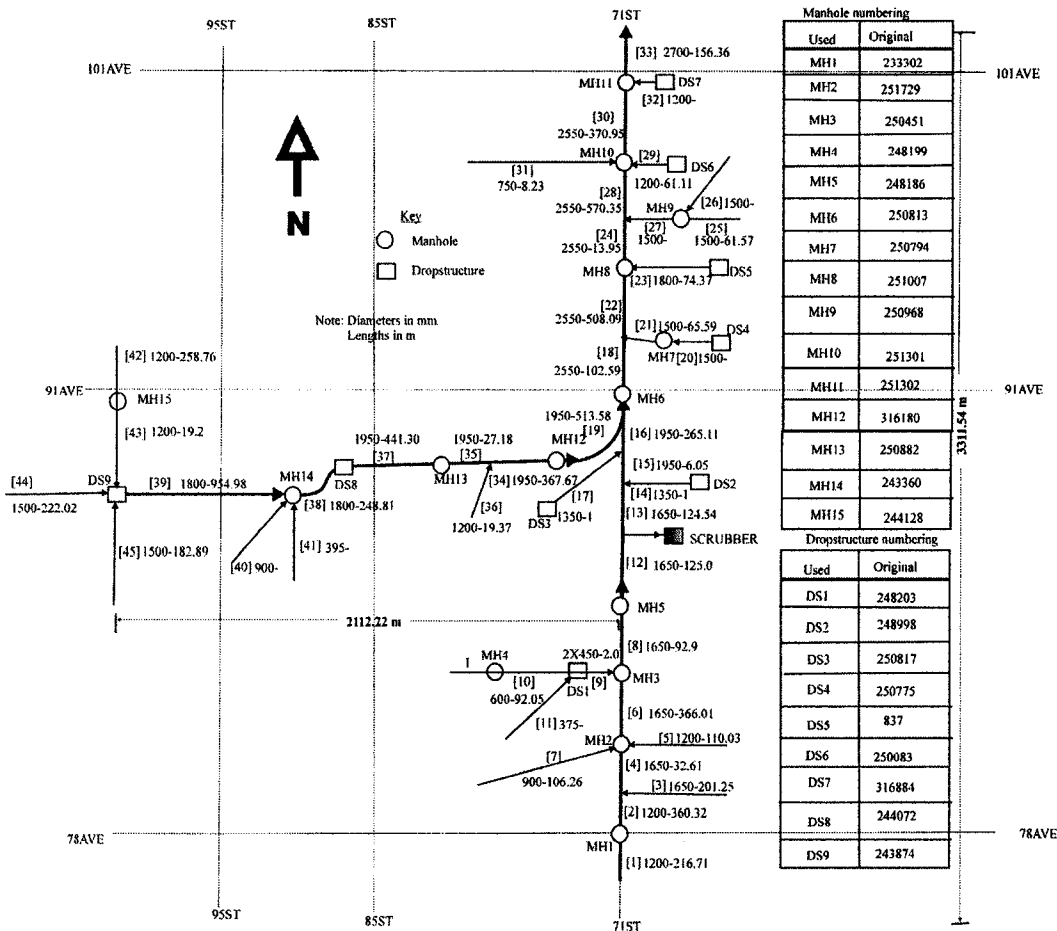


**Figure 5-5: The Kenilworth sewer system (Not drawn to scale)**

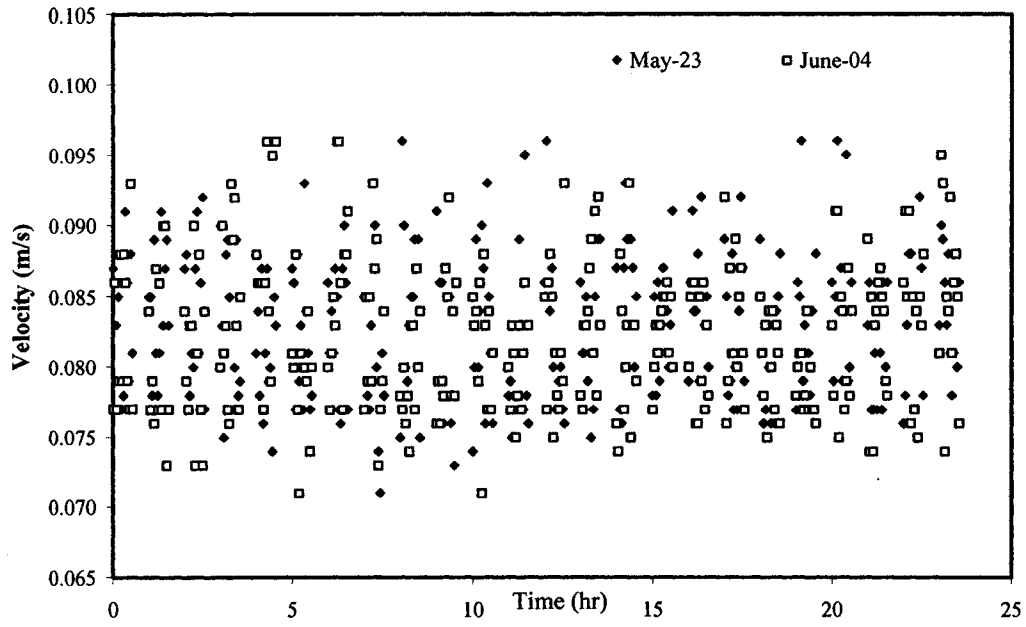


**Figure 5-6a: Diurnal wastewater velocity in pipe [1]  
(May/June 2003)**

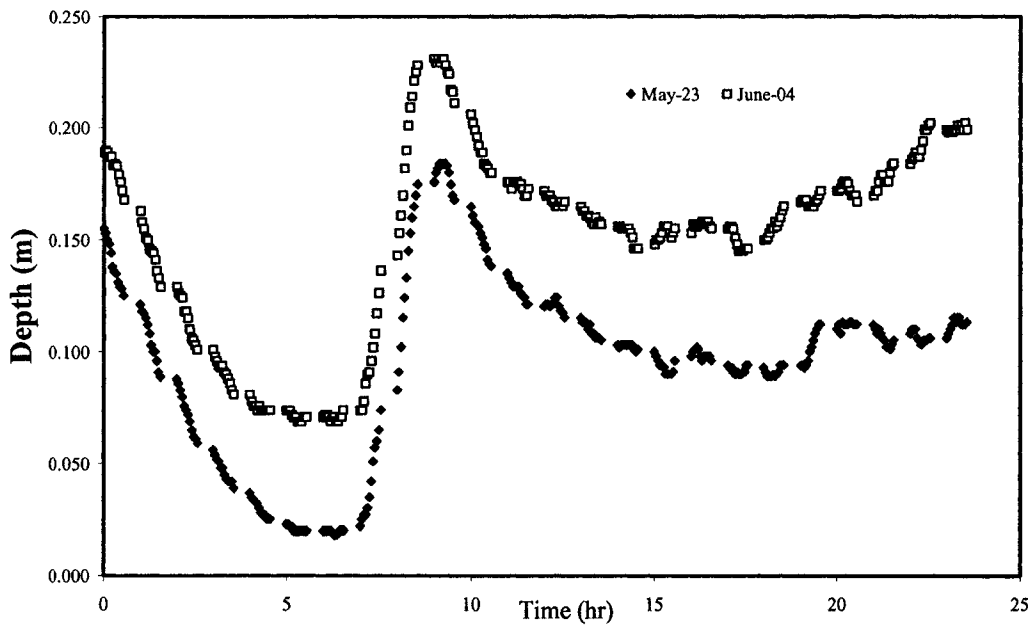


**Figure 5-6b: Diurnal wastewater flow depth in pipe [1]  
(May/June 2003)**

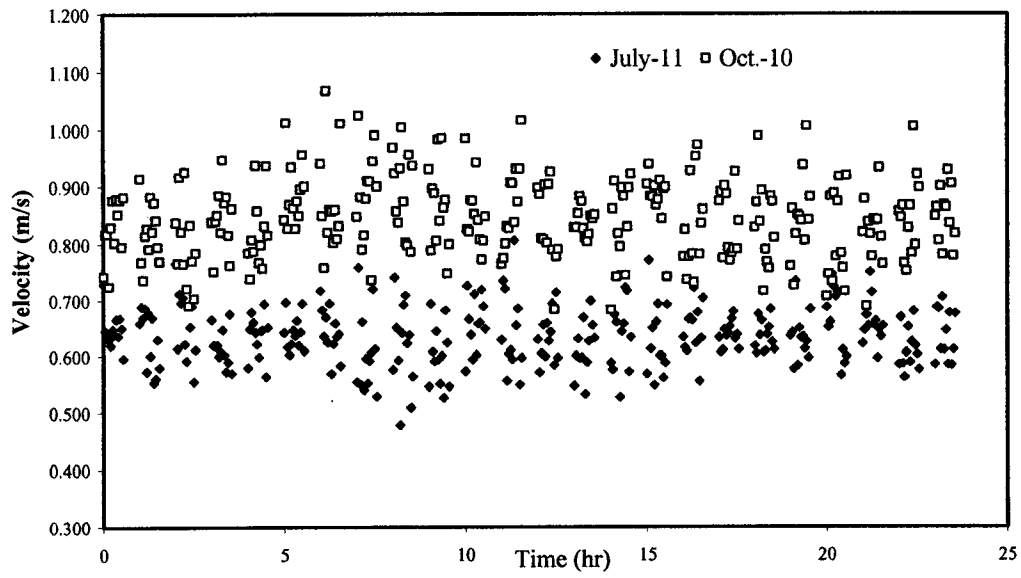


**Figure 5-7a:Diurnal wastewater velocity in pipe [33] (July/October 2003)**

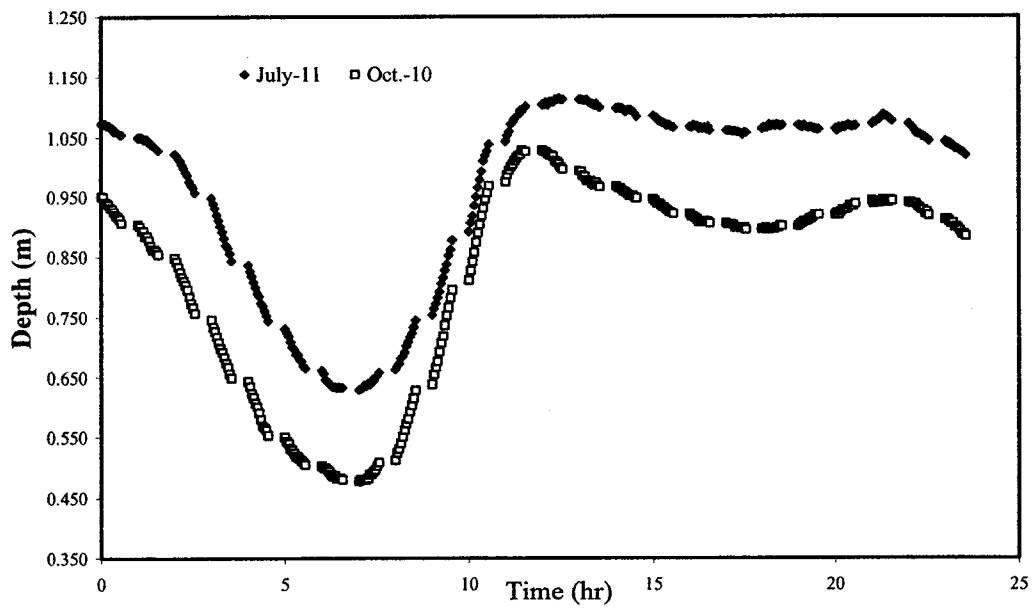


**Figure 5-7b:Diurnal wastewater flow depth in pipe [33] (July/October 2003)**

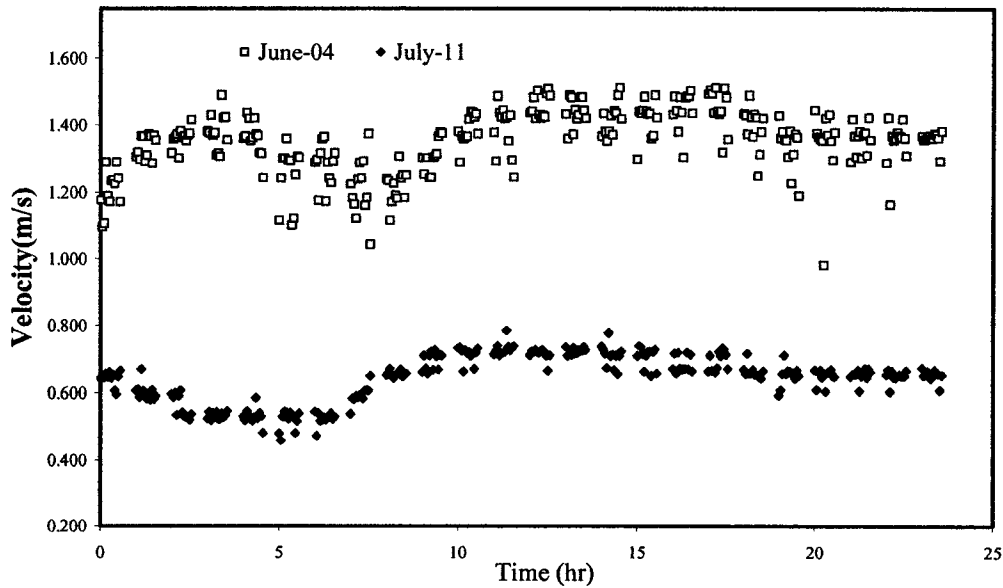


**Figure 5-8a: Diurnal wastewater velocity in pipe [44]  
(June/July 2003)**

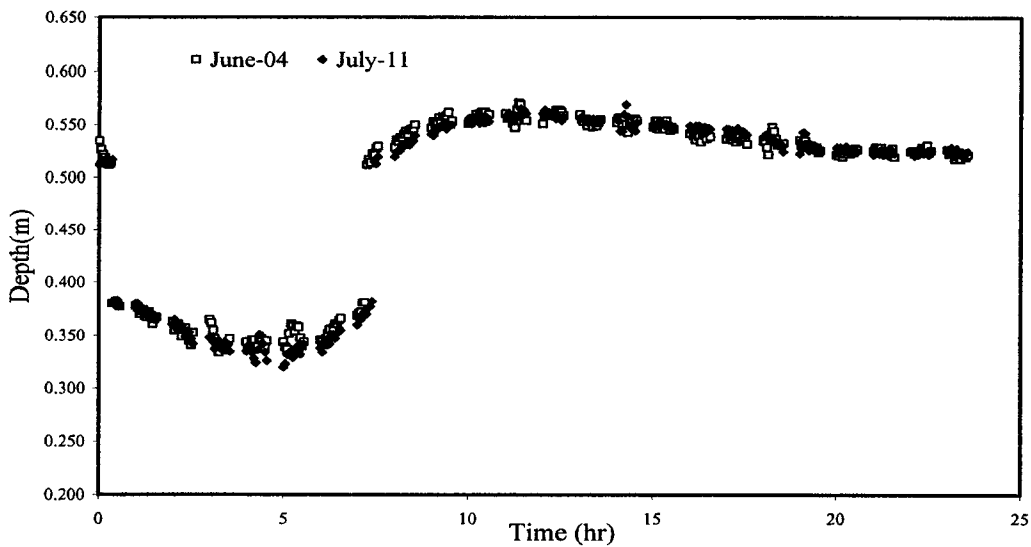


**Figure 5-8b: Diurnal wastewater flow depth in pipe [44]  
(June/July 2003)**

Available anemometric field measurements of educting velocities via manholes MH1, MH4, MH11 and MH12 are plotted in Figure 5-9a for the two cases of the scrubber in 'shut down' and in 'sucking' modes. The high educting velocities and

the low reported wastewater velocities speculatively suggest that the air flow in this system is caused predominantly by dropstructure pressurization phenomenon. Anemometric test measurements available also indicate that some manholes within the system induct ambient air into the system. Typical measured average values of air velocity via such manholes are indicated in Figure 5-9b. It is interesting to observe that manholes MH9 and MH14 exhibit dual dynamic tendencies. On one test occasion they admit fresh air into the system and another test day they expunge foul air into the ambient environment. It is not clear at this point if this phenomenon is caused by the internal driving forces or external unknown forces such as wind speed or barometric variations. One thing is however certain: If the pressures in these manholes are less than the atmospheric pressure, air will be forced in and it appears this condition prevails sometimes at these manhole locations.

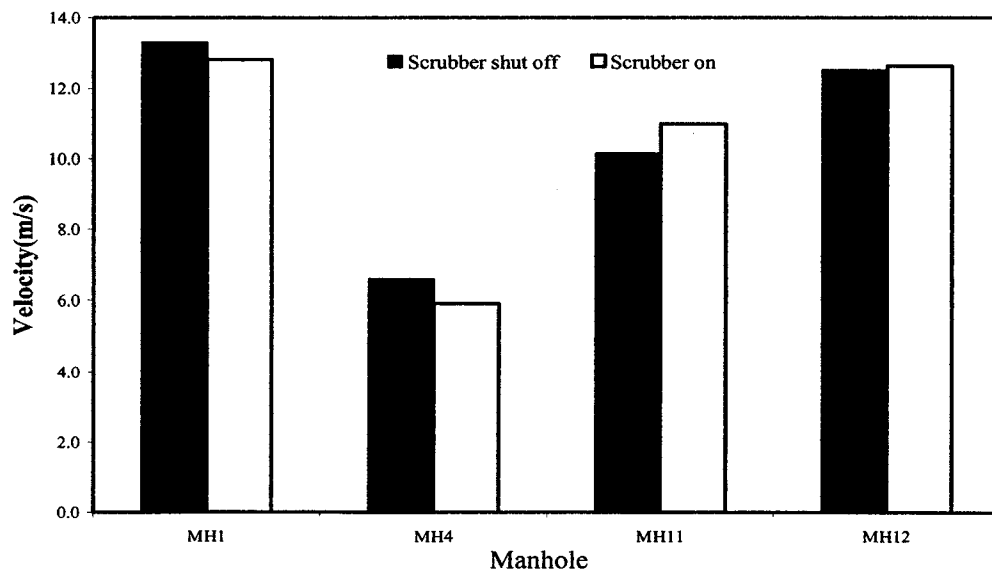


**Figure 5-9a: Field measurement of average educting velocity**

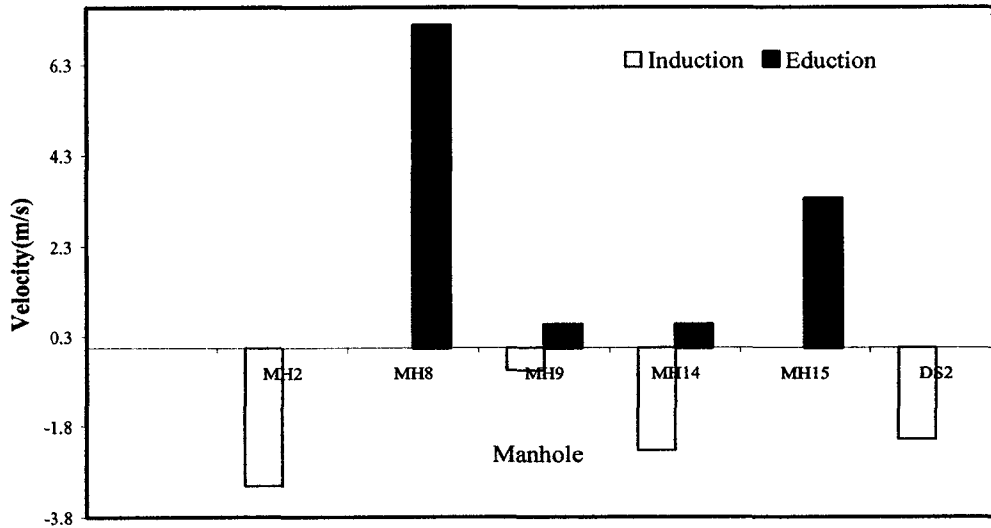


**Figure 5-9b: Field measurement of average educting/inducting velocity**

#### 5.4.2.2 Theoretical predictions

Just as in the hypothetical case, the Kenilworth sewer system is first represented as a closed network with the ambient atmosphere as a reference line as shown in Figure 5-10. All the terms required for the theoretical analysis are indicated in the figure. Closed junctions are designated as CJ in the network. The air flow directions in all manholes and connecting pipes are arbitrarily assumed.

There are twenty-five (25) nodes and thirty-eight (38) loops which lead to a system of twenty-five (25) linear and thirty-eight (38) non-linear equations to solve. These equations are given in Appendix B.

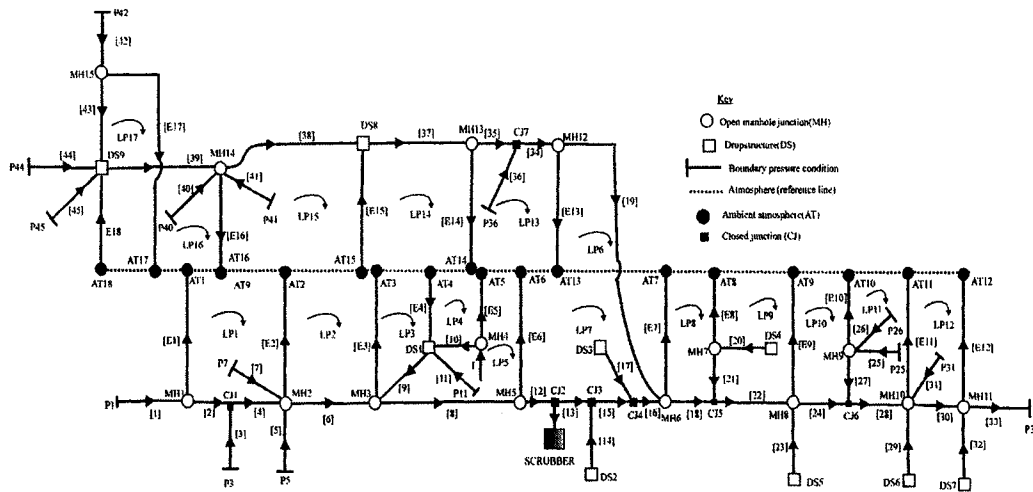


**Figure 5-10: Network representation of Figure 5-5**

Of significance is to determine the overall system air flow response to pressure, dropstructures and wastewater drag phenomena. However in order to make any meaningful theoretical predictions, a number of assumptions would have to be made due to lack of detailed system data. These assumptions are:

- The quadratic characteristic function (Equation [5-9]) is valid to describe the dropstructure pumping dynamics. The characteristic function parameters assumed for this application exercise are  $\gamma = -0.25$ ,  $\alpha = -0.55$  and  $\beta = 19.55$ .
- The externally-imposed pressures  $P_1, P_3, \dots, P_{45}$  at the end of the adjoining pipes (Figure 5-10) are arbitrarily chosen, but ensured that they are within reported pressure data measurements in the City of Edmonton's sewer systems. Some air pressure tests within this system and nearby systems indicate that the mean pressure varies in the range of  $\pm 23$  m of air (Odor

and Corrosion Technology Consultants 1999a; Asset Management and Public Works 2003). The assumed pressures given in Appendix B serve as boundary conditions for the isolated system.

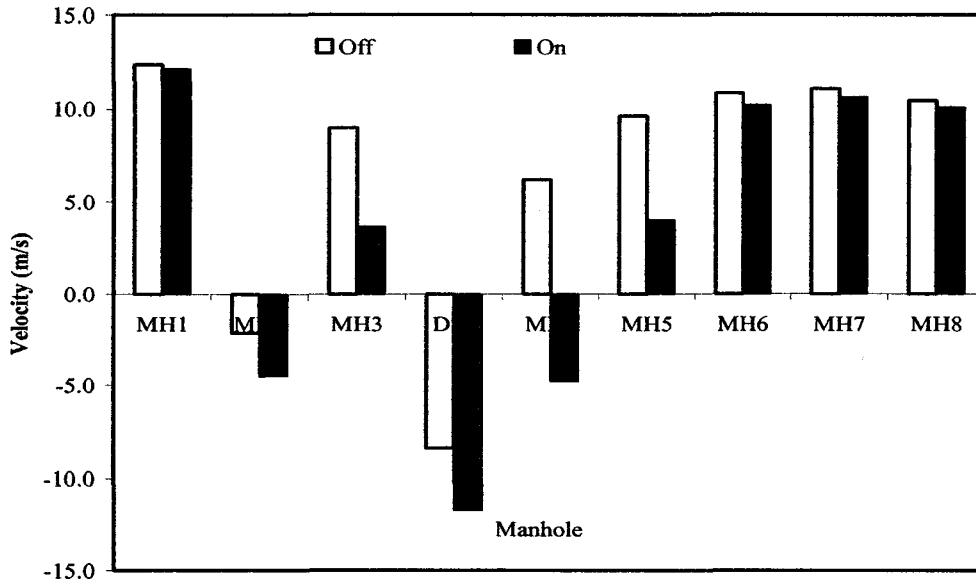
- The atmospheric pressure variations within the neighborhood (due to wind or barometric pressure) are assumed zero (since no data on wind speed or atmospheric pressure variations are available). Thus the driving forces for air movement in the system are friction between the sewer headspace air and moving wastewater, and dropstructure pumping phenomenon. This assumption may lead to serious miscalculations if indeed these external forces are operative and vary in the area.
- The air flow in the system is in the turbulent flow regime.
- In the absence of wastewater flow data, both flow depths and velocities are assumed. The assumed wastewater velocities and relative depths for all pipes are given in Figure B-2 in Appendix B.
- Pickholes are assumed to have coefficient of discharge value of 0.65.
- The scrubber performance characteristic curve is assumed to be 'flat'. Thus the scrubber is assumed to deliver a constant effective discharge of  $424.7\text{m}^3/\text{min}$  of air over a range of static pressures.

Based on the aforementioned assumptions the air flow dynamics has been analyzed by solving the system of equations in Appendix B using the Newton's algorithm described in Section 5.4.1. Figure 5-11 shows predicted air velocities via all system manholes (including those at the dropshaft locations namely DS1,

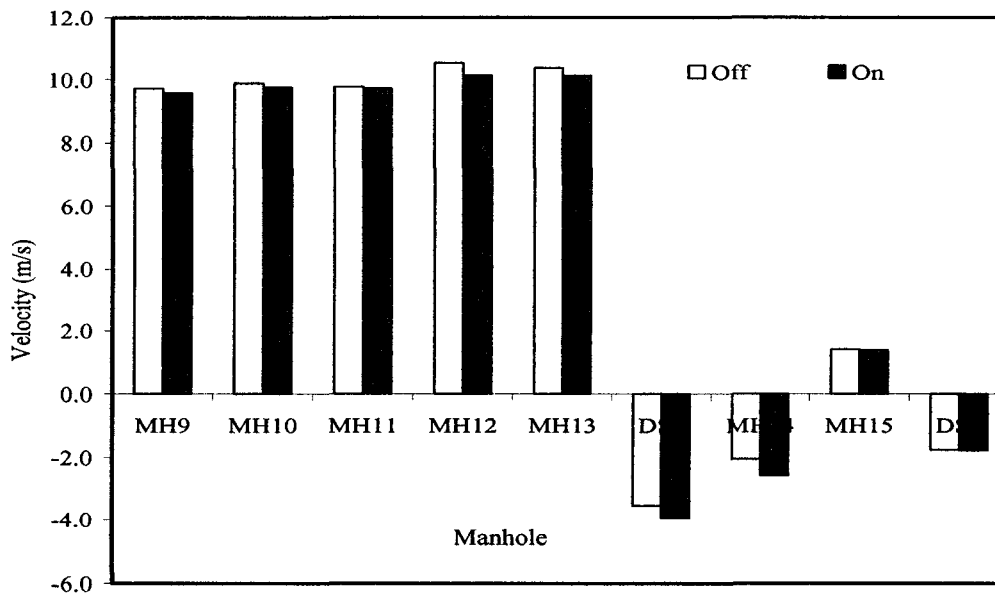


DS8 and DS9) with and without the scrubber in operation. Based on this simulation, it appears that the odourous tendencies would occur at all junction manholes with the exception of junction manholes MH2 and MH14 which act as sources of fresh air into the system. Inductions at MH2 and MH14 occur as a result of negative induced pressure at these manhole junctions and flow reversals in some of the adjoining pipes. As would be expected all the dropshaft manholes (DS locations) induct fresh air from the ambient environment into the sewer system as a result of the negative pressures created at the drop inlet pipes by the sucking-phenomenon of the dropstructures. The prediction further indicates that when the scrubber is in operation, it increases induction at DS1, MH2, MH14 and DS8 and reduces eduction noticeable at MH3, MH4 and MH5. It does not appear to have any appreciably effect on flows in the other system manholes further away from the installed location such as MH1, MH9, MH10, MH11, MH15 and DS9. Clearly the scrubber is not capable of averting eduction (averting odour into the ambient environment).

Figure 5-12 presents the predicted air flow rates in atmospheres of all the pipes. As can be seen from the bar charts, both forward and reversal flows occur in the sewer headspaces even without the scrubber in operation. The scrubber is found to affect headspace flows in a large number of pipes with the exception of pipes [31], [32], [35] and [37]-[45] which are further away from its installed location. It completely reverses flows in pipe [18] against the direction of the wastewater flow and either increases or decreases flows in other affected pipes.

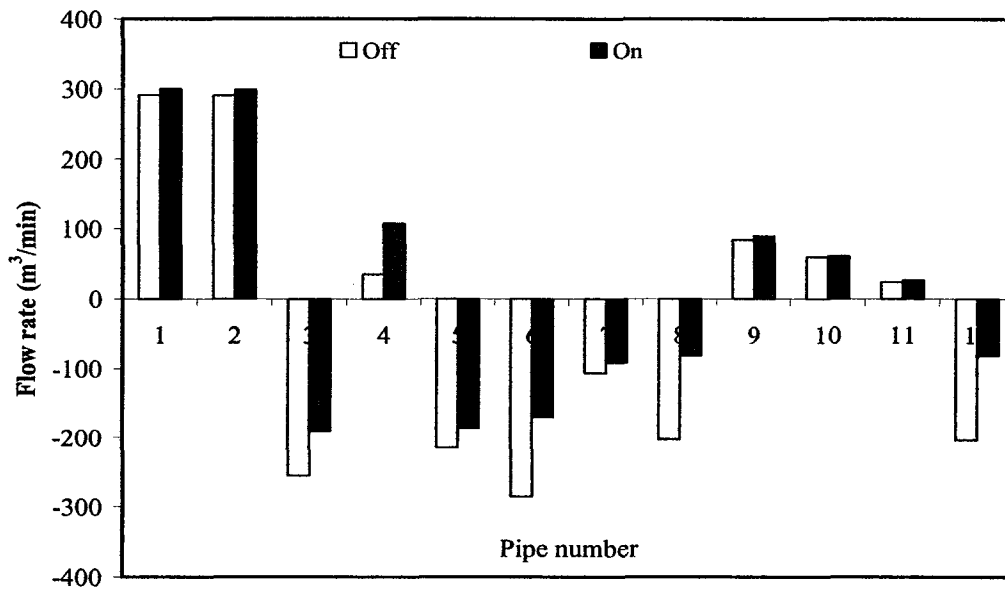


a)

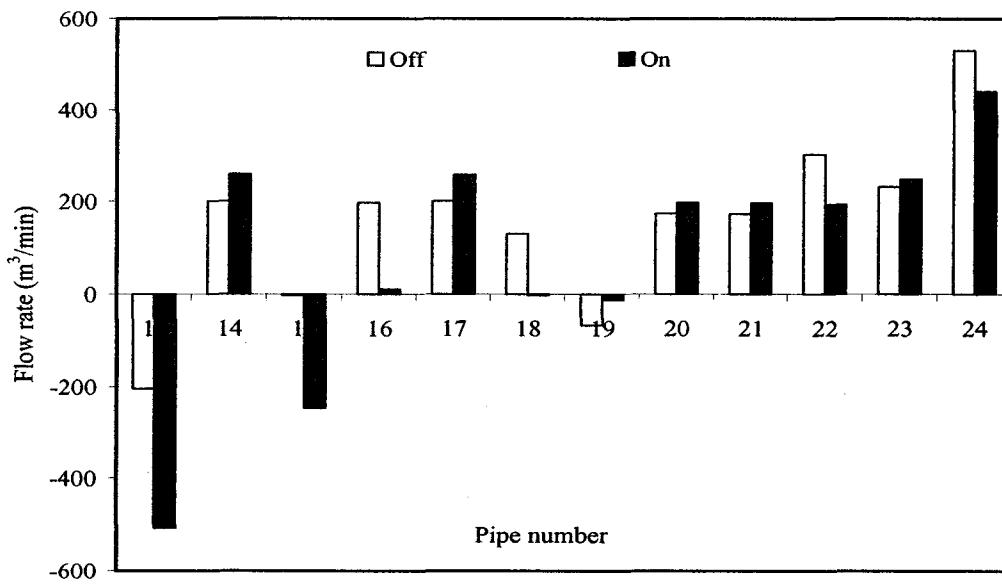


b)

Figure 5-11(a & b): Influence of scrubber on eduction/induction,  $C_d=0.65$

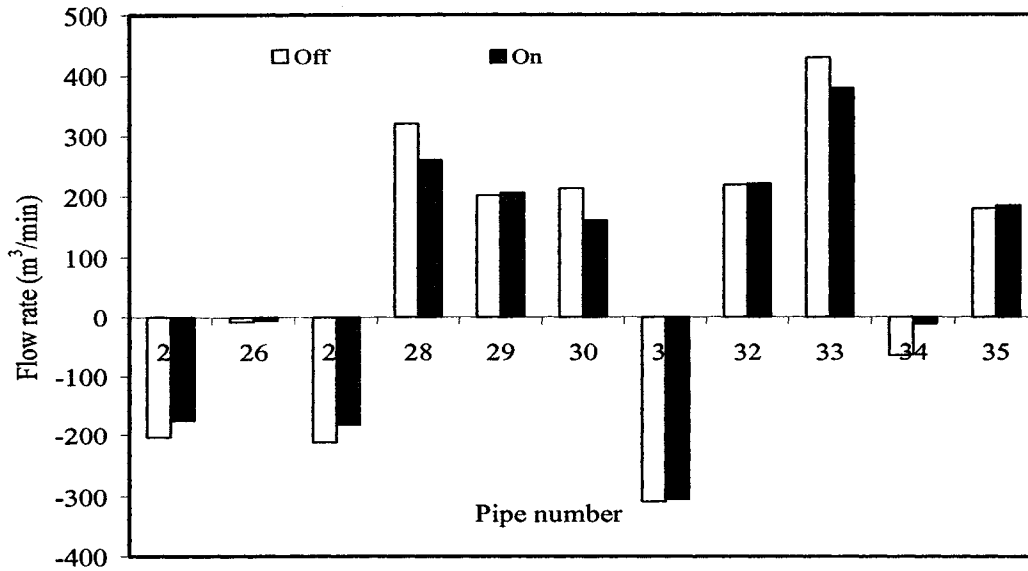


a)

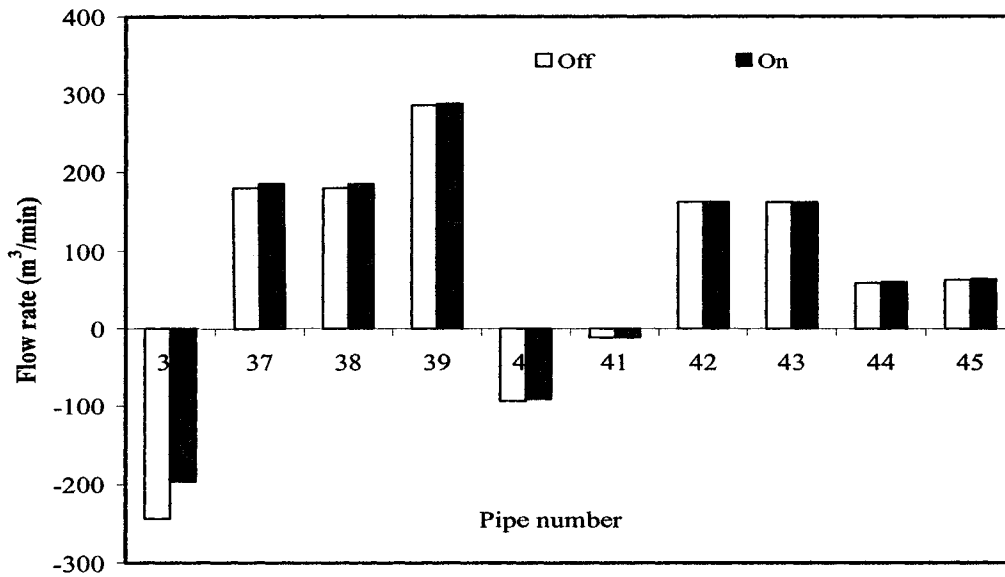


b)

Figure 5-12(a, b, c & d): Influence of scrubber on headspace flow rate



c)



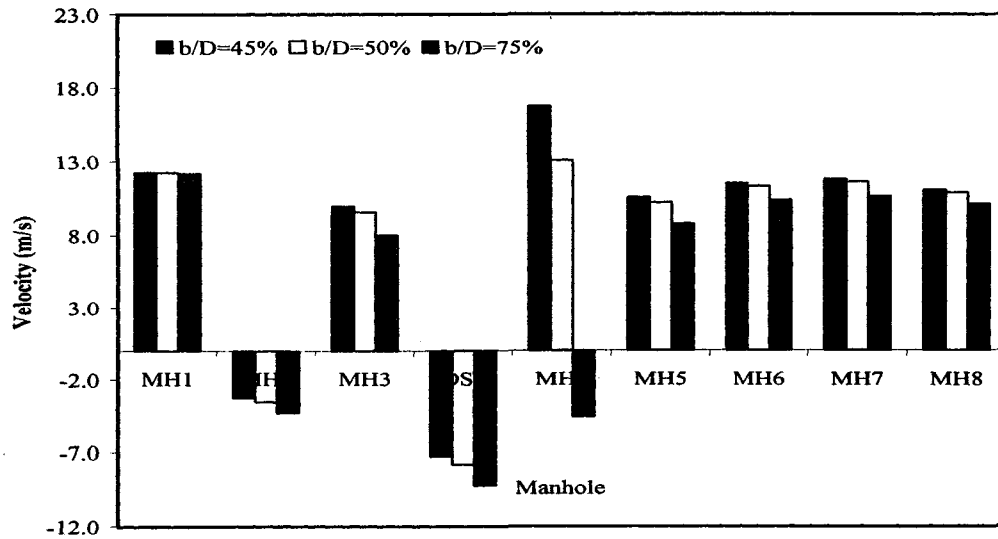
d)

**Figure 5-12(Continued): Influence of scrubber on headspace flow rate**

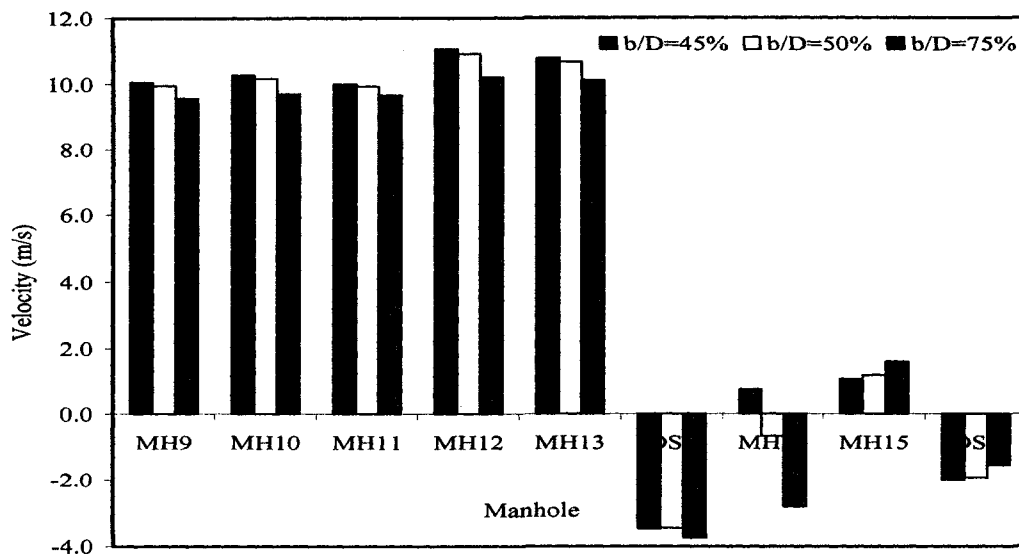
It should be acknowledged here that in this application, we have assumed that the system variables such as wastewater velocities and dropstructure characteristic

curve parameters, etc., are constant, but the only thing 'constant' in a sewer is change. This contributes another level of complexity to the art of deducing air flow in sewers. It is this constantly changing feature which allows the air in a sewer to sometimes move in one direction in the morning and the opposite direction in the afternoon. Thus using system average values instead of diurnal data may not help in identifying the pattern of air flow dynamics in the system. Therefore, it is only through continuous predictions using diurnal data input such as those in Figures 5-6 to 5-8 that the system diurnal patterns of air flow can effectively be recognized. Figure 5-13 examines the effect of wastewater depth changes (dropstructure characteristic functions and wastewater velocity assumed to be the same as in previous simulations) on eduction/induction. Relative depths of 45%, 50% and 75% are examined. It is observed from the figure that eduction generally increases with decreasing headspace depth.

Due to the unknown contributions from the dropstructures at this juncture and lack of documentation of environmental conditions at the system location, it is recommended that future effort be devoted to the modeling of the dropstructures within the system and documentation of any environmental conditions such as barometric pressure and wind speed variations. Particular attention should be paid to the occurrence, frequency and duration of wind speeds. Given all these inputs, the above formulation would be able to predict the air exchanges and identify the odour 'hot spot' locations within the system.



a)



b)

**Figure 5-13(a & b): Effect of wastewater level changes on  
 eduction/induction,  $C_d = 0.65$**

## **5.5 DESIGN CONSIDERATIONS FOR A NEW SEWER SYSTEM**

The analyses presented so far have evaluated modeling of ventilation as a corrective measure for odour control principally for existing sewers, based upon accumulated data. The important question that comes in mind is how can a new system be designed from the scratch to avoid airspace pressurization and hence reduce odour nuisance during the use of the system? Another question is what conditions are most crucial in this regard?

There are two distinct types of problems that confront engineers in designing municipal sewer systems- the conceptual and detailed design of system elements, and corrosion and odour control strategies. In most cases, the former is given prominence at the expense of the latter. These two should remain in designers' mind not as unrelated ideas, but rather as two integral and interwoven entities always to be considered and taken together while developing both concepts and detailed designs. Thus sewer layouts should take appropriate account of the hydraulics of both the flowing sewage and the sewer air.

The representation of sewer flow and other system variables in a new sewer is highly uncertain partly because the wastewater flow is uncertain at the time of design. Under such circumstance the only appropriate approach would be to perform a comprehensive range of modeling scenarios of air movement based

upon a variety of projected flow conditions (to be experienced throughout the life of the system) and conceptual design data. The first line of defense, for odour control purposes, will be to minimize or prevent headspace and junction pressurizations during the system design stage. For example pressurization of interceptor airspaces can occur where: there are few, if any, wastewater connections to the interceptor, manhole covers are solid, dropstructures are unavoidable or improperly designed for ventilation, and there are siphons, force mains, pumping stations, or surcharged sewer upstream or downstream (or both), blocking the movement of air along the interceptor. Aside from these, a decrease in pipe diameter in the downstream direction and poor junction structure design can cause localized pressure zones in the system. Designers should analyze the effects of all these design choices on air flow and modify their structural/hydraulic designs or avoid them where necessary. The designer may need to use air flow modeling to evaluate alternative interceptor designs so that long-term economic and environmental impact comparisons between options can be made. If pressurization can not be eliminated (or reduced) to acceptable levels (to avoid odour education) by design and anticipated operating practices, then controls will be needed. The idea of a control will be to maintaining a slight negative pressure in the headspace or at a junction and thus preventing fugitive odours from escaping the system.



## 5.6 CONCLUSIONS

A theoretical framework for modeling sanitary sewer system ventilation and pressurization is presented. To implement any efficient odour control technology it is imperative that air flowing through manhole openings be quantified. The emphasis in this paper therefore has been the development of a framework that provides a means of identifying the severity and causes of an odour episode via such an appurtenance.

The model development has been based on system theoretic assumptions where the entire system is broken down into components (elements and nodes) and formulating flow equations for each system component. The developed model offers novel insights about the nature of the air flow dynamics at a level of detail that is not easily achievable by field studies. It can be used for predicting the causes of air flow as well as the amount and direction of the transporting air within a given sewer system. Input data for predictions are: meteorological data, system configuration dimensions, wastewater flow, dropstructure pumping characteristic parameters and other ventilating energy sources. The flow of air via manholes and the effect of dropstructures are modelled as orifices and pumps, respectively. The coefficient of discharge of the orifice and the dropstructure pumping characteristic coefficients are the required parameters to calibrate for a given system. Knowing these parameters and further identifying the major driving forces for a given system would allow the estimation of volume of air that would

be forced out which in turn would allow the determination of the size and cost of odourous air treatment alternatives or would lead to appropriate system modifications.

The model formulation has been applied to the Kenilworth sewer system in the City of Edmonton with the objective of laying down a predictive tool for analyzing air flow in the system. Based upon the data which have been accumulated and analyzed, the assumption of quadratic characteristic function for the dropstructures on the system, and assumed additional system data, the ventilation dynamics of the sewer system has been theoretically characterized. It should be noted that for the developed formulation to be applied to modern sewer systems, such as those in the City of Edmonton, which are associated with numerous dropstructures, contributions from dropstructures should be accurately modelled. It is therefore recommended that future studies be directed at studying dropstructure ventilation and hydraulics with a view to developing a characteristic performance function to be used.

Based on the analysis presented, the following steps and input data required for any effective system modeling task are summarized as follows.

- The first important step is to look for sources of energy inputs and losses that cause air pressurization and odour release in the sewer system. Primary sources of energy inputs are flowing wastewater, dropstructures, barometric pressure and wind speed variations. Energy losses include

wastewater velocity decrease or in some places where all of the energy in the air is 'dumped' such as at pump station wet wells and inverted siphons. In identifying the energy inputs, it should be recognized that some energy sources may only operate part of the time.

- Diurnal wastewater levels and velocities patterns in major connecting sewer pipes should be noted. In reality, the wastewater flow is not constant and changes every time of the day. This constant change in wastewater flow would also affect diurnal patterns of air flow in the entire system. The formulation presented in this paper requires the use of the wastewater velocity inputs  $U_{wc}$  and  $U_w$ , but in practice these may not be measured or known so resorting to the use of the average wastewater velocity would need some adjustment. For example using experimental data of Pescod and Price (1978) a relation between the water surface average velocity and the average wastewater velocity has been established as  $U_w = 1.21V_w$ . This relationship should not be accepted as a general norm. Such relationship should be established for a given system where appropriate. The use of  $V_w$  instead of  $U_{wc}$  or  $U_w$  would undoubtedly under predict the air flow rate contributions from wastewater drag.
- Energy inputs from sources as such as scrubbers/blowers, wind speed and barometric pumping should be quantified. These inputs would serve as boundary conditions or driving forces for the system being modelled. This would require field data gathering efforts or an understanding of the particular energy source.

- Air flow directions are then assigned either arbitrarily or based upon energy inputs and losses. Algebraic expressions for the pressure head drops in all connecting conduit headspaces, manholes and dropstructures, etc., on the sewer network are then written down using the applicable equations. The nodal equations using flow balance at nodes and loop equations using work-energy principles are then assembled. The air flow rates through the entire system are subsequently calculated by solving these equations simultaneously. Predictions should include both the magnitude and direction of flows in the system.

## REFERENCES

- Arora, K. R. 1993. Fluid mechanics, hydraulics and hydraulic machines. Standard Publishers Distributors, Delhi.
- ASCE. 1989. Sulphide in wastewater collection and treatment systems. ASCE Manuals and Reports on Engineering Practice, No. 69.
- Asset Management and Public Works. 2003. Kenilworth scrubber field data and plans. Drainage Services, City of Edmonton Odour Control Project.
- Asset Management and Public Works. 2001. Odour control project. Project No. 234-010, Drainage Services, City of Edmonton.
- Chow, V. T. 1959. Open-channel hydraulics. MacGraw-Hill, London.
- Corsi, R. L., Chang, P. Y., Schroeder, E. D. 1989. Assessment of the effect of ventilation rates on VOC emission from sewers. Air & Water Management Ass. 82nd Annual Meeting & Exhibition. Anaheim, California.
- Corsi, R. L., Chang, P. Y., Schroeder, E. D. 1992. A modeling approach for VOC emissions from sewers, Water Env. Research. **64** (5), 734-741.
- Davidson, S., Green, J., Mann, J., Lamb, E. 2004. Design challenges in sewer foul air extraction and treatment. WEF/A & WMA Odors and Air Emission Conference, Bellevue, Seattle.
- Edwini-Bonsu, S., Steffler, P. M. 2004a. A physically-based model for computing natural ventilation rate in sanitary sewer atmosphere. WEF/ A & WMA Odors and Air Emission Conference, Bellevue, Seattle.
- Edwini-Bonsu, S., Steffler, P. M. 2003. Air flow in sanitary sewer conduits due

- to wastewater drag: A CFD approach. *J. Environ. Eng. Sci.* Accepted.
- Edwini-Bonsu, S. and Steffler, P. M. 2004b. Combined effects of wastewater drag and pressure gradient on air flow in sanitary sewer conduits. *J. of Environ. Eng. ASCE.* Submitted.
- Edwini-Bonsu, S., Steffler, P. M. 2004c. Dynamics of air flow in sanitary sewer conduits due to differential pressure. *J. of Environ. Eng. ASCE.* Submitted.
- Haecker, S., Cheatham, J. B, Gaudes, R. J. 2004. Biological treatment of collection system odors is the most cost effective solution. WEF/A & WMA Odors and Air Emission Conference, Bellevue, Seattle.
- Hager, H. W. 1999. Wastewater hydraulics-theory and practice. Springer-Verlag, Berlin.
- Henderson, F. M. 1966. Open-channel flow. London: Collier-Macmillan.
- Jeppson, W. R. 1976. Analysis of flow in pipe network. Ann. Arbor Science Publishers, Ann Arbor, Mich.
- Larock, E. B., Jeppson, W. R., Watters, Z. G. 1999. Hydraulics of pipeline systems. CRC Press, N. Y.
- Marsalek, J. 1981. Energy losses at straight-flow through sewer junctions. Research report no. 111. Ministry of the Environment, Ontario.
- Matos, J. S., de Sousa, E. R. 1992. The forecasting of hydrogen sulphide gas build-up in sewerage collection systems. *Wat. Sci. Tech.* **26** (3-4): 915-922.
- Odor and Corrosion Technology Consultants, Inc. 1999a. Air movement and odour transport characteristics within the Ritchie Neighborhood and Mill Creek Ravine areas. TM No.5, City of Edmonton Odour Control Project,

Alberta.

Odor and Corrosion Technology Consultants, Inc. 1999b. Analysis and evaluation of dropstructure ventilation phenomena in deep sewer tunnels. TM No.2, City of Edmonton Odour Control Project, Alberta.

Odor and Corrosion Technology Consultants, Inc. 1999c. The use of modeling techniques to evaluate and correct odour releases from trunk sewers. TM No.4, City of Edmonton Odour Control Project, Alberta.

Odor and Corrosion Technology Consultants, Inc. 1999d. Trunk sewer odour monitoring program. TM No.1, City of Edmonton Odour Control Project, Alberta.

Olson, D. 1996. Gas exchange rates between industrial process drains and the ambient atmosphere. MSc. Thesis, University of Texas.

Olson, D., Rajagopalan, S., Corsi, R. L. 1997. Ventilation of industrial process drains: mechanisms and effects on VOC emissions, Jr. *Env. Eng.* **123** (9), 939-947.

Pescod, M. B., Price, A. C. 1978. A study of sewer ventilation for the Tyneside sewerage scheme. Final research report, Department of Civil Engineering, University of Newcastle upon Tyne, U. K.

Pescod, M. B., Price, A. C. 1981. Fundamentals of sewer ventilation as applied to the Tyneside sewerage scheme. *Water Pollution Control*: **90** (1): 17-33.

Pescod, M. B., Price, A. C. 1982. Major factors in sewer ventilation. *J. Water Pollution Control Fed.* **54** (4): 385-397.

Pomeroy, R. 1945. Pros and cons of sewer ventilation. *Sewage Works Journal*, **17**

(2): 203-208.

Quigley, C. J., Corsi, R. L. 1995. Emission of VOCs from a municipal sewer. *J.*

*Air and Waste Mgmt. Assn.* **45** (5): 395-403.

Thistlethwayte, D. K. B. (Ed.). 1972. *The control of sulphides in sewerage systems.*

Butterworths, Sydney.

U. S. Environmental Protection Agency (EPA). 1994. *Air emission models for*

*waste and wastewater.* EPA-453/R-94-080A-Part 1.

Yih, C. S. 1969. *Fluid mechanics.* McGraw-Hill Book Company, N. Y.

Zhou, F. 2000. *Effects of trapped air on flow transients in rapidly filling sewers.*

PhD. Thesis, University of Alberta.

Zytner, R. G., Madani-Isfahani, M., Corsi, R. L. 1997. *Oxygen uptake and VOC*

*emissions at enclosed sewer dropstructures,* *Water Env. Research.* **69** (3),

286-294.



---

## **CHAPTER SIX**

### **SUMMARY, CONCLUSIONS AND RECOMMENDATIONS**

---

#### **6.1 SUMMARY AND CONCLUSIONS**

The overall goal of this research has been to improve and build upon the existing knowledge-base related to ventilation and pressurization of sanitary sewer system airspaces. New models for predicting the causes of sewer air flow as well as the amounts and directions of the transporting air current have been developed. The models can also be used to assess the capacity of ventilators (scrubbers/blowers) for controlling odour releases from sewers. The research study has considered air flow due to wastewater drag and pressure in conduit headspaces in addition to air exchanges via manholes as summarized below.

##### **6.1.1 Headspace Ventilation and Pressurization**

The major part of the research has been devoted to air flow in sewer conduit atmosphere without the possibility of manhole eduction or induction. In this case, the computational approach first considers ventilation mechanisms of wastewater drag and pressure gradient separately and then their combined effects. The

analyses have been conceptually viewed as Poiseuille-Couette flows with the wastewater effect formulated as a moving boundary condition, and the effects of pressure motive forces as a longitudinal pressure gradient in the momentum equation. Both turbulent and laminar regimes have been considered. The turbulence modeling takes into consideration the turbulence-driven secondary currents associated with flows in the sewer headspace and hence the Reynolds-averaged-Navier-Stokes equations governing the air flow field have closed with an anisotropic turbulence model which consists of two sub-models: a generalized eddy viscosity-biharmonic mixing length model for the turbulent shear stresses and semi-empirical models for the turbulent normal stresses. The resulting formulations are numerically integrated using a Galerkin finite element algorithm and an iterative solver. Comparisons of the predicted mean velocity field with available laboratory experiments show that the models capture most experimental trends with reasonable accuracy. The models reproduce known flow pattern and provide novel insights about the complex nature of the air flow field at a level of detail that would not be easily attainable by laboratory or field studies. For the laminar flow case, analytical (in the form of infinite series) and finite difference models have been developed with the main objective of assessing the predictive capacity of the finite element method which has been the main computational tool in this research. The finite element method has been chosen for this work because of its consistency, generality and ability to conform well to complex domains.

Using the simulated results, curves and formulae that can be used directly by

municipal engineers for calculating cross-sectional average longitudinal velocities have been developed. These curves and formulae suggest that the amount and characteristics of ventilation induced by wastewater drag and pressure gradient depend upon the unwetted wall perimeter, interfacial surface width and the headspace depth in addition to the magnitude and directions of the driving forces. The developed models further suggest that the methods currently in use for estimating ventilation and modeling corrosion are incapable of detailing the air flow field and generally overpredict the mean velocity, especially in turbulent flow regimes.

The effects of turbulence-driven secondary currents on the longitudinal mean velocity distribution have been studied. The numerical simulation shows that the strength of the secondary currents generally increases with decreasing relative depth ( $b/D$ ). The secondary velocity computed is generally within 5-8 %, 6-10 % and 6-12 % of the bulk streamwise mean velocity for wastewater-driven, pressure-induced and the combined case, respectively. The pattern of the calculated secondary flow is found to be independent of the driving mechanism. There is a single identical secondary flow cell on either side of the vertical plane dividing the headspace into symmetric quadrants. The only apparent observed difference of the secondary flow lies in the location of the center of the secondary flow cell. It is found that the centers of the secondary cells, to some extent, are located nearer the curved wall than the interface in the presence of a pressure gradient. The secondary motion is also noted to depress the location of the

maximum velocity towards the interface in pressure-driven flows as well as in the combined case. The distortion of the isovels by the secondary current is found to be more pronounced in wastewater-only-driven flows than either pressure-only-induced or when the two forces act simultaneously. The predictions also indicate that when the air flow is wastewater-only-driven, the computed average streamwise velocity is consistently less than half the water surface velocity. This is found to be independent of the wastewater level or the flow regime.

With application of a positive pressure gradient to a forward moving wastewater drag induced flow, the air flow rate could change direction depending on the value of the pressure gradient and apart from the stagnant sewer walls, there are also spots where the longitudinal air velocity is zero. As might be expected in wastewater-only-driven flows, all air in the headspace moves downstream and there is no zero velocity in the headspace. The model simulations also suggest that there is a possibility of zero average velocity even when both positive pressure gradient and wastewater drag act simultaneously. It has been found that ventilation rates caused by pressure forces are likely to be higher than those caused by wastewater drag for a given in-service trunk sewer and environmental conditions. The wastewater drag effect appears subservient to pressure, particularly where there is a large space above low-velocity fluid flow. When high pressure forces act in the same direction as liquid drag, the resulting average velocity is almost the same as that with no liquid drag present. In turbulent flow regime, when both wastewater drag and pressure forces simultaneously act either

in the same direction or in the opposite direction, the cross-sectional average velocity due to the individual effects is not linearly additive. Computations further indicate that the bulk velocity in a turbulent regime for the combined case, unlike the laminar flow, is less than the simple algebraic addition of the contributions from the individual mechanisms and that ventilation rates can be overestimated by employing the simple superposition of the individual effects especially in low pressure and high wastewater induced air flows. A reduction factor has been introduced to account for the overestimation that may result.

Interfacial drag coefficient is also predicted. It is found that the variation of the predicted average interfacial drag coefficient with Reynolds number follows a Moody-like diagram. The interfacial drag coefficient is found to be approximately equal to the predicted average wall friction coefficient in wastewater-driven flows. The reverse is true for the combined effect where the wall friction factor is consistently greater than the interfacial drag coefficient. The coefficient is further noted to decrease with increasing relative depth.

### **6.1.2 System Modeling**

The second part of the research study has been devoted to the development of a system framework for computing eduction/induction via manholes and sewer atmospheres. The approach adopted applies both continuity and work-energy principles and models air exchanges via manholes using the standard orifice equation. A quadratic characteristic pump model, whose parameters have to be

calibrated for a given system, is proposed to describe the pumping effects of dropstructures in deep collection systems. Applications to both hypothetical and real sewer systems are presented to show procedural calculations and to demonstrate the applicability of the framework. The Kenilworth sewer system in the City of Edmonton is used for the latter case. This sewer system consists of nine (9) dropstructures whose pumping performance functions are unknown and hence this study as of now only serves as a computational tool and groundwork for future studies in the design of corrective ventilation measures to minimize odour problems in the neighborhoods. The system model inputs are:

- Wastewater velocity/depth in all sewer pipes (interceptors, trunk & laterals).
- Meteorological data (barometric pressure and wind speed).
- Sewer system configuration and geometric data (diameter, length, manhole location and number/size of pickholes, etc.).
- Dropstructure location & pumping function (calibration required).
- Auxiliary ventilator (scrubber/blower) capacity/performance function.
- Other ventilating energy sources (where possible).

Outputs from the model are:

- Air flow rates in headspaces (sewer atmospheres) and
- Air flow rates out of/into manholes (eduction/induction rates).

## 6.2 RECOMMENDATIONS FOR FUTURE WORK

The research described herein should significantly improve the existing knowledge-base related to ventilation and pressurization in sanitary sewer airspaces, and should provide reasonable estimates of the air flow dynamics in sewer systems. This research addresses many, but not all, issues regarding air movement in sewer systems. There is still a need for additional research which will ultimately lead to improved air flow estimates and odour control technologies. Recommendations for future research therefore include the following:

- It should be emphasized here that an important factor to the modeling effort reported in this thesis has been the access to limited experiments in the literature. For further progress to be made in this area, it is critical therefore that, experimental investigations as detailed as those reported by Pescod and Price (1978) continue to enrich the literature. Testing and validation of the developed models should be made with both detailed experimental data and field studies completed in operating sanitary sewers so as to unveil their tremendous potential, identify their weaknesses, and define areas for further research.
- In the current study, the issue of dynamic interaction between the wastewater and the air (along the air interface), involving wave generation, and propagation, was essentially untouched. This of course requires further work study. It is recommended that investigation be made

on the possibility of secondary flows due to interfacial waves.

- This research has attempted to address the issue regarding air eduction via manholes in deep sewer systems using system theory and a proposal of a new model for dropstructure pumping phenomenon. A great deal of work is required in this case. Future effort should be directed at the calibration of the proposed model or the development of other mathematical models. The dynamics of entrainment and eduction in dropstructures and hydraulic jumps should also be considered.
- Future studies should also consider effects of temperature on air movement. This factor may be important in industrial sewers and in some cases in sanitary sewers during winter periods. A change in ambient temperature (and therefore a change in air density) may cause convection of air into and out of sewers depending upon the temperature gradient.
- Consideration should also be given to air flow dynamics at inverted siphons, pump station wet wells and treatment plants.
- Future research should also consider oxygen concentration (oxygen-demand) and hazardous pollutant transport modeling issues in collection systems.



## REFERENCE

Pescod, M. B., Price, A. C. 1978. A study of sewer ventilation for the Tyneside sewerage scheme. Final research report, Department of Civil Engineering, University of Newcastle upon Tyne, U. K.

---

## **APPENDIX A**

### **COMPUTATIONAL METHOD:**

### **FINITE ELEMET METHOD**

---

#### **A.1 INTRODUCTION**

In Chapters 2-4, the governing equations of the air flow in the sewer conduit headspace were adopted, and a corresponding model of the fluid turbulence was selected. The system of equations governing the turbulent flow case is parabolic whereas that in the laminar case is elliptic. The nature of the flow equations and the 2-D geometry preclude a direct generalized analytical solution. The use of a finite difference approximation even in the laminar flow regime is difficult to implement for such geometry. The choice of the computational method in these chapters therefore has been the finite element method (FEM). An important advantage of this method is its ability to deal with arbitrary geometries, consistency and, the easy at which meshes are constructed and refined. The FEM is however not described in detail in these chapters. The inclusion of this in the main body of the various chapters would have disrupted the flow of the text, and therefore distracted readers. This appendix details the transformation of the model formulations presented in Chapters 2-4 into a finite element framework, and in particular, into the framework used in FEMLAB programming language. The

solver algorithms employed to solve the resulting discretized equations are also discussed.

Unlike other channel shapes (e.g. full circular and rectangular sections), the present uniquely-shaped (lenticular) channel formed by the curved sewer wall and the air-water interface has not been studied extensively. As such there are limited data against which comparisons with the computational results may be made. Although some attempts have been made to validate the numerical results via available experiments in chapters 2 and 3, having alternative means of assessing the predictive capacity of the numerical tool would be of great asset. To achieve this, computational experiments are carried out where the FEM is tested against other solution methods. In these experiments, the equation of the laminar flow is solved using approximate analytical method which utilizes elliptic-cylinder coordinate system and a finite difference method derived in a generalized curvilinear co-ordinate system. The outputs from the two models are compared (within their range of validities) with the FEM. All the laminar models are based on the assumptions of constant interfacial drag and smooth interfacial surfaces.

## **A.2 FEMLAB IMPLEMENTATION**

The FEMLAB algorithm used involves four (4) main steps in its implementation:

- Geometric modeling
- Generation of unstructured meshes

- Discretization of PDE(s)
- Solution of the discretized equation (s)

Each of these steps is explained below.

### A.2.1 Geometric Modeling

In FEMLAB, simple geometry objects are used to form the geometry of a PDE problem. Here the headspace geometry is modelled as an algebraic sum of a circular section object and a rectangle object with the top side of the rectangle as the interface. i.e. [Headspace] = [Circle]-[Rectangle]. The circle is construction using a rational Bezier curve of degree 2 and the rectangular section made from rational Bezier patches. The parameterized curve of the general rational Bezier curve is given as (FEMLAB 2002):

$$\mathbf{b}(t) = \frac{\sum_{i=0}^p \mathbf{b}_i w_i B_i^p(t)}{\sum_{i=0}^p w_i B_i^p(t)}, \quad 0 \leq t \leq 1 \quad [\text{A.1}]$$

where the functions  $B_i^p(t) = \binom{p}{i} t^i (1-t)^{p-i}$  are the Bernstein basis functions of degree  $p$  ( $p=2$  in this case),  $\mathbf{b}_i = (x_1, \dots, x_n)$  are the control vertices of the  $n$ -dimensional space (2 in this case), and  $w_i$  are the weights which should always be positive real numbers to get a properly defined rational Bezier curve. A rectangular rational Bezier patch has the form described by:

$$S(s,t) = \frac{\sum_{i=0}^p \sum_{j=0}^q \mathbf{b}_{i,j} w_{i,j} B_i^p(s) B_j^q(t)}{\sum_{i=0}^p \sum_{j=0}^q w_{i,j} B_i^p(s) B_j^q(t)}, \quad 0 \leq s, t \leq 1 \quad [\text{A.2}]$$

where  $B_i^p$  and  $B_j^q$  are the Bernstein basis functions of degree  $p$  and  $q$ , respectively. A rectangular patch of degree (1, 1) is used here. All the above expressions are executed with the FEMLAB syntax: *Headspace= circ2(x, y, r)-r2(xmin, xmax, ymin, ymax)*. The function *circ2(...)* creates a solid circle geometry object with center in  $(x, y)$  and radius  $r$ . The function *r2(...)* creates a solid rectangle geometry object with corner co-ordinates defined by  $xmin, xmax, ymin, ymax$ .

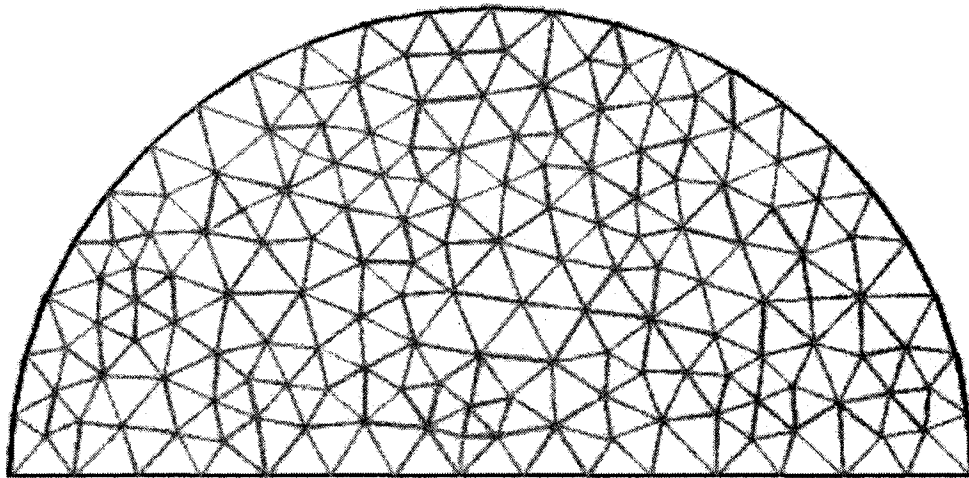
### A.2.2 Generation of Unstructured Meshes

The starting point of the finite element method is the partitioning of the flow domain (headspace) into triangles. Of course, this is only an approximation since the sewer wall is curved. In FEMLAB the initial mesh is created with a function *meshinit(...)*, which uses a Delaunay triangulation algorithm in MATLAB. Typical generated finite element meshes are shown in Figures A-1, A-2 and A-3. The meshes in Figure A-2 are those of Figure A-1 refined using regular and total refinement method, where all of the triangles are divided into four triangles of the same shape. This is accomplished with the function *meshrefine(...)*. It must be stated here that the refinement can also be carried out a number of times in a loop if desired. Figures A-1b and A-2b show the corresponding triangle quality  $q$  (given by Equation A.3) of the finite element meshes.  $q$  is a number between 0

and 1. If  $q > 0.6$  the triangle is of acceptable quality. This quality is to ensure that the curved walls are appropriately approximated to straight edges of the triangles. High values are also noted to enhance computations by decreasing the number of iterations required to achieve convergence. Throughout this study, it is ensured that the quality is at least 0.7 in all computations. This quantity is assessed using the formula (FEMLAB 2002):

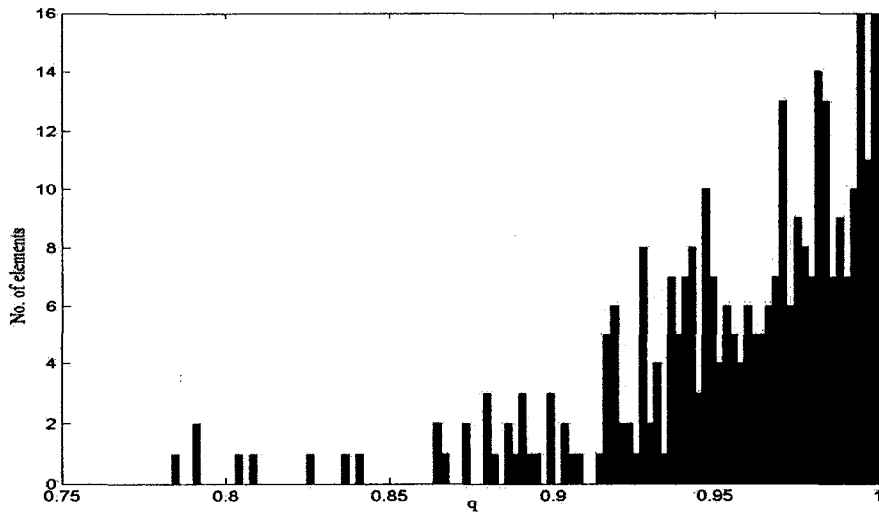
$$q = \frac{4\sqrt{3}a}{h_1^2 + h_2^2 + h_3^2} \quad [\text{A.3}]$$

where  $a$  is the area and  $h_1$ ,  $h_2$ , and  $h_3$  the side length of the triangle. Figure A-3 illustrates the capability of the meshing algorithm to do selective meshing in some regions of the domain where needed (cases where the integration is carried out to the viscous sublayer).



a)

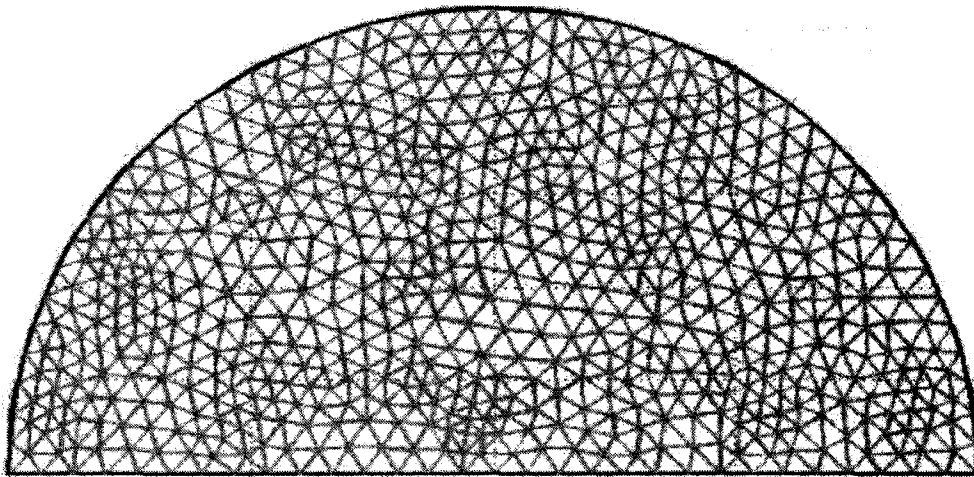
**Figure A-1(a & b): Typical unstructured mesh: a) initial mesh; nodes= 173, boundary elements = 39, elements = 305, b) corresponding mesh quality histogram**



b)

**Figure A-1(Continued): Typical unstructured mesh: a) initial mesh; nodes= 173, boundary elements = 39, elements = 305, b) corresponding mesh quality**

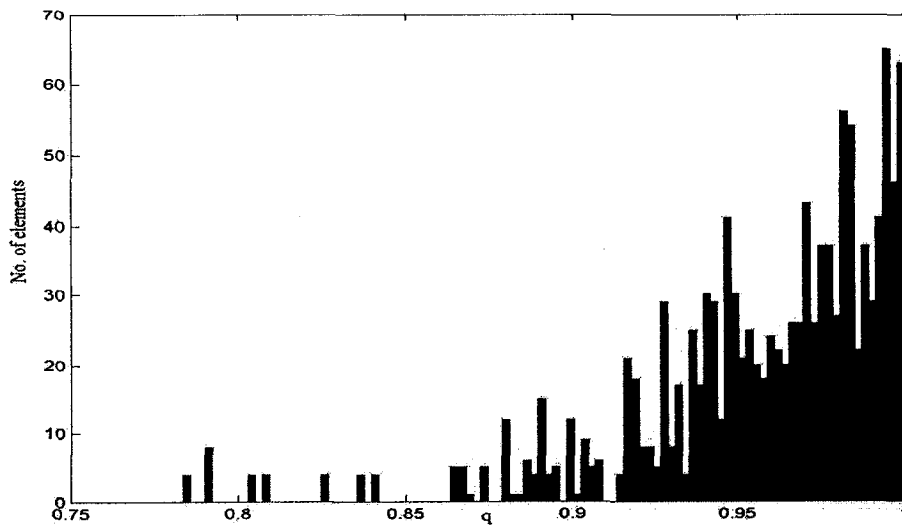
**histogram**



a)

**Figure A-2(a &b): Typical unstructured mesh: a) refined mesh; nodes= 650, boundary elements = 78, elements = 1220, b) corresponding mesh quality**

**histogram**



b)

**Figure A-2(Continued): Typical unstructured mesh: a) refined mesh; nodes= 650, boundary elements = 78, elements = 1220, b) corresponding mesh quality histogram**

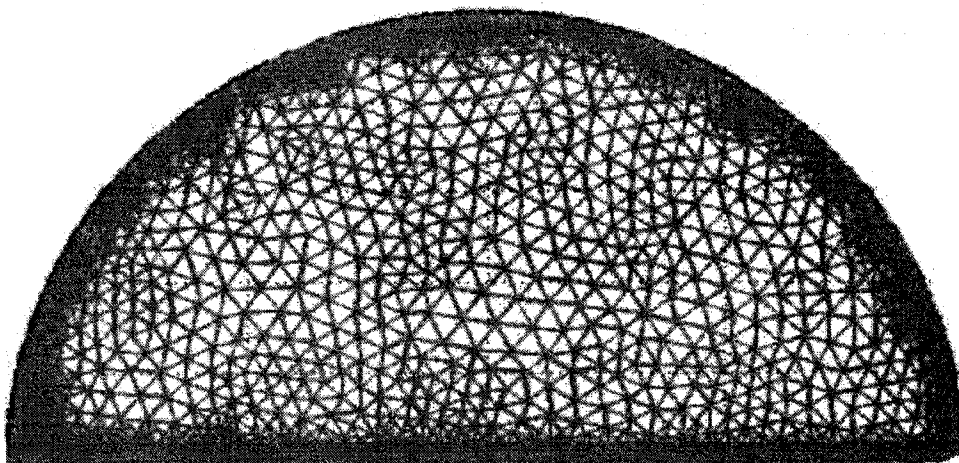


**Figure A-3: Typical unstructured mesh using selective refinement close to the boundary regions: nodes= 5177, boundary elements = 535, elements = 9817, minimum  $q= 0.78$**



## A.2.3 Discretization of PDEs

To illustrate the discretization of the PDEs in the FEMLAB framework, the non-dimensionalized turbulent flow equations in Chapter 4 are used. These equations are:

Streamwise averaged momentum equation:

$$X_*: V_* \frac{\partial U_*}{\partial Y_*} + W_* \frac{\partial U_*}{\partial Z_*} - \frac{\partial}{\partial Y_*} \left[ (1/\text{Re} + \nu_{t*}) \frac{\partial U_*}{\partial Y_*} \right] - \frac{\partial}{\partial Z_*} \left[ (1/\text{Re} + \nu_{t*}) \frac{\partial U_*}{\partial Z_*} \right] = \lambda \quad [\text{A.4}]$$

Secondary averaged momentum equations:

$$Y_*: V_* \frac{\partial V_*}{\partial Y_*} + W_* \frac{\partial V_*}{\partial Z_*} - \frac{1}{\text{Re}} \left[ \frac{\partial^2 V_*}{\partial Y_*^2} + \frac{\partial^2 V_*}{\partial Z_*^2} \right] = -\frac{\partial P_*}{\partial Y_*} - \frac{\overline{\partial v_*'^2}}{\partial Y_*} + \frac{\partial}{\partial Z_*} \left[ \nu_{t*} \left( \frac{\partial V_*}{\partial Z_*} + \frac{\partial W_*}{\partial Y_*} \right) \right] \quad [\text{A.5}]$$

$$Z_*: V_* \frac{\partial W_*}{\partial Y_*} + W_* \frac{\partial W_*}{\partial Z_*} - \frac{1}{\text{Re}} \left[ \frac{\partial^2 W_*}{\partial Y_*^2} + \frac{\partial^2 W_*}{\partial Z_*^2} \right] = -\frac{\partial P_*}{\partial Z_*} - \frac{\overline{\partial w_*'^2}}{\partial Z_*} + \frac{\partial}{\partial Y_*} \left[ \nu_{t*} \left( \frac{\partial V_*}{\partial Z_*} + \frac{\partial W_*}{\partial Y_*} \right) \right] \quad [\text{A.6}]$$

Continuity:

$$\frac{\partial V_*}{\partial Y_*} + \frac{\partial W_*}{\partial Z_*} = 0 \quad [\text{A.7}]$$

Eddy viscosity:

$$\nu_{t*} = \ell_{m*}^2 \left[ \left( \frac{\partial U_*}{\partial Y_*} \right)^2 + \left( \frac{\partial U_*}{\partial Z_*} \right)^2 + 2 \left( \frac{\partial V_*}{\partial Y_*} \right)^2 + 2 \left( \frac{\partial W_*}{\partial Z_*} \right)^2 + \left( \frac{\partial V_*}{\partial Z_*} + \frac{\partial W_*}{\partial Y_*} \right)^2 \right]^{\frac{1}{2}} \quad [\text{A.8}]$$

Each equation and boundary condition is first written in a general form:

$$\nabla \cdot \Gamma = F \quad \text{in } \Omega \quad [\text{A.9}]$$

$$-\underline{n} \cdot \Gamma = G + \left( \frac{\partial R}{\partial u} \right)^T \mu \quad \text{on } \partial\Omega \quad [\text{A.10}]$$

$$0 = R \quad \text{on } \partial\Omega \quad [\text{A.11}]$$

where  $\Omega$  is the bounded region,  $\partial\Omega$  is the boundary of the region, and  $\underline{n}$  is the outward unit normal vector. Equation [A.9] is the PDE. Equations [A.10] and [A.11] are the Neumann and Dirichlet boundary conditions, respectively. The terms  $\Gamma$ ,  $F$ ,  $G$ , and  $R$  are known as coefficients. They are functions of the space co-ordinates  $(Z_*, Y_*)$ , the solution  $u$  ( $U_*$ ,  $V_*$ ,  $W_*$ ,  $P_*$ ), and the derivatives of the solution vector components.  $F$ ,  $G$ , and  $R$  are scalars, while  $\Gamma$  is a vector.  $\Gamma$  is called the flux vector. The  $T$  in the Neumann boundary condition denotes the transpose, which in single variable case is unnecessary. The variable  $\mu$  is an unknown function, called the Lagrange multiplier. For convenience the non-dimensionalized quantities will be replaced with their dimensionalized equivalents from this point. The flux vector can be written as:

$$\Gamma = \begin{bmatrix} \Gamma_{U1} & \Gamma_{U2} \\ \Gamma_{V1} & \Gamma_{V2} \\ \Gamma_{W1} & \Gamma_{W2} \\ \Gamma_{P1} & \Gamma_{P2} \end{bmatrix} \quad [A.12]$$

where

$$\begin{aligned} \Gamma_{U1} &= -(1/\text{Re} + \nu_t) \frac{\partial U}{\partial Y} + WU, \quad \Gamma_{U2} = -(1/\text{Re} + \nu_t) \frac{\partial U}{\partial Z} + VU, \\ \Gamma_{V1} &= \nu_t \left( \frac{\partial V}{\partial Z} + \frac{\partial W}{\partial Y} + \frac{1}{R_e} \frac{\partial V}{\partial Z} \right) - VW, \quad \Gamma_{V2} = - \left( V^2 + P - \frac{1}{R_e} \frac{\partial V}{\partial Y} \right), \\ \Gamma_{W1} &= - \left( W^2 + P - \frac{1}{R_e} \frac{\partial W}{\partial Z} \right), \quad \Gamma_{W2} = \nu_t \left( \frac{\partial V}{\partial Z} + \frac{\partial W}{\partial Y} + \frac{1}{R_e} \frac{\partial W}{\partial Y} \right) - VW \end{aligned} \quad [A.13]$$

$$\Gamma_{P1} = 0, \Gamma_{P2} = 0$$

The source term is worked out as:

$$F = \begin{bmatrix} F_U \\ F_V \\ F_W \\ F_P \end{bmatrix} \quad [\text{A.14}]$$

$$\text{where } F_U = \lambda, F_V = \frac{\overline{\partial v^2}}{\partial Y}, F_W = \frac{\overline{\partial w^2}}{\partial Z} \text{ and } F_P = \frac{\partial W}{\partial Z} + \frac{\partial V}{\partial Y}$$

The Dirichlet condition, on expanded form, reads:

$$\begin{bmatrix} 0 \\ 0 \\ 0 \\ 0 \end{bmatrix} = \begin{bmatrix} R_U \\ R_V \\ R_W \\ - \end{bmatrix} \quad [\text{A.15}]$$

In Chapter 4 for example,  $R = [0,0,0,-]$  at the curved wall boundary and  $R = [U_{ws}, 0,0,-]$  at the interface. The Neumann condition is used for P as

$$-\underline{n} \cdot \Gamma = G. \text{ The normal component of the flux vector is defined as}$$

$$\underline{n} \cdot \Gamma = (n_z, n_y) \cdot [\Gamma_P]$$

Due to the non-linear nature of the PDE formulations in the turbulent flow regime, they are first approximated with a set of linear problem when the solution  $u$  is close to some function  $u_0$ . The linearization around the ‘‘point’’  $u_0$  is achieved using a symbolic differentiation in FEMLAB such that:

$$\begin{cases} \nabla \cdot (-c\Delta\tilde{u} - \alpha\tilde{u} + \gamma) + \beta \cdot \nabla\tilde{u} + a\tilde{u} = f & \text{in } \Omega \\ \underline{n} \cdot (c\Delta\tilde{u} + \alpha\tilde{u} - \gamma) + q\tilde{u} = g - h^T \mu & \text{on } \partial\Omega \\ h\tilde{u} = r & \text{on } \partial\Omega \end{cases} \quad [\text{A.16a,b,c}]$$

where

$\tilde{u} = u - u_0$  and the coefficients

$$c = -\frac{\partial \Gamma}{\partial \nabla u}, \alpha = -\frac{\partial \Gamma}{\partial u}, \gamma = \Gamma, \beta = -\frac{\partial F}{\partial \nabla u}, a = -\frac{\partial F}{\partial u}, f = F, q = -\frac{\partial G}{\partial u}, g = G,$$

$$h = -\frac{\partial R}{\partial u}, r = R \text{ are evaluated for } u = u_0 \quad [\text{A.17}]$$

The above formulation is known as the coefficient form. The conversion of the general form to the coefficient form is accomplished in a single FEMLAB syntax:

*femdiff (fem,...)*, where *fem* contains the coefficients in the PDE given in the general form.

The next step is the discretization of the resulting formulation using the finite element approximations to the dependent variables. The idea is to approximate  $\tilde{u}$  with a function that can be described by a finite number of parameters, the so-called degree of freedom (DOF). Then this approximation is inserted into the weak form of the equation to obtain a system of equations for the degrees of freedom. This means that the dependent variables are expressed in terms of the degree of freedom as:

$$\tilde{u} = \sum_i \tilde{S}_i \varphi_i^l \quad [\text{A.18}]$$

where  $\varphi_i^l$  are the basis functions for the variables  $\tilde{u}$ . Let  $\tilde{S}$  be the vector with the degrees of freedom  $\tilde{S}_i$  as the components. This vector is called the solution vector, since it is what we want to compute in order to obtain  $\tilde{u}$ . Now, let  $\tilde{v}$  be an arbitrary function on  $\Omega$  called the test function (the function  $\tilde{v}$  should belong

to a suitably chosen well-behaved class of functions). Multiplying the PDE of Equation [A.16a] with this function, rearranging terms, and integrating, leads to:

$$\int_{\Omega} \tilde{v} \nabla \cdot (-c \nabla \tilde{u} - \alpha \tilde{u} + \gamma) dA = \int_{\Omega} \tilde{v} (f - \beta \cdot \nabla \tilde{u} - a \tilde{u}) dA \quad [\text{A.19}]$$

where  $dA$  is the area element.

Now we use integration by parts (in other words, Gauss law or the divergence theorem) to get:

$$\int_{\partial\Omega} \tilde{v} (-c \nabla \tilde{u} - \alpha \tilde{u} + \gamma) \cdot \mathbf{n} ds - \int_{\Omega} \nabla \tilde{v} \cdot (-c \nabla \tilde{u} - \alpha \tilde{u} + \gamma) dA = \int_{\Omega} \tilde{v} (f - \beta \cdot \nabla \tilde{u} - a \tilde{u}) dA \quad [\text{A.20}]$$

where  $ds$  is the length element. Now, using the Neumann boundary condition in Equation [A.16b] we get:

$$0 = - \int_{\Omega} (\nabla \tilde{v} \cdot (-c \nabla \tilde{u} - \alpha \tilde{u} + \gamma) + \tilde{v} (f - \beta \cdot \nabla \tilde{u} - a \tilde{u})) dA + \int_{\partial\Omega} \tilde{v} (-q \tilde{u} + g - h^T \mu) ds \quad [\text{A.21}]$$

Equations [A.21] and [A.16c] (the Dirichlet condition), give the weak formulation of Equation [A.16a,b,c]. The above steps are all accomplished in a single FEMLAB syntax: *flform (fem,...)*. The weak formulation can simply be written as:

$$0 = \int_{\Omega} W_1 dA + \int_{\partial\Omega} W_2 ds - \int_{\partial\Omega} \tilde{v} \cdot h^T \mu ds \quad [\text{A.22}]$$

where the integrands  $W_1$  and  $W_2$  are expressions in  $\tilde{u}, \nabla \tilde{u}, \tilde{v}$  and  $\nabla \tilde{v}$ . Here the test functions are approximated with the same finite elements (this is the Galerkin method):

$$\tilde{v} = \sum_i \tilde{V}_i \varphi_i^{(l)} \quad [\text{A.23}]$$

Since the test functions occur linearly in the integrands of the weak equation, it is enough to require that the weak equation holds when we choose the test functions as basis functions,  $\tilde{v} = \varphi_i^{(l)}$ . When substituted into the weak equation, this gives one equation for each  $i$ . Here the dependent variables are approximated with functions in the Lagrange quadratic space. Now the Lagrange multipliers have to be discretized. Let

$$\Lambda_{mj} = \mu x_{mj} w_{mj} \quad [\text{A.24}]$$

where  $x_{mj}$  are the Lagrange points and  $w_{mj}$  is the integral of  $ds$  over the appropriate part of the mesh element. The term

$$\int_{\partial\Omega} \varphi_i^l \cdot h^T \mu ds \quad [\text{A.25}]$$

is approximated as a sum over all mesh elements. The contribution from mesh element number  $m$  to this sum is approximated with the Riemann sum

$$\sum_j \varphi_i^l x_{mj} \cdot h^T x_{mj} \mu x_{mj} w_{mj} = \sum_j \varphi_i^l x_{mj} \cdot h^T x_{mj} \Lambda_{mj} \quad [\text{A.26}]$$

All this means that the discretization of the weak equation can be written

$$0 = L - N^T \Lambda \quad [\text{A.27}]$$

where  $L$  is the vector whose  $i$ th component is

$$\int_{\Omega} W dA + \int_{\partial\Omega} W ds \quad [\text{A.28}]$$

evaluated for  $\tilde{v} = \varphi_i^l$ .  $\Lambda$  is the vector containing all the discretized Lagrange multipliers  $\Lambda_{mj}$ .  $N$  is a matrix whose *ith* column is a concatenation of the vectors

$$h \ x_{mj} \varphi_i^l \ x_{mj} \quad [A.29]$$

To sum up, the discretization of the coefficient form is given as:

$$K(\tilde{S}_0)(\tilde{S} - \tilde{S}_0) + N(\tilde{S}_0)^T \Lambda = L(\tilde{S}_0) \quad [A.30a]$$

$$N(\tilde{S}_0)(\tilde{S} - \tilde{S}_0) = M(\tilde{S}_0) \quad [A.30b]$$

Introducing  $X_T = \tilde{S} - \tilde{S}_0$ , we can write these equations as:

$$\begin{bmatrix} K & N^T \\ N & 0 \end{bmatrix} \begin{bmatrix} X_T \\ \Lambda \end{bmatrix} = \begin{bmatrix} L \\ M \end{bmatrix} \quad [A.31]$$

where  $K, L, N$  and  $M$  are evaluated for  $\tilde{S} = \tilde{S}_0$ .  $K$  is called the stiffness matrix,  $M$  is called the constraint residual and  $L$  is the load vector (also called the residual vector). The entries in the stiffness matrix and the residuals are computed numerically. This computation is called assembly and is performed by the function *assemble* in FEMLAB. This computation uses a quadrature formula. Such a formula computes the integral over a mesh element by taking a weighted sum of the integrand evaluated in a finite number of points in the mesh element. The order of a quadrature formula is the maximum number  $k$  such that it integrates all polynomials of degree  $k$  exactly. Thus, the accuracy of the quadrature increases with the order. On the other hand, the number of evaluation points also increases with the order. As a rule of thumb one takes the order to be twice the order of the finite element you are using. The order of the quadrature

formula is denoted by *gporder* in FEMLAM's data structures (*gp* stands for Gauss points)

For the laminar flow case where the original governing equation is linear, the discretization can be written as:

$$K\tilde{S} + N^T \Lambda = L(0) \quad [\text{A.32a}]$$

$$N\tilde{S} = M(0) \quad [\text{A.32b}]$$

or

$$\begin{bmatrix} K & N^T \\ N & 0 \end{bmatrix} \begin{bmatrix} \tilde{S} \\ \Lambda \end{bmatrix} = \begin{bmatrix} L \\ M \end{bmatrix} \quad [\text{A.33}]$$

Here  $K, L, N$  and  $M$  are evaluated for  $\tilde{S} = 0$ .

The Lagrange multiplier vector  $\Lambda$  is typically underdetermined and it is not solved for. The constraint  $N\tilde{S} = M$  often contains the same equation several times, and special case is taken to handle this. There are several ways to do this in FEMLAB. Here a MATLAB backslash operator is used.

## A.2.4 Solution of the Discretized Equations

Now the object is to solve the resulting discretized system of equations for the solution vector  $X_T$  or  $(\tilde{S})$ , the Lagrange multiplier vector  $\Lambda$  and ultimately the variables of interest  $u$ .



In the laminar flow case, the matrix is solved using Gaussian elimination method. This method involves the reduction of the matrix to an upper triangular one by elimination of the elements below the main diagonal of the matrix. Then the triangular system is solved by successive substitution beginning with the last equation. This is performed using the command *femlin(... 'method'='eliminate'..)*. In the case of the turbulent modeling, a combination of parametric sweeping algorithm and Good Broyden method based on the Broyden family type of solvers is used. The idea is to solve a series of increasingly difficult non-linear problems. The solution of a slightly non-linear problem, which is easy to solve, is used as the input to a more difficult non-linear problem by increasing a parameter that represents the degree of non-linearity. The sweeping parameter used here is the Reynolds number,  $Re$ . In this way the solutions of a low Reynolds number flow is subsequently used as initial guess for the next iteration step. This method leads to a fast and efficient convergence. To illustrate the iterative solver, we consider the linear system:

$$Ax = b \quad [A.34]$$

where  $A$  is a square matrix, the solution  $x$  and the right-hand side  $b$  are vectors. The iterative method solves this linear system by generating a sequence of approximate solutions  $x_k$  that converge towards the solution  $x = A^{-1}b$ . Given an initial guess  $x_0$  and an initial preconditioned  $H_0 \sim A^{-1}$ , the algorithm involved is:

Initialization:  $r_0 = b - Ax_0$  (initial residual vector)

$$\Delta_0 = H_0 r_0 \text{ (initial preconditioned residual vector)}$$

$$\sigma_0 = \Delta_0^* \Delta_0 \quad (* \text{ denotes the conjugate})$$

Iteration loop:  $k = 0, 1, \dots, k_{\max}$  :

$$q_k = A \Delta_k$$

$$\tilde{z}_0 = H_0 q_k \text{ (based on quasi-Newton condition)}$$

Update loop:  $i = 0, \dots, k-1$  (for  $k \geq 1$ ) :

$$\tilde{z}_{i+1} = \tilde{z}_i + \frac{\Delta_i^* \tilde{z}_i}{\gamma_i \tau_i} (\Delta_{i+1} - (1-t_i) \Delta_i)$$

$$z_k = \tilde{z}_k$$

$$\gamma_k = \Delta_k^* z_k$$

$$\tau_k = \sigma_k / \gamma_k$$

if  $\tau_k < \tau_{\min}$  : restart

$$t_k = \tau_k$$

if  $\tau_k > \tau_{\max}$   $t_k = 1$

$$x_{k+1} = x_k + t_k \Delta_k$$

$$r_{k+1} = r_k - t_k q_k$$

$$\Delta_{k+1} = (1-t_k + \tau_k) \Delta_k - \tau_k z_k$$

$$\sigma_{k+1} = \Delta_{k+1}^* \Delta_{k+1}$$

[A.35]

where the parameters  $\tau_{\min}, \tau_{\max}$  are set internally such that  $0 < \tau_{\min} < 1, \tau_{\max} \geq 1$

In each iteration, the new approximation  $x_{k+1}$  to  $x$  is obtained by correcting the previous iterate  $x_k$  along the preconditioned residual  $\Delta_k$ . The convergence of the

solution to the next iterative step within a given parametric sweep is assessed using the solution error criterion formulation given as (Deuflhand et al. 1990):

$$\frac{\sqrt{\sigma_{k+1}}}{\|x_{k+1}\|} \leq \varepsilon \quad [\text{A.36}]$$

where  $\|x_{k+1}\|$  is the norm of vector of unknowns at  $k+1$  iterative step, the numerator is simply the norm of the preconditioned residual of the iterate  $x_{k+1}$  and  $\varepsilon$  is a relative accuracy parameter to be specified. Here the Incomplete LU is implemented in preconditioning the matrix. In this case the iterative method is applied on the transformed system  $\tilde{A}\tilde{x} = \tilde{b}$ , where  $\tilde{A} = \tilde{L}^{-1}A\tilde{U}^{-1}$ ,  $\tilde{b} = \tilde{L}^{-1}b$ , and  $\tilde{x} = \tilde{U}x$ , where  $\tilde{L}$  and  $\tilde{U}$  are the incomplete LU factors of A. These factors are generated by the MATLAB function *luinc*.

### A.3 ASSESSING THE PREDICTIVE CAPACITY

To assess the predictive capacity of the finite element method, finite difference and analytical solutions are used to approximate the laminar flow equation. The governing equation in the laminar flow regime in both wastewater-driven and pressure-induced flows can be written in non-dimensionalized form as:

$$\left[ \frac{\partial^2 U_*}{\partial Y_*^2} + \frac{\partial^2 U_*}{\partial Z_*^2} \right] = \alpha_* \quad [\text{A.37}]$$

where the length and velocity scales are  $b$  and  $U_w$ , respectively. The boundary conditions required to solve Equation [A.37] are  $U_* = 1$  at the interface for wastewater-only induced flow and combined flow (both pressure and wastewater

drag acting altogether), and  $U_* = 0$  for pressure-only induced flow. Evidently, in pressure-only flow, the velocity cannot be non-dimensionalized since our velocity scale  $U_w$  is zero.  $U_* = 0$  at the wall (no-slip condition) is further used for all cases. All dimensionless quantities are replaced with their dimensionalized equivalents for convenience from this point.

### A.3.1 Analytical Modeling

The airspace cross-section is transformed into half-elliptic shape facilitating the use of elliptic orthogonal and conformal curvilinear co-ordinates. Although this transformation is an approximation, it is far better than assuming a 1-D approximation for such geometry. Here expressions, in the form of infinite series, are derived for the longitudinal velocity distributions and average velocities. The models are valid for headspace sections with eccentricity,  $\epsilon$ , less than unity or  $b/D < 0.5$ .

In this method, the headspace is bounded by the equations

$$Y = 0 \text{ and } \frac{4Z^2}{C^2} + Y^2 = 1 \quad [\text{A.38}]$$

where  $|Z| \leq C/2$ ,  $0 \leq Y \leq 1$  and  $C$  is the dimensionless interfacial width. Figure A-4 shows the elliptic system placed on the flow geometry. This transformation is necessary to eliminate the cumbersome mathematical analysis associated with the Cartesian co-ordinate system for this flow geometry. The analysis presented here is based on placing the foci on the  $Z$ -axis at the points  $F_1(-t, 0)$  and  $F_2(t, 0)$  so that

$C > 2$ . In this system, surfaces of constant  $\eta$  are represented by elliptic cylinders and the sewer wall is defined by  $\eta = \eta_1$  (Equation [A.40]). The value  $\theta = \pi/2$  corresponds to the positive Y-axis, and  $\theta = 0$  and  $\pi$  correspond to the positive and negative Z-axes, respectively.

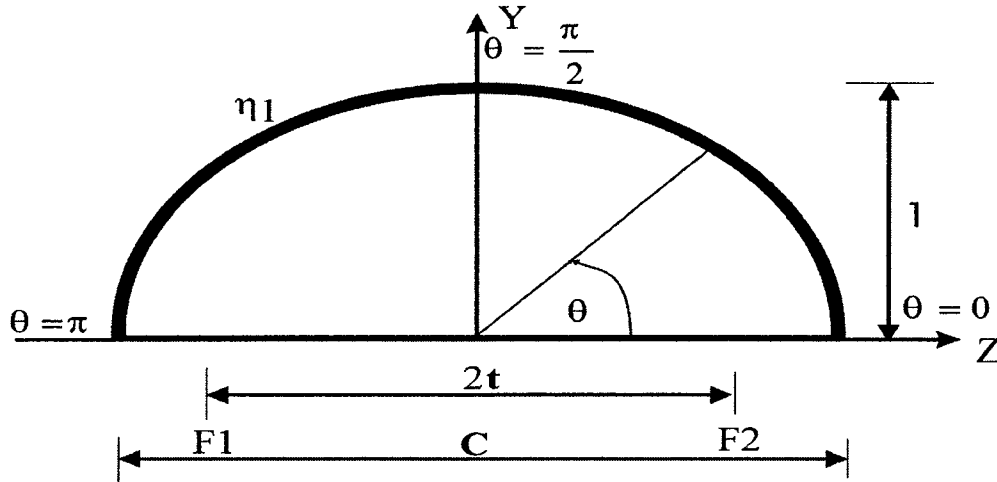


**Figure A-4: Headspace in an elliptic system**

The following transformation is utilized (Moon et al. 1961):

$$Z = t \cosh \eta \cos \theta, \quad Y = t \sinh \eta \sin \theta \quad [\text{A.39}]$$

Where  $t = C/2 \cosh \eta_1$

In which (Borjini et al. 1999)

$$\eta_1 = \frac{1}{2} \ln \left[ \frac{(1 + \sqrt{1 - \epsilon^2})}{(1 - \sqrt{1 - \epsilon^2})} \right] \quad [\text{A.40}]$$

where  $\epsilon$  is the eccentricity of the approximated headspace given as:

$$\varepsilon = \frac{\sqrt{C^2 - 4}}{2C} \quad [\text{A.41}]$$

Let us designate the co-ordinate system by the metric coefficients  $g_{11}$  and  $g_{22}$ , where

$$g_{11} = \left( \frac{\partial Z}{\partial \eta} \right)^2 + \left( \frac{\partial Y}{\partial \eta} \right)^2 = t^2 (\cosh^2 \eta - \cos^2 \theta) \quad [\text{A.42}]$$

$$g_{22} = \left( \frac{\partial Z}{\partial \theta} \right)^2 + \left( \frac{\partial Y}{\partial \theta} \right)^2 = t^2 (\cosh^2 \eta - \cos^2 \theta) \quad [\text{A.43}]$$

Equation [A.37] in the curvilinear co-ordinates  $(\eta, \theta)$  can therefore be written as:

$$g^{-1/2} \left( \frac{\partial}{\partial \eta} \left( \frac{g_{22}}{g^{1/2}} \frac{\partial U}{\partial \eta} \right) + \frac{\partial}{\partial \theta} \left( \frac{g_{11}}{g^{1/2}} \frac{\partial U}{\partial \theta} \right) \right) = \alpha \quad [\text{A.44}]$$

where  $g^{1/2} = g_{11}^{1/2} g_{22}^{1/2}$ . Note that the other metric coefficients  $g_{21} = g_{12} = 0$  and also  $g_{11} = g_{22}$  because of the orthogonal and conformal co-ordinate system. With these coefficients, we can write the transformed equation as:

$$\frac{\partial^2 U}{\partial Z^2} + \frac{\partial^2 U}{\partial Y^2} = \frac{1}{t^2 [\cosh^2 \eta - \cos^2 \theta]} \left[ \frac{\partial^2 U}{\partial \eta^2} + \frac{\partial^2 U}{\partial \theta^2} \right] = \alpha \quad [\text{A.45}]$$

The boundary conditions in this transformation become:

$$1. U(\eta, 0) = U(\eta, \pi) = 1 \quad [\text{A.46}]$$

$$2. U(\eta_1, \theta) = 0 \quad [\text{A.47}]$$

Equations [A.45], [A.46] and [A.47] are amenable to analytical solution using the method of eigenfunction expansion in one-dimension. To do this the equation is divided into homogeneous and inhomogeneous parts and then using the method of superposition to obtain the complete solution.

a) Homogeneous Part

The homogeneous formulation of Equation [A.45] is given by

$$\frac{\partial^2 U}{\partial \eta^2} + \frac{\partial^2 U}{\partial \theta^2} = 0 \quad [\text{A.48}]$$

with the boundary conditions:

$$1. U(\eta, 0) = U(\eta, \pi) = 1 \quad [\text{A.49a}]$$

$$2. U(\eta_1, \theta) = 0 \quad [\text{A.49b}]$$

If the homogeneous solution is denoted by  $U_H$  then

$$U_H(\eta, \theta) = 1 + U_1(\eta, \theta) \quad [\text{A.50}]$$

where  $U_1(\eta, \theta) = H(\eta)\vartheta(\theta)$

The boundary conditions for  $U_1$  are:

$$1. U_1(\eta, 0) = U_1(\eta, \pi) = 0 \quad [\text{A.51a}]$$

$$2. U_1(\eta_1, \theta) = -1 \quad [\text{A.51b}]$$

We still have inhomogeneous boundary conditions and homogeneous equation in  $U_1$ . Substituting Equation [A.50] into Equation [A.48] and separating variables, lead to

$$H(\eta) = Ae^{\sqrt{\lambda}\eta} + Be^{-\sqrt{\lambda}\eta}, \quad \vartheta(\theta) = E \sin \sqrt{\lambda}\theta + D \cos \sqrt{\lambda}\theta \quad [\text{A.52}]$$

$\lambda$  is a separation constant, and A, B, D and E are constants. Using Equation [A.51] (boundary conditions for  $U_1$ ), the eigenfunctions in  $\theta$  are  $\sin m\theta$ , where m are the eigenvalues ( $m = 1, 2, 3, \dots$ ).

$U_1$  could have the general solution

$$U_1(\eta, \theta) = \sum_{m=1}^{\infty} (A_m \sin m\theta \sinh m\eta) \quad [\text{A.53}]$$

where  $A_m$  is determined as

$$A_m = -\frac{\int_0^\pi \sin m\theta d\theta}{\sinh m\eta_1 \int_0^\pi \sin^2 m\theta d\theta} = -\frac{4}{\pi n \sinh m\eta_1} \quad [\text{A.54}]$$

The homogeneous solution therefore becomes

$$U_H(\eta, \theta) = \left[ 1 - \frac{4}{\pi} \sum_{m=1}^{\infty} \frac{\sin m\theta \sinh m\eta}{m \sinh m\eta_1} \right] \quad [\text{A.55}]$$

$m=1, 3, 5\dots$

b) Non-homogeneous Part

The non-homogeneous part comprises Equation [A.45] and boundary conditions:

$$1. U(\eta, 0) = U(\eta, \pi) = 0 \quad [\text{A.56a}]$$

$$2. U(\eta_1, \theta) = 0 \quad [\text{A.56b}]$$

The solution is first expanded in eigenfunctions of the homogeneous part in  $\theta$  by the method of separation of variables as,

$$U_p(\eta, \theta) = H(\eta)\vartheta(\theta) \quad [\text{A.57}]$$

where

$$H(\eta) = Ae^{\sqrt{\lambda}\eta} + Be^{-\sqrt{\lambda}\eta}, \quad \vartheta(\theta) = E \sin \sqrt{\lambda}\theta + D \cos \sqrt{\lambda}\theta \quad [\text{A.58}]$$

where A, B, D and E are constants. Using Equation [A.56], the eigenfunctions in  $\theta$  are  $\sin m\theta$  where  $m$  ( $m= 1, 2, 3\dots$ ) are the eigenvalues. Expanding  $U_p(\eta, \theta)$  in a series of these eigenfunctions:

$$U_p(\eta, \theta) = \sum_{m=1}^{\infty} V_m(\eta) \sin m\theta \quad [\text{A.59}]$$



where the sine coefficients  $V_m(\eta)$  are functions of  $\eta$ . Substituting Equation [A.59] into Equation [A.45] gives

$$\sum_{m=1}^{\infty} \left[ \frac{d^2 V_m}{d\eta^2} - m^2 V_m \right] \sin m\theta = \alpha^2 [\cosh^2 \eta - \cos^2 \theta] \quad [\text{A.60}]$$

Since  $U_P(\eta, \theta)$  and  $\sin m\theta$  satisfy the same homogeneous boundary conditions, the Fourier sine coefficients satisfy the following second-order ordinary differential equation:

$$\left( \frac{d^2 V_m}{d\eta^2} - m^2 V_m \right) = \frac{\alpha^2 \int_0^{\pi} [\cosh^2 \eta - \cos^2 \theta] \sin m\theta d\theta}{\int_0^{\pi} \sin^2 m\theta} = k \cosh^2 \eta - p \quad [\text{A.61}]$$

$$\text{where } k = \frac{4\alpha^2}{m\pi}; \quad p = \frac{4\alpha^2}{m\pi} \left( \frac{m^2 - 2}{m^2 - 4} \right) \quad [\text{A.62}]$$

Solving the resulting equation with the boundary conditions gives

$$V_m = v_1 e^{m\eta} + v_2 e^{-m\eta} + R \cosh^2 \eta + p_0 \quad [\text{A.63}]$$

where

$$R = \frac{k}{4 - m^2}; \quad p_0 = \frac{p - 2R}{m^2}; \quad v_2 = -\frac{z_1 - k_1 e^{m\eta_1}}{2 \sinh m\eta_1}; \quad z_1 = -R \cosh^2 \eta_1 - p_0; \quad k_1 = -R - p_0; \quad v_1 = k_1 - v_2 \quad [\text{A.64}]$$

The solution of the non-homogeneous part  $U_P$  is worked out as

$$U_P(\eta, \theta) = \sum_{m=1}^{\infty} (v_1 e^{m\eta} + v_2 e^{-m\eta} + R \cosh^2 \eta + p_0) \sin m\theta \quad [\text{A.65}]$$

The general solution therefore is a linear superposition of  $U_H$  and  $U_P$  given as:

$$U(\eta, \theta) = \sum_{m=1}^{\infty} \left( v_1 e^{m\eta} + v_2 e^{-m\eta} + R \cos^2 \eta + p_0 \right) \sin m\theta + \left( 1 - \frac{4}{\pi} \sum_{m=1}^{\infty} \frac{\sin m\theta \sinh m\eta}{m \sinh m\eta_1} \right) \quad [\text{A.66}]$$

I

II

$m=1, 3, 5, \dots$

The cross-sectional average velocity is calculated as

$$U_{av} = \frac{4}{\pi C} \int_0^{\eta_1} \int_0^{\pi} U(\eta, \theta) (g_{11}^{1/2} d\eta) (g_{22}^{1/2} d\theta) \quad [\text{A.67a}]$$

$$U_{av} = \frac{4t^2}{\pi C} \left[ \sum_{m=1}^{\infty} (I_{m1} I_{m2} - I_{m3} I_{m4}) \right] + \left[ 1 - \frac{16t^2}{\pi^2 C} \sum_{m=1}^{\infty} \frac{(I_{m5} I_{m6} - I_{m7} I_{m8})}{m \sinh m\eta_1} \right] \quad [\text{A.67b}]$$

I

II

$m=1, 3, 5, \dots$

where

$$I_{m1} = \frac{2}{m}$$

$$I_{m2} = \frac{1}{4} \left[ \frac{v_1 e^{\eta_1(m+2)} - v_2 e^{-\eta_1(m+2)}}{m+2} + \frac{v_1 e^{\eta_1(m-2)} - v_2 e^{-\eta_1(m-2)}}{m-2} + 2I_{m3} - 2I_{m4}(v_1 - v_2) + G \right]$$

$$I_{m3} = \frac{v_1 e^{m\eta_1} - v_2 e^{-m\eta_1}}{m} + \frac{R}{4} \sinh 2\eta_1 + \eta_1 (p_0 + R/2) - \frac{(v_1 - v_2)}{m}; I_{m4} = \frac{2(m^2 - 2)}{m(m+2)(m-2)}$$

$$G = (p_0 + R) \sinh 2\eta_1 + \eta_1 (2p_0 + 3R/2) + \frac{R}{8} \sinh 4\eta_1$$

$$I_{m5} = \frac{2}{m}; I_{m6} = \frac{1}{2} (I_{m9} + I_{m8}); I_{m7} = \frac{2(m^2 - 2)}{m(m+2)(m-2)}$$

$$I_{m8} = \frac{\cosh m\eta_1 - 1}{m}$$

$$I_{m9} = \frac{(m-2) \cosh(2+m)\eta_1 + (m+2) \cosh(m-2)\eta_1 - 2m}{2(m+2)(m-2)}$$

Term I in Equations [A.66] and [A.67b] is the contribution of the pressure forces whereas term II in the same equations is due to wastewater drag.

### A.3.2 Finite Difference Modeling

In this method, a transfinite algebraic grid generation technique is employed to transform the governing equation and the flow geometry into a body-fitted unit-square co-ordinate system that allows co-incidence of all boundary lines with a co-ordinate line. A finite difference formulation of the resulting equation, in the computational domain, is solved iteratively using the method of successive over-relation (SOR) from which the longitudinal velocity distribution and average velocity are generated.

Thus here Equation [A.37] is transformed into the generalized co-ordinate system  $(\xi, \eta)$ . It is assumed that there is a unique, single-valued mapping between the computational co-ordinates  $(\xi, \eta)$  and the physical co-ordinates  $(Z, Y)$ , which can be written as  $\xi = \xi(Z, Y)$ ,  $\eta = \eta(Z, Y)$  and by implication

$Z = Z(\xi, \eta)$ ,  $Y = Y(\xi, \eta)$ . In terms of these new variables, the governing equation is written as:

$$\frac{\partial}{\partial \xi} \left( \frac{g_{22}}{g^{1/2}} \frac{\partial U}{\partial \xi} - \frac{g_{12}}{g^{1/2}} \frac{\partial U}{\partial \eta} \right) + \frac{\partial}{\partial \eta} \left( -\frac{g_{21}}{g^{1/2}} \frac{\partial U}{\partial \xi} + \frac{g_{11}}{g^{1/2}} \frac{\partial U}{\partial \eta} \right) = \alpha \quad [\text{A.68}]$$

where  $g^{1/2} = g_{11}^{1/2} g_{22}^{1/2}$ . The metric coefficients  $g_{11}$ ,  $g_{12}$ ,  $g_{21}$  and  $g_{22}$  are contained in  $g$  as

$$\mathbf{g} = \begin{bmatrix} g_{11} & g_{12} \\ g_{21} & g_{22} \end{bmatrix} = \begin{bmatrix} (Z_\xi^2 + Y_\xi^2) & (Z_\xi Z_\eta + Y_\xi Y_\eta) \\ (Z_\xi Z_\eta + Y_\xi Y_\eta) & (Z_\eta^2 + Y_\eta^2) \end{bmatrix} = \frac{1}{J^2} \begin{bmatrix} (\eta_Z^2 + \eta_Y^2) & -(\xi_Z \eta_Z + \xi_Y \eta_Y) \\ -(\xi_Z \eta_Z + \xi_Y \eta_Y) & (\xi_Z^2 + \xi_Y^2) \end{bmatrix} \quad [\text{A.69}]$$

where  $Z_\xi \equiv \partial Z / \partial \xi$ , etc., as above, and  $J$  is the determinant of the Jacobian matrix

$$\mathbf{J} \equiv \begin{bmatrix} \frac{\partial \xi}{\partial Z} & \frac{\partial \xi}{\partial Y} \\ \frac{\partial \eta}{\partial Z} & \frac{\partial \eta}{\partial Y} \end{bmatrix} \quad [\text{A.70}]$$

The metric tensor is related to the inverse Jacobian by  $\mathbf{g} = (\mathbf{J}^{-1})^T \mathbf{J}^{-1}$  from which it can be shown that  $g^{1/2} = J^{-1}$  by taking determinants of both sides. Unlike the analytical modeling, none of the metric coefficients is zero due to the non-conformal and non-orthogonal system used. Substitution for the various terms, after some manipulation, gives

$$-\left\{ \left( \frac{\Delta^2 \xi}{J} \right) U \right\}_\xi - \left\{ \left( \frac{\Delta^2 \eta}{J} \right) U \right\}_\eta + \left\{ \left( \frac{\sigma}{J} \right) U \right\}_{\xi\xi} + \left\{ \left( \frac{\beta}{J} \right) U \right\}_{\xi\eta} + \left\{ \left( \frac{\gamma}{J} \right) U \right\}_{\eta\eta} = \alpha J^{-1} \quad [\text{A.71}]$$

where

$$\sigma = \xi_Z^2 + \xi_Y^2; \quad \beta = 2(\xi_Z \eta_Z + \xi_Y \eta_Y); \quad \gamma = \eta_Z^2 + \eta_Y^2; \quad J = \xi_Z \eta_Y - \xi_Y \eta_Z; \quad \Delta^2 \xi = \xi_{ZZ} + \xi_{YY}, \text{ etc.}$$

The new terms appearing in Equation [A.71] represent terms in the computational domain that result from the transformation of the physical domain into the computational domain. Expressing Equation [A.71] in terms of the transformation parameters  $Z_\xi$ , etc., instead of  $\xi_Z$ , etc., the various terms become:

$$GTT \equiv \frac{\sigma}{J} = \frac{Z_\eta^2 + Y_\eta^2}{J^{-1}}; GWT \equiv \frac{\beta}{J} = \frac{-2(Z_\xi Z_\eta + Y_\xi Y_\eta)}{J^{-1}}; GWW \equiv \frac{\gamma}{J} = \frac{Z_\xi^2 + Y_\xi^2}{J^{-1}} \quad [A.72]$$

where the determinant of the inverse Jacobian  $J^{-1} = Z_\xi Y_\eta - Z_\eta Y_\xi$ . It can also be established that

$$\xi_{ZZ} = \frac{\xi_Z Y_{\xi\eta} + \eta_Z Y_{\eta\eta}}{J^{-1}} - \frac{\xi_Z^2 J_\xi^{-1} + \xi_Z \eta_Z J_\eta^{-1}}{J^{-1}} \quad [A.73]$$

Obtaining similar expression for  $\xi_{YY}$  and further manipulation allows the terms  $(\Delta^2 \xi / J)$  and  $(\Delta^2 \eta / J)$  (in Equation [A.71]) to be written

$$\begin{aligned} DELZI \equiv \frac{\Delta^2 \xi}{J} &= \frac{GTT(Z_\eta Y_{\xi\xi} - Y_\eta Z_{\xi\xi})}{J^{-1}} \\ &+ \frac{GWT(Z_\eta Y_{\xi\eta} - Y_\eta Z_{\xi\eta})}{J^{-1}} \\ &+ \frac{GWW(Z_\eta Y_{\eta\eta} - Y_\eta Z_{\eta\eta})}{J^{-1}} \end{aligned} \quad [A.74]$$

$$\begin{aligned} DELET \equiv \frac{\Delta^2 \eta}{J} &= \frac{GTT(Y_\xi Z_{\xi\xi} - Z_\xi Y_{\xi\xi})}{J^{-1}} \\ &+ \frac{GWT(Y_\xi Z_{\xi\eta} - Z_\xi Y_{\xi\eta})}{J^{-1}} \\ &+ \frac{GWW(Y_\xi Z_{\eta\eta} - Z_\xi Y_{\eta\eta})}{J^{-1}} \end{aligned} \quad [A.75]$$

The numerical computation is effectively performed on the equation:

$$-(DELZI.U)_\xi - (DELET.U)_\eta + (GTT.U)_{\xi\xi} + (GWT.U)_{\xi\eta} + (GWW.U)_{\eta\eta} - WWW = 0 \quad [A.76]$$

where  $WWW = \alpha J^{-1}$

A transfinite algebraic grid generation technique is used in mapping the physical domain to the logical domain. This transformation maps a unit square in the logical space to the physical domain through vector functions which specify both Z and Y co-ordinates of the image point. Figure A-5 shows the correspondence between the physical domain (ABLD) and the computational domain ( $A'B'L'D'$ ), where calculations are performed over one quadrant of the cross-section due to symmetry.

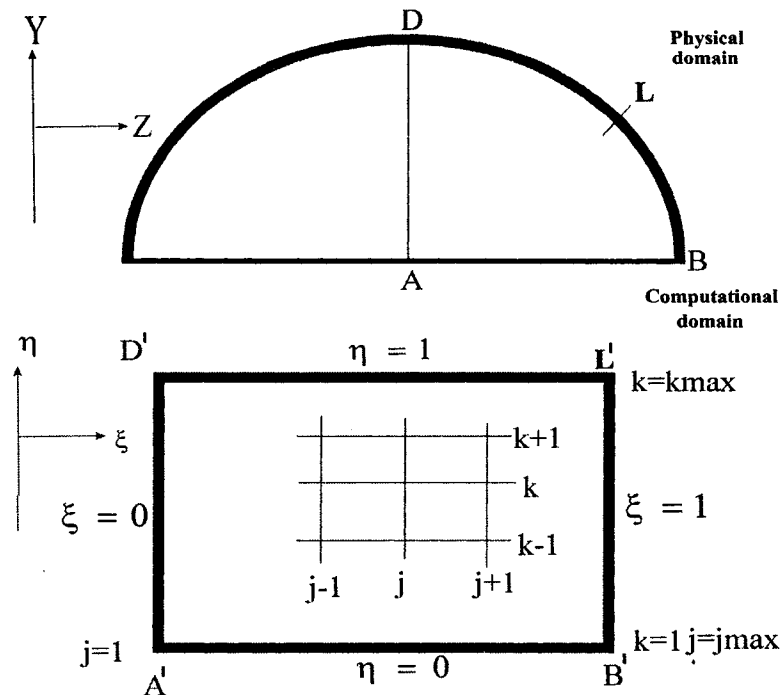


**Figure A-5: Correspondence between physical and computational domains**

The vector functions for the flow geometry are worked out as:

$$\begin{aligned}
F_{AD} &= \begin{bmatrix} Z_{AD} \\ Y_{AD} \end{bmatrix} = \begin{bmatrix} 0 \\ \eta(D/2 - y_0) + y_0 \end{bmatrix} \\
F_{AB} &= \begin{bmatrix} Z_{AB} \\ Y_{AB} \end{bmatrix} = \begin{bmatrix} \xi C/2 \\ 0 \end{bmatrix} \\
F_{BL} &= \begin{bmatrix} Z_{BL} \\ Y_{BL} \end{bmatrix} = \begin{bmatrix} \xi C/2 + \eta(e_a - C/2) \\ ((D/2)^2 - Z^2)^{1/2} \end{bmatrix} \\
F_{LD} &= \begin{bmatrix} Z_{LD} \\ Y_{LD} \end{bmatrix} = \begin{bmatrix} \xi e_a \\ ((D/2)^2 - Z^2)^{1/2} \end{bmatrix}
\end{aligned} \tag{A-77}$$

where  $y_0 = D/2 - 1$ ;  $C/2 = ((D/2)^2 - y_0^2)$ ,  $e_a = \delta C/2$ ,  $D$  is the diameter

(dimensionless) of the sewer pipe and  $\delta$  gives the position of point L. The interior co-ordinate vector function for this transformation is (Chen et al. 2000).

$$\begin{bmatrix} Z(\xi, \eta) \\ Y(\xi, \eta) \end{bmatrix} = \begin{bmatrix} (1-\eta)Z_{AB}(\xi) + \eta Z_{LD}(\xi) + (1-\xi)Z_{AD}(\eta) + \xi Z_{BL}(\eta) - m_Z(\xi, \eta) \\ (1-\eta)Y_{AB}(\xi) + \eta Y_{LD}(\xi) + (1-\xi)Y_{AD}(\eta) + \xi Y_{BL}(\eta) - m_Y(\xi, \eta) \end{bmatrix} \tag{A.78}$$

where

$$m_Z = \xi \eta Z_{LD}(1) + \xi(1-\eta)Z_{AB}(1) + \eta(1-\xi)Z_{LD}(0) + (1-\xi)(1-\eta)Z_{AB}(0)$$

$$m_Y = \xi \eta Y_{LD}(1) + \xi(1-\eta)Y_{AB}(1) + \eta(1-\xi)Y_{LD}(0) + (1-\xi)(1-\eta)Y_{AB}(0)$$

$$0 \leq \eta \leq 1 ; 0 \leq \xi \leq 1$$

Both Neumann and Dirichlet boundary conditions are defined in the computational domain as:

$$U(\xi, 0) = 1, U(1, \eta) = U(\xi, 1) = 0,$$

$$k_1 \frac{\partial U(0, \eta)}{\partial \xi} + k_2 \frac{\partial U(0, \eta)}{\partial \eta} = 0, \quad k_1 = \frac{\partial \xi}{\partial Z}, \quad k_2 = \frac{\partial \eta}{\partial Z} \text{ (Due to symmetry).}$$

The various parameters and the governing equation are evaluated at each nodal point using the centred finite difference scheme. The resulting equation becomes:

$$\begin{aligned}
& - \left[ \frac{(DELZIU)_{j+1,k} - (DELZIU)_{j-1,k}}{2\Delta\xi} \right] - \left[ \frac{(DELETU)_{j,k+1} - (DELETU)_{j,k-1}}{2\Delta\eta} \right] \\
& + \left[ \frac{(GTTU)_{j-1,k} - 2(GTTU)_{j,k} + (GTTU)_{j+1,k}}{\Delta\xi^2} \right] \\
& + \left[ \frac{(GWTU)_{j+1,k+1} - (GWTU)_{j-1,k+1} + (GWTU)_{j-1,k-1} - (GWTU)_{j+1,k-1}}{4\Delta\xi\Delta\eta} \right] \\
& + \left[ \frac{(GWWU)_{j,k-1} - 2(GWWU)_{j,k} + (GWWU)_{j,k+1}}{\Delta\eta^2} \right] - (WWW)_{j,k} = 0
\end{aligned} \tag{A.79}$$

This equation is solved iteratively using the method of successive over-relation (SOR) by making  $\Delta\xi = \Delta\eta$  in the computational domain. Equation [A.79] provides an estimate of  $U_{j,k}^{n+1}$  as:

$$U_{j,k}^* = \left\{ 2(GTT_{j,k} + GWW_{j,k}) \right\}^{-1} \left\{ \begin{aligned} & - \left[ \frac{\Delta\eta((DELZIU^n)_{j+1,k} - (DELZIU^n)_{j-1,k})}{2} \right] \\ & - \left[ \frac{\Delta\eta((DELETU^n)_{j,k+1} - (DELETU^n)_{j,k-1})}{2} \right] \\ & + \left[ \begin{aligned} & (GTTU^n)_{j-1,k} + (GTTU^n)_{j+1,k} \\ & + (GWWU^n)_{j,k-1} + (GWWU^n)_{j,k+1} \end{aligned} \right] + \\ & \left[ \frac{\begin{aligned} & (GWTU^n)_{j+1,k+1} - (GWTU^n)_{j-1,k+1} \\ & + (GWTU^n)_{j-1,k-1} - (GWTU^n)_{j+1,k-1} \end{aligned}}{4} \right] - WWW_{j,k} \Delta\eta^2 \end{aligned} \right\} \tag{A.80}$$

the improved solution is

$$U_{j,k}^{n+1} = U_{j,k}^n + \lambda(U_{j,k}^* - U_{j,k}^n) \tag{A-81}$$

where  $\lambda$  is the relaxation parameter. Here  $\lambda = 1.5$  is used. The above formulation is incorporated into a FORTRAN program. For the purpose of selecting a suitable mesh size that yields accurate results, the effect of the grid points on the numerical solution is tested by a series of runs of the computer program. The



number of grid points employed in the numerical experiments is taken from 55 x 55 to 300 x 300 grid points. It has been observed that a grid of 105 x 105 nodal points and beyond showed no difference in the solution output.

### **A.3.3 Comparisons of Developed Models**

Headspace velocity contour plots computed using the three models (finite element, analytical and finite difference methods) are compared in Figures A-6, A-7 and A-8 for wastewater-driven, pressure-induced and the combined case, respectively. Also shown in Figures A-9, A-10 and A-11 are the comparisons of the calculated average velocities from the three models for the same driving forces. There is some degree of agreement in relation to the pattern of air isovels and magnitude of the mean velocities simulated. It must be indicated here again that the analytical and finite difference models are only developed to serve as a predictive capacity test for the FEM, which is the main discretization numerical tool in this research study, but not for predicting the air flow field.

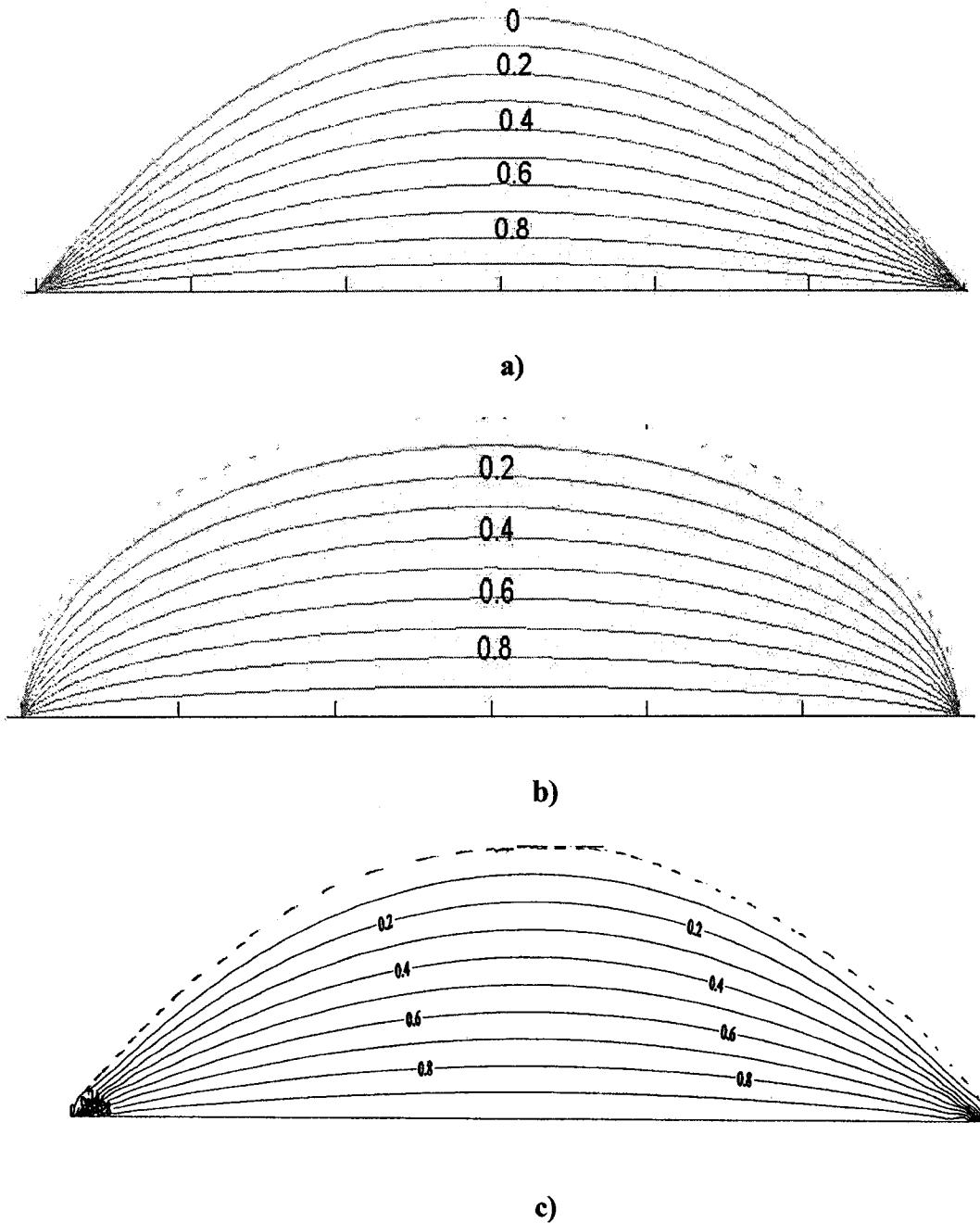
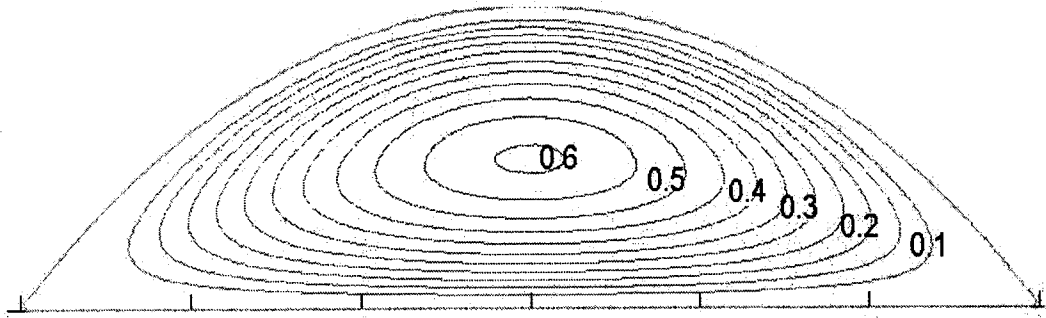
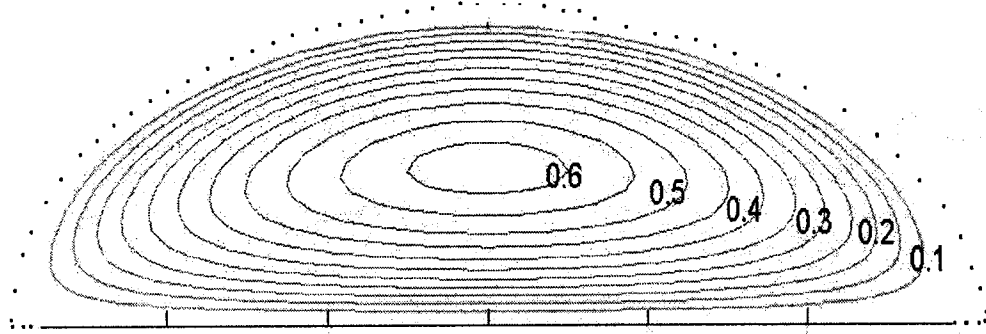


**Figure A-6(a, b & c): Wastewater-induced isovels computed for  $b/D= 10\%$ :**

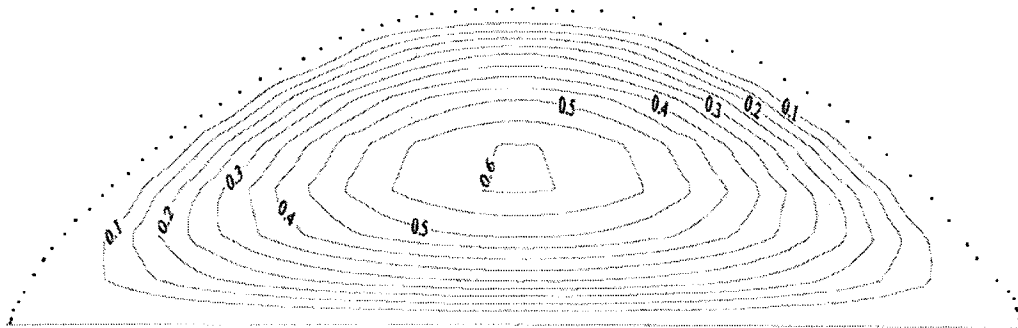
**a) finite element, b) analytical, c) finite difference**



a)



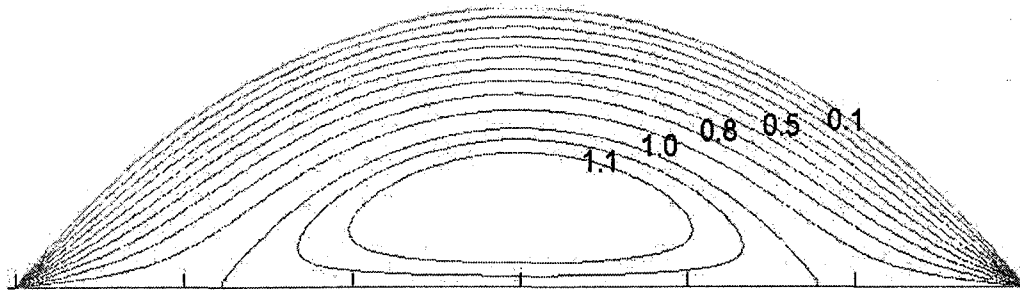
b)



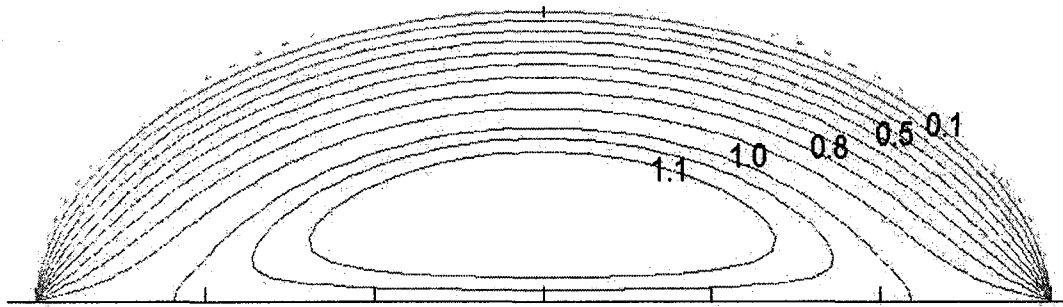
c)

**Figure A-7(a, b & c): Pressure-induced isovels computed for  $\alpha = -5$ ,  $b/D = 10$**

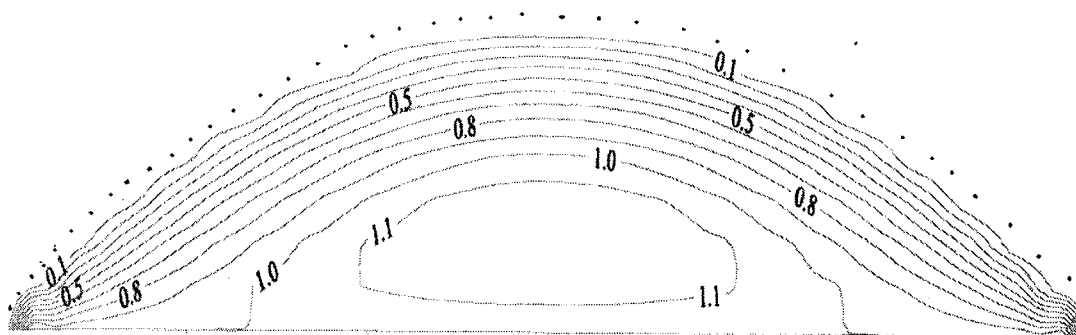
**%: a) finite element, b) analytical, c) finite difference**



a)



b)



c)

**Figure A-8(a, b & c): Combined pressure and wastewater induced isovels for**

**$\alpha = -5$ ,  $b/D = 10\%$ : a) finite element, b) analytical, c) finite difference**

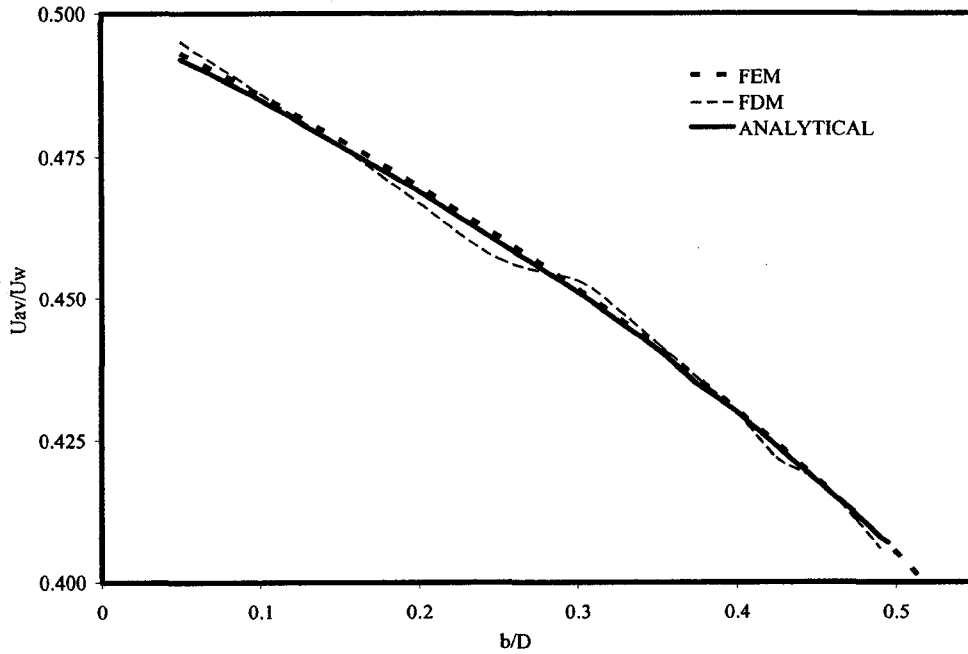


**Figure A-9: Comparative performance of the three models in computing wastewater-induced average velocity**

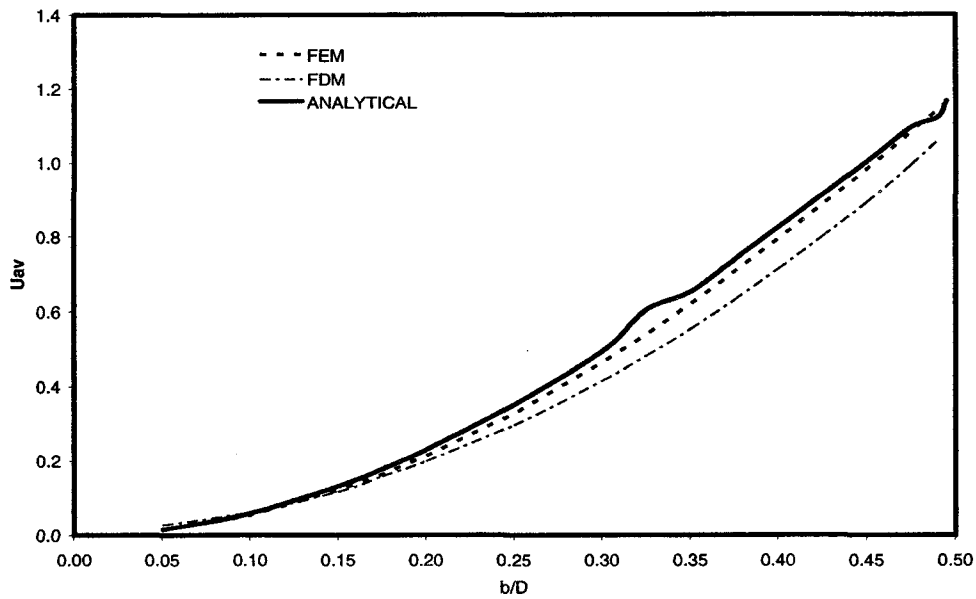


**Figure A-10: Comparative performance of the three models in computing pressure-induced average velocity for  $(dp/dx)/(v\rho) = -100$**

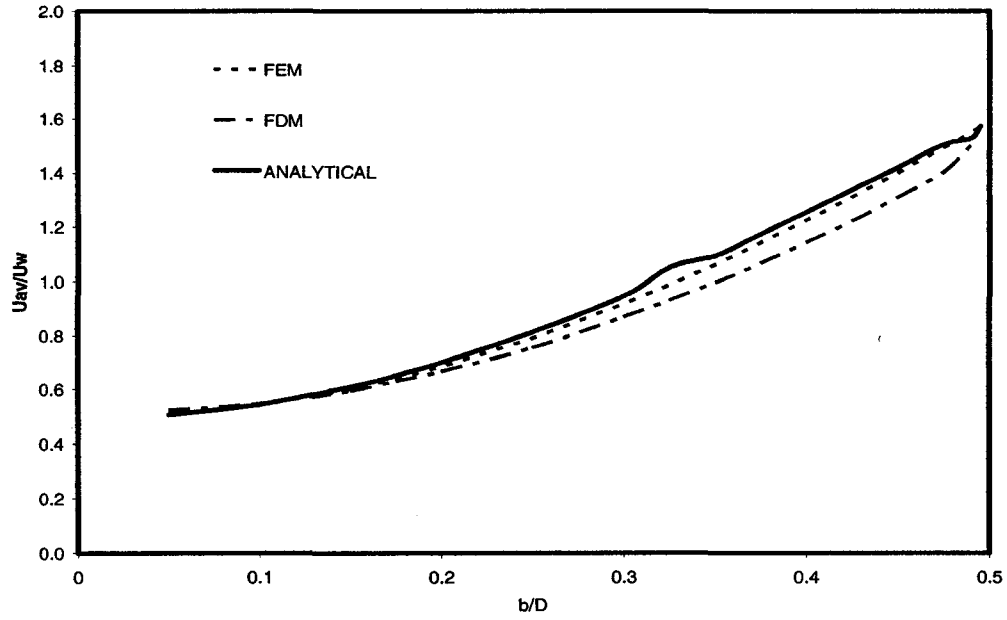


**Figure A-11: Comparative performance of the three models in computing combined average velocity for  $(dp/dx)/(v\rho U_w) = -100$**

## REFERENCES

- Ames, W. F. 1977. Numerical methods for partial differential equations. Academic Press, Toronto.
- Borjini, M. N., Mbow, C., Daguene, M. 1999. Numerical analysis of the effect of radiation on laminar steady natural convection in a two-dimensional participation medium between two horizontal confocal elliptic cylinders. Numerical Heat Transfer, Part A, 35, 467-494.
- Chen, C. J., Bernatz, R., Carlson, K. D., Lin, W. 2000. Finite analytic method in flows and heat transfer. Taylor and Francis, N. Y.
- Chorlton, F. 1967. Textbook of fluid dynamics. D. Van Nostrand Company Ltd., London.
- Deuffhard, P., Freund, R., Walter, A. 1990. Fast secant methods for the iterative solution of large nonsymmetric linear systems. IMPACT Comp. Sci. Eng. 2: 244-276.
- FEMLAB. 2002. Version 2.3a. Comsol Inc.
- Finlayson, B. A. 1972. The method of weighted residuals and variation principles. Academic Press, N. Y.
- Fletcher, C. A. J. 1988. Computational techniques for fluid dynamics 2. Springer-Verlag, N. Y.
- Moon, P., Spencer, D. E. 1961. Field theory handbook. Springer-Verlag, Berlin.
- Munson, B. R., Young, D. F., Okiishi, T. H. 1990. Fundamentals of fluid mechanics. John Willey & Sons, Inc, N. Y.

- Myint-U, T. 1973. Partial differential equations of mathematical physics. Elsevier Publishing Company, Inc., N. Y.
- Stewart, J. 1999. Calculus. 4<sup>th</sup> Edition. ITP Company, N. Y.
- Yih, C. S. 1969. Fluid mechanics. McGraw-Hill Book Company, N. Y.
- Zauderer, E. 1983. Partial differential equations of applied mathematics. John Willey & Sons, Inc., N. Y.



## APPENDIX B

# NETWORK FORMULATION AND DATA FOR THE KENILWORTH SEWER SYSTEM

This appendix provides the model formulation, and assumed pressure and wastewater velocities used for solving the Kenilworth sewer system in Chapter 5.

### Formulation

There are sixty-three (63) set of independent equations obtained using the principles of continuity and work-energy loss around the loops. All symbols required for the formulation are indicated in Figure B-1.

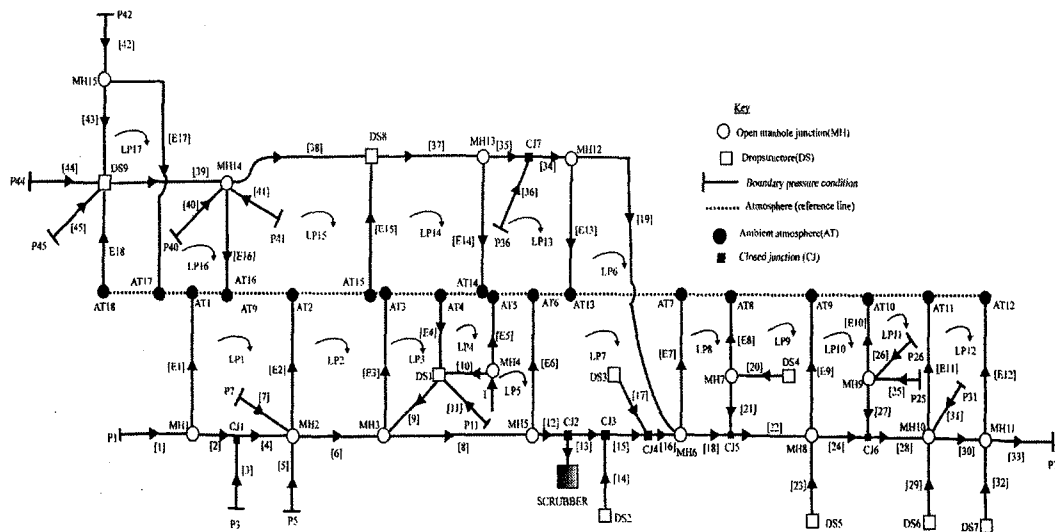


**Figure B-1: Network representation of the Kenilworth sewer system**

From the figure, the following Q-equations can be written for all junctions using continuity at open junction manholes, closed junctions, and in-line dropstructure

manholes as follows:

**Junction manholes (with possibility of eduction/induction):**

$$\text{MH1: } F_1 = Q_1 - Q_2 - Q_{E1} = 0, \text{ MH2: } F_2 = Q_7 + Q_4 + Q_5 - Q_6 - Q_{E2} = 0$$

$$\text{MH3: } F_3 = Q_6 - Q_8 + Q_9 - Q_{E3} = 0, \text{ MH4: } F_4 = Q_I - Q_{10} - Q_{E5} = 0$$

$$\text{MH5: } F_5 = Q_8 - Q_{12} - Q_{E6} = 0, \text{ MH6: } F_6 = Q_{16} - Q_{18} + Q_{19} - Q_{E7} = 0$$

$$\text{MH7: } F_7 = -Q_{21} + Q_{20} - Q_{E8} = 0, \text{ MH8: } F_8 = Q_{22} - Q_{24} + Q_{23} - Q_{E9} = 0$$

$$\text{MH9: } F_9 = Q_{25} + Q_{26} - Q_{27} - Q_{E10} = 0, \text{ MH10: } F_{10} = Q_{28} + Q_{29} - Q_{30} + Q_{31} - Q_{E11} = 0$$

$$\text{MH11: } F_{11} = Q_{30} + Q_{32} - Q_{33} - Q_{E12} = 0, \quad \text{MH12: } F_{12} = Q_{34} - Q_{19} - Q_{E13} = 0$$

$$\text{MH13: } F_{13} = Q_{37} - Q_{35} - Q_{E14} = 0, \text{ MH14: } F_{14} = Q_{39} + Q_{40} + Q_{41} - Q_{38} - Q_{E16} = 0$$

$$\text{MH15: } F_{15} = Q_{42} - Q_{43} - Q_{E17} = 0$$

[B-1]

**Closed junctions (no eduction/induction):**

$$\text{CJ1: } F_{16} = Q_2 + Q_3 - Q_4 = 0, \text{ CJ2: } F_{17} = Q_{12} - Q_{13} - Q_S = 0 \text{ (scrubber location)}$$

$$\text{CJ3: } F_{18} = Q_{13} - Q_{15} + Q_{14} = 0, \text{ CJ4: } F_{19} = Q_{15} - Q_{16} + Q_{17} = 0$$

$$\text{CJ5: } F_{20} = Q_{21} - Q_{22} + Q_{18} = 0, \text{ CJ6: } F_{21} = Q_{27} + Q_{24} - Q_{28} = 0$$

$$\text{CJ7: } F_{22} = Q_{36} - Q_{34} + Q_{35} = 0$$

[B-2]

**In-line dropstructure manholes (with possibility of eduction/induction):**

$$\text{DS1: } F_{23} = Q_{10} + Q_{11} - Q_9 + Q_{E4} = 0, \text{ DS8: } F_{24} = Q_{38} - Q_{37} + Q_{E15} = 0$$

$$\text{DS9: } F_{25} = Q_{43} + Q_{44} + Q_{45} - Q_{39} + Q_{E18} = 0$$

[B-3]

Now applying work-energy around loops LP1-LP17 plus the loops formed by the lateral pipes (boundaries), and the isolated dropstructures (i.e. those other than DS1, DS8 and DS9), we have a set of thirty-eight (38) non-linear Q-equations as follows:

$$F_{26} = P_{AT1} - P_{AT2} - \frac{|Q_{E2}|Q_{E2}}{2g(A_{02}C_{d2})^2} - \frac{|(Q_2 - W_2)|(Q_2 - W_2)}{gT_2^2} +$$

LP1:  $\frac{|Q_{E1}|Q_{E1}}{2g(A_{01}C_{d1})^2} - \frac{|(Q_4 - W_4)|(Q_4 - W_4)}{gT_4^2} = 0$

$$F_{27} = P_{AT2} - P_{AT3} - \frac{|Q_{E3}|Q_{E3}}{2g(A_{03}C_{d3})^2} - \frac{|(Q_6 - W_6)|(Q_6 - W_6)}{gT_6^2} +$$

LP2:  $\frac{|Q_{E2}|Q_{E2}}{2g(A_{02}C_{d2})^2} = 0$

$$F_{28} = P_{AT3} - P_{AT4} + \frac{|Q_{E4}|Q_{E4}}{2g(A_{04}C_{d4})^2} + \frac{|(Q_9 - W_9)|(Q_9 - W_9)}{gT_9^2} - \Delta P_{DS1}(Q_9) +$$

LP3:  $\frac{|Q_{E3}|Q_{E3}}{2g(A_{03}C_{d3})^2} = 0$

$$F_{29} = P_{AT4} - P_{AT5} - \frac{|Q_{E5}|Q_{E5}}{2g(A_{05}C_{d5})^2} + \frac{|(Q_{10} - W_{10})|(Q_{10} - W_{10})}{gT_{10}^2} -$$

LP4:  $\frac{|Q_{E4}|Q_{E4}}{2g(A_{04}C_{d4})^2} = 0$

$$F_{30} = P_{AT5} - P_{AT6} - \frac{|Q_{E6}|Q_{E6}}{2g(A_{06}C_{d6})^2} - \frac{|(Q_8 - W_8)|(Q_8 - W_8)}{gT_8^2} + \Delta P_{DS1}(Q_9) -$$

LP5:  $\frac{|(Q_{10} - W_{10})|(Q_{10} - W_{10})}{gT_{10}^2} - \frac{|(Q_9 - W_9)|(Q_9 - W_9)}{gT_9^2} + \frac{|Q_{E5}|Q_{E5}}{2g(A_{05}C_{d5})^2} = 0$

$$\begin{aligned}
F_{31} &= P_{AT6} - P_{AT13} + \frac{|Q_{E6}|Q_{E6}}{2g(A_{06}C_{d6})^2} - \frac{|Q_{E13}|Q_{E13}}{2g(A_{013}C_{d13})^2} + \\
&\frac{|(Q_{19} - W_{19})|(Q_{19} - W_{19})}{gT_{19}^2} - \frac{|(Q_{12} - W_{12})|(Q_{12} - W_{12})}{gT_{12}^2} \\
\text{LP6: } &\frac{|(Q_{13} - W_{13})|(Q_{13} - W_{13})}{gT_{13}^2} - \frac{|(Q_{15} - W_{15})|(Q_{15} - W_{15})}{gT_{15}^2} - \\
&\frac{|(Q_{16} - W_{16})|(Q_{16} - W_{16})}{gT_{16}^2} = 0 \\
F_{32} &= P_{AT6} - P_{AT7} + \frac{|Q_{E6}|Q_{E6}}{2g(A_{06}C_{d6})^2} - \frac{|Q_{E7}|Q_{E7}}{2g(A_{07}C_{d7})^2} - \\
\text{LP7: } &\frac{|(Q_{12} - W_{12})|(Q_{12} - W_{12})}{gT_{12}^2} - \frac{|(Q_{13} - W_{13})|(Q_{13} - W_{13})}{gT_{13}^2} - \\
&\frac{|(Q_{15} - W_{15})|(Q_{15} - W_{15})}{gT_{15}^2} - \frac{|(Q_{16} - W_{16})|(Q_{16} - W_{16})}{gT_{16}^2} = 0 \\
F_{33} &= P_{AT7} - P_{AT8} - \frac{|Q_{E8}|Q_{E8}}{2g(A_{08}C_{d8})^2} + \frac{|(Q_{21} - W_{21})|(Q_{21} - W_{21})}{gT_{21}^2} - \\
\text{LP8: } &\frac{|(Q_{18} - W_{18})|(Q_{18} - W_{18})}{gT_{18}^2} + \frac{|Q_{E7}|Q_{E7}}{2g(A_{07}C_{d7})^2} = 0 \\
F_{34} &= P_{AT8} - P_{AT9} - \frac{|Q_{E9}|Q_{E9}}{2g(A_{09}C_{d9})^2} - \frac{|(Q_{22} - W_{22})|(Q_{22} - W_{22})}{gT_{22}^2} - \\
\text{LP9: } &\frac{|(Q_{21} - W_{21})|(Q_{21} - W_{21})}{gT_{21}^2} + \frac{|Q_{E8}|Q_{E8}}{2g(A_{08}C_{d8})^2} = 0 \\
F_{35} &= P_{AT9} - P_{AT10} - \frac{|Q_{E10}|Q_{E10}}{2g(A_{010}C_{d10})^2} + \frac{|(Q_{27} - W_{27})|(Q_{27} - W_{27})}{gT_{27}^2} - \\
\text{LP10: } &\frac{|(Q_{24} - W_{24})|(Q_{24} - W_{24})}{gT_{24}^2} + \frac{|Q_{E9}|Q_{E9}}{2g(A_{09}C_{d9})^2} = 0
\end{aligned}$$

$$\text{LP11: } F_{36} = P_{AT10} - P_{AT11} - \frac{|Q_{E11}|Q_{E11}}{2g(A_{011}C_{d11})^2} + \frac{|Q_{E10}|Q_{E10}}{2g(A_{010}C_{d10})^2} - \frac{|(Q_{28} - W_{28})|(Q_{28} - W_{28})}{gT_{28}^2} - \frac{|(Q_{27} - W_{27})|(Q_{27} - W_{27})}{gT_{27}^2} = 0$$

$$\text{LP12: } F_{37} = P_{AT11} - P_{AT12} - \frac{|Q_{E12}|Q_{E12}}{2g(A_{012}C_{d12})^2} + \frac{|Q_{E11}|Q_{E11}}{2g(A_{011}C_{d11})^2} - \frac{|(Q_{30} - W_{30})|(Q_{30} - W_{30})}{gT_{30}^2} = 0$$

$$\text{LP13: } F_{38} = P_{AT13} - P_{AT14} - \frac{|Q_{E14}|Q_{E14}}{2g(A_{014}C_{d14})^2} + \frac{|Q_{E13}|Q_{E13}}{2g(A_{013}C_{d13})^2} + \frac{|(Q_{35} - W_{35})|(Q_{35} - W_{35})}{gT_{35}^2} + \frac{|(Q_{34} - W_{34})|(Q_{34} - W_{34})}{gT_{34}^2} = 0$$

$$\text{LP14: } F_{39} = P_{AT14} - P_{AT15} + \frac{|Q_{E15}|Q_{E15}}{2g(A_{015}C_{d15})^2} + \frac{|Q_{E14}|Q_{E14}}{2g(A_{014}C_{d14})^2} + \frac{|(Q_{37} - W_{37})|(Q_{37} - W_{37})}{gT_{37}^2} - \Delta P_{DS8}(Q_{37}) = 0$$

$$\text{LP15: } F_{40} = P_{AT15} - P_{AT16} - \frac{|Q_{E16}|Q_{E16}}{2g(A_{016}C_{d16})^2} - \frac{|Q_{E15}|Q_{E15}}{2g(A_{015}C_{d15})^2} + \frac{|(Q_{38} - W_{38})|(Q_{38} - W_{38})}{gT_{38}^2} = 0$$

$$\text{LP16: } F_{41} = P_{AT16} - P_{AT18} + \frac{|Q_{E18}|Q_{E18}}{2g(A_{018}C_{d18})^2} + \frac{|Q_{E16}|Q_{E16}}{2g(A_{016}C_{d16})^2} + \frac{|(Q_{39} - W_{39})|(Q_{39} - W_{39})}{gT_{39}^2} - \Delta P_{DS9}(Q_{39}) = 0$$

$$\text{LP17: } F_{42} = P_{AT17} - P_{AT18} + \frac{|Q_{E18}|Q_{E18}}{2g(A_{018}C_{d18})^2} + \frac{|Q_{E17}|Q_{E17}}{2g(A_{017}C_{d17})^2} - \frac{|(Q_{43} - W_{43})|(Q_{43} - W_{43})}{gT_{43}^2} = 0$$

(Other loops formed by laterals and isolated dropstructures)

$$\text{LP18: } F_{43} = P_1 - \frac{|Q_{E1}|Q_{E1}}{2g(A_{01}C_{d1})^2} - \frac{|(Q_1 - W_1)|(Q_1 - W_1)}{gT_1^2} - P_{AT1} = 0$$

$$\text{LP19: } F_{44} = P_3 - \frac{|Q_{E1}|Q_{E1}}{2g(A_{01}C_{d1})^2} - \frac{|(Q_3 - W_3)|(Q_3 - W_3)}{gT_3^2} + \frac{|(Q_2 - W_2)|(Q_2 - W_2)}{gT_2^2} - P_{AT1} = 0$$

$$\text{LP20: } F_{45} = P_5 - \frac{|Q_{E2}|Q_{E2}}{2g(A_{02}C_{d2})^2} - \frac{|(Q_5 - W_5)|(Q_5 - W_5)}{gT_5^2} - P_{AT2} = 0$$

$$\text{LP21: } F_{46} = P_7 - \frac{|Q_{E2}|Q_{E2}}{2g(A_{02}C_{d2})^2} - \frac{|(Q_7 - W_7)|(Q_7 - W_7)}{gT_7^2} - P_{AT1} = 0$$

$$\text{LP22: } F_{47} = P_{11} + \frac{|Q_{E4}|Q_{E4}}{2g(A_{04}C_{d4})^2} - \frac{|(Q_{11} - W_{11})(Q_{11} - W_{11})}{gT_{11}^2} - P_{AT4} = 0$$

$$\text{LP23: } F_{48} = \Delta P_{DS2}(Q_{14}) - \frac{|Q_{E6}|Q_{E6}}{2g(A_{06}C_{d6})^2} - \frac{|(Q_{14} - W_{14})(Q_{14} - W_{14})}{gT_{14}^2} + \frac{|(Q_{12} - W_{12})(Q_{12} - W_{12})}{gT_{12}^2} + \frac{|(Q_{13} - W_{13})(Q_{13} - W_{13})}{gT_{13}^2} - P_{AT6} = 0$$

$$\text{LP24: } F_{49} = \Delta P_{DS3}(Q_{17}) - \frac{|Q_{E7}|Q_{E7}}{2g(A_{07}C_{d7})^2} - \frac{|(Q_{17} - W_{17})(Q_{17} - W_{17})}{gT_{17}^2} - \frac{|(Q_{16} - W_{16})(Q_{16} - W_{16})}{gT_{16}^2} - P_{AT7} = 0$$

$$\text{LP25: } F_{50} = \Delta P_{DS4}(Q_{20}) - \frac{|Q_{E8}|Q_{E8}}{2g(A_{08}C_{d8})^2} - \frac{|(Q_{20} - W_{20})(Q_{20} - W_{20})}{gT_{20}^2} - P_{AT8} = 0$$

$$\text{LP26: } F_{51} = \Delta P_{DS5}(Q_{23}) - \frac{|Q_{E9}|Q_{E9}}{2g(A_{09}C_{d9})^2} - \frac{|(Q_{23} - W_{23})(Q_{23} - W_{23})}{gT_{23}^2} - P_{AT9} = 0$$

$$\text{LP27: } F_{52} = P_{26} - \frac{|Q_{E10}|Q_{E10}}{2g(A_{010}C_{d10})^2} - \frac{|(Q_{26} - W_{26})|(Q_{26} - W_{26})}{gT_{26}^2} - P_{AT10} = 0$$

$$\text{LP28: } F_{53} = P_{25} - \frac{|Q_{E10}|Q_{E10}}{2g(A_{010}C_{d10})^2} - \frac{|(Q_{25} - W_{25})|(Q_{25} - W_{25})}{gT_{25}^2} - P_{AT10} = 0$$

$$\text{LP29: } F_{54} = P_{31} - \frac{|Q_{E11}|Q_{E11}}{2g(A_{011}C_{d11})^2} - \frac{|(Q_{31} - W_{31})|(Q_{31} - W_{31})}{gT_{31}^2} - P_{AT11} = 0$$

$$\text{LP30: } F_{55} = \Delta P_{DS6}(Q_{29}) - \frac{|Q_{E11}|Q_{E11}}{2g(A_{011}C_{d11})^2} - \frac{|(Q_{29} - W_{29})|(Q_{29} - W_{29})}{gT_{29}^2} - P_{AT11} = 0$$

$$\text{LP31: } F_{56} = \Delta P_{DS7}(Q_{32}) - \frac{|Q_{E12}|Q_{E12}}{2g(A_{012}C_{d12})^2} - \frac{|(Q_{32} - W_{32})|(Q_{32} - W_{32})}{gT_{32}^2} - P_{AT12} = 0$$

$$\text{LP32: } F_{57} = P_{33} - \frac{|Q_{E12}|Q_{E12}}{2g(A_{012}C_{d12})^2} + \frac{|(Q_{33} - W_{33})|(Q_{33} - W_{33})}{gT_{33}^2} - P_{AT12} = 0$$

$$\text{LP33: } F_{58} = P_{36} - \frac{|Q_{E13}|Q_{E13}}{2g(A_{013}C_{d13})^2} - \frac{|(Q_{36} - W_{36})|(Q_{36} - W_{36})}{gT_{36}^2} - \frac{|(Q_{34} - W_{34})|(Q_{34} - W_{34})}{gT_{34}^2} - P_{AT13} = 0$$

$$\text{LP34: } F_{59} = P_{40} - \frac{|Q_{E16}|Q_{E16}}{2g(A_{016}C_{d16})^2} - \frac{|(Q_{40} - W_{40})|(Q_{40} - W_{40})}{gT_{40}^2} - P_{AT16} = 0$$

$$\text{LP35: } F_{60} = P_{41} - \frac{|Q_{E16}|Q_{E16}}{2g(A_{016}C_{d16})^2} - \frac{|(Q_{41} - W_{41})|(Q_{41} - W_{41})}{gT_{41}^2} - P_{AT16} = 0$$

$$\text{LP36: } F_{61} = P_{42} - \frac{|Q_{E17}|Q_{E17}}{2g(A_{017}C_{d17})^2} - \frac{|(Q_{42} - W_{42})|(Q_{42} - W_{42})}{gT_{42}^2} - P_{AT17} = 0$$

$$\text{LP37: } F_{62} = P_{44} + \frac{|Q_{E18}|Q_{E18}}{2g(A_{018}C_{d18})^2} - \frac{|(Q_{44} - W_{44})|(Q_{44} - W_{44})}{gT_{44}^2} - P_{AT18} = 0$$

$$\text{LP38: } F_{63} = P_{45} + \frac{|Q_{E18}|Q_{E18}}{2g(A_{018}C_{d18})^2} - \frac{|(Q_{45} - W_{45})|(Q_{45} - W_{45})}{gT_{45}^2} - P_{AT18} = 0$$

[B-4]

where  $Q$ 's are the air flow rates in the sewer pipes,  $Q_E$  are the educting/inducting flows via manholes,  $P_{AT}$ 's are the local atmospheric pressure (due to wind speed or barometric pressure or a combination of the two forces),  $P$ 's are boundary pressures at the end the lateral pipes and  $\Delta P_{DS}(Q)$ 's are the pumping characteristic function modelled as:

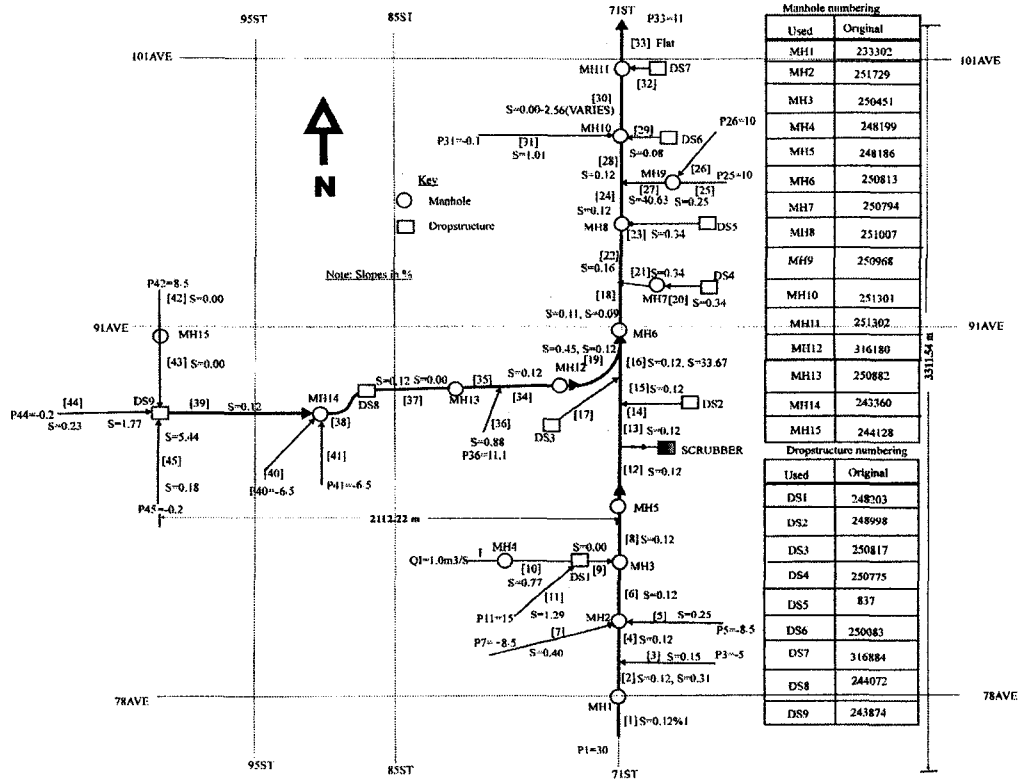
$$\Delta P_{DS}(Q) = \gamma Q^2 + \alpha Q + \beta \quad [\text{B-5}]$$

in which  $Q$  is the dropstructure outlet air flow rate, and  $\gamma$ ,  $\alpha$  and  $\beta$  are constants. Other symbols are explained in Chapter 5.

### 1. Data

Figure B-2 shows the slopes (available) for the Kenilworth sewer pipes. Also shown are the assumed boundary pressure heads and wastewater velocities/depths used in the theoretical simulation. The choice of the pressure values was somehow aided by reported pressure data measurements in the City of Edmonton's sewer systems. The velocities/depths assigned are also aided by the reported data in Chapter 5.





**Note:**

Pipe [1] and pipe [2] are assigned water surface velocity of 0.2 m/s and relative depth b/D= 81%

Pipe [33] is assigned water surface velocity of 1 m/s and relative depth b/D= 63%

All lateral pipes are assigned water surface velocity of 1 m/s and relative depth b/D= 63%

Other pipes on interceptors are assigned water surface velocity of 1.2 m/s and relative depth b/D= 63%

Lengths of sewer pipes not available and not shown in Figure 5-5 (Chapter 5) are assumed as follows:

[11],[20],[40],[41] assigned 100 m, [26] assigned 150 m, [27] assigned 75 m, [32] assigned 45 m

**Figure B-2: Sewer system showing available slopes and assumed boundary pressure heads (m) (Not drawn to scale)**